Studies of lipid bilayers incorporating a peptide or small molecule

ANDREW JAMES ANDERSON CUDMORE

Submitted in satisfaction of the requirements for the degree of PhD in the University of Edinburgh, 1995.

Abstract

Synthetic phospholipid membrane structures have been studied, primarily by X-ray diffraction and the swelling series phase assignment method. The first part of this thesis describes a study of the interaction of a small lipophilic molecule in two different charge forms, amantadine free base and hydrochloride, with fluid phase dioleoylphosphatidylcholine (DOPC) bilayers. Although diffraction data were collected out to eight orders from these bilayers, the swelling series method could only phase the first five orders of diffraction. Measurement of the meridional diffraction spacing showed that the DOPC bilayer thickness decreased by 1 to 2.5Å on addition of either charge form of amantadine. Little more could be deduced about the interaction of amantadine with DOPC bilayers, because of the limited ability of the swelling series method to phase the diffraction data.

The second part of this thesis describes the study of a brominated phospholipid, which might provide an alternative to the swelling series phasing method. The synthetic brominated phospholipid is an analogue of dipalmitoyl-phosphatidylcholine (DPPC), where the terminal methyl group of the *sn*-2 chain has been exchanged for a bromine atom. This bromine atom 'label' has been incorporated into a phospholipid by substitution for a group of similar atomic radius, 1.85Å versus 2.00Å, thus creating a molecule which is sterically similar to its unlabelled analogue.

The bromolipid and DPPC were studied independently, in both the gel ($L_{\beta'}$) and fluid (L_{α}) phase, and as mixtures, solely in the gel ($L_{\beta'}$) phase. Comparison of the gel and fluid phase electron density maps showed that the major difference between the DPPC and bromolipid bilayers was the presence of an electron dense region at the centre of the bromolipid lipid layer. The mixture bilayer data (1:1, 7:2 and 4:1 DPPC:bromolipid mixtures) showed that the size of the bromine atom peak correlated with the concentration of bromolipid in the bilayer. In the gel phase, the electron dense region could be described by two Gaussian distributed atoms placed 2Å apart.

The DPPC and bromolipid molecules did, however, form bilayers that differed in thickness by 1 to 2.3Å in the gel phase, and 2.2 to 3.8Å in the fluid phase. The 1:1 mixture formed bilayers with a thickness intermediate between those of the pure forms. As well as the bromine atom peak, the gel and fluid phase electron density maps also indicate that the bromolipid and DPPC bilayers differ in their lipid layer structure, at $\pm$10Å from the centre of the lipid layer in the gel phase structures. The disruptive effects of bromolipid on the DPPC structure can be limited, however, by placing only a small quantity of bromolipid into the bilayer.

In general, the addition of bromolipid to DPPC bilayers shifted the structure factor amplitudes in the positive direction. This effect of the electron dense bromine atoms on the diffraction data showed that the bromolipid may be used as a phasing agent for future X-ray diffraction work. The bromolipid may also act as a phasing agent in multiple anomalous diffraction (MAD) experiments.

Declaration

I declare that this thesis has been composed by myself, and that the work described herein is my own, except where stated.

Acknowledgements

I would like to thank Dr. Jeremy Bradshaw for being my supervisor. My thanks also go out to my second supervisor, Dr. Richard Ashley, who helped to guide me through to this final product. I would also like to thank my industrial supervisor Dr. Robert Alecio for designing the bromolipid and for his help and hospitality in Sittingbourne. I would also like to express my graitude to Shell Research Ltd., Sittingbourne Research Centre, Sittingbourne, Kent, ME9 8AG, for supporting me as a CASE student, in collaboration with the SERC.

Acknowledgements also go out to Dr. Kevin Campbell Duff and Dr. Larry Hayward, for their advise and friendship. My biggest thanks go to my wife Dr. Sarah Cudmore for help and support beyond the call of duty.

List of contents

List of exhibits

Figures

Plates

Abbreviations

1:1 mixture	1:1 (wt:wt) mixture of DPPC and Bromolipid
4:1 mixture	4:1 (wt:wt) mixture of DPPC and Bromolipid
7:2 mixture	7:2 (wt:wt) mixture of DPPC and Bromolipid
BHT	Butylated hydroxytoluene
Bromolipid	1-palmitoyl, 2-n-pentadeca-15-bromo-*sn*-glycero-3-phosphocholine
D	Bilayer thickness
DMPC	1, 2-dimyristoyl-*sn*-glycero-3-phosphocholine
DOPC	1, 2-dioleoyl-*sn*-glycero-3-phosphocholine
DPG	Diphosphatidylglycerol
DPNH	Diphosphopyridine nucleotide
DPPC	1, 2-dipalmitoyl-*sn*-glycero-3-phosphocholine
DSC	Differential scanning calorimetry
DSPC	1, 2-disteroyl-*sn*-glycero-3-phosphocholine
ER	Endoplasmic recticulum
FAB	Fast atom bombardment
FB	Free base
HA	Haemagglutinin
HCl	Hydrochloride
IR	Infrared
M/e	Mass to charge ratio
M1	First Influenza M protein discovered
M2	Second Influenza M protein discovered
MAD	Multiple anomalous dispersion
NADH	Nicotinamide adenine dinucleotide
NMR	Nuclear magnetic resonance spectroscopy
PC	Phosphatidylcholine
PE	Phosphatidylethanolamine
PG	Phosphatidylglycerol
pH	potenz hydrogens
PI	Phosphatidylinositol
ppm	Parts per million
PS	Phosphatidylserine
RH	Relative humidity
SM	Sphingomyelin
SRS	Synchrotron radiation source
vol	Volume
wt	Weight

Chapter 1.

X-ray diffraction of biological membranes

1.1 Introduction.

The work presented in this thesis has been based on the X-ray diffraction technique, applied to phospholipid membrane samples. The aims were two-fold:

1) To study the interaction of a small drug molecule with phospholipid bilayers using X-ray diffraction and the swelling series phasing method.

2) To develop an alternative phasing method to the swelling series approach.

During this project, the interaction of an anti-influenza drug, amantadine, with dioleoylphosphatidylcholine (DOPC) bilayers has been studied by X-ray diffraction and the swelling series phasing method. In recognition of the limitations of the swelling series method, a novel bromolipid has been synthesised and characterised which might offer an improved method of phasing diffraction data. The layout of the thesis is as follows:

Chapter 1 Membrane biology is introduced and the importance of phospholipids as building blocks of the membrane bilayer structure is emphasised.

Chapter 2 The theory behind X-ray diffraction studies of membrane structures is described.

Chapter 3 Materials and methods of X-ray diffraction and differential scanning calorimetry (DSC) experiments described later in the thesis are discussed. The synthesis and characterisation of a novel synthetic bromolipid is also described.

Chapter 4 A study of the interaction of the anti-influenza drug, amantadine, with fluid phase DOPC bilayers by X-ray diffraction is discussed, that employs the established swelling series method to aid the analysis of the

diffraction data. While this phasing technique has proved its worth over many years, its limitations are highlighted.

Chapter 5 Studies of a novel brominated structural isomorph of DPPC (the bromolipid described in Chapter 3) are described, in comparison with DPPC, in the gel phase by X-ray diffraction. Studies of the two phospholipids by DSC are also discussed.

Chapter 6 An X-ray diffraction study of three different bilayer mixtures of the bromolipid and DPPC (1:1, 7:2 and 4:1 DPPC:bromolipid mixtures) are described. While the diffraction studies of the bromolipid have employed the swelling series phasing method, it was hoped that the work would produce an alternative phasing method for the analysis of X-ray diffraction data.

Chapter 7 This final experimental chapter describes the study of pure bromolipid and DPPC bilayers, above the gel to fluid phase transition temperature, by X-ray diffraction.

Chapter 8 The swelling series and bromolipid phasing methods are evaluated and the findings of this thesis are concluded.

1.2 Introduction to membrane biology.

While the bilayer membranes studied in this thesis are artificial, the driving force for such research is the importance of membranes to all living cells (Finean *et al.*, 1984). Membranes cover the outside of all living cells and also form the basis of many internal organelle structures. The following four functions are general features of all living membranes:

1) Membranes form the physical boundaries of compartments whose composition can be controlled to permit biochemical processes to occur efficiently.
2) Membranes allow the transportation of a restricted range of molecules from one compartment to another, i.e. they are selectively permeable.
3) Membranes act as interfaces which allow the transduction of energy or chemical signals from one compartment to another.
4) Membranes provide the optimum environment for the functioning of certain molecules (e.g. enzymes, ion pumps and receptors).

1.2.1 The surface membrane.

The surface membrane covers all cells, and divides the external medium from the internal cytoplasm. Prokaryotes rarely have any membrane structures, other than the surface or limiting membrane (Margulis and Schwartz, 1982). While many viruses possess no membrane structures whatsoever, those such as influenza have a relatively simple membrane envelope (Luria *et al.*, 1978; Fields, 1985). The surface membrane is freely permeable to a restricted range of small molecules, such as water, urea, glycerol and many lipid soluble molecules (Kregenow, 1981). The transportation of more complex molecules into the cell, such as glucose and amino-acids, is facilitated by proteins embedded in the surface membrane (Mueckler *et al.*, 1985; Thorens *et al.*, 1990). Another embedded protein, the Na^+/K^+ ATPase, pumps Na^+ ions out of the cell in exchange for K^+ ions (Sweadner and Goldin, 1980; Cantley, 1981; Pedersen and Carafoli, 1987). Peptide hormones, such as insulin and glucagon, bind to the external surface of cell membranes, eliciting a

response from the internal surface via embedded plasma membrane proteins (Ullrich *et al.*, 1985; Schlessinger and Ullrich, 1992).

The surface membrane of many cells is divided into separately functioning regions. The plasma membrane of epithelial cells, such as those found in the gut or kidney, is segregated by a tight junction into apical and basolateral domains (Da Silva and Kachar, 1982; Schneeberger and Lynch, 1992; Anderson *et al.*, 1993). In hepatocytes, the basolateral membrane is subdivided into a blood-bathed sinusoidal domain and a lateral domain that interacts with neighbouring cells (Bartles *et al.*, 1985; Simons and Fuller, 1985). The hepatocyte membrane regions have been shown to differ in both their physical and biochemical properties (Evans, 1977).

1.2.2 Internal membranes of eukaryotic cells.

Unlike prokaryotes, eukaryotes have a variety of membrane-bound organelles within their cytoplasm (de Duve, 1975; Tolbert and Essner, 1981), several examples of which are given below:

1) The mitochondrion has a double membrane structure which encapsulates a central matrix compartment containing all the enzymes associated with the final oxidation of carbohydrate, lipid and protein metabolites (Lanoue and Schoolwerth, 1979; Bereiter-Hahn, 1990). The inner mitochondrial membrane is highly folded into cristae and holds the membrane proteins of the electron transport system (Srere, 1982). As well as having proton pumping capabilities, these membranes have transport systems for metabolites and breakdown products that are used or produced in the central matrix.
2) Lysosomes are membrane bound organelles which typically have a low pH that is generated by a proton pumping ATPase (Ohkuma *et al.*, 1982). The organelle contains a wide variety of hydrolytic enzymes such as phosphatases, sulphatases, esterases, proteases and glycosidases (Bainton, 1981; Kornfeld and Mellman, 1989) which must be prevented from digesting other cell components by the barrier qualities of the surrounding membrane.

3) Peroxisomes, another form of membrane bound organelle, contain a variety of oxidases that produce hydrogen peroxide during the oxidation of substrates such as D-amino acids and hydroxyl acids (e.g. lactate) that must be prevented from digesting other cell components by the membrane barrier (Tolbert and Essner, 1981; Taiz and Zeiger, 1991).
4) The nuclear membrane is a double membrane structure, with large well defined pores, that surrounds the genetic material of cells (Franke *et al.*, 1981; Forbes, 1992).
5) The endoplasmic recticulum and Golgi membranes separate the cytoplasm from the cisternal space (Novikoff, 1976; Farquhar and Palade, 1981; Griffing, 1991). The rough endoplasmic recticulum bears ribosomes on its cytoplasmic face and is the site of membrane protein synthesis (Lake, 1981). The smooth endoplasmic recticulum synthesises membrane lipids such as cholesterol and phospholipids (Bishop and Bell, 1985).
6) Membrane vesicles transport proteins and lipids to specific destinations in the cell, and act as carriers in exocytosis and endocytosis (Helenius *et al.*, 1983; Davey *et al.*, 1985; Bradshaw, 1989; Watts and Marsh, 1992).

From this great diversity of roles, it is easy to appreciate the importance of membranes to life and the understanding of their function and mechanism of action is well worth studying and characterising (Evans and Graham, 1989).

1.3 The structure of membranes.

Membranes are composed mainly of protein and lipid molecules (Wallach and Zahler, 1966; Unwin and Henderson, 1984) which may be modified by covalent attachment of carbohydrate residues (Hirano *et al.*, 1972; Hakomori, 1986). It is generally accepted that the molecular organisation of cell membranes broadly conform to the fluid-mosaic model of Singer and Nicholson (1972), a general structure which has a hydrophobic (non-polar) interior and hydrophilic (polar) exterior. Amphipathic molecules, such as phospholipids and glycolipids,

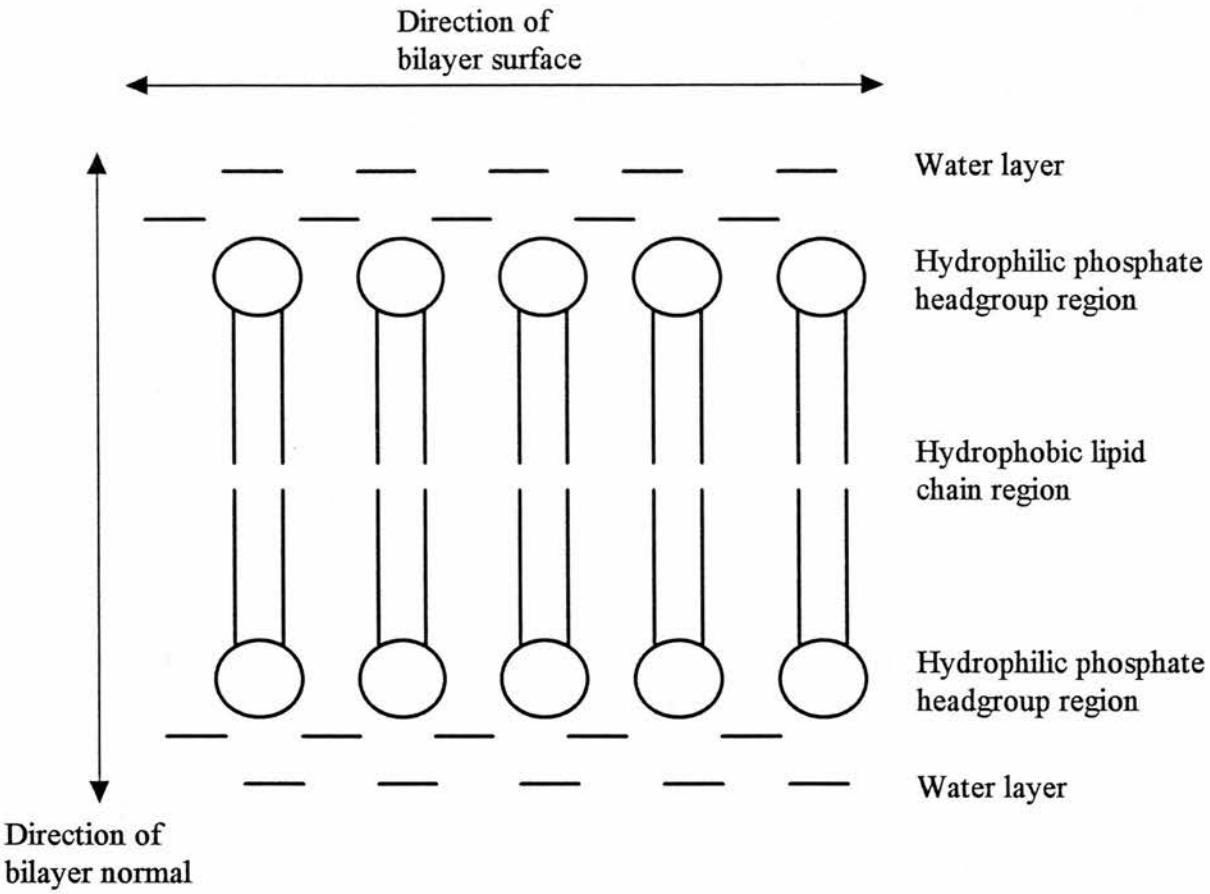

Figure 1.1 The general structure of phospholipid bilayers (Luzzati, 1968). Phospholipids are amphipathic molecules, comprised of a hydrophilic phosphate headgroup attached to hydrophobic lipid chains, which spontaneously form ordered structures. The bilayer structure, drawn above in two dimensions, is the structural basis of membranes which cover all living cells, where two layers of phospholipid molecules form opposing sides of the structure. The membrane exterior is hydrophilic (phosphate headgroups), whilst the centre of the membrane is hydrophobic (lipid chains).

form the basis of the membrane structure, where two layers of molecules facing one another form a bilayer (Figure 1.1). Protein molecules can either bind to the surface of, or penetrate into, the bilayer structure. Sterols, typically ergosterol in plants and cholesterol in animals, are also found in eukaryotic cell membranes.

The major classes of membrane amphipathic molecules, in both prokaryotes and eukaryotes, are based predominantly on a diacylglycerol backbone structure (phospholipids), although animal cell membranes are also comprised of amphipathic molecules based on a ceramide (N-acylsphingosine) structure (Quinn, 1976). In phospholipids, the free primary hydroxyl group of the diacylglycerol backbone is phosphorylated. A variety of headgroup residues can be attached to the phosphate group, forming a large family of related molecules (Figure 1.2). Phospholipids commonly found in nature include: Phosphatidylcholines (PC), Phosphatidylethanolamines (PE), Phosphatidylserines (PS), Phosphatidylinositols (PI) and Phosphatidyl- and Diphosphatidyl- glycerols (PG and DPG).

Table 1.1 Phospholipid, glycolipid and cholesterol content of membranes (Evans and Graham, 1989).

Membrane Type	Glycolipid (% weight) in membrane	Phospholipid (% weight) in membrane	Cholesterol (% weight) in membrane
Human erythrocyte	11	61	22
Myelin	28	41	22
Rat liver mitochondria	<5	80	4
Rat liver E.R.	<5	75	8
Bacterial protoplast	trace	80 - 90	0
Plant chloroplast	80	12	0

The amphipathic molecules that are incorporated into membrane structures vary with membrane type (Bollen and Higgins, 1980; Nillson and Dallner, 1977; Crain and Marinetti, 1979). The relative amounts of phospholipid, glycolipid and cholesterol, for example, have been found to vary widely between the membrane structures of different organisms (Table 1.1). The individual phospholipid types forming a membrane structure can also vary (Table 1.2) as can the sphingomyelin composition (Figure 1.3, rat liver cells). The proportion of cholesterol in a

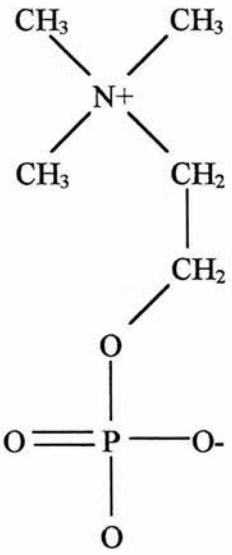

a) Phosphatidylcholine (PC)

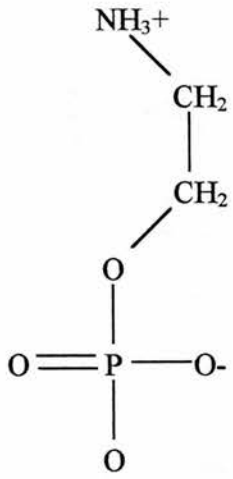

b) Phosphatidylethanolamine (PE)

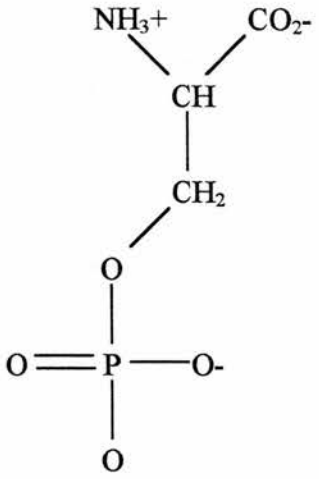

c) Phosphatidylserine (PS)

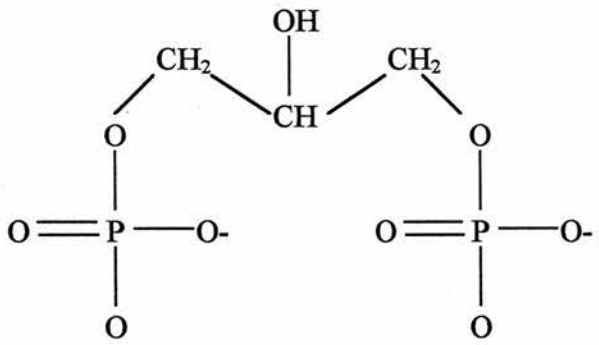

d) Diphosphatidylglycerol ("Cardiolipin", DPG)

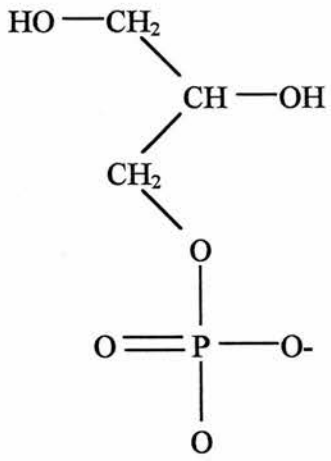

e) Phosphatidylglycerol (PG)

Figure 1.2 Phosphatidyl headgroups commonly found in nature (Bach, 1983). Many different headgroups can be attached to a phosphate group to form phospholipids that have varied characteristics.

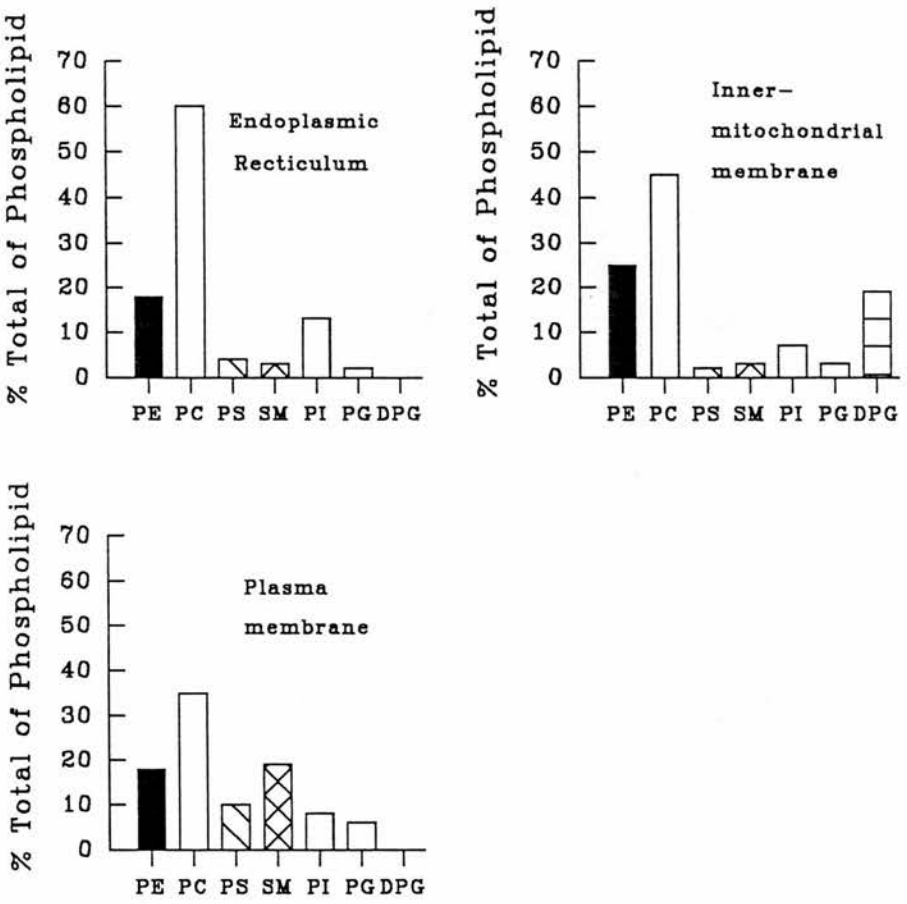

PE –Phosphatidylethanolamine PC –Phosphatidylcholine
PS –Phosphatidylserine PI –Phosphatidylinositol
PG –Phosphatidylgylcerol PDG –Diphosphatidylgylcerol
SM –Sphingomyelin

Figure 1.3 The phospholipid compositions of the rat hepatocyte endoplasmic recticulum, inner-mitochondrial and plasma membranes. The data show that the phospholipid composition varies between the different membranes of the same organism cell type (Evans and Graham, 1989).

membrane structure has also been shown to be dependent on the membrane type, with cholesterol content tending to be highest in the plasma membrane and lowest in the intracellular membranes (Yeagle, 1985). It appears, therefore, that the molecules comprising a membrane are specifically selected to contribute to the properties of that membrane.

Table 1.2 Percentage of each main phospholipid class present in the outer leaflet of various animal membranes.

Cell membrane	SM	PC	PE	PS	Reference
Human erythrocyte	80	77	20	<4	Zachowski, 1993
Human platelet	93	45	20	9	Peret *et al.*, 1979
Rat erythrocyte	100	62	20	6	Renooij *et al.*, 1976
Rat cardiac sarcolemna	93	43	25	0	Post *et al.*, 1988
Rat Hepatocyte bile canalicular surface	65	85	50	0	Higgins and Evans, 1978
Rat liver rough ER	58	68	40	26	Bollen and Higgins, 1988

Transverse asymmetry has been shown to exist in natural membranes, where the lipid composition is different on each side of the bilayer (Zachowski, 1993). Since membranes separate two physiologically dissimilar compartments, they are also likely to perform asymmetric functions. For example, the internal face of the peroxisomal membrane must act as a barrier under harsher conditions (due to presence of hydrogen peroxide) than the external face. Reconstitution experiments indicate a marked variation in the lipid requirement of membrane associated functions:

1) The P_i-ATP exchange and calcium pump reconstituted with lipid vesicles containing F_1-ATPase and Ca^{2+}-ATPase from mitochondria and sarcoplasmic recticulum respectively, require the amino group of phosphatidylethanolamine (PE) to be present, but the proton pump reconstituted with bacteriorhodopsin functions actively in vesicles made from acetylated lipid instead of PE (Singer and Nicholson, 1972).

2) Cytochrome C activity requires the presence of long chain unsaturated fatty acids that provide a fluid environment.
3) The purified (Na^+/K^+)-ATPase contains the phospholipids PC, PS and PE. Removal of these phospholipids leads to the loss of enzymatic activity, which returns when the phospholipids are reintroduced (Hokin, 1976).

Lipids also serve other roles in membrane function (Lenaz, 1977), such as providing a suitable non polar environment in which lipid soluble membrane components, for example ubiquinone (a coenzyme of the electron transport chain in the inner mitochondrial membrane), may function. Lipids may also serve as a barrier separating two different aqueous media and impose vectorial properties on specific proton transport systems, as in oxidative phosphorylation.

1.4 Phospholipids.

Phospholipids are a major class of molecules which can spontaneously form membrane structures (Table 1.1; Figure 1.1; Luzzati, 1968; Ceve and Marsh, 1987). As well as bilayer structures, phospholipids can form a wide variety of other structures (e.g. micelle, inverted micelle, cubic), whose existence and stability is dependant on environmental factors e.g. temperature; pressure; and water content (Cullis and de Kruijff, 1979; de Kruijff *et al.,* 1984). These diverse phases have been extensively studied by X-ray and neutron diffraction as well as many other methods, such as differential scanning calorimetry, infrared (IR) spectroscopy, nuclear magnetic resonance (NMR) spectroscopy and freeze fracture electron microscopy (Nilsson *et al.*, 1991; de Kruijff *et al.,* 1985; Tate and Gruner, 1989; Sjolund *et al.,* 1989; Turner and Gruner, 1992; Seddon, 1990). In this thesis only the well characterised, biologically relevant structures formed by phospholipids have been studied, namely the lamellar phases that many phospholipids form naturally under physiological conditions (Luzzati, 1968).

The phase diagram of a typical phospholipid (Figure 1.4, from Stumpel *et al.,* 1983), especially those with identical lipid chains, shows how the structural

form (phase) of DPPC varies with temperature. The nomenclature most commonly used for describing bilayer lamellar phases is as follows:

L - lamellar bilayers, which run flat and parallel with one another;

P - a bilayer structure with a periodic ripple and 2 dimensional order either centred or oblique.

subscripts often encountered include:

α - alpha, denoting that the bilayer is in the fluid phase, the lipid tails having melted apart;

β - beta, the bilayer is in the gel phase, the lipid chains being close packed and stabilised by hydrophobic interactions;

β' - beta prime, states that the lipid chains are tilted, at an angle other than perpendicular to the normal of the lamellae;

ε - epsilon, the subtransition phase found in samples cooled for a long period of time, having a two dimensional orthorhombic unit cell (Chen *et al.*, 1980).

1.5 Molecular conformation of phosphatidylcholines.

Phosphatidylcholine is the most abundant phospholipid in rat liver cell membranes (Figure 1.3). The two lipid chains attached to the PC headgroup, even when chemically identical, are conformationally distinct (Figure 1.5). The conformational difference between the two lipid chains at the glycerol backbone results in the *sn*-1 chain penetrating deepest into the bilayer (Zaccai *et al.*, 1979). The phosphatidylcholine headgroup is hinged at the phosphate group (Figure 1.5) and its orientation can alter as a result of changes in humidity and additions into the bilayer of small molecules (Bechinger and Seelig, 1991).

The crystal structure of 1,2 dimyristoyl-*sn*-glycero-3-phosphorylcholine (DMPC), reported by Pearson and Pascher (1979), is similar to the molecular conformation found for most symmetric chain PC bilayers studied to date. The structure proposed for C(18):C(18) PC under none crystalline conditions is based on the DMPC crystal structure (Figure 1.6). Although the phospholipid conformation shown is based on the gel phase state, it still has many similarities

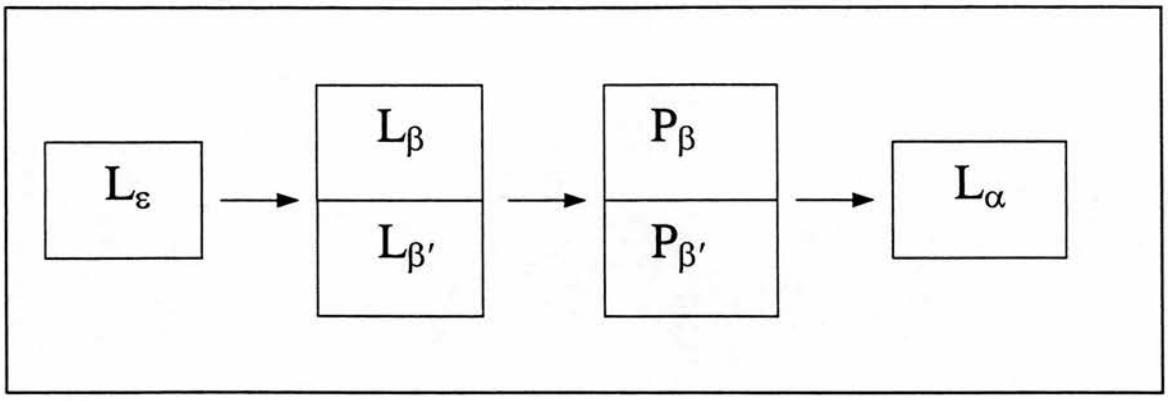

Figure 1.4 Phases formed by phospholipids such as DPPC under physiological conditions. The arrows denote the direction of increasing temperature (from Stumpel *et al.*, 1983).

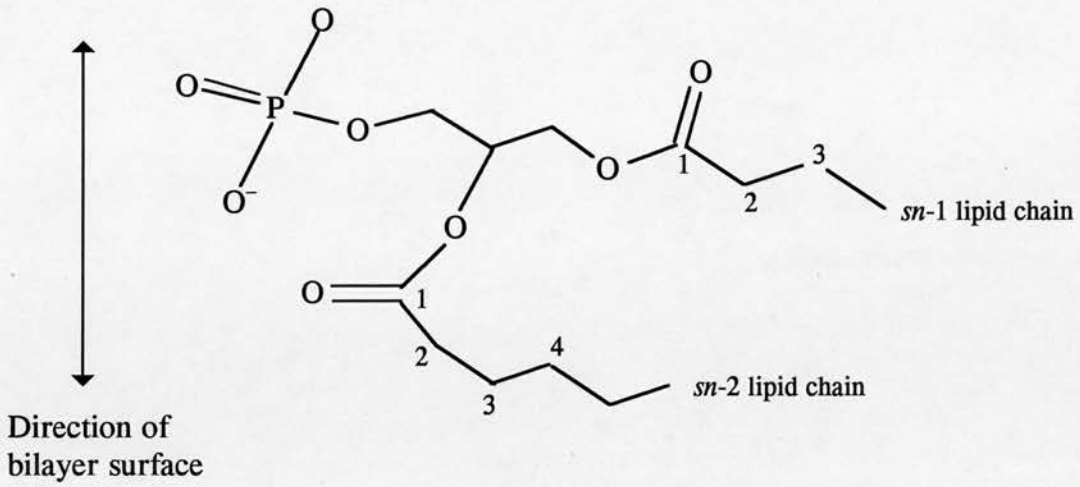

a) The conformational inequivalence of the two lipid chains in a symmetric chain phospholipid. It has been found that the lipid chains of symmetric chain phospholipids in bilayer structures differ conformationally. The *sn*-2 chain at first travels parallel with the bilayer surface before heading down into the lipid layer, compared with the *sn*-1 chain which heads directly into the lipid layer. The chain length difference has been measured as 3 carbon bonds in the phospholipid crystal structure (Pearson and Pascher, 1979) and 1.5 carbon bonds in gel phase DPPC (Zaccai *et al.*, 1979). The chain inequivalence is exaggerated in the above diagram.

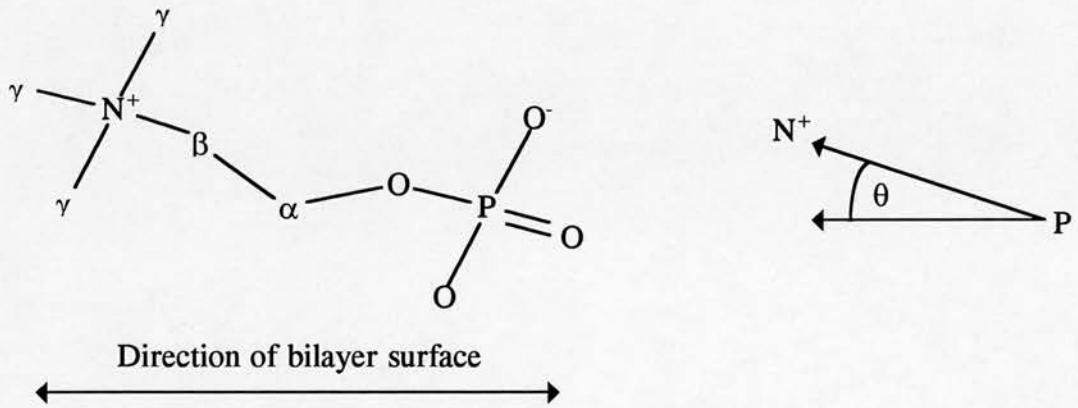

b) Conformation of the choline headgroup. The choline headgroup is hinged about the phosphate group and the choline group to bilayer surface angle can vary with humidity (Bechinger and Seelig, 1991).

Figure 1.5 Two aspects of the typical conformation of phosphatidylcholine molecules in bilayers. (a) The two lipid chains are conformationally inequivalent. (b) The phosphatidylcholine headgroup is hinged at the phosphate group.

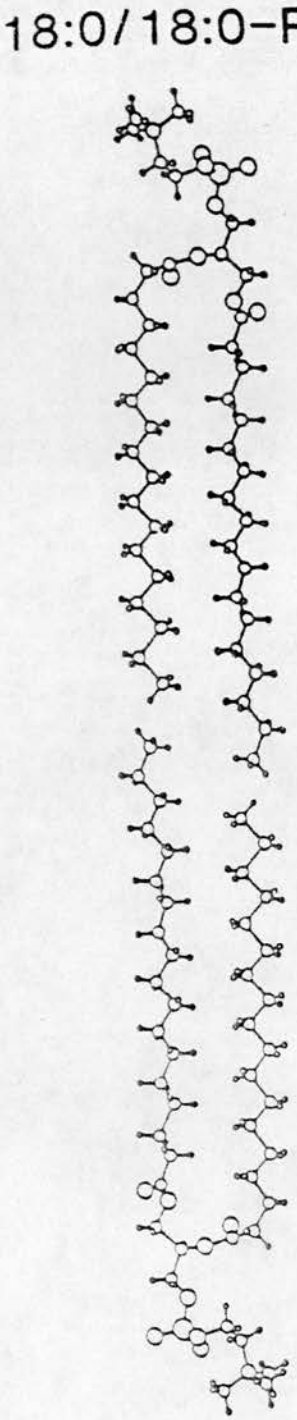

Figure 1.6 A molecular model of a gel phase bilayer structure, based on the conformation of C(18)C(18)PC (from Mattai *et al.*, 1987). In spite of being in the gel phase, the lipid conformation is still based on that found for crystalline lipids (Pearson and Pascher, 1979).

with the crystal structure of DMPC. The structure shown in Figure 1.6 exhibits the lipid chain conformational inequivalence found in both crystalline and non-crystalline bilayer arrays of phospholipids (Pearson and Pascher, 1979; Zaccai *et al.*, 1979). Bilayers of the PC molecule can be divided up into 3 regions for conformational analysis; the head group, glycerol backbone and the lipid chain region. Each of the 3 regions are discussed separately below.

1.5.1 Phosphatidylcholine head group conformation.

Although X-ray diffraction experiments can locate the main electron density groups in the bilayer, additional conformational information of the bilayer molecules can come from other sources. Phosphorus NMR has been of some use in elucidating the behaviour of the head group in bilayers. Studies of hydrated $L_{\beta'}$ phase DPPC bilayers by NMR (Griffin *et al.*, 1978) show that the PC head group is orientated perpendicular to the plane of the bilayer normal (see Figure 1.6). Neutron diffraction experiments on deuterated DPPC (Buldt *et al.*, 1979) also show the head group to be roughly perpendicular to the bilayer normal in both the gel ($L_{\beta'}$) and fluid (L_{α}) phases.

The head group dipole angle has been shown to change either with hydration (Bechinger and Seelig, 1991) or due to the penetration into the bilayer by amphiphiles (Scherer and Seelig, 1989). The hydration state of the head group has also been shown to affect the lipid chain conformation (Buldt *et al.*, 1979). At 20°C and low hydration the DPPC lipid chains were found to be tilted at 11 degrees. On increasing the hydration more water molecules penetrate around the head group, decreasing the bilayer thickness and increasing both the area per lipid and the lipid chain tilt angle (Katsaras *et al.*, 1991).

1.5.2 Backbone or interface region.

The hydrophobic hydrophilic interface region of phospholipid bilayers extends from the phospholipid glycerol backbone to the ester linkages and the α-

methylenes of both the *sn*-1 and *sn*-2 acyl chains. The ester bond linking the acyl chain to the glycerol moiety can exist in two resonance forms, imparting double bond character on the ester bond (Figure 1.7). Since rotation around the axis of a double bond is highly restricted, the five atoms of the ester-glycerol group are essentially co-planar. The *sn*-1 acyl chain and the carbon atoms of the glycerol backbone are oriented almost parallel to the bilayer normal. The initial section of the *sn*-2 acyl chain extends out from the glycerol backbone at a right angle, running perpendicular to the bilayer normal (Zaccai *et al.*, 1979), before bending abruptly by about 90°, at the α-methylene segment, allowing the remainder of the acyl chain to run parallel with the *sn*-1 chain. Because of the unique conformation of the initial segment of the *sn*-2 chain, the terminal ends of a phospholipid with symmetric chains display an axial displacement.

A variety of spectroscopic techniques have demonstrated that the inequivalence of the two phospholipid chains, seen in the crystal structure, persists in hydrated phospholipid phases (Zaccai *et al.*, 1979; Gaber *et al.*, 1978). Neutron diffraction studies on DPPC specifically deuterated at the α-methylenes of the acyl chains have confirmed the bent conformation of the *sn*-2 chains (Zaccai *et al.*, 1979), in both the gel and liquid crystalline phases. In these hydrated phases the lipid chain inequivalence is reduced, from the 3Å found for crystal structures, to 1.8Å (≈1.5 carbon bond lengths). Deuterium NMR studies (Browning, 1981; Seelig and Seelig, 1980) have been performed on a wide variety of phospholipids, with the results suggesting that this interface region conformation is a general feature of most phosphatidylcholines.

1.5.3 Lipid chain conformations.

Depending on temperature, humidity, pressure and lipid chain type, phospholipid chains in the hydrophobic layer can pack together in a number of ways. The close packing of lipid chains results in the formation of equilateral diffraction maxima. The most common packing arrangement for lamellar phase phospholipids, and their characteristic diffraction patterns, are summarised below.

1.5.3.1 The α conformation.

Lipid chains in the α conformation have a liquid-like disorder, producing X-ray diffraction patterns which are characterised by a broad band at around 4.6Å^{-1} that is very similar to a band observed with liquid paraffins (Luzzatti *et al.*, 1960). The hydrocarbon chains in the α conformation behave like molecules in miscible liquids. The α conformation is, to a large extent, insensitive to chemical heterogeneity of the chain groups, which is in contrast to phases of a more ordered nature where the chemical composition plays a critical role in phase stability. Studies of oriented membrane preparations in the lamellar L_α phase (Levine and Wilkins, 1971) have shown that even these 'fluid' bilayers are anisotropic at low water content i.e. there is still some order in the lipid chain conformation. Phospholipid bilayers in the α conformation exhibit a peculiar temperature effect, in that the bilayer thickness decreases as the temperature increases (Luzzati, 1968). This phenomenon, recognised in rubber, is typical of a polymer with a highly disordered conformation, moderately stretched by an external force: a rise in temperature increases disorder and decreases the elongation.

1.5.3.2 The β conformation.

X-ray diffraction patterns of oriented phospholipid samples in the β conformation are characterised by a sharp equilateral reflection at 4.2Å^{-1}. Phospholipids in the β conformation have their lipid chains oriented parallel to the plane of the bilayer normal. This conformation tends to appear in phospholipid samples whose chains are of a chemically heterogeneous nature or contain only a small amount of water (Luzzati, 1968).

1.5.3.3 The β′ conformation.

Sharp reflections at 4.1Å^{-1} and 4.4Å^{-1} are characteristic of phospholipids in the β′ conformation (Stumpel *et al.*, 1983). The lipid chains are stiff and

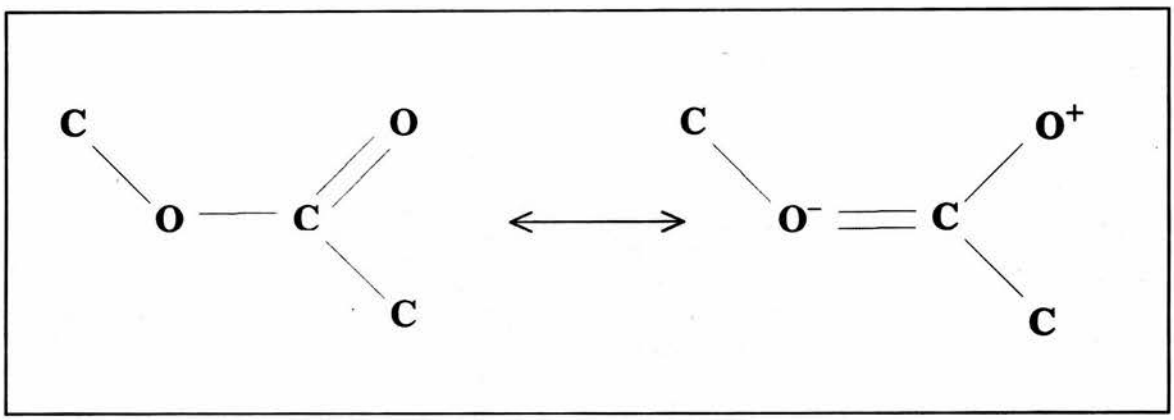

Figure 1.7 The two resonance forms of the ester linkage region. All five atoms are coplanar imparting structural rigidity to the interface region.

parallel, as is the case for the β conformation, packed with rotational disorder in a two dimensional quasi-hexagonal lattice. The chains are, however, tilted with respect to the normal plane of the lamellae. The amount of water incorporated into β′ type phases can be larger than for β type phases, with the angle of chain tilt increasing with increasing water content (Katsaras *et al.*, 1991).

For fully hydrated gel state phosphatidylcholines, the phosphorylcholine head groups adopt a layer aligned orientation with surface areas in the range of 43 to 53Å^2, depending upon the hydrocarbon chain length (Tardieu *et al.*, 1973). Thus the observed chain tilting compensates for the large head group area, allowing the chains to pack with optimal van der Waals contacts. Spectroscopic work has shown that the carbon-carbon bonds are predominantly all-*trans* in the gel phase (Mendelsohn *et al.*, 1989) with an average of two *gauche* conformers in DPPC bilayers (Casal and McElhaney, 1990). Due to the inequivalence of the two acyl chains in symmetric chain phospholipids, there is a small segment at the terminal end of the *sn*-1 chain which must be distorted, possibly by *trans-gauche* isomerism, to fill the space under the methyl terminus of the shorter *sn*-2 acyl chain so as not to leave a region void of van der Waals contacts (Mason and Huang, 1981; Nagle, 1980). This region may well be the predominate source of the gel phase *gauche* conformers seen by spectroscopic methods.

1.5.3.4 The ripple phase.

The $P_{\beta'}$ two dimensional ripple phase is an intermediate between the $L_{\beta'}$ and L_α phases (Caffrey *et al.*, 1990). Its formation, also known as the pretransition, is associated with a change from a one-dimensional to a two-dimensional monoclinic lattice consisting of lipid lamellae distorted by a periodic undulation or ripple. X-ray diffraction photographs of this ripple phase have been presented (Alecio *et al.*, 1985) suggesting the ripple to have a wavelength of 165Å (DPPC at 39.5°C and 98% RH). The period of the ripple increases with decreasing water content, reaching a minimum value at the swelling limit of the lecithin. The hydrocarbon chains are tilted with respect to the plane of the bilayer and are packed in a

hexagonal array. DPPC exhibits a pretransition endotherm at 35°C and a main chain melting endotherm at 42°C, when studied by DSC (Rand *et al.*, 1975). Techniques such as NMR spectroscopy show that there is an increase in molecular mobility of the polar head group at the pretransition temperature (Velski *et al.*, 1969; Chapman and Chen, 1972; Darke *et al.*, 1972; Okamura *et al.*, 1990).

The pretransition endotherm has been shown to be affected by the presence of small amounts of other molecules added into the bilayer, e.g. cholesterol (Ladbrooke *et al.*, 1968), drug molecules (Cater *et al.*, 1974) and also by the effects of various salts present in the aqueous channels separating the bilayers (Chapman *et al.*, 1977). Adding 7.5 mole percent cholesterol to DPPC bilayers was shown to be enough to remove the pretransition, with the tilted lipid chains of DPPC being forced into the untilted β form. Including small amounts of related lipids, e.g. phosphatidylethanolamines (Chapman *et al.*, 1974) removes the pretransition, presumably by affecting the chain organisation. The effect of salts on the pretransition endotherm suggests that the polar head group has the ability to organise into ripples, as the salts are in the water layer bathing the head groups.

1.5.3.5 The ε subtransition phase conformation.

The ε subtransition, discovered more recently than the phases previously described, is a phase whose formation is dependant on the thermal history of the sample (Chen *et al.*, 1980; Fuldner, 1981). Typically the sample must be held at 5°C for several days to achieve the formation of this phase. Using DSC it is only on the first pass of a run that the phase is observed, at a temperature below that of the pretransition. Joint X-ray and DSC results (Stumpel *et al.*, 1983) suggest this phase has a two-dimensional orthorhombic unit cell.

1.5.3.6 Conformations found in mixed chain phospholipids.

The reported crystal structure of a lysophosphatidylcholine (C(16):C(0) PC, Hauser *et al.*, 1980) shows that the phospholipids pack as a fully interdigitated

lamellar layer with a greatly reduced thickness, of 24.5Å, compared with the equivalent bilayer thickness of a symmetric chain phospholipid (C(8):C(8) PC). The head group of lysophosphatidylcholine pack in a layer parallel orientation, with a large head group area of 52.1$Å^2$. The chains are observed to be tilted with respect to the bilayer normal by 41°. A similar interdigitated packing has been proposed for C(18):C(10) PC (Hui and Huang, 1986).

It has been observed that the unit cell dimensions of C(18):C(10) PC are identical to those found for C(14):C(14) PC (Tardieu *et al.*, 1973). This observation supports the idea of an interdigitated packing mode for C(18):C(10) PC where the long lipid chain pairs with a short chain to produce a continuous chain of 28 carbons, as found in C(14):C(14) PC.

1.6 Phospholipids studied in the course of this thesis.

Phosphatidylcholine is the head group chosen exclusively for study in this thesis. Various PC molecules, that vary in the lipid chain region, have been studied during the course of this project.

1.6.1 Dipalmitoylphosphatidylcholine (DPPC)

Attached to the glycerol backbone of DPPC are two fully saturated, 16 carbon (palmitoyl), lipid chains. The carbon atoms are arranged topologically as a straight chain formation, with no branching. The bonds between each carbon along the chain are SP_3 hybrids, which means that each atom is free to rotate about each bond axis. The carbon atoms are free to arrange into a tightly packed arrangement, via hydrophobic interactions. This packing allows DPPC to be in the gel phase at up to about 43°C, with the exact temperature being dependent upon the membrane hydration state (Chapman *et al.*, 1967).

1.6.2 Bromolipid (1-Palmitoyl, 2-n-pentadecyl, 15-bromo-phosphatidylcholine)

The bromolipid molecule is a synthetic phospholipid derivative, not known to exist in nature, that has been synthesised purely as an aid to the analysis of X-ray diffraction data. The bromolipid differs from DPPC solely in the exchange of a terminal methyl group, on the *sn*-2 lipid chain, for a bromine atom.

1.6.3 Dioleoylphosphatidylcholine (DOPC)

The two identical lipid chains of DOPC are 18 carbons long and have a double bond located between carbons 9 and 10 (oleoyl). The double bond orbitals are SP_2 hybrids, which have a different geometry to SP_3 orbitals. Rotation cannot take place around the double bond with the result that DOPC cannot pack as tightly together as the single bond equivalent disteroylphosphatidylcholine (DSPC). For the same headgroup and extent of hydration, increasing the lipid chain unsaturation reduces the transition temperature (Ladbrooke *et al.*, 1968). Thus DOPC has a chain melting transition temperature of *ca* –22°C whereas DSPC melts at *ca* 58°C (Philips *et al.*, 1969). The geometry of the oleoyl chain double bond forces a tilt on the lipid chain, reducing the bilayer thickness (54Å for DOPC at 20°C (Chapter 4) versus 67Å for DSPC (Stumpel *et al.*, 1983).

Chapter 2

Theory of X-ray diffraction of membrane structures.

2.1 Introduction.

The first X-ray diffraction patterns recorded from biological membranes were published in the early 1930s, although it was only in the late 1960s that substantial progress was made in this field (Luzzati, 1968; Velski, 1969). X-ray diffraction is a powerful technique which can identify the conformation of molecules down to atomic detail. Present day membrane studies also employ a host of other physical techniques, such as calorimetry, nuclear magnetic resonance spectroscopy, and infra-red spectroscopy (Nilsson *et al.*, 1991; de Kruijff *et al.*, 1985; Tate and Gruner, 1989; Sjolund *et al.*, 1989; Turner and Gruner, 1992; Seddon, 1990).

Pure phospholipid systems, the most commonly studied 'biological' membranes, have been shown by X-ray diffraction to form a remarkable variety of structures (e.g. lamellar, micelle, inverted micelle and cubic phases), depending on environmental conditions such as temperature, humidity and pressure (Cullis and de Kruijff, 1979; de Kruijff *et al.*, 1984). The interaction of many small molecules with phospholipid systems have also been studied by X-ray diffraction, including studies on the interactions of cholesterol, drugs, toxins, anaesthetics, and peptides (Katsaras *et al.*, 1991; Duff *et al.*, 1993; Dickinson *et al.*, 1993; Brockerhoff *et al.*, 1990; Worcester and Franks, 1976; Franks and Leib, 1979).

2.2 Theory and practice of low angle X-ray diffraction.

In a typical diffraction experiment, X-rays (electromagnetic waves of typical wavelength 1.54Å) are fired at a sample and the resultant diffraction pattern collected and analysed. If the pattern is analysed correctly and completely, structural information about the sample can be obtained from the resultant diffraction (Franks and Leib, 1981). X-rays are scattered by the electrons in the sample and are collected as intensities of diffraction at a particular position, using either X-ray sensitive photographic film or a radiation detector. The sample gives rise to a diffraction pattern whenever it has some repeating nature, so that X-rays

scattered from each repeat add together to give a pattern that is sufficiently intense to detect. The amount of information that can be obtained in a diffraction experiment is therefore limited by the degree of disorder in the structure averaged over the time it takes to record the diffraction pattern.

Whilst the bilayer repeat distance (D) of a membrane can be obtained simply by measuring the relative positions of intensity on the collected diffraction pattern, there are two main problems to be overcome in order to completely analyse a diffraction pattern.

1) In order to reconstruct the electron density profile both the amplitudes of the scattered waves and their relative phases must be known, yet only the intensity of the scattered wave can be measured (i.e. the phase information is lost).
2) The second problem is that even if the correct phases can be deduced there is no simple way of assigning the various levels of electron density to the chemical constituents; hydrated protein and lipid head groups, for example, have a similar electron density (Nagle and Wiener, 1989).

Despite these problems, the technique of X-ray diffraction can provide valuable information about the structure of both biological membranes and model systems, which cannot be obtained by other methods.

2.3 Origin of the diffraction pattern.

X-rays fired at a sample interact with electrons, which then act as secondary X-ray sources. The amplitude of the scattered radiation from each bilayer region is directly proportional to the local electron density, and the interference between the waves scattered by different regions gives rise to the diffraction pattern. Spots of intensity on the diffraction pattern correspond to directions where waves 'in phase' have interfered constructively to produce a peak or spot. Areas on the film lacking intensity spots indicates that either no X-rays were scattered in that direction or scattered waves have interfered destructively, cancelling one another out. The diffraction pattern conveys information about the geometric arrangement in space of the scattering centres, i.e. the time averaged position in space of electron density.

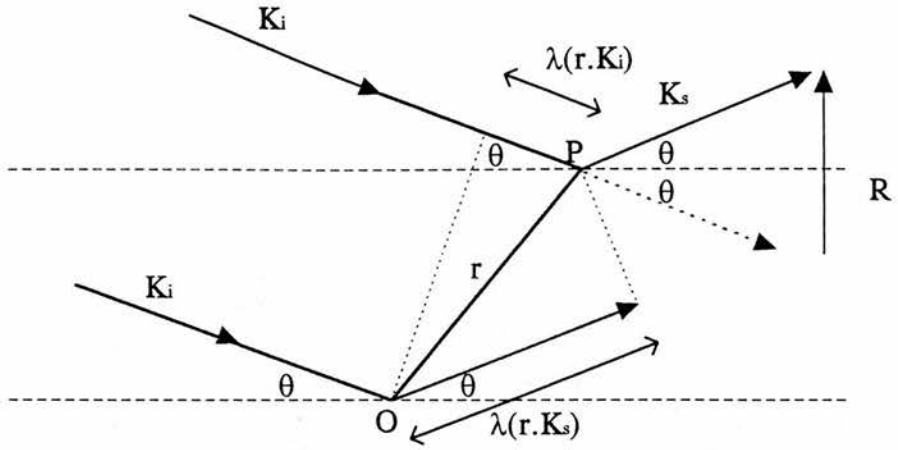

Figure 2.1 A plane wave of X-rays incident upon two scattering centres, O and P (from Makowski and Li, 1983). In a diffraction experiment the incident wave can be represented by a vector K_i of modulus $1/\lambda$ pointing in the direction of propagation. In the direction of the scattered wave represented by the vector K_s, the path difference between rays which have passed through the points O and P, separated by a distance r, is $\lambda r.(K_s - K_i)$.

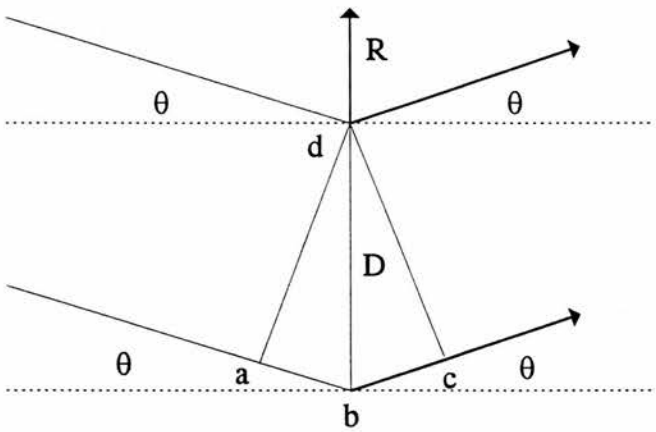

Figure 2.2 A plane wave of X-rays incident upon two planes of constant electron density, separated by the bilayer thickness, D, the distance b to d. All angles θ are equal and the angles b-a-d and b-c-d are right angles. The lower wave must travel an extra distance before emerging from the multilayer stack, compared with the upper wave. This extra path length a-b-c is equal to $2D\sin\theta$, and is therefore related to the bilayer thickness. For the two waves to exit the sample in phase, this path difference must be exactly one X-ray wavelength or an integral number of wavelengths ($h\lambda$) in size, as described by Bragg's law (equation 2.2).

Figure 2.1 demonstrates the interaction between a plane of X-radiation and just two scattering centres, one of which is at an arbitrary origin in space while the other is at a point P, whose position is described by the vector r from the origin. The incident X-radiation can be characterised in terms of a wave vector K_i which lies in the direction of propagation and has modulus $|K_i| = 1/\lambda$, where λ is the wavelength of the radiation. In the direction of the scattered wave (Figure 2.1), represented by the vector K_s, the path difference between rays which have passed through the points O and P is $\lambda r.(K_s - K_i)$. The phase difference in radians is obtained by multiplying by $(2\pi/\lambda)$ which gives

$$\text{phase difference} = 2\pi r.(K_s - K_i) = 2\pi\,(r.R) \qquad (2.1)$$

where we have defined a new vector $R=(K_s - K_i)$. This vector has a simple geometric interpretation since it is perpendicular to imaginary planes which contain the scattering centres and from which the X-rays can be considered to have been 'reflected'.

W.L. Bragg was the first to suggest that X-ray scattering from crystals could be described in terms of 'reflections' from planes of constant electron density (Bragg and Perutz, 1952). The construction Bragg used is shown in Figure 2.2. For planes of distance D apart, total constructive interference occurs only when the angle of incidence is such that the path difference between the two rays is an integral number of wavelengths, as shown in Bragg's law,

$$2\,D \sin\theta = h\,\lambda \qquad (2.2)$$

The integer h is called the order of the 'reflection'. The analogy with normal reflection is not complete since X-ray 'reflections' only occur at specific angles for a given D.

Figure 2.2 shows two 'in phase' waves incident on corresponding regions of two bilayers separated by the bilayer repeat distance D which are 'reflected'. For the two waves to interfere constructively on emerging from the sample they must still be in phase. The lower wave (Figure 2.2) must travel an extra path distance, $2D\sin\theta$, before emerging from the multilayer stack, compared with the upper wave.

For the two waves to be in phase this path difference must be exactly one, or an integral number of, wavelengths in size (Bragg's law, equation 2.2).

The angular deviation (2θ) of the scattered X-rays from the main beam direction can be related to distances between planes of constant electron density in the structure (Bragg's law, equation 2.2). When X-rays are diffracted from a stack of membranes, long range structural periodicity gives rise to diffraction at low angles, whereas the finer details of the membrane structure gives rise to diffraction at higher angles. Thus X-ray diffraction patterns are recorded out to as high an angle as possible so that these fine details may be resolved. The Bragg spacing D, between membrane stacks, divided by h_{max} ,the highest angle order of diffraction observed, is usually said to be the resolution of the pattern.

The reciprocal relationship between distances in the diffraction pattern and distances in the structure can be seen more clearly by relating Bragg's law to the vector R (Figure 2.2), which has a modulus

$$|R| = 2 \sin \theta/\lambda \qquad (2.3)$$

(The amplitude of the wave vector does not change during the diffraction process) Combining equations (2.2) and (2.3) gives

$$|R| = h/D. \qquad (2.4)$$

The vector R is called the *reciprocal space* vector and is the co-ordinate used to describe the positions of reflections in the diffraction pattern. Distances in the structure, on the other hand, are said to be in *real space*.

One can then consider the diffraction pattern from a number of membranes stacked regularly on top of one another, separated by fluid layers of constant width. Most membranes that are studied have no well ordered repeating structure within the plane of the bilayer, and can therefore be considered to have a characteristic time averaged electron density distribution. The one-dimensional projection in the direction of the bilayer normal can be thought of as a continuous distribution of electron density $\rho(x)$ at a distance x from some arbitrary origin, relative to the electron density of the fluid. The amplitude of the scattered wave from this point

will be proportional to $\rho(x)$ and its phase relative to the origin will be $2\pi Rx$ (equation 2.1). To obtain the total resultant amplitude scattered from the whole membrane array one integrates over the thickness of the array, thus

$$F(R) = \int_{x}^{\infty} \rho(x) \exp(2\pi iRx)\, dx \qquad (2.5)$$

F(R) is called the *structure factor* or *structure amplitude* and defines both the amplitude and phase of the scattered radiation (i is the square root of minus one).

The integral of equation (2.5) has the form of a Fourier integral and therefore defines a unique and reciprocal relationship between the electron density structure factor F(R) and the distribution $\rho(x)$. The structure factor F(R), therefore, is the *Fourier transform* of $\rho(x)$, so that if F(R) is known at every value of R then the electron density distribution can be obtained using the inverse relationship

$$\rho(x) = \int_{R}^{\infty} F(R) \exp(-2\pi iRx)\, dR \qquad (2.6)$$

$\rho(x)$ is referred to as being the Fourier transform of F(R) and therefore F(R) is the inverse Fourier transform of $\rho(x)$. Because of this reciprocal nature of the Fourier transform one can think of either of the above as being the Fourier transform of the other.

F(R) in equation (2.5) relates to the entire stack of membranes, but the structure factor of a single bilayer still has to be extracted from it. If the membrane stack consists of N membranes each of thickness D_m separated by fluid layers each of thickness D_f, then the electron density distribution will then be periodic in x, repeating itself every distance $D=(D_m+D_f)$ i.e.,

$$\rho(x + nD) = \rho(x) \; ; \; 0 \geq x \geq D \quad \text{for } n = 1, 2 \ldots N-1 \qquad (2.7)$$

Equation (2.5) can therefore be rewritten as a sum of integrals and factorised to give

$$F(R) = \{ \sum_{n=0}^{N-1} \exp(2\pi iRnD) \} \int_0^D \rho(x) \exp(2\pi iRx)\, dx$$

$$= \{ \sum_{n=0}^{N-1} \exp(2\pi iRnD) \} F_u(R) \qquad (2.8)$$

where

$$F_u(R) = \int_0^D \rho(x) \exp(2\pi iRx)\, dx \qquad (2.9)$$

is the structure factor of an isolated repeat unit of the array. It is thus apparent that the structure factor of the array can be factorised into a product of the structure factor of a single repeat unit and a sum of terms which represent the phase differences introduced into the scattering waves by the spatial separation of the repeat units. This sum is a geometric series, called the interference function G(R)

$$G(R) = \sum_{n=0}^{N-1} \exp(2\pi iRnD)$$

$$= \exp[\pi iR(N-1)D] \frac{\sin(N\pi RD)}{\sin(\pi RD)} \qquad (2.10)$$

The interference function has maxima whenever all the terms in the series have the same value of +1, and this happens only when

$$RnD = m \; ; \; m = 0, \pm 1, \pm 2 \ldots \qquad (2.11)$$

Since both n and m are integers, then equation (2.11) will be satisfied for all n if R times D is also an integer, i.e.,

$$RD = h \; ; \; h = 0, \pm 1, \pm 2 \ldots \qquad (2.12)$$

which is a restatement of Bragg's law (equation 2.2). In other words, the interference function has peaks in reciprocal space at positions where reflections are predicted to occur by Bragg's law.

The wave interference function for a stacked multilayer sample consists of a series of sharp peaks at points $R = \pm h/D$ in reciprocal space. Since the amplitude of the interference function is

$$|G(R)| = \frac{\sin(N\pi RD)}{\sin(\pi RD)} \qquad (2.13)$$

(the exponential factor of equation (2.10) giving the phase) then the maxima in the interference function will have height $|G(h/D)| = N$. The half-widths will be of order $1/(ND)$ so that the widths of the Bragg reflections will be inversely proportional to the number of coherently diffracting units in the array. Thus for large N the interference function exists only in the neighbourhood of the points $R = h/D$ and effectively samples the function $F_u(R)$, the Fourier transform of the single repeat unit, at equal intervals of reciprocal space. Because diffracted X-rays are concentrated into small regions of reciprocal space, membrane stacks can diffract X-rays out to quite high angles, giving high resolution structural information.

As discussed above, there is a unique relationship between the structure factor F(R) and the electron density distribution $\rho(x)$, through the Fourier transformation, so that if one is known the other can be calculated. Unfortunately, in a diffraction experiment we do not observe the function F(R) but rather the diffracted intensity I(R). The observed intensity distribution is related to the diffracted amplitude by

$$I(R) = F^*(R).F(R) = |F(R)|^2 \qquad (2.14)$$

where F*(R) is the complex conjugate of F(R). Thus from the observed intensity we can only directly calculate the modulus of the structure factor, while we lose the phase information. This is the well-known phase problem and constitutes the principal difficulty in the complete analysis of X-ray diffraction patterns.

2.4 Corrections to the value of the measured intensity.

Due to technical difficulties in measuring absolute intensities (Luzzati, 1960; Kratky, 1967) only relative intensities are recorded in an experiment and thus electron density profiles can only be calculated on a relative scale. The measured intensity value has to be corrected by a number of geometrical factors, the most important of which is the Lorentz factor, which takes into account the disorientation of the membranes with respect to the X-ray beam. For a point focus beam the diffracted intensity will spread out in reciprocal space at constant R so that the measured intensities will be reduced by a factor proportional to R^2. If the intensities on a film are integrated around an arc or a circle, as is the case in this thesis, then they need only be multiplied by R rather than R^2.

A minor correction is needed because oscillating electrons, which act as the secondary X-ray sources, do not radiate energy isotropically and the measured intensities have to be divided by $[1+\cos^2(2\theta)]/2$ to take this effect into account, although it is only a small correction at low angles.

2.5 Centrosymmetric structures.

The phase problem is greatly simplified when studying centrosymmetric structures, i.e. $\rho(x) = \rho(-x)$. As this is always the case in this thesis (but not true for all membranes) equation (2.9) can be rewritten as

$$F_u(R) = \int_{-D/2}^{D/2} \rho(x) \exp(2\pi i R x)\, dx$$

$$= \int_{-D/2}^{D/2} \rho(x) \cos(2\pi R x)\, dx + i \int_{-D/2}^{D/2} \rho(x) \sin(2\pi R x)\, dx \qquad (2.15)$$

The sine transform, the second term of equation (2.15), is zero since the sine function is anti symmetric (i.e. $\sin(x) = -\sin(-x)$). In general, we can also write the structure factor $F_u(R)$ in terms of its amplitude $|F_u(R)|$ and phase (α) as

$$F_u(R) = |F_u(R)| \exp(i\alpha)$$

$$= |F_u(R)| \cos\alpha + i|F_u(R)| \sin\alpha \qquad (2.16)$$

and since equation (2.15) shows that $F_u(R)$ is purely real for a centrosymmetric structure, we see that for this case

$$\sin\alpha = 0 \text{ so that } \alpha = n\pi;\ n=0, \pm1, \pm2 \ldots \qquad (2.17)$$

i.e. the phase angles of the structure factor $F_u(R)$ can only be integral multiples of π. These phase angles correspond to the structure factor having either positive or negative values and thus the phase problem reduces to simply determining the sign associated with the observed structure factor amplitude $|F_u(R)|$.

2.6 Analysis of diffraction patterns.

When a membrane is centrosymmetric then, in principle, all that has to be done in order to calculate the electron density distribution $\rho(x)$ is to identify the zeros in intensity, i.e. where the sign changes. The Fourier cosine transform can then be applied to the phase assignments together with the observed $|F_u(R)|$ to calculate an electron density profile. One problem that immediately arises however, is that, since there is a practical limit to how close to the main beam direction scattered X-rays can be observed, the region close to and including the origin in reciprocal space has to be extrapolated from the observed data. The value of the transform at the origin has a simple physical interpretation. From equation (2.9) we can see that when $R=0$

$$F_u(0) = \int_0^D \rho(x)\, dx \qquad (2.18)$$

Thus, as $\rho(x)$ is a contrast function defined relative to the electron density of the fluid, $F_u(0)$ is simply the total number of electrons in the structure in excess of the

number in an equivalent volume of the fluid. In most membrane experiments $F_u(0)$ will be positive. If the sign is not known then, strictly speaking, even if the relative signs of the peaks could be deduced, this would still leave an ambiguity between the electron density distribution and its negative. In practice this choice is not difficult as a bilayer type profile can be assumed.

A more serious difficulty is that the observation of zero intensity is only a necessary but not a sufficient condition for the phase sign to change, and accurate intensity data are required to determine whether or not a sign change in fact occurs. If zeros are not observed between the peaks then this may mean that the membrane electron density profile is asymmetric, although there are a number of other factors that may result in diffraction being observed where zeros should occur. For example, if either the incident beam is not sufficiently monochromatic, the membrane thickness is not uniform or there is scattering from structures within the plane of the membrane or indeed from non membranous structures in the sample, then clear zeros will not be observed. Also, if the membranes are not large sheets but have significant curvature, then transform zeros will not be expected either (Moody, 1975).

2.7 The Fourier series.

The relationship between the electron density distribution $\rho(x)$ and the structure factors $F_u(h/D)$ can be conveniently represented in terms of a Fourier series rather than a Fourier transform. The Fourier series for a centrosymmetric electron density function is

$$\rho(x) = F_u(0)/D + 2/D \sum_{h=1}^{h_{max}} F(h/D) \cos(2hx/D) \qquad (2.23)$$

where h_{max} is the order of highest observed reflection. The term $\rho(x)$ therefore consists of a sum of harmonics whose amplitudes are the structure factor amplitudes $|F_u(h/D)|$ and whose frequency increases with increasing Bragg order. Therefore, as higher orders are added to the Fourier synthesis, finer detail can be resolved in

the structure. The first term on the right hand side of equation (2.23) is a constant and defines the mean value of $\rho(x)$; note that if the electron density is defined relative to the fluid level, it does not represent the mean absolute electron density. In general, it is more difficult to assign phases to the weaker reflections but, luckily, these same terms have the least effect in the Fourier synthesis.

2.8 Truncation (termination) error.

It is not permissible to calculate a Fourier synthesis using only the low orders and consider the resulting electron density map to be an accurate representation of the structure at low resolution, if there are higher order terms of significant amplitude. The exclusion of important higher orders introduces a truncation artefact, which appears as a ripple in the electron density map.

2.9 Methods of solving the phase problem.

As has been stated previously, the outstanding difficulty in diffraction lies in solving the phase problem. Several methods have been devised to overcome the phase problem in X-ray diffraction, which include the now well-known "swelling series" and "isomorphous replacement" approaches (Perutz, 1954; Wilkins, 1972; Torbet and Wilkins, 1976). There are some methods which attempt the determination of phases using only a single data set. Luzzati *et al.* (1972) used a pattern recognition approach where all possible phase combinations were considered and the correct solution chosen on the basis of known or postulated properties of the electron density profile, such as levels of electron density and partial specific thickness of particular components. For a high resolution pattern, however, with a large number of orders, there are a large number of possible phase assignment combinations.

2.9.1 Shannon's sampling theorem.

The Shannon sampling theorem states that the complete continuous Fourier transform $F_u(R)$ can be reconstructed using just the set of observed $|F_u(h/D)|$ together with their chosen signs, and a value of $F_u(0)$ (Moody, 1963). Thus

$$F_u(R) = \sum_{-h_{max}}^{h_{max}} F_u(h/D) \frac{\sin[\pi(RD-h)]}{\pi(RD-h)} \qquad (2.24)$$

This means that in principle only two sets of intensities, collected at different sample humidities so that the bilayer thickness changes, are needed. Since for a constant structure, only the correct combination of signs for the two sets of amplitudes will result in the same continuous Fourier transform ($F_u(R)$) of equation 2.24) as calculated using the Shannon theorem (Worthington *et al.*, 1973). However, the use of just two data sets relies heavily on both the accuracy of the experimental measurements and the assumption that the bilayer structure does not change whilst swelling. It is therefore more prudent to measure as many sets of data as possible so as to reduce and quantify random experimental errors.

2.9.2 The swelling series method.

If the repeat units of a multilayer sample can be swollen apart, provided the structure does not change, then the signs of the structure factors can be obtained. Since the values of $F_u(h/D)$ represent sampled values on the continuous Fourier transform then, if enough swelling states can be measured, the transform can be mapped out and zero values (phase changes) identified. Before the data for a swelling series can be plotted, the intensities from these different swelling states have to be scaled together. Blaurock (1973) showed that the intensities in any one data set at a spacing D could be scaled so that

$$\sum_{-\infty}^{\infty} I(h/D) = D/D_{min} \qquad (2.25)$$

where D_{min} is the minimum spacing in the swelling series. Blaurock also pointed out that since in practice I(0) is not observed and that only a finite number (h_{max}) of reflections are recorded, only an inexact version of equation (2.25) can be used.

The basis of the swelling series phasing method is to construct a smooth continuous Fourier transform by sampling different parts of the continuous transform. The size of the water layer, that separates the phospholipid bilayers in the multilayer stack, is varied by changing the sample humidity as part of the swelling series process. There are several assumptions that are made when utilising the swelling series method:

a) A structure which remains constant with hydration is physically plausible. It is possible to assign phases if during swelling the bilayer structure remains constant except for the thickness of the solvent layer (Perutz, 1954).
b) Phases can still be assigned as long as any structural changes that occur with swelling are simple and continuous through the experiment (Torbet and Wilkins, 1976).
c) A simple and unique solution is more likely to be correct than any one of a number of complicated alternative solutions.

The swelling series method, if successful, will result in electron density maps being constructed at each of the humidities that experiments were carried out. From assumption (b) of the swelling series method, we would expect the electron density maps to vary with humidity in a predictable way, i.e. any major change as the humidity is varied should only affect the size and possibly the shape of the water layer. Assumption (c), above, states that the phases of each diffraction order, between differing humidity data sets, should vary in a simple way that is predictable by the form of the plotted continuous Fourier transform.

If a smooth continuous Fourier transform is plotted during the swelling series process it is sometimes thought that no structural changes can have taken place in the sample during swelling i.e. the modulus of a single continuous Fourier transform has been sampled. This is not so, as continuous changes in the sample structure will also result in the plotting of a smooth continuous Fourier transform. If, on the other hand, the data points for each order vary gradually but these

individual curves do not make up a smooth function, then this is clear evidence of a structural change. What is important is that the changes are small and continuous in nature, so that phases can still be assigned on the assumption that the reconstructed Fourier transforms should change in a reasonable and consistent way with swelling.

2.9.3 The isomorphous replacement method.

Isomorphous replacement is a phasing method used extensively in protein crystallography, where a heavy atom is added into a native sample. The method requires that the addition of the heavy atom does not substantially alter the native structure. The use of heavy atom methods have had limited success when used on biological membrane samples (Akers and Parsons, 1970; Harker, 1972; Blaurock, 1973). Phases have been determined for bilayers of fatty acids associated with a series of alkaline earth metals (McIntosh *et al.*, 1976) using a method similar to that of Hargreaves (1946). Franks *et al.* (1978) have used halogenated cholesterol analogues in isomorphous experiments, that were used to phase the signs of the lamellar reflections (for orders up to h=7). This method works well, but can only be used when studying a system containing inserted molecules, such as cholesterol, that can be labelled with a heavy atom.

2.9.4 The multiple anomalous dispersion (MAD) method.

Anomalous scattering as a method of phasing is still relatively new to protein crystallography (Hendrickson, 1985a, b), although it has already been used to analyse complex crystal structures such as that of crambin (Hendrickson and Teeter, 1981). Although the MAD technique has yet to be used in membrane diffraction experiments, it would be a possible application for a synthetic phospholipid such as the bromolipid that has been synthesised and studied during this thesis. The MAD technique has been made possible by major advances in the field of X-ray instrumentation, such as the introduction of synchrotron radiation. Synchrotron radiation is a high intensity source of X-rays, produced in a wide

spectrum of wavelengths. A desired wavelength for study can be chosen from this spectrum and tuned onto a sample. Diffraction patterns can be collected from the same sample at different X-ray wavelengths, the crux of the MAD technique.

X-ray scattering is perturbed through resonance between the electronic vibrations excited by an incident X-ray wave and the natural oscillations of bound electrons in atoms. The resulting anomalous scattering includes a phase shift that makes anomalous scattering centres distinct. The effect increases sharply as the X-ray energy approaches an atomic absorption edge, although they are also appreciable throughout the range of wavelengths of interest in X-ray diffraction experiments for all but the lightest of atoms. Bijvoet (1949) first recognised the potential of anomalous scattering in structure analysis long before the instrumentation was available. Conventional diffraction analysis takes scattering by electrons to be directly proportional to electron density and insensitive to atom type. Such a description is only adequate for the lightest of elements (e.g. nitrogen or lighter). In general, resonance between electronic vibrations, induced by the incident X-rays, and the characteristic frequencies of bound electrons modifies the diffraction scattering. This change, the 'anomalous' scattering, has two especially pertinent features: the magnitude of the effect varies with X-ray wavelength, and each type of atom gives a distinctive response.

For most systems of interest, the diffraction due to anomalous scattering is very small compared with the total scattering. Effective exploitation of anomalous diffraction therefore requires precise measurements of small differences between relatively large values. Thus experimental methods must be designed so that systematic errors are minimised, Hendrickson (1985a, b). It may be that for membrane diffraction the sample is too disordered, with the natural thermal and stacking disorder of a typical sample being too great for such small differences in diffraction to be measured. Membrane diffraction has the advantage over crystal diffraction that with each phospholipid unit containing an anomalous scatterer, the ratio of anomalous scatterers to normal scatterers is much higher, as a typical phospholipid is much smaller than a typical crystal protein. As MAD is a multi-wavelength experiment, diffraction data can be collected at either side of a suitable

atom's absorption edge, thus greatly enhancing the magnitude of the anomalous scattering effects. Complementary to this, extra phase information is obtained, due to the experiment having been performed at different wavelengths (Hendrickson, 1985a, b).

MAD experiments have a major advantage over isomorphous replacement experiments. In a typical isomorphous replacement experiment one might study several samples, each with increasing amounts, or type, of heavy atom present, and hope that there is no major structural change around the heavy atom. In the MAD experiment one need only study a single sample, incorporating a heavy atom. Throughout the MAD experiment, therefore, there would be no structural variations whatsoever, as it is the X-ray wavelength and not the sample that is varied.

The bromolipid that has been synthesised and studied in this thesis appears to satisfy all predictable requirements for a membrane based MAD experiment to be successful. It contains an anomalous scatterer, the bromine atom, which sits in a precise position in the bilayer. The bromine atom was specifically chosen in the design of a structural isomorph of DPPC, so that MAD experiments might be possible in the future. Other atoms, such as other halogens, could have sufficed if the requirement was to have a synthetic phospholipid to use purely in isomorphous replacement experiments. The bromine K shell electrons have an absorption edge energy (*ca* 1Å X-rays) which can be obtained by existing synchrotron facilities, such as the SRS at the Daresbury laboratories, Warrington, England (Hendrickson, 1991). There is a natural heavy atom in a phospholipid, the phosphorus atom, which is an anomalous scatterer. Unfortunately the absorption edges for a phosphorus atom are not obtainable with modern synchrotron sources, and so a synthetic lipid must be used instead.

Chapter 3.

Materials and methods.

3.1 X-ray diffraction set-up.

The X-ray diffraction experiments were carried out using a Marconi-Elliot GX-13 rotating anode X-ray generator (Plates 3.1 and 3.2). The GX-13 accelerates electrons towards a copper target using a potential difference of up to 70 kilovolts (kV). A usable X-ray beam was generated by a minimum voltage of 30kV and a current of 30kA, with higher voltages reducing the exposure time required to collect a photograph. The X-ray diffraction experiments used the 1.54Å (K_α) wavelength radiation emitted by the copper target. Other wavelengths produced by a copper target, which make up 15% of the total beam (mostly copper K_β with a 1.39Å wavelength), were removed by passing the beam through nickel foil (Franks and Levine, 1981).

X-rays were directed into a purpose built sample holder, through mylar windows (Plate 3.1), using a thin metal tube that collimated the X-rays into a parallel 0.30mm beam. Diffraction patterns were collected by a stack of X-ray sensitive films, positioned 175cm behind the sample holder. A small lead backstop was positioned between the sample holder and film to absorb any undiffracted main beam X-rays that would otherwise fog the film. Air was evacuated from the main camera casing during an exposure to reduce noise from air-scattered radiation.

3.1.1 X-ray camera sample holder.

The sample holder was constructed from a metal can which contained mylar windows. Shelves allowed a bilayer sample, mounted on a curved glass slide, and a perspex bath to be loaded into the sample holder (Plate 3.2). The salt solution placed in the perspex bath allowed the humidity of the membrane sample to be controlled. Around the sample holder were metal tubes that carried water from a temperature controlled bath. An electronic probe, inserted into a hole in the sample holder, measured the sample temperature, which over a 24 hour exposure was maintained to within ± 0.5°C of the desired temperature.

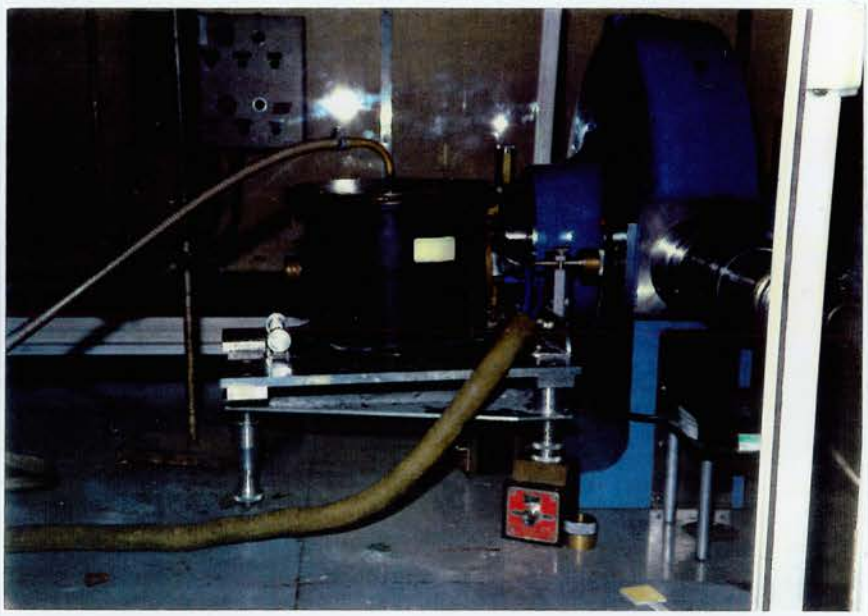

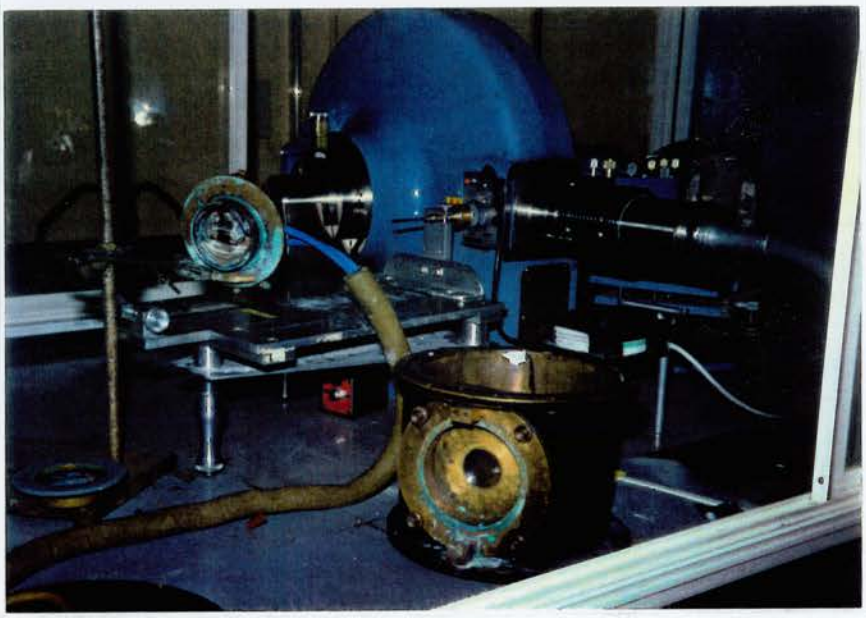

PLATE 3.1 (top) GX-13 X-ray generator and sample camera. X-rays, from the rotating anode, feed into the camera via a 0.30mm collimator. A tube inserted into the top of the camera allows a vacuum to be created between the sample holder and the X-ray sensitive film. Another tube carries water, from a water bath, to allow the temperature of the sample to be controlled.

PLATE 3.2 (bottom) Camera and sample holder. The camera, taken off its support mounting, is turned to show how the sample holder fits into the camera. The sample holder has been opened up to show the position of the water bath under the sample.

3.2 Collection of X-ray diffraction patterns.

X-ray patterns were collected on multiple packs of 130×180 mm and 130×90mm Agfa-Gevaert Osray film. A stack of films were used so that all orders of diffraction could be recorded in an unsaturated form. Relating all the diffraction orders to each other requires an overlap of unsaturated intensity spots on consecutive films in the stack, i.e. the same unsaturated order on sequential pieces of film so that a scaling factor between films can be estimated. Four to six films were typically used in a pack, depending on the predicted number of diffraction orders and the likely intensity ratio of strongest to weakest order.

Collecting the whole diffraction pattern on one stack of film was not always feasible during a single exposure. The length of exposure required to collect weak outer orders often resulted the first order being saturated, or fogged by background noise, on all films in the stack. Separate short exposures onto a few pieces of film, typically for 5 to 20 minutes depending on sample and power of X-ray generator, were therefore regularly used to collect the lower (1-4) diffraction orders.

3.2.1 X-ray film analysis.

Diffraction photographs were scanned on a Joyce Loebl Chromoscan 3 microdensitometer. Scanning involved positioning the film on a glass surface which then allowed each diffraction order to be passed through a light beam. The ability of the light beam to penetrate through the X-ray film provides a measure of the darkness of the film. As the light beam passes through the centre of each diffraction spot, a record is obtained of the position and intensity of each meridional order. The scan peaks were background corrected by constructing a baseline under each peak, using the Chromoscan 3 microdensitometer software, which also calculated the integral of each peak. Any saturated peaks were ignored, with the data for that order coming from other films in the film stack.

The intensity data for each humidity were then scaled to one another using equation 2.25 (Blaurock, 1973). The Lorentz factor was then used to correct each

order for the spreading of intensity in reciprocal space and the sampling of peaks by the Ewald sphere. This factor multiplies each order by $\sin(2\theta_h)$, where θ is the Bragg angle and h the order of diffraction. A further correction is then applied for absorption of the incident and diffracted beams by the lipid film (Franks and Leib, 1979). The square root of each corrected intensity value gives the structure factor amplitude value. The phase of the calculated amplitude is, however, unknown and must be deduced using techniques such as the swelling series method.

3.3 Phase assignment using the swelling series method.

X-ray diffraction patterns obtained during the course of this thesis have been analysed using the swelling series method, which involves collecting diffraction patterns from the same membrane sample at different humidities. The basis of the swelling series phase assignment method is to analyse changes that occur in diffraction patterns with increasing humidity. Whilst the bilayer thickness at each humidity can be calculated without phase information (Bragg's Law; equation 2.2), further diffraction analysis requires phases to be assigned to the data.

A swelling series plot aims to reconstruct the form of a continuous Fourier transform, by plotting each diffraction amplitude against (h/D), where h is the order number and D the bilayer thickness. Swelling series data are phased by judging the goodness of fit of the reconstructed continuous Fourier transform through the putatively phased data points. The electron density maps, constructed using the putative phase assignments, are then inspected. Phase assignments that result in the construction of electron density maps incompatible with the accepted bilayer structure are rejected (Franks and Leib, 1981).

3.4 Assessment of errors in the swelling series data.

Many errors can combine during experimentation to affect the accuracy of the final product of the swelling series method, the bilayer electron density map. The assessment of these errors is discussed below.

3.4.1 The Monte Carlo simulation method of estimating confidence limits for the bilayer electron density distribution.

The uncertainty in electron density map distributions can be determined by the Monte Carlo sampling procedure (Press *et al.*, 1989), using each structure factor amplitude and an associated error level to define a normal distribution of the structure factor (Wiener and White, 1991). The upper and lower 95% confidence limits of the electron density distribution are generated and stored during the Monte Carlo simulation process. Sets of mock diffraction data are repeatedly generated, by random sampling from the structure factor normal distributions, and used to construct electron density maps, typically for 1000 cycles. During each cycle, if the latest calculated electron density value lies outwith (either maximum or minimum) a previous value then the new value is stored in its place. Figures 3.2 and 3.3 depict the 95% confidence limits for the electron density distribution of bromolipid and DOPC bilayers respectively calculated using a Monte Carlo simulation program.

3.4.2 Accuracy of data collected from X-ray film scanning.

X-ray diffraction patterns collected on film were scanned manually, using a Chromoscan 3 microdensitometer. There are systematic errors associated with the scanning method, namely:

1) The film must be aligned by hand so that, when the glass table moves, the light beam passes through the centre of all spots on the film. In practice, lining up films accurately is difficult as, especially on a film with twelve diffraction spots, minimal error can result in the centre of extreme orders being missed. The alignment error acts to reduce the measured size of a spot and may result in the existence of a weak spot being missed altogether.
2) As X-ray diffraction pattern spots from membranes tend to be arced in shape, the finite sized scanning beam of light may not capture the whole of some diffraction spots. Thus, some spots may register as being smaller than they really are. This error can be avoided by using the next film in the film stack.

3) Many intensity spots on the X-ray films are overexposed, i.e. the X-ray film has been blackened non-linearly, so that the intensity spots appear smaller than reality. Care had therefore to be taken so that these over-saturated intensity spots were discarded.

A single film was repeatedly scanned to assess the accuracy of the scanning process. A film, taken from a 1:1 (DPPC:bromolipid) mixture sample at 20°C and 57% RH, with eleven orders of diffraction was scanned fifteen times. Between each scan reading, the film was taken out and then realigned in the microdensitometer the machine. The results (Table 3.1) illustrate the variation observed in each of unsaturated orders of the X-ray film being scanned. Using the same scan data, the bilayer repeat distance was also estimated fifteen times and was shown to be 56.55Å ±0.06Å (SD). The level of error in the electron density distribution, as a result of film scanning errors, has been estimated for the 1:1 (DPPC:bromolipid) mixture sample (Figure 3.1) using a Monte Carlo simulation program and an intensity data standard deviation error estimate of 6% for all twelve orders of diffraction. The 95% confidence limits were calculated to be displaced approximately ±0.5 relative units from the central 1:1 mixture electron density distribution.

Table 3.1 Results of scanning a single film fifteen times to assess the reproducibility of the scanning process (film scanned was used to collect data from 1:1 (DPPC:bromolipid) mixture bilayers at 20°C and 57% RH).

Unsaturated diffraction orders	Average spot intensity from 15 scans (Absorbence)	Standard deviation (SD) of spot intensity	Percentage SD
2	0.172	0.011	6%
5	0.157	0.005	3%
6	0.304	0.007	2%
8	0.164	0.010	6%
9	0.124	0.005	4%
11	0.079	0.010	12%

3.4.3 Reproducibility of bilayer sample preparation, data collection and analysis.

Diffraction patterns were collected out to four orders from five separate oriented samples of DOPC at 20°C and 57% RH. After film scanning and analysing each sample separately, the five sets of data were then averaged and variations in the diffraction data assessed (Table 3.2). The average electron density map of DOPC, at 20°C and 57% RH, has been calculated (Figure 3.2), as have the DOPC electron density distribution confidence limits, using the diffraction order accuracy values (SD) in a Monte Carlo simulation program.

Table 3.2 Diffraction data collected from five oriented DOPC bilayer samples at 20°C and 57% RH.

	DOPC X-ray structure factor data (from samples at 20°C and 57% RH)					
Diffraction order	Sample 1	Sample 2	Sample 3	Sample 4	Sample 5	Sample Mean ± SD (±%)
1	0.180	0.183	0.173	0.182	0.181	0.180±0.004 (±2%)
2	0.069	0.066	0.071	0.069	0.074	0.070±0.003 (±4%)
3	0.073	0.068	0.094	0.070	0.073	0.075±0.011 (±15%)
4	0.060	0.049	0.082	0.048	0.047	0.057±0.015 (±26%)
Bilayer Repeat (Å) ± SD	51.9±0.2	52.1±0.2	52.3±0.2	52.2±0.1	51.8±0.1	52.1±0.2

The 95% confidence limits of the bilayer electron density distribution show that large variations are possible in the bilayer profiles as a result of the diffraction intensity data accuracy limits (Figure 3.2). The measured DOPC bilayer thickness varied between 51.8 ±0.1Å and 52.3 ±0.2Å, where the variation in bilayer thickness between 'identical' samples was greater than the accuracy with which a single sample's bilayer thickness could be measured from the film stack data. The five sets of diffraction data plot as a swelling series (Figure 3.3), indicating a correlation between variations in bilayer thickness and the measured diffraction intensity of each order, the basis of phasing by the swelling series method. The

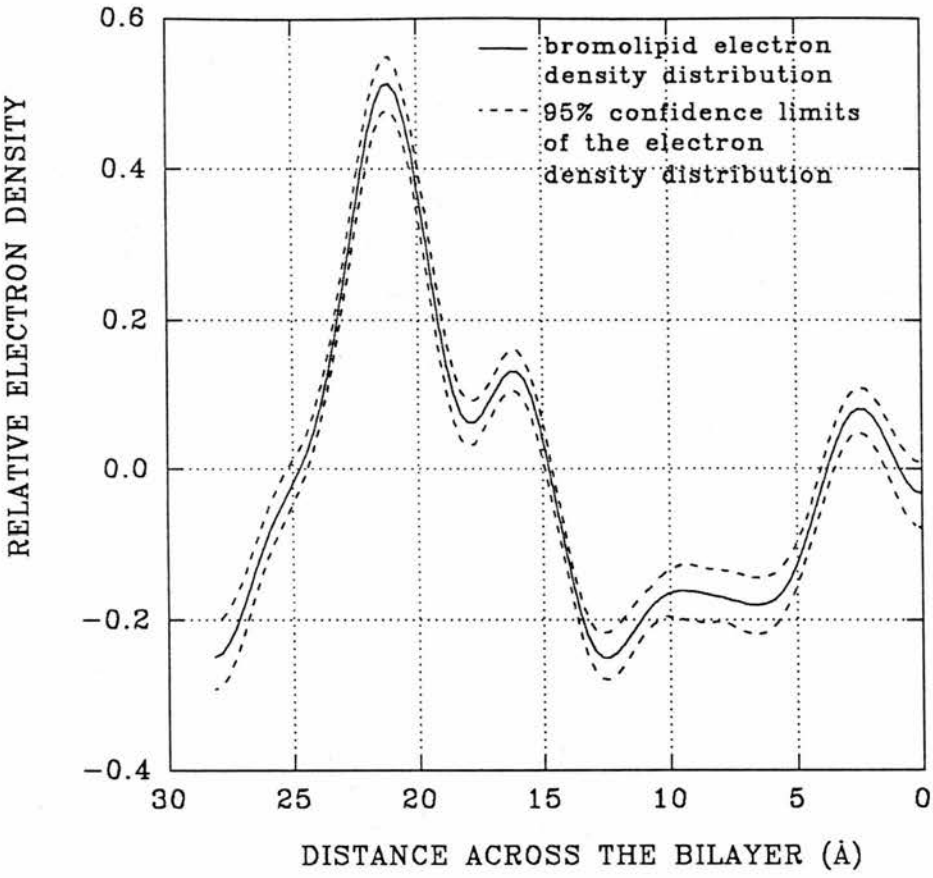

Figure 3.1 The average position and 95% confidence limits for the electron density distribution of bromolipid bilayers (one half of bilayer shown). X-ray diffraction data were collected from oriented membrane samples at 20°C and 90% RH and phased using the swelling series method. The bromolipid electron density map, above, was constructed using twelve orders of diffraction. The 95% confidence limits for the electron density distribution were calculated using a Monte Carlo simulation program and a structure factor amplitude error limit of 6% (SD). The bromolipid phosphate headgroup, ester linkages and centre of the lipid layer can be located at 21Å, 17Å and 0Å respectively. The 95% confidence limits, displaced approximately ±0.05 relative units from the central electron density distribution, were created to assess the level of uncertainty introduced into bilayer profiles by the accuracy with which X-ray films can be scanned.

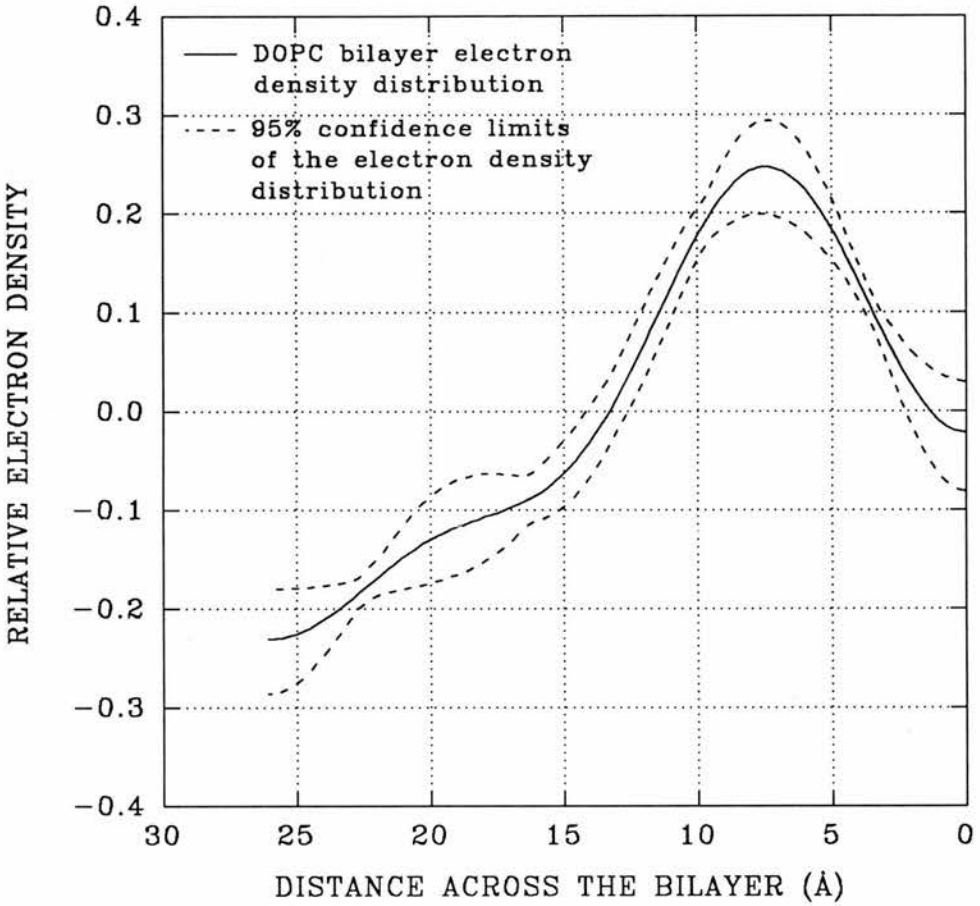

Figure 3.2 One half of the electron density map of DOPC bilayers at 20°C and 57% RH. Four orders of diffraction data were collected from five separate DOPC samples and used to create an averaged electron density map (above). The 95% confidence limits for the DOPC electron density distribution were calculated using a Monte Carlo simulation program. The centre of the water layer, the DOPC phosphate headgroup, and the centre of the lipid layer can be located at 0Å, 8Å and 26Å respectively.

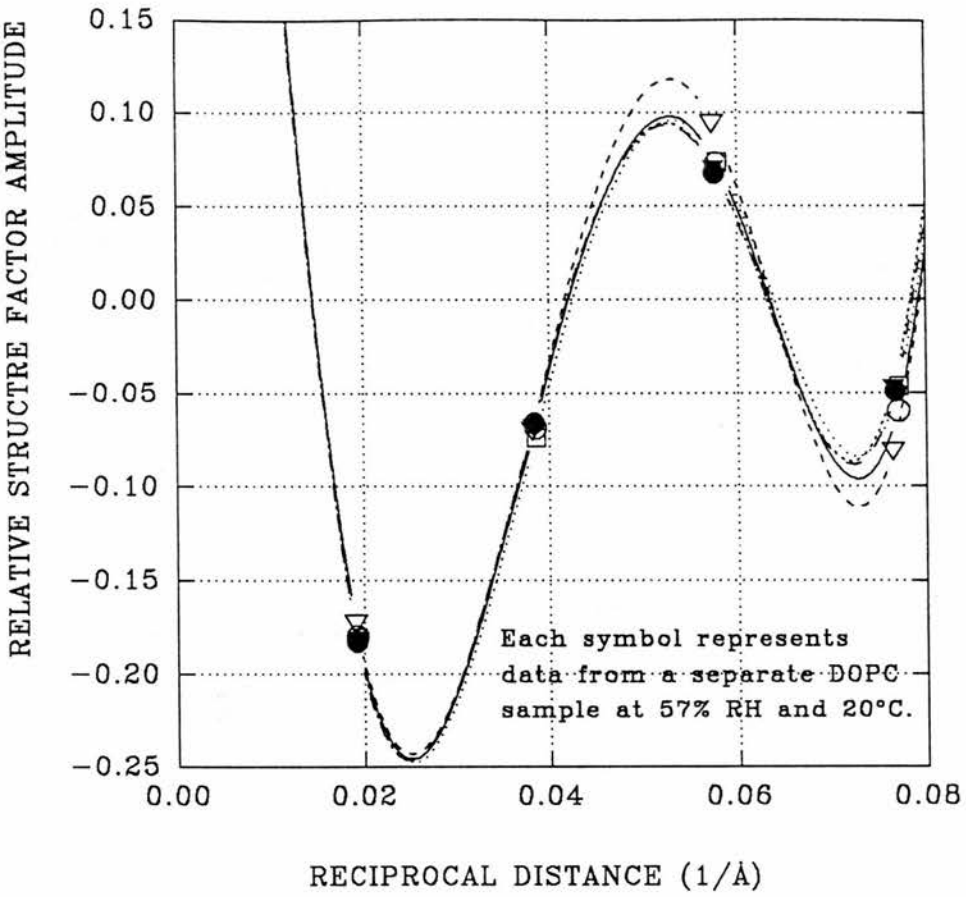

Figure 3.3 A swelling series plot of the diffraction data collected from five oriented DOPC bilayer samples at 20°C and 57% RH. Variations in structure factor amplitude and bilayer thickness data were measured between the five DOPC samples. The swelling series method works on the premise that changing the sample humidity allows the continuous Fourier transform to be sampled at multiple points. The plot, above, suggests that the structure factor amplitude data varies with the bilayer thickness (i.e. the '57%' RH sample humidity actually varies), rather than as a result of random noise acting on the data.

relationship suggests that variations in the measured intensity between samples may be a result of variation in the hydration state and therefore structure of the bilayer. The ability to obtain data from a bilayer sample may, therefore, be better than that suggested by the 'error levels' quoted in Table 3.2.

Variations observed in the structure factor data collected from a membrane sample (Table 3.2) may be introduced by variations in the hydration state of that sample (Figure 3.3). The difference in bilayer thickness of DOPC based bilayers at 20°C, between 98% and 57% RH, has been measured as 2.7Å (Chapter 4, Tables 4.1, 4.2 and 4.3). The variation in bilayer thickness of 0.5Å, found in the five DOPC samples, might then represent a random variation in humidity about 57% of ((98-57/2.7)*0.5≅ 8% RH) i.e. 57% RH ± 4%. This sample humidity error is additive upon the error with which diffraction data can be recorded on film and must be considered when comparing bilayer structures i.e. bilayers with and without a drug present. Failure to take into account variations in sample hydration could result in the conclusion that the systems under study differ significantly, when in fact they only differ in their hydration states.

3.5 Preparation of oriented multilayer samples for X-ray diffraction experiments.

X-ray diffraction experiments have been performed exclusively on oriented stacked bilayer samples. The membrane systems studied during this thesis include:

1) Pure phospholipid systems (DOPC, DPPC and bromolipid)
2) Mixed phospholipid systems (DPPC:bromolipid mixtures of varying ratios)
3) Phospholipid systems incorporating small molecules (DOPC+amantadine FB and HCl).

The preparation of oriented membrane samples required the phospholipids, phospholipid mixtures and phospholipid/drugs to be dissolved and mixed together as chloroform solutions. The chloroform solutions were then pipetted onto glass slides. As the chloroform evaporates, multilayer samples spontaneously form on the glass surface. The sample preparation process is described below.

3.5.1 Preparation of DOPC and DOPC+5% (mol) amantadine solutions in chloroform.

DOPC in chloroform (20mg/ml), amantadine hydrochloride (HCl) and amantadine free base (FB) were all purchased from Sigma Chemical Company Ltd, Fancy Road, Poole, UK. DOPC was used without further preparation in diffraction experiments. Five molar percent amantadine (FB and HCl) in DOPC samples were prepared by weighing out and dissolving amantadine in chloroform, which was then mixed with DOPC in chloroform.

3.5.2 Preparation of DPPC and bromolipid solutions in chloroform.

DPPC was ordered from the Sigma Chemical Company Ltd, Poole, UK., in a crystalline form. Solutions (20mg/ml) of DPPC were prepared by dissolving the phospholipid in chloroform. The bromolipid was synthesised at Shell Research Centre, Sittingbourne, Kent, under the guidance of Dr. M. R. Alecio and stored as a (20 mg/ml) chloroform solution, under nitrogen and at -70°C. Samples requiring mixtures of bromolipid and DPPC were prepared by mixing measured chloroform solutions and vortexing.

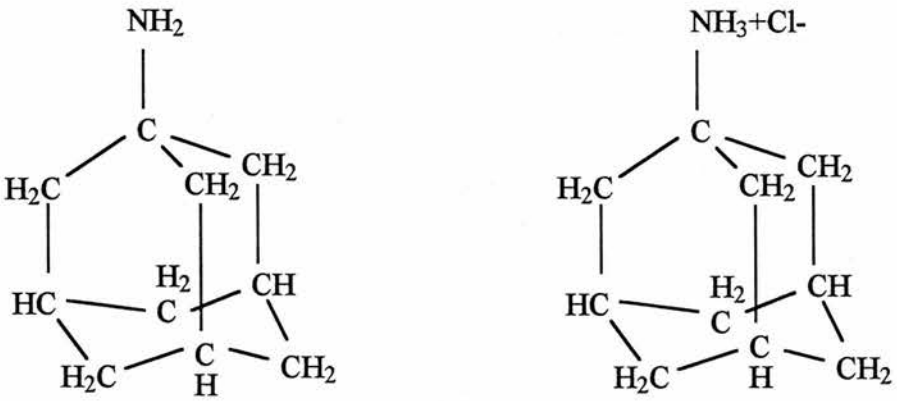

a) Amantadine Freebase (FB)

b) Amantadine Hydrochloride (HCl)

Figure 3.4 The structures of amantadine freebase (FB) and hydrochloride (HCl).

3.5.3 Preparation of multilayer samples.

Solutions of phospholipids in chloroform were slowly pipetted onto a clean glass slide, made from a tube of 20 mm radius, that had a surface area of $1cm^2$. The chloroform was then slowly evaporated off, using a stream of nitrogen. Samples were then placed in a vacuum, for at least two hours, to remove any further traces of chloroform. The samples were then rehydrated, by placing the glass slides over water in a glass dessicator, at 80°C for two hours.

The slowly cooled sample was then transferred from the dessicator to the X-ray camera sample holder. Into this environmental cell was then placed a perspex bath, loaded with the appropriate salt solution for the relative humidity required. Saturated salt solutions used were $ZnSO_4$, KCl, NaCl, and NaBr, these giving relative humidities of 90%, 81%, 74%, and 57% respectively (Handbook of Chemistry and Physics, 1986-1987). In addition, water produces a 98% RH.

3.6 Differential scanning calorimetry (DSC) of membrane samples.

The principle of DSC is given by Steim (1974). A sample pan and a reference pan having similar heat capacities are simultaneously heated at identical rates. Each sample pan has a temperature sensor and heating element so that the temperature of both pans can be identically matched i.e. the temperature differential between the pans is always maintained at zero. The difference in power input, necessary to keep the heating rates of both the sample and reference pans the same, is recorded during the experiment, producing a plot of differential heating rate against temperature.

When the sample and reference pans are precisely matched thermally over a temperature range, the recorder traces a straight baseline at zero differential power input. If a thermal event in the sample pan is not shared by the reference pan then the heat requirements of the two are different, and the recorder pen is deflected from the baseline. The direction of the deflection is dependent upon whether the event was endothermic or exothermic. When the thermal event is completed, the

pen returns to the baseline and a peak will have been traced whose position on the temperature scale indicates the temperature of the event and whose area is a direct measurement of the enthalpy of the event (Steim, 1974).

The thermal events measured in biological membrane calorimetric studies, such as bilayer transitions, are often broad, ill defined and not very energetic. Also, the unavoidably large amount of water in biological systems limits the mass of sample that can be placed in a calorimeter pan and so the heat change cannot be greatly improved by increasing the size of the sample. A DSC experiment is expensive with respect to the amount of lipid consumed, usually using 7-8mg of lipid per sample prepared, which compares unfavourably with the 2mg of lipid that can generate a swelling series data set in X-ray diffraction experiments.

3.6.1 Materials and methods for the DSC experiments.

As *per* the diffraction experiments, DPPC was obtained from the Sigma Chemical Company Ltd, Poole, UK., in a crystalline form. The bromolipid was synthesised at Shell Research Centre, Sittingbourne, Kent, under the guidance of Dr. M. R. Alecio and stored as a (20mg/ml) chloroform solution, under nitrogen and at -70°C. Samples requiring mixtures of bromolipid and DPPC were prepared by mixing measured chloroform solutions and vortexing.

Chloroform solutions of DPPC, Bromolipid and 1:1 (DPPC:bromolipid) mixtures were first dried down in a rotary evaporator. The phospholipid samples were then washed twice with acetone and dried down in a rotary evaporator to a solid. The dry sample was then placed in a platinum pan and the total mass of lipid weighed using a four point balance. Water (5.7µl water/mg) was injected by syringe into the pan containing the dried lipid sample. A reference pan containing only water was also prepared for the experiments. Pan lids were sealed onto the sample pans by cold welding using a Perkin Elmer sealing press. As the sample pans had to accommodate at least 5mg of dry phospholipid sample plus the water of hydration, to get a large enough signal, 50µl volume sample pans were used. To keep the pans clean, all sample pan operations were performed using tweezers.

Samples were loaded into a Perkin Elmer DSC 7 machine with a Perkin Elmer Tac 7/7 instrument controller. Samples were then cycled, typically from 10°C to 70°C, to anneal and homogenise the sample. The sample was then allowed to equilibrate at 10°C for 30 minutes before an experimental run from 10°C to 70°C was recorded.

3.7 Synthesis of the bromolipid.

The bromolipid was synthesised and purified at the Shell Research Centre, Sittingbourne, Kent, under the guidance of Dr. M. R. Alecio. *Sn*-1 palmitoyl, lysophosphatidylcholine and pentadecanolide were both purchased from the Sigma Chemical Company Ltd., Poole, England, and stored at -70°C. Hydrogen bromide, in a 30% (wt/vol) solution of acetic acid was purchased from the Aldrich Chemical Company Ltd., New Road, Gillingham, Dorset, England. The synthesis of the bromolipid (Figure 3.5) can be broken down into the following stages:

a) Preparation of a bromoacid.

The starting products of the bromolipid are 15-pentadecanolide (15-hydroxy-pentadecanoic acid lactone), hydrogen bromide and lysophosphatidylcholine. The first stage of the synthesis is to use the lactone and hydrogen bromide to make a bromoacid. Lactone (2g) was dissolved, with warming, in glacial acetic acid (*ca* 2ml), before being cooled and added to a hydrogen bromide solution (10ml of 30% (wt) solution in acetic acid). The solution was then stoppered and stored for 48 hours. The mass of crystals that formed during this period were suspended in cold water, to wash out unreacted reagents. The crystals were then collected in a filter and washed with more water, before being recrystallised in methanol, at low temperature (5-10°C), and dried in a vacuum over phosphorus pentoxide overnight.

b) Preparation of the symmetrical bromoacid anhydride.

The symmetric bromoacid anhydride was prepared by following the method of Selinger and Lapidot (1966). All equipment and reagents had to be water-free for this stage of the synthesis. Chloroform was distilled and dried over

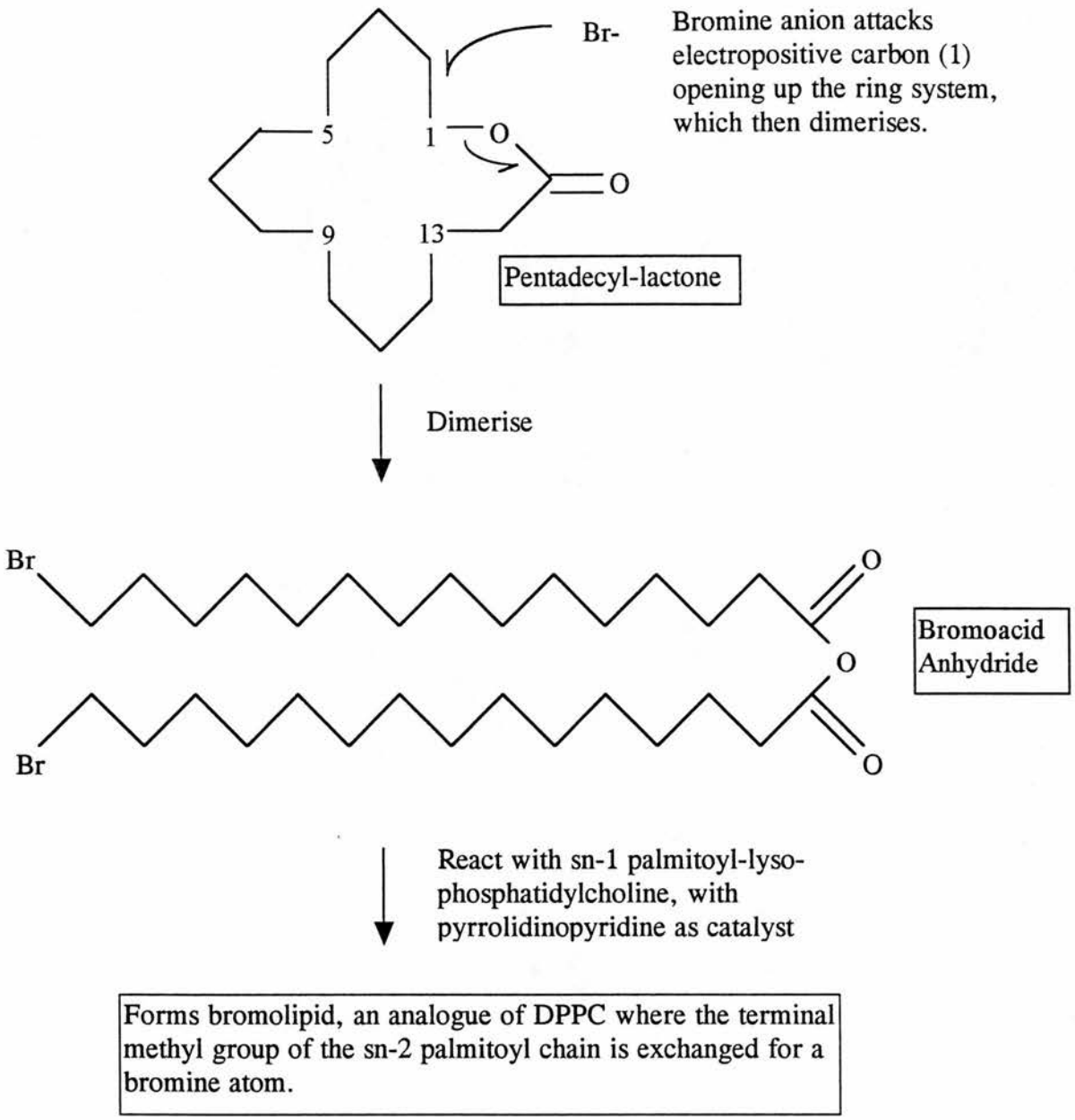

Figure 3.5 The synthesis of the novel bromolipid, a structural analogue of DPPC. A bromoacid is formed by the opening of a lactone ring. A bromolipid is then formed by reacting the bromoacid anhydride with a lyso-phosphatidylcholine.

phosphorus pentoxide overnight and all glassware and syringes to be used were washed with acetone and oven dried. The synthesised bromoacid (2.2g) was dissolved in chloroform, as was 0.7g of DCCI (N,N'-Dicyclocarbohexylcarbodiimide). The bromoacid and DCCI solutions were then mixed together in a sealed flask and stirred overnight at room temperature. Excess DCCI and solvents were filtered off and the remaining crystals recrystallised twice from acetone to give 1.4g of crystals.

c) Coupling of the symmetric bromoacid anhydride and lysophosphatidylcholine to form the bromolipid.

The symmetric bromoacid anhydride was coupled to lysophosphatidylcholine to form the bromolipid, using the method of Mason *et al.*, (1981). As in the previous stage of the synthesis all equipment and reagents were ensured to be water free. Lysophosphatidylcholine was dried, in a vacuum over phosphorus pentoxide, then suspended in dried chloroform. The symmetrical anhydride was similarly treated, before being injected into the lysophosphatidylcholine suspension. Finally, 4-pyrrolidinopyridine (75mg in 1ml of chloroform) was injected into the suspension, to act as a catalyst. The suspension was then stirred for 4 hours at a constant temperature of 35°C. Towards the end of the 4 hours, all the precipitate dissolved to give a clear yellow solution of bromolipid.

To the clear yellow bromolipid solution was added chloroform (12ml). The solution was then poured into a separating funnel, to which was then added methanol (6ml), water (4.5ml), and concentrated hydrochloric acid (4.5ml). The funnel was then shaken and the upper organic layer extracted, with more chloroform. The extract was then rotary-evaporated at room temperature to dryness, producing a white, semi-solid residue (bromolipid).

The bromolipid was then purified using an open column chromatography method. The bromolipid was applied to the top of a silica gel column, and washed with a chloroform/methanol/ammonium hydroxide (200/15/1) mixture. This mixture ratio was then gradually changed to a 65/15/1 mixture, to wash the bromolipid. Finally, switching the wash mixture to 65/35/5 eluted the purified

bromolipid. The bromolipid was again rotary-evaporated to dryness, before being stored as a 20mg/ml solution in chloroform, at -70°C.

3.8 Thin-layer chromatography (TLC) of the bromolipid.

Thin-layer chromatography of lipids employs two different immiscible phases, making use of the fact that solutes in the liquid organic phase will have differing affinities for the hydrophilic solid phase. Thus, as the liquid phase runs through the solid gel, different lipids will be retained to different extents by the gel, and will spread out at different distances behind the solvent front. The mobile phase can be made either more or less hydrophilic (e.g. by variation of the quantity of polar solvents, such as methanol in chloroform, or by the addition of water), altering the partition coefficient of solutes between the two phases. For phospholipids, the most commonly used stationary phase is silica gel, which is moderately hygroscopic, and consists of granules which under normal conditions are surface coated with a layer of tightly-bound water. The mobile phase is usually a mixture of solvents including chloroform (New, 1990).

At the end of the chromatography run, lipids are visualised by either specific stains, which are sprayed on to the plate, or by non-specific stains, using methods such as charring, or iodine uptake. TLC can give information about the purity of a lipid sample, as a compound that is pure should run to a single spot. Phospholipids which have undergone degradation can be observed as a long smear with a tail trailing to the origin.

3.8.1 Materials and methods for the TLC experiments.

Silica gel TLC plates, a molybdenum blue spray reagent and DPPC were bought from the Sigma Chemical Company Ltd, Fancy Road, Poole, UK. Solid DPPC was dissolved in chloroform to a form 20mg/ml solution, to be spotted onto a TLC plate. The bromolipid was stored as a 20mg/ml solution in chloroform after its synthesis, and so needed no further preparation. A TLC solvent mixture of

freshly made chloroform:methanol:water:ammonium hydroxide (65:35:2.5:2.5 v/v) was used in the TLC experiments. Chloroform (65ml) was mixed thoroughly with methanol (35ml), ammonium hydroxide (2.5ml) and distilled water (2.5ml), in a glass cylinder before use.

A TLC chromatography tank was lined with a Whatman No. 1 filter paper sheet and filled with the solvent mixture. The tank was then sealed and left to equilibrate for two hours. DPPC and bromolipid, 5μl, 8μl and 10μl of each 20mg/ml sample, were spotted 2.5cm from the lower edge of a TLC plate and allowed to dry. The TLC plate was then placed into the tank and covered. The solvent was allowed to ascend to within 3-4cm of the top of the plate, before the plate was removed from the tank. The solvent front was then marked with a pencil and the plate air-dried in a fume cupboard.

Two lipid visualisation methods were used.

1) The molybdenum blue reagent spray stains phosphate containing compounds. The TLC plate was sprayed evenly with molybdenum blue spray, using a back and forth motion across the entire plate. Care was taken to avoid saturating the plate. The plate was then air dried in a fume cupboard for 10 minutes, before the results were recorded.
2) The uptake of iodine is a method which stains for general lipids. Approximately 10g of solid iodine crystals were sprinkled on the bottom of a glass tank. The dry TLC plate was then left in the closed tank for 1 hour, to allow the uptake of iodine, before the results were recorded.

3.8.2 Results of TLC

TLC chromatograms of the bromolipid and DPPC have been obtained. The aim of the chromatography experiments were to:

1) check that a pure phospholipid species (the bromolipid) has been synthesised and purified;
2) show that neither the bromolipid nor the DPPC were contaminated with impurities or breakdown products;

3) test that the bromolipid and DPPC have similar hydrophilic/hydrophobic affinities, as measured by their R_f values for the chromatography system used.

Plates 3.3 and 3.4 show the chromatograms recorded by staining the TLC plates with molybdenum blue and iodine respectively. The R_f values for each lipid have been measured directly from the TLC plates (Table 3.3).

Table 3.3 The R_f values, measured from TLC plates stained with either molybdenum blue or iodine, for bromolipid and DPPC samples.

	Bromolipid	DPPC
R_f value measured from molybdenum blue stained plate	0.38 ±0.01	0.37 ±0.01
R_f value measured from iodine stained plate	0.40 ±0.01	0.38 ±0.03

Both bromolipid and DPPC produced single spots on the TLC plates (Plates 3.3 and 3.4). Staining the plates using either molybdenum blue or iodine located the phospholipids in the same positions. The lipid groups (iodine) and the phospholipid phosphate groups (molybdenum blue) are therefore located at the same position on the plates. Both of the phospholipids therefore appear to be single, pure species that have not degraded. Unknown phospholipids (such as the bromolipid) are often run against standards. As the bromolipid appears to perform identically to DPPC in the TLC experiments, it has not been necessary to run any other standards on the plates.

3.9 Mass spectroscopy.

In the classical mass spectrometer, molecules are bombarded with a beam of energetic electrons. The molecules are ionised and broken up into many fragments, some of which are positive ions (Chapman, 1993). Each kind of ion has a particular ratio of mass to charge, or m/e value. For most ions, the charge is 1, so that m/e is

simply the mass of the ion. The mass spectrum obtained from a compound is highly characteristic of that compound. The mass spectrum can help to establish the structure of a compound by either giving a molecular weight for the compound or by indicating the presence of a molecule made up of certain structural units.

There are additional methods, to an electron beam, of ionising the molecules under study (Rose and Johnstone, 1982). A beam of ions such as Xe^+ (xenon) can be produced by ionising xenon atoms and accelerating the resulting ions through an electric field. The resulting (fast) ions are directed through a xenon gas chamber where charge exchange occurs to give fast atoms,

$$Xe^+ \text{ (fast)} + Xe \text{ (thermal)} \rightarrow Xe \text{ (fast)} + Xe^+\text{(thermal)}$$

Excess of fast Xe ions can be deflected leaving a beam of fast atoms.

When such beams of fast atoms impinge onto (bombard) a metal plate coated with a sample of the substance being investigated, the large amounts of kinetic energy in the atoms is dissipated in various ways, some of which lead to volatilisation and ionisation of the sample. By maintaining a suitable electric gradient from the plate, either positive or negative ions can be directed into the analyser of the mass spectrometer. This technique is known as fast atom bombardment (FAB). Usually best results are obtained by coating the plate with a relatively involatile polar liquid such as glycerol and mixing the substance under investigation into the glycerol. Due to the nature of FAB, the technique is especially useful for studying thermally unstable compounds.

3.9.1 Mass (FAB) spectra of the bromolipid.

An MAT90 mass spectrometer machine, using the (Xe) FAB method, was used to collect a mass spectrum of the bromolipid (Figure 3.6). Glycerol was used to coat the metal sample plate. The sample was bombarded with atoms of energy 8.0kEv using a gun current of 2.0ma. Positive ions, produced by the bombardment method, were directed into the mass spectrometer analyser.

The bromolipid mass spectrum has a base peak at 184.1 m/e, whose intensity was set to 100 for reference. Two other major peaks were also recorded,

at 798.7 and 86.1 m/e (Table 3.4). The presence of the peak at 798.7 confirms that the anticipated bromolipid (Figure 3.6) has been synthesised. The base peak, at 184.1 m/e, confirms that the bromolipid has a phosphatidylcholine headgroup, with the peak at 86.1 m/e (choline) further supporting this conclusion. The mass spectroscopy results, therefore, are consistent with the conclusion that the bromolipid (1-palmitoyl, 2-n-pentadeca-15-bromo-*sn*-glycero-3-phosphocholine) has been synthesised. I would like to acknowledge the help that was received from Mr T. Beer and Shell Research, Sittingbourne, Kent in collecting the Mass spectrum of the bromolipid.

Table 3.4 Mass (FAB) spectrum results for the bromolipid.

M/e peak position	molecular assignment
86.1	$CH_2{=}CH.N(CH_3)_3+$
184.1	$O.OH.P{=}O.O.(CH_2)_2.\ N(CH_3)_3+$
798.7	Positive ion bromolipid

3.10 Nuclear magnetic resonance (NMR) of phospholipids.

Nuclear magnetic resonance (NMR) can be used to elucidate the atomic structure of molecules and can also provide conformational information about the structure. The NMR technique is therefore very useful for testing the structure of newly synthesised molecules. NMR occurs as a result of the interaction of a static magnetic field with a nucleus possessing a magnetic moment. Only particles with both an electric charge and a spin angular momentum, such as the proton (^1H), and isotopes of carbon and phosphorus (^{13}C and ^{31}P), have a magnetic moment.

For example, if a proton is placed in an external magnetic field, its magnetic moment can be aligned either with or against the external field. Alignment with the field is the more stable, and energy must be absorbed to 'flip' the tiny proton magnet over to the less stable alignment, against the field. It is the measurement of this absorption of energy as the nuclei flips between states that is the basis of the NMR experiment. The frequency at which a proton absorbs energy depends on the

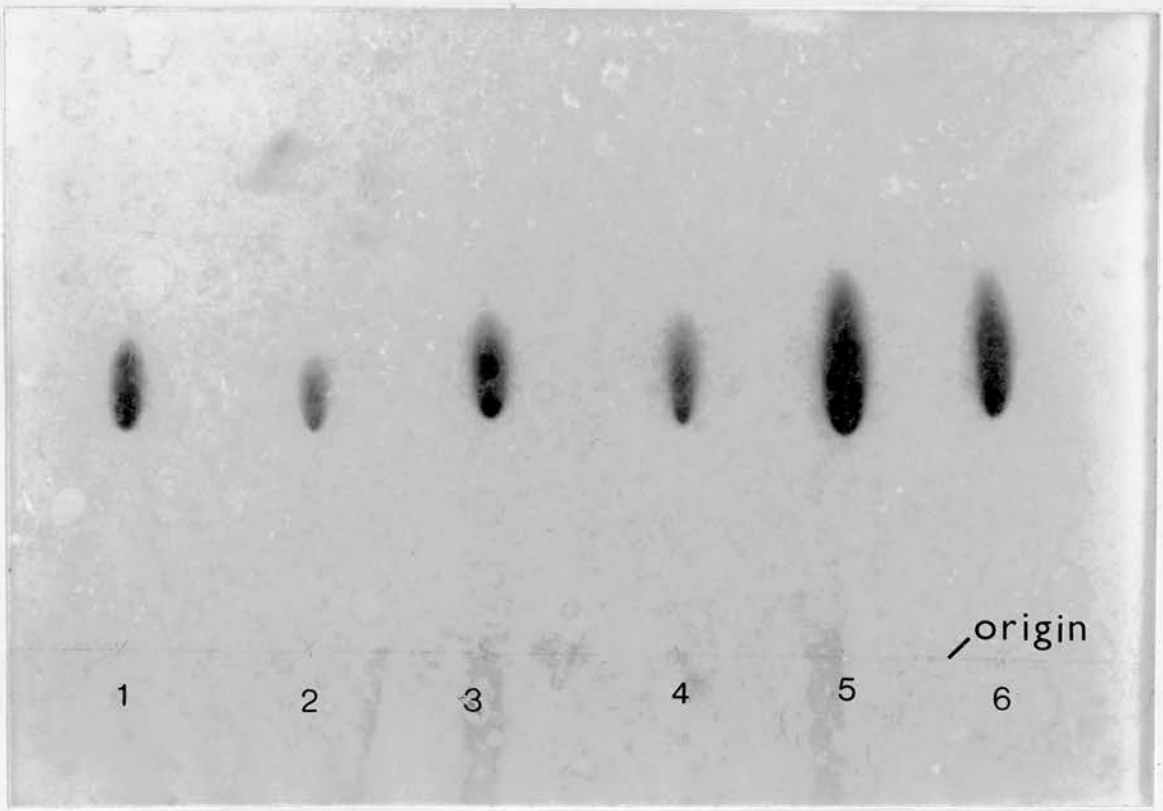

Plate 3.3 Analysis of DPPC and the bromolipid by TLC, using a molybdenum blue stain. A TLC chromatography tank was lined with a Whatman No.1 filter paper sheet and filled with freshly prepared chloroform:methanol:water:ammonium hydroxide (65:35:2.5:2.5 v/v). The TLC plate was spotted with three different quantities of DPPC and bromolipid. Lanes 1, 3 and 5 were loaded with 5μl, 8μl and 10μl, respectively, of 20mg/ml bromolipid in chloroform and lanes 2, 4 and 6 were loaded with 5μl, 8μl and 10μl, respectively, of 20mg/ml DPPC in chloroform. The molybdenum blue reagent spray was used to visualise any phosphate containing compounds that might be present on the plate. The bromolipid and DPPC samples produced single spots on the TLC plate, suggesting a single species to be present in each sample. The two phospholipids also had a similar R_f value, suggesting that a bromolipid, similar to DPPC has indeed been synthesised.

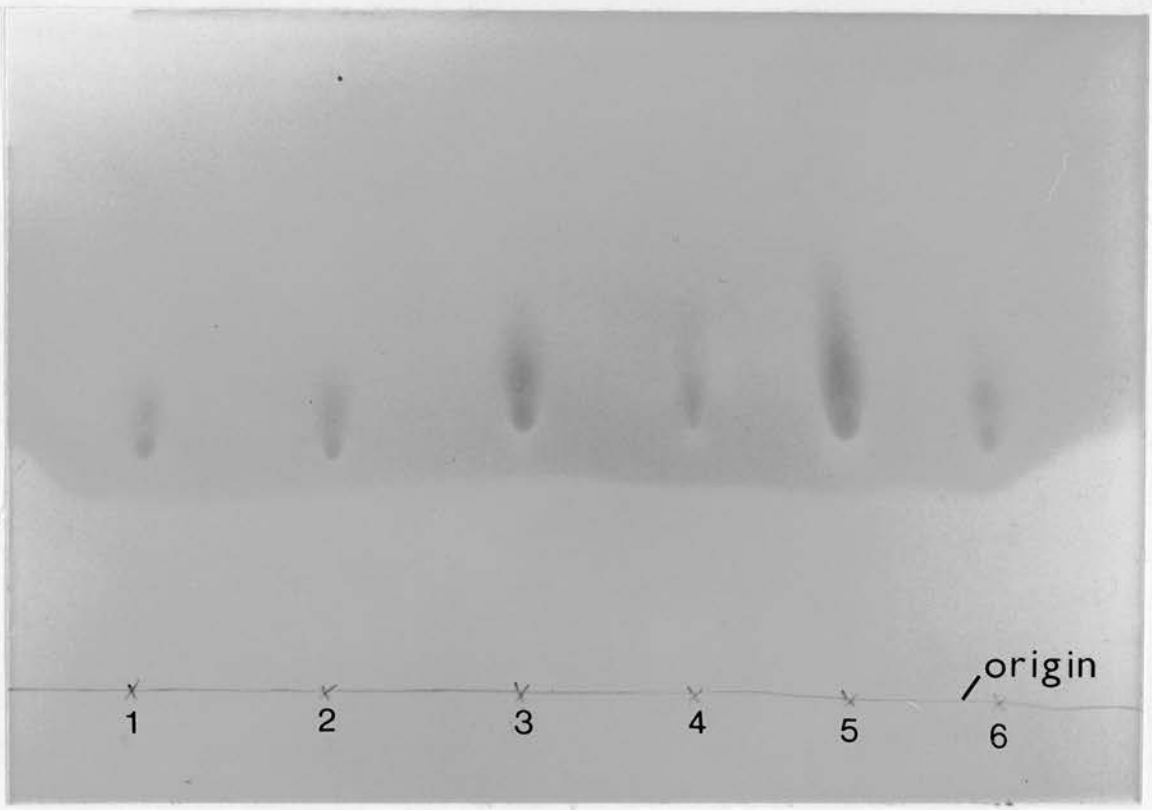

Plate 3.4 Analysis of DPPC and the bromolipid by TLC, using the iodine method of staining. A TLC chromatography tank was lined with a Whatman No.1 filter paper sheet and filled with freshly prepared chloroform:methanol:water:ammonium hydroxide (65:35:2.5:2.5 v/v). The TLC plate was spotted with three different quantities of bromolipid and DPPC. Lanes 1, 3 and 5 were loaded with 5μl, 8μl and 10μl, respectively, of 20mg/ml bromolipid in chloroform and lanes 2, 4 and 6 were loaded with 5μl, 8μl and 10μl, respectively, of 20mg/ml DPPC in chloroform. The iodine uptake method was used to visualise any lipids in general that might be present on the plate. The bromolipid and DPPC samples produced single spots on the TLC plate, suggesting a single species to be present in each sample. The two phospholipids also had a similar R_f value, suggesting that a bromolipid, similar to DPPC has indeed been synthesised.

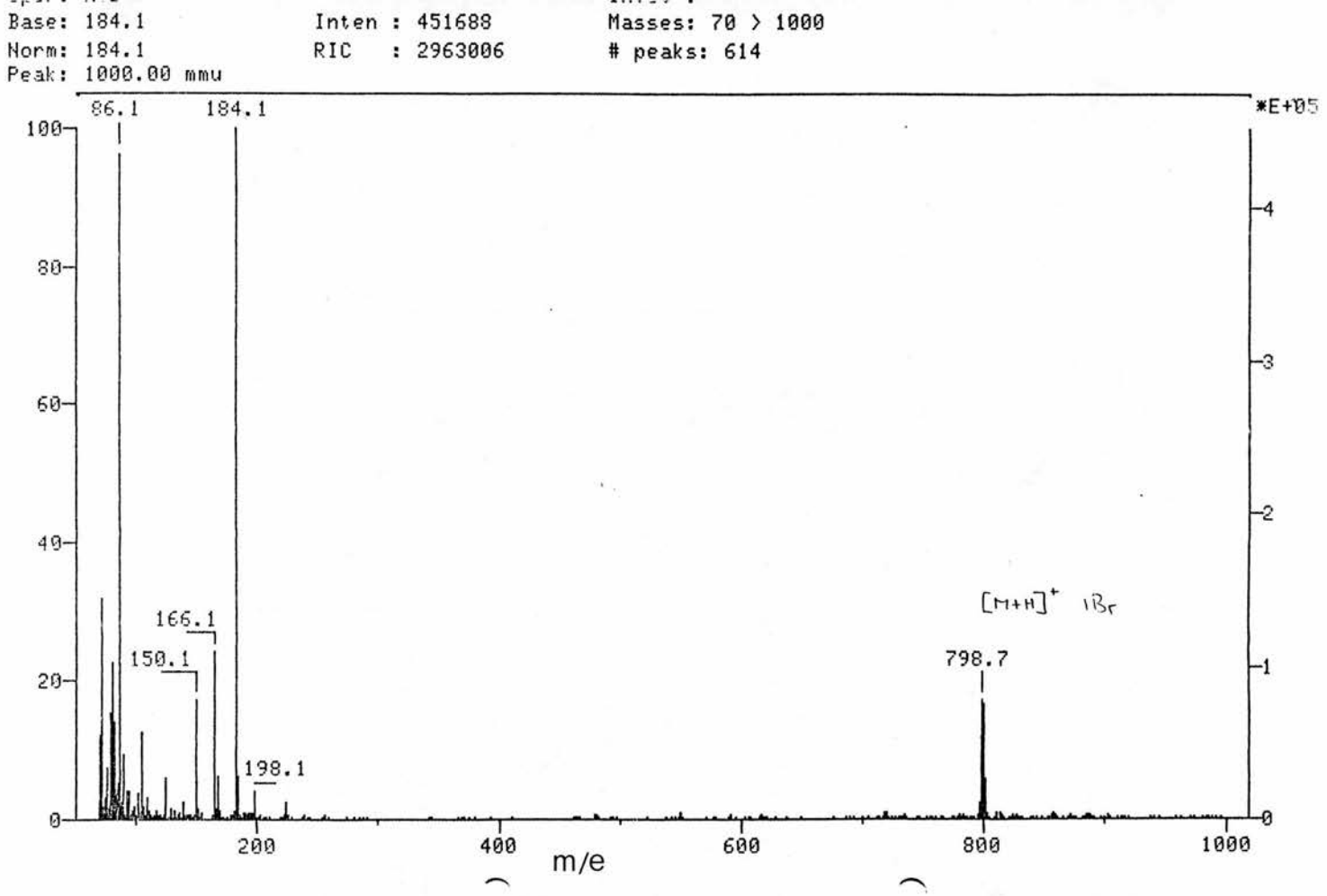

Figure 3.6 Mass (FAB) spectra of the bromolipid. Mass spectra were collected on a MAT90 mass spectrometer using the (Xe) fast atom bombardment (FAB) method. Glycerol was used to coat the metal sample plate. The sample was bombarded with atoms of energy 8.0kEv using a gun current of 2.0ma. After bombardment, the sample positive ions were directed into the mass spectrometer analyser. The spectra synthesised molecule has a relative molecular mass of 798.7, that fragments into molecules of mass 184.1 and 86.1.

magnetic field local to the proton, which is dependent not only on the experimentally applied external field but also the local environment of the proton. Each proton, or set of equivalent protons, in a structure has a slightly different electronic environment from every other set of protons, absorbing energy at a slightly different frequency.

The result of a proton NMR experiment is a spectrum showing many absorption peaks, whose relative position reflect the differences in the electronic environment of each of the protons. Differences between protons are measured as chemical shifts, expressed in parts per million (ppm) of the total applied field. The most commonly used scale is the δ (delta) scale, whose origin is marked by the tetramethylsilane ($(CH_3)_4Si$) NMR peak. Chemical shifts previously assigned to components of dilauroyl-lecithin (Table 3.5, from Hauser *et al.*, 1975) indicate the relationship between the electron environment and chemical shift. Electronegative groups neighbouring a proton, for example, increase the chemical shift of that proton. The area under each NMR signal indicates, relative to other peaks, the number of equivalent protons giving rise to that peak. Areas under NMR signals are measured by an electronic integrator, and are usually given on the spectrum chart in the form of a stepped curve, whose heights are proportional to the peak areas.

NMR spectra are typically complicated by a process known as spin-spin coupling, that splits the observed spectrum peaks into multiple peaks (multiplet). Splitting reflects the environment of the absorbing protons, with respect to other nearby protons. The distance between the peaks in a multiplet is a measure of the effectiveness of the spin-spin coupling, and is called the coupling constant (J). Spin-spin coupling is only observed between non-equivalent neighbouring protons. A secondary proton with a neighbouring tertiary proton at a particular instant will have its chemical shift slightly increased or decreased, depending on the orientation of the neighbouring proton's magnetic moment. On average, half of the molecules protons will be shifted upfield and half downfield, splitting the spectrum peak in two, forming a doublet. Similarly a proton with two neighbouring tertiary protons can have its NMR peak split into a triplet and in general, a set of n equivalent protons will split an NMR signal into $n+1$ peaks. Many atomic structures can split

the NMR signal into even more complex signals, such as pentets and double doublets.

Table 3.5 Chemical shifts of selected components of dilauroyl lecithin in $CDCl_3$ (from Hauser *et al.*, 1975).

Dilauroyl lecithin component assigned to signal	Chemical shift (ppm)
$(CH_3).(CH_2)_n$	0.9
$CH_3.(CH_2)_n$	1.25
$O.CO.CH_2.CH_2$	1.6
$O.CO.CH_2.CH_2$	2.3
$N^+.(CH_3)_3$	3.4
$P.O.CH_2.CH_2.N^+.(CH_3)_3$	3.8
$CH.CH_2.O.P$	3.9
$CH_2.O.CO.R$	4.1
$P.O.CH_2.CH_2.N^+.(CH_3)_3$	4.3
$CH.O.CO.R$	5.2

3.10.1 NMR of DPPC and bromolipid.

Samples were prepared by dissolving approximately 10mg of phospholipid in deuterated chloroform ($CDCl_3$). NMR (^1H) spectra of the bromolipid and DPPC in $CDCl_3$ were taken on a General Electrics QE-300 machine and then analysed (Tables 3.6 and 3.7). The spectral peak chemical shifts and proton assignments compare well with those previously assigned to phospholipids (Table 3.5, from Hauser *et al.*, 1975). DPPC and bromolipid share many of the ^1H NMR spectrum features, due to protons remote from, and therefore unaffected by, the *sn*-2 chain bromine atom. The DPPC and bromolipid headgroup, glycerol backbone, *sn*-1 chain and the *sn*-2 chain methylene groups from C(2) to C(12), protons all give rise to similar peaks in the ^1H NMR spectrum. Compared with DPPC, bromolipid lacks a proton signal from the *sn*-2 terminal methyl group (3 rather than 6 protons make up the peak at 0.85 ppm, as it has been exchanged for the bromine atom. The electronegativity of the bromine atom also alters the NMR peaks of protons attached to the *sn*-2, C(13) to C(15), palmitoyl carbons. The closer the protons are to the bromine atom, the greater are they chemically shifted by the increased electron

negative environment created by the bromine atom. At the extreme, the methylene protons on the carbon adjacent to the bromine atom, are shifted from 1.2 ppm (DPPC methylenes) to 3.4 ppm. The analysis of the ^1H NMR spectrum indicates that the bromolipid, whose structure is described in Figure 3.5, has indeed been synthesised. I would like to acknowledge the help of Dr R. Alecio and Shell Research that was received in obtaining the DPPC and bromolipid NMR spectra.

Table 3.6 ^1H NMR chemical shifts of DPPC in $CDCl_3$

Chemical Shift	Peak shape	Number of protons	Proton position in molecule
0.85	Triplet	6	$(C\underline{H}_3).(CH_2)_{12}.(CH_2)_2$
1.2	Broad singlet	48	$CH_3.(C\underline{H}_2)_{12}.(CH_2)_2$
1.55	Multiplet	4	$O.CO.CH_2.C\underline{H}_2$
2.25	Multiplet	4	$O.CO.C\underline{H}_2.CH_2$
3.3	Broad singlet	9	$N^+.(C\underline{H}_3)_3$
3.7	Broad singlet	2	$P.O.CH_2.C\underline{H}_2.N^+.(CH_3)_3$
3.9	Multiplet	2	$CH.C\underline{H}_2.O.P$
4.1	Double doublet (J= 7.5, 12.5)	1	$C\underline{H}_2.O.CO.R$
4.25	Broad singlet	2	$P.O.C\underline{H}_2.CH_2.N^+.(CH_3)_3$
4.35	Double doublet (J= 2.5, 12.5)	1	$C\underline{H}_2.O.CO.R$
5.2	Multiplet	1	$C\underline{H}.O.CO.R$
7.25	Singlet		Chloroform contaminant

Table 3.7 ^{1}H NMR chemical shifts of bromolipid in $CDCl_3$

Chemical Shift	Peak shape	Number of protons	Proton position in molecule
0.85	Triplet	3	$CH_3.(CH_2)_{12}$
1.25	Broad singlet	42	$CH_3.(CH_2)_{12}.(CH_2)_2$, $Br.(CH_2)_3.(CH_2)_9.(CH_2)_2$
1.4	Multiplet	2	$CH_2.CH_2.CH_2.Br$
1.55	Multiplet	4	$O.CO.CH_2.CH_2$
1.85	Pentet	2	$CH_2.CH_2.CH_2.Br$
2.25	Multiplet	4	$O.CO.CH_2.CH_2$
3.3	Broad singlet	9	$N^+.(CH_3)_3.$
3.4	Triplet	2	$CH_2.CH_2.(CH_2)$ .Br
3.75	Broad singlet	2	$P.O.CH_2.CH_2.N^+.(CH_3)_3$
3.9	Multiplet	2	$CH.CH_2.O.P$
4.1	Double doublet (J= 7.5, 12.5)	1	$CH.CH_2.O.CO.R$
4.25	Broad singlet	2	$P.O.CH_2.CH_2.N^+.(CH_3)_3$
4.35	Double doublet (J= 2.5, 12.5)	1	$CH.CH_2.O.CO.R$
5.2	Multiplet	1	$CH.O.CO.R$
7.25	Singlet		Chloroform contaminant

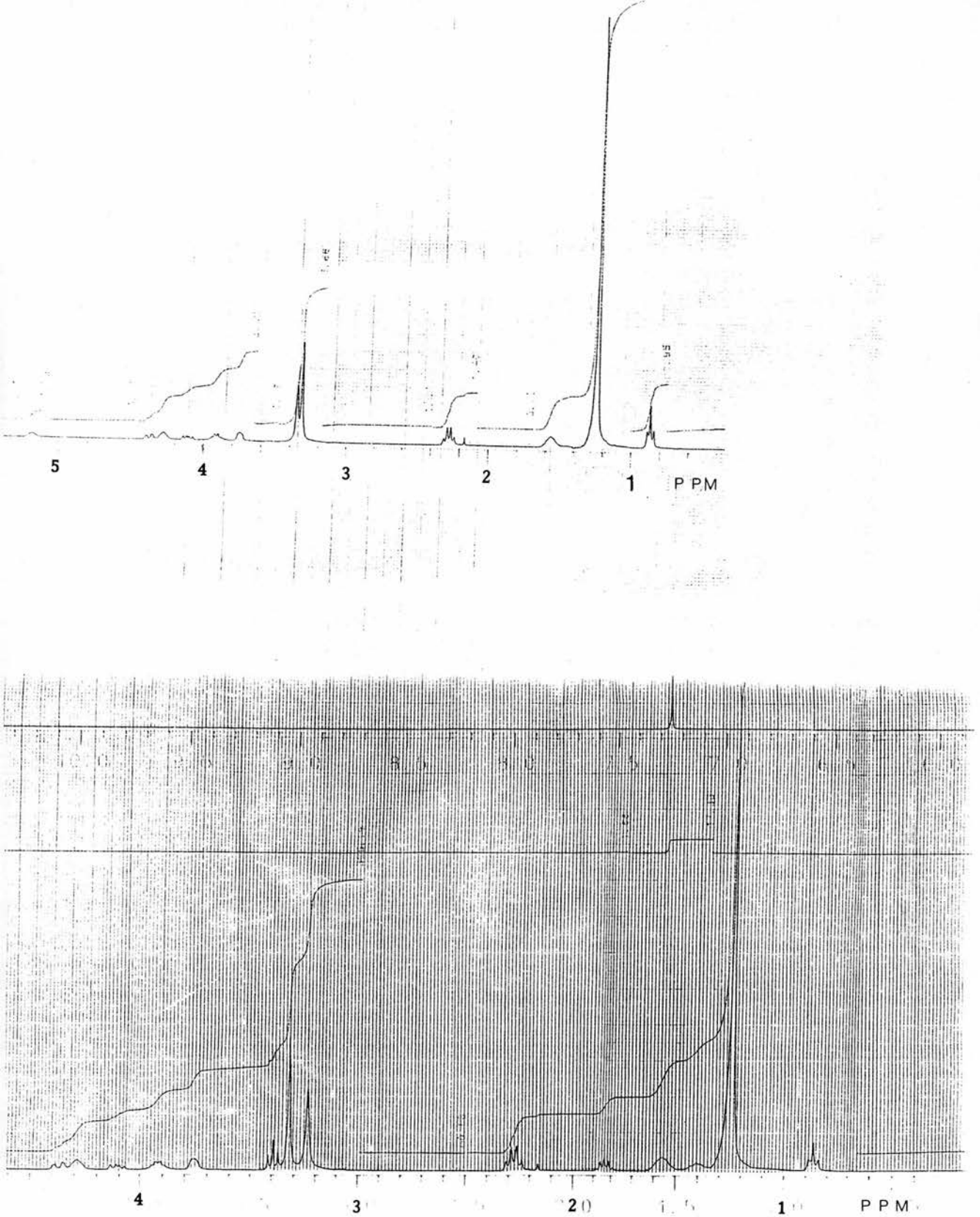

Figure 3.7 Proton ^{1}H NMR spectra of DPPC (top) and bromolipid (bottom). Differences between the two are due to the electro-negativity effect the bromine atom has on nearby methylene protons. Samples were prepared by dissolving approximately 10mg of phospholipid in deuterated chloroform ($CDCl_3$). NMR (^{1}H) spectra of the bromolipid and DPPC in $CDCl_3$ were then taken on a General Electrics QE-300 machine.

Chapter 4.

A study of fluid phase DOPC and DOPC plus amantadine (FB and HCl) bilayers by X-ray diffraction and the swelling series method.

4.1 Aim of studying the interaction of amantadine with DOPC bilayers.

Amantadine is a small drug molecule used in the treatment of influenza and Parkinson's disease (Oxford and Galbraith, 1980; Obeso and Martinez-Lage, 1987; Gilman *et al.*, 1990). The aim of this work was to study the interaction of two different charge states of amantadine with DOPC bilayers by X-ray diffraction, using the swelling series phase assignment method. There were several reasons behind the study of the DOPC-amantadine system:

1) To model studies of the small amphipathic molecule with fluid bilayers.
2) To study the effect of molecular charge on the lipid-drug interaction.
3) To evaluate the swelling series phasing method.

4.2 Background of amantadine.

A major component in the prevention and control of influenza is the use of killed influenza vaccines, which may give protection from infection for over a year (Ruben, 1987). Killed vaccines work by inducing serum antibodies against the heamagglutinin and neuraminidase of the vaccine strains, with sufficient antibodies ensuring protection against infection. Although no substitute for vaccination, an alternative to vaccination is the use of amantadine, which is effective in the prophylaxis and treatment of all strains of influenza A (Nicholson, and Wiselka, 1991). Prophylactic amantadine can be particularly helpful in high risk groups, including those with cardiovascular and pulmonary diseases and those in chronic care settings (Fedson, 1987). Amantadine does, however, have several known side effects, including nausea and vomiting, loss of appetite and central nervous system effects such as nervousness and insomnia (Monto, 1983).

Amantadine (1-aminoadamantane hydrochloride and 1-aminoadamantane freebase), a small molecule comprised of a tri-cyclohexane ring structure polarised by an amine group, can be purchased commercially in both the freebase (FB) and hydrochloride (HCl) salt forms. The molecular structure of the two forms of amantadine are depicted in Figure 3.4. The amphipathic amantadine molecule has a

hydrophilic amine group and a lipophilic main body. NMR studies have shown that amantadine perturbs the organisation and motional properties of phospholipid bilayers (Cheetham and Epand, 1987), presumably by the insertion of the lipophilic body of amantadine into the bilayer. The therapeutic effect of amantadine is thought to involve the hydrophobic, lipophilic properties of the molecule (Phonphok *et al.*, 1991) and has been suggested to involve interruption of viral-host cell membrane fusion or interference with haemagglutinin maturation (Hay, 1989; Sugrue *et al.*, 1990). More recently, amantadine has been linked to the influenza virus M2 protein (Sugrue and Hay, 1991; Duff and Ashley, 1992).

4.2.1 The influenza A virus M2 protein.

The viral M2 transmembrane protein is a disulphide-bonded homotetramer that forms a proton channel (Sugrue and Hay, 1991). The M2 protein is expressed on the cell surface during viral synthesis (Lamb *et al.*, 1985) and has been identified in viral particles (Zebedee and Lamb, 1988). The protein has been suggested to be important at two separate phases in the viral replication cycle (Belshe and Hay, 1989). Immediately after viral endocytosis, and concomitant with pH-induced fusion between the endosomal and viral membranes (Skehel *et al.*, 1982), mediated by haemagglutinin (HA), M2 is thought to conduct protons into the interior of the virus leading to uncoating, acid-induced release of ribonucleoprotein from the matrix protein (M1), and eventual nuclear infection (Martin and Helenius, 1991). When HA is transported to the cell surface in post-Golgi vesicles (Sugrue *et al.*, 1990), M2 may also facilitate influenza synthesis and assembly by countering any vesicular acidification. Amantadine is thought to inhibit these processes by impeding proton flow during these events (Hay, 1989).

4.2.2 Interaction of amantadine with M2.

A wealth of evidence now supports the theory that amantadine interacts directly with the viral transmembrane protein M2. It has recently been reported that

the efficacy of amantadine is not due to any possible effects on the secondary structure of the transmembrane domain (Duff and Ashley, 1992). In addition, synthetic peptides representing this domain have been shown to possess an amantadine-sensitive, proton channel function when incorporated into planar lipid bilayers, suggesting that amantadine may operate via physical blockade.

A molecular modelling study has been published, in which an energy minimum location for amantadine within the M2 transmembrane domain is specified (Sansom and Kerr, 1993). The modelling work identified the energy minimum as being in the vicinity of the M2 serine 31 oxygen atoms, when energy interactions were evaluated as amantadine was moved along the length of the channel made of a tetrameric association of M2. This minimum was shown to be derived from a favourable electrostatic interaction between the cationic amine group and the ring of serine 31 oxygen atoms. In addition, van der Waals contacts were observed between the valine 27 side-chains of M2 and the amantadine cyclic ring structure. Overall the ring structure of amantadine fitted into a hydrophobic pocket formed by the valine 27 side-chains of M2, as the protonated amine group formed favourable electrostatic interactions with the serine 31 oxygens. It was concluded that the combination of a steric cut-off at isoleucine 42, and the favourable interaction at valine 27/serine 31, provided a molecular explanation for block of M2 channels by amantadine. Neutron diffraction work (Duff, 1993) shows that deuterium labelled amantadine can indeed be located in an M2 transmembrane segment as predicted by the modelling work.

4.2.3 Effect of charge on the interaction of small molecules with lipid bilayers.

An objective of this work was to study the effect that molecular charge, on the amine group of amantadine, has on the DOPC-drug interaction. The local anaesthetic tetracaine interacts with phospholipids in a manner influenced by the charge state of the drug's tertiary amine group (Smith *et al.*, 1991; Shinooka *et al.*, 1992). NMR has shown that drugs which contain an amino group have the ability to interact strongly with the lipid phosphate group (Datta *et al.*, 1992).

The passive permeability of lipid bilayers is considerably greater for anions than for cations (Franklin and Cafiso, 1993; Leiberman and Topaly, 1969; Leblanc, 1969, 1970; Flewelling and Hubbell, 1986). The bilayer translocation rate and partition coefficient are both several orders of magnitude greater for the anion tetraphenylboron (TPB^-) than they are for the structurally similar tetraphenyl-phosphonium (TPP^+) cation (LeBlanc, 1969, 1970; Anderson and Fuchs, 1975). It has been proposed that the observed differential permeability to anions and cations can be explained by an electrostatic potential in the interior of the bilayer which is positive relative to the aqueous medium (Leiberman and Topaly, 1969; Leblanc, 1970; Haydon and Hladky, 1972; Hladky and Haydon, 1983; McLaughlin, 1977; Flewelling and Hubbell, 1986; Honig *et al.,* 1986).

The internal potential of fully hydrated phosphatidylcholine vesicles and planar bilayers has been measured to be 240mV (Flewelling and Hubbell, 1986). This internal potential is a dipole potential since it is found in phosphatidylcholine where the head group has no net charge. There are three possible sources for this internal dipole: oriented water molecules; the lipid polar head group; or the glycerol acyl esters (McLaughlin, 1977; Zheng and Vanderkooi, 1992). If the internal potential of a bilayer is indeed positive, cations will tend to be excluded from the hydrophobic region, compared with anions or neutral species, thereby causing a relative decrease in both the membrane/water partition coefficient and bilayer translocation rate for cations. Zheng and Vanderkooi (1992) calculated that increasing the water content of a bilayer will make the membrane potential more positive, thus further excluding cations. This effect of hydration has also recently been shown to be important by others (Gawrisch *et al.,* 1992).

4.3 X-ray diffraction study of DOPC bilayers containing amantadine (FB or HCl).

The interaction of amantadine (both FB and HCl forms) with DOPC bilayers has been studied by X-ray diffraction and the swelling series method (described in Chapters 2 and 3). Swelling series data were compiled for three different systems:

1) Pure DOPC bilayers at 20°C and 98%, 90%, 81%, 74% or 57% RH.

2) DOPC plus 5% (mol) amantadine freebase (FB) bilayers at 20°C and 98%, 90%, 81%, 74% or 57% RH.
3) DOPC plus 5% (mol) amantadine hydrochloride (HCl) bilayers at 20°C and 98%, 90%, 81%, 74% or 57% RH.

Diffraction patterns were collected from oriented samples of each system, using the sample preparation and diffraction methods described in Chapter 3.

4.3.1 Phasing of diffraction patterns using the swelling series method.

X-ray diffraction patterns were collected from oriented multilayer samples on X-ray sensitive films. Plate 4.1 shows typical meridional diffraction patterns collected from these fluid (L_α) phase bilayers. Meridional diffraction data were collected out to seven orders from pure DOPC bilayers, to eight orders from bilayers of DOPC+amantadine FB, and to six orders from bilayers of DOPC+amantadine HCl (Tables 4.1, 4.2 and 4.3). The bilayer thickness can be calculated, without phase information, using the meridional diffraction data and Bragg's law (equation 2.2). Plotting the calculated bilayer thickness (including the water layer) against the relative humidity shows that the bilayer thickness decreases with decreasing humidity for all three systems studied (Figure 4.1). The bilayer thickness also decreases by 1-2·5Å, on addition of amantadine (FB or HCl) to DOPC bilayers, at each relative humidity studied.

4.3.2 Phasing the diffraction data collected from pure DOPC bilayers.

The swelling series phase assignment method involves plotting each structure factor amplitude (Tables 4.1 to 4.3) against (h/D) (h is the diffraction order, D is the bilayer thickness), in order to reconstruct the form of a continuous Fourier transform. The 'phase-problem' is whether each structure factor

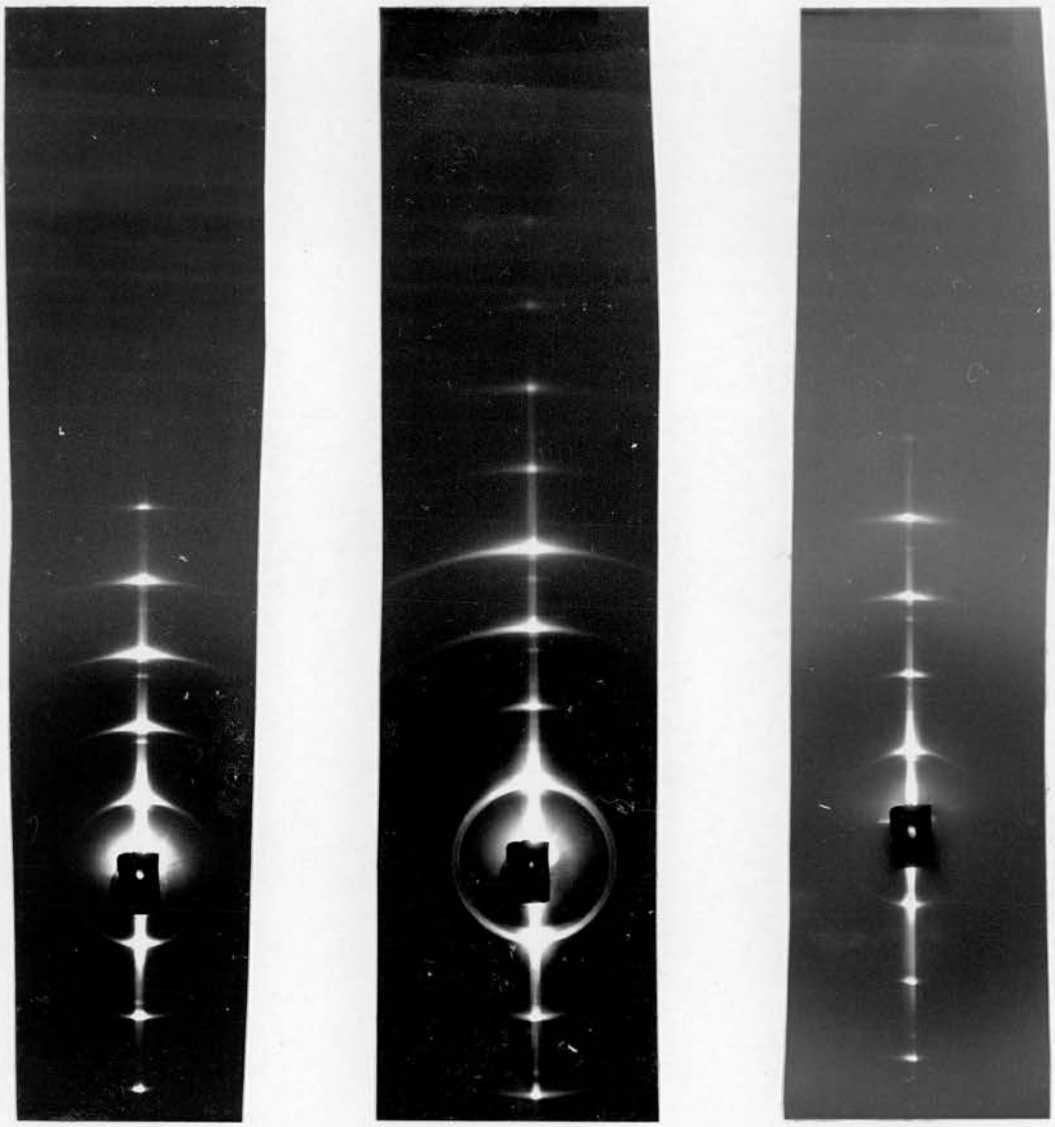

(a) (b) (c)

PLATE 4.1 Diffraction patterns collected from (a) DOPC bilayers at 98% RH, (b) DOPC+amantadine HCl bilayers at 81% RH and (c) DOPC+amantadine FB bilayers at 57% RH. Each diffraction pattern was collected from a membrane sample oriented on a glass slide, that was held in an environmental cell at 20°C.

Table 4.1 Diffraction data collected from DOPC bilayers at 20°C.

Diffraction order	Relative intensity of diffraction				
1	0.726	0.672	0.730	0.789	0.733
2	0.138	0.171	0.120	0.037	0.069
3	0.096	0.093	0.098	0.091	0.172
4	0.031	0.050	0.043	0.080	0.027
5	0.008	0.013	0.009	0.003	0.002
6	0.001	0.001	0	0	0
7	0.001	0.001	0	0	0
Relative humidity	98%	90%	81%	74%	57%
Bilayer thickness ± SD (Å)	54.0 ±0.2	53.6 ±0.2	53.2 ±0.2	52.3 ±0.2	52.1 ±0.2

Table 4.2 Diffraction data collected from DOPC+amantadine FB bilayers at 20°C.

Diffraction order	Relative intensity of diffraction				
1	0.849	0.849	0.791	0.779	0.782
2	0.056	0.057	0.072	0.039	0.025
3	0.058	0.059	0.084	0.076	0.066
4	0.037	0.036	0.052	0.080	0.092
5	0	0	0	0.011	0.017
6	0	0	0	0.011	0.012
7	0	0	0	0.004	0.004
8	0	0	0	0.001	0.003
Relative humidity	98%	90%	81%	74%	57%
Bilayer thickness ± SD (Å)	52.5±0.2	52.4±0.2	51.7±0.2	50.4±0.2	50.0±0.2

Table 4.3 Diffraction data collected from DOPC+amantadine HCl bilayers at 20°C.

Diffraction order	Relative intensity of diffraction				
1	0.739	0.745	0.881	0.876	0.690
2	0.128	0.131	0.019	0.037	0.137
3	0.095	0.100	0.039	0.055	0.151
4	0.038	0.024	0.057	0.030	0.002
5	0	0	0.002	0.001	0.001
6	0	0	0.002	0	0
Relative humidity	98%	90%	81%	74%	57%
Bilayer thickness ± SD (Å)	53.1±0.2	52.1±0.2	51.4±0.2	50.7±0.2	49.5±0.2

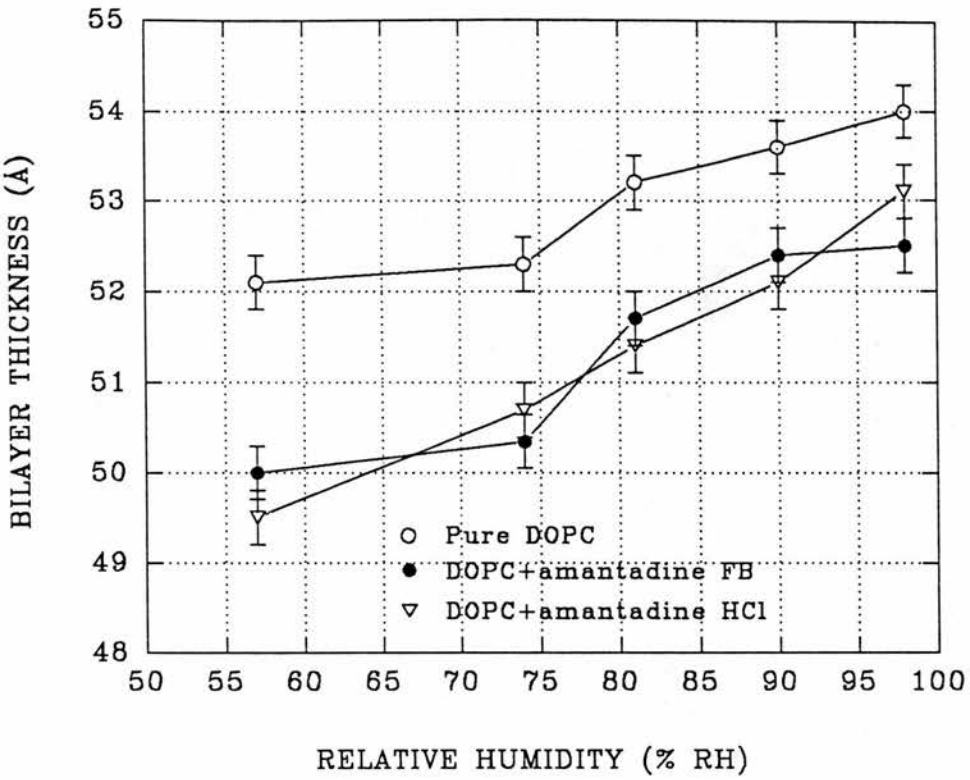

Figure 4.1 The effect of relative humidity on the DOPC, DOPC+amantadine FB and DOPC+amantadine HCl bilayer thickness. Diffraction data were collected from oriented bilayer samples at 20°C and either 98%, 90%, 81%, 74% or 57% RH. The bilayer thickness of each of three systems increases with relative humidity. The plots also show that adding amantadine (FB or HCl) to DOPC decreases the bilayer thickness by *ca* 2Å.

amplitude is a positive or a negative value, information which is lost during the diffraction process. Phase assignments that result in the construction of electron density maps which differ markedly from known bilayer structures can be discounted (Franks and Leib, 1981).

The phasing process for the first five orders of diffraction, collected from the pure DOPC bilayers at 20°C, is illustrated in Figure 4.2. Assuming that the first diffraction order phase is negative, the form of reconstructed continuous Fourier transforms [solid and dotted lines of Figure 4.2, (A)] suggest that the second order phase assignment is most likely to be negative, as the negative assignment continuous Fourier transform (solid line) passes smoothly through the second order data points. Assigning the third order phase [Figure 4.2 (B)] is less obvious from the swelling series plot, but has been phased positive by assessing the form of the continuous Fourier transform when higher orders were included in the analysis. Both the fourth and fifth order data fitted a smooth continuous Fourier transform when assigned a negative phase [Figure 4.2, (C) and (D)].

Whilst phases have been assigned out to five orders for the pure DOPC bilayer data, further swelling series and electron density map reconstruction work (Figures 4.3 and 4.4) do not differentiate between the four possible phase assignments for the higher order data (h=6, 7). Due to the outer structure factor amplitude values being small, all four possible outer order phase assignments plot as plausible continuous Fourier transforms. The electron density maps, using the seven order data set collected from DOPC bilayers 20°C and 98% RH, constructed using the four plausible phase assignments to the higher orders (Figure 4.4), all display characteristics of phospholipid bilayers (Danielli and Davson, 1934; Lesslauer *et al.*, 1972; Tardieu *et al.*, 1973). The electron dense phosphate headgroups (8-9Å) are separated by a water layer (0Å) and the lipid chain terminal region is low in electron density (26Å). As the phase assignment differences are confined to the weaker, higher orders, they make only small differences to the electron density distribution construction. A DOPC electron density map has also been constructed using five orders of diffraction (Figure 4.4, a truncated Fourier series construction), five orders being the limit of unambiguous phase assignment.

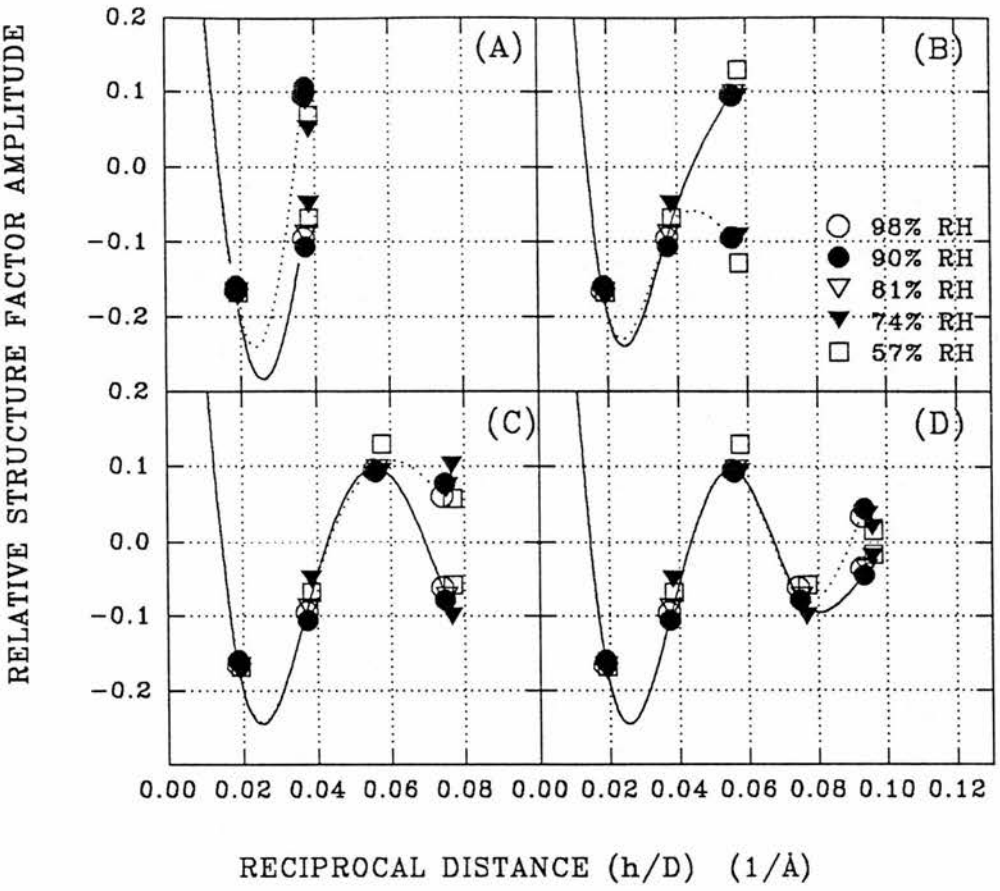

Figure 4.2 Phasing the DOPC bilayer diffraction data using the swelling series method. Diffraction data were collected from oriented DOPC bilayer samples at 20°C and between 98% and 57% RH. The four graphs (A, the second order to D, the fifth order) show different stages of the phasing process, where the next order to be phased is shown plotted both positively and negatively. The solid lines represent the accepted, and the dashed lines the rejected, phase assignments. Although diffraction data have been collected out to seven orders from the DOPC bilayer samples, the swelling series method has only successfully phased the first five orders.

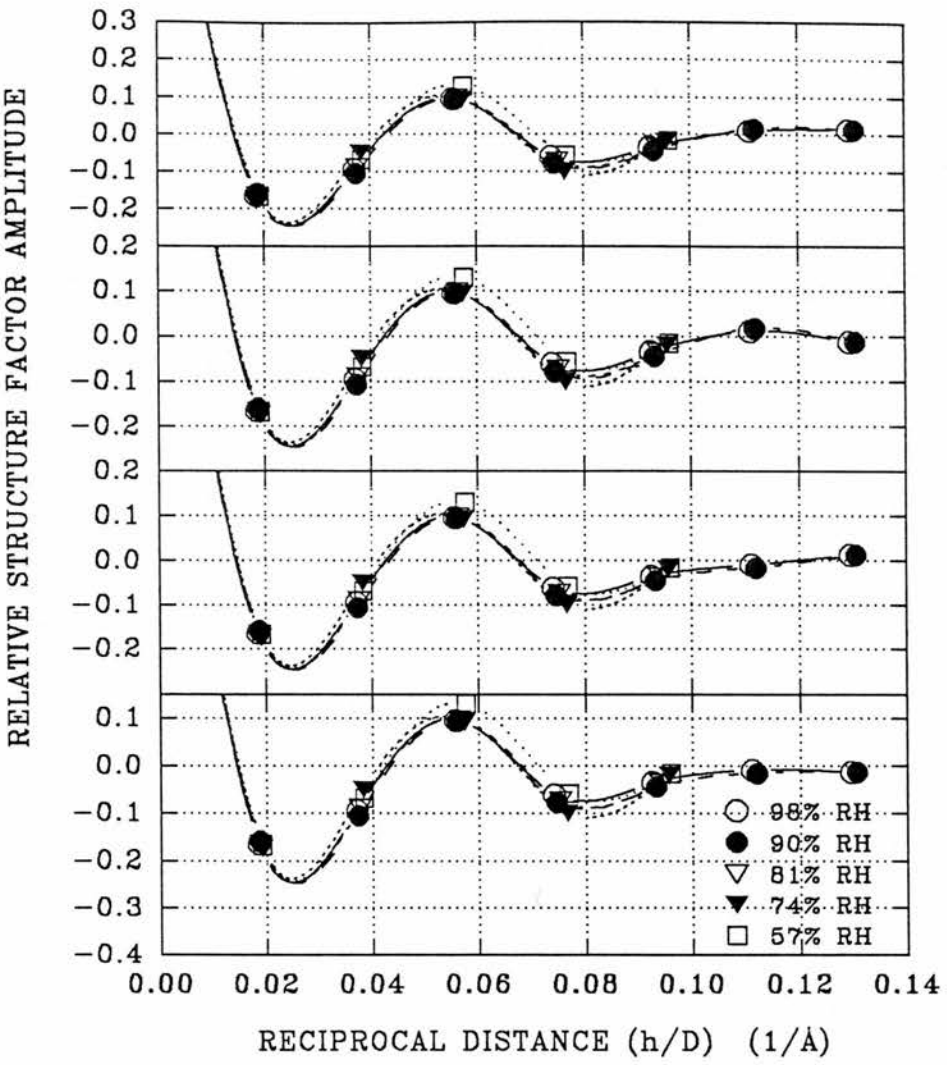

Figure 4.3 Phasing the DOPC bilayer higher (6 or 7) order diffraction data using the swelling series method. Diffraction data were collected out to seven orders from oriented DOPC bilayer samples at 20°C and between 98% and 57% RH. The swelling series phase assignment method has successfully phased the first five orders of diffraction (Figure 4.2), leaving four possible combinations for the final two orders of diffraction unresolved. All four phase assignment combinations produce feasible continuous Fourier transform plots.

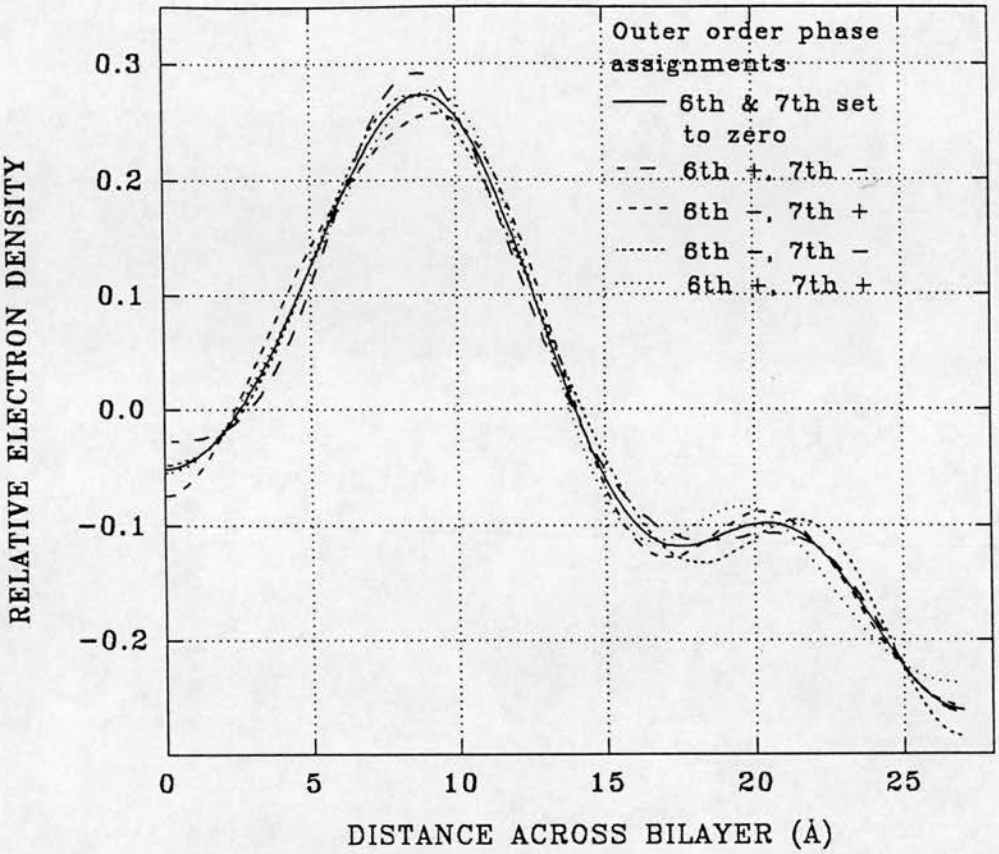

Figure 4.4 Construction of the possible DOPC bilayer electron density maps, using each of the four phase assignment combinations unresolvable by the swelling series method (Figure 4.3). Diffraction data were collected out to seven orders from oriented DOPC bilayer samples at 20°C and between 98% and 57% RH. The swelling series phase assignment method has successfully phased the first five orders of diffraction (Figure 4.2), leaving four possible combinations for the final two orders of diffraction unresolved. The electron density maps have been constructed using either all seven orders, and each of the possible phase assignments, or using only five orders of diffraction, the limit of successful phase assignment. All of the electron density maps display the characteristics of phospholipid bilayers; a water layer (0Å); a phosphate headgroup (9Å); a lipid chain terminal methyl region characterised by low electron density (26Å). For clarity, only half of the bilayer unit is shown above. The five order structure, compared with the possible seven order structures, gives an indication of the level of truncation error present in a five order electron density map construction.

The truncated construction has therefore been made with the higher orders set to zero, resulting in the construction of electron density maps containing half the error of incorrectly phasing an order (truncation error). The possible seven order versus five order electron density map comparisons therefore provide an estimate of the truncation error involved in constructing the DOPC electron density maps when using only five orders of diffraction (approximately ± 0.025 relative electron density units across the bilayer).

The structures of DOPC bilayers at 20°C and between 98% and 57% RH have been calculated using the truncated Fourier series of five orders of diffraction (Figure 4.5). Decreasing the humidity reduced the DOPC bilayer thickness (Figure 4.1), an observation independent of phase information. The truncated DOPC electron density distributions (Figure 4.5) suggest that the decrease in bilayer thickness is caused by a reduction in the spacing between the phospholipid headgroups across the water layer. To make this observation assumes that the truncation error affects all the bilayer structures in a similar manner and to the same degree. It would be impossible however, because of truncation error, to state an absolute position for the phospholipid headgroups.

4.3.3 Phasing the diffraction data collected from bilayers of DOPC containing amantadine FB.

Two of the five data sets collected from DOPC+amantadine FB bilayers contain eight orders of diffraction (Table 4.2). As with the DOPC bilayer data, the DOPC+amantadine FB diffraction data have been phased out to five orders (Figure 4.6). The swelling series method could not, however, resolve which of three plausible combinations of phase assignments, for orders six to eight, might be the correct ones (Figure 4.6). Electron density maps have been calculated using an eight order data set (DOPC + amantadine FB at 20°C and 74% RH) and the three higher order phase assignment combinations suggested by the swelling series method (Figure 4.7). All three of the generated electron density maps represent plausible phospholipid bilayer structures, especially as any unusual features in the

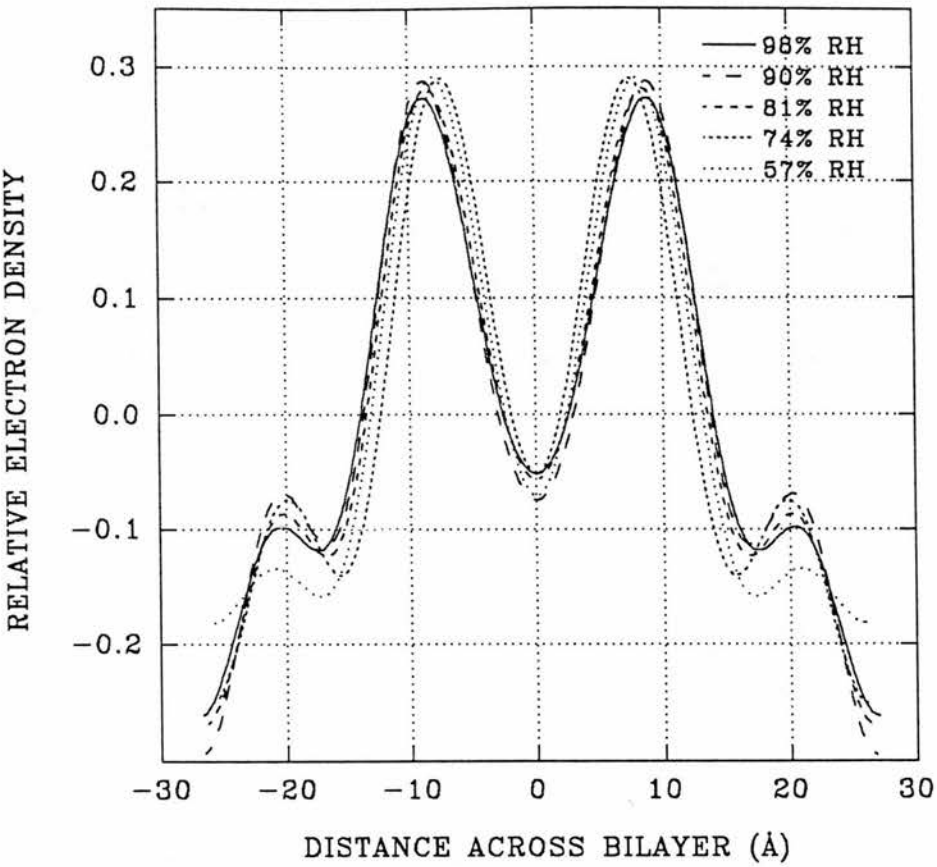

Figure 4.5 Construction of DOPC bilayer electron density maps using five orders of diffraction. Seven orders of diffraction were collected from oriented DOPC bilayer samples at 20°C and between 98% and 57% RH. The swelling series phase assignment method, however, only successfully phased the first five orders of diffraction (Figure 4.2), leaving four possible combinations for the final two orders of diffraction unresolved. The DOPC electron density maps have, therefore, been constructed using only five orders of diffraction, the limit of successful phase assignment. The maps show that the size of the water layer (0Å) decreases with the sample humidity, closing together the phosphate headgroups (±9Å). The electron density maps do not, however, take into account truncation errors (Figure 4.4) or data accuracy limits.

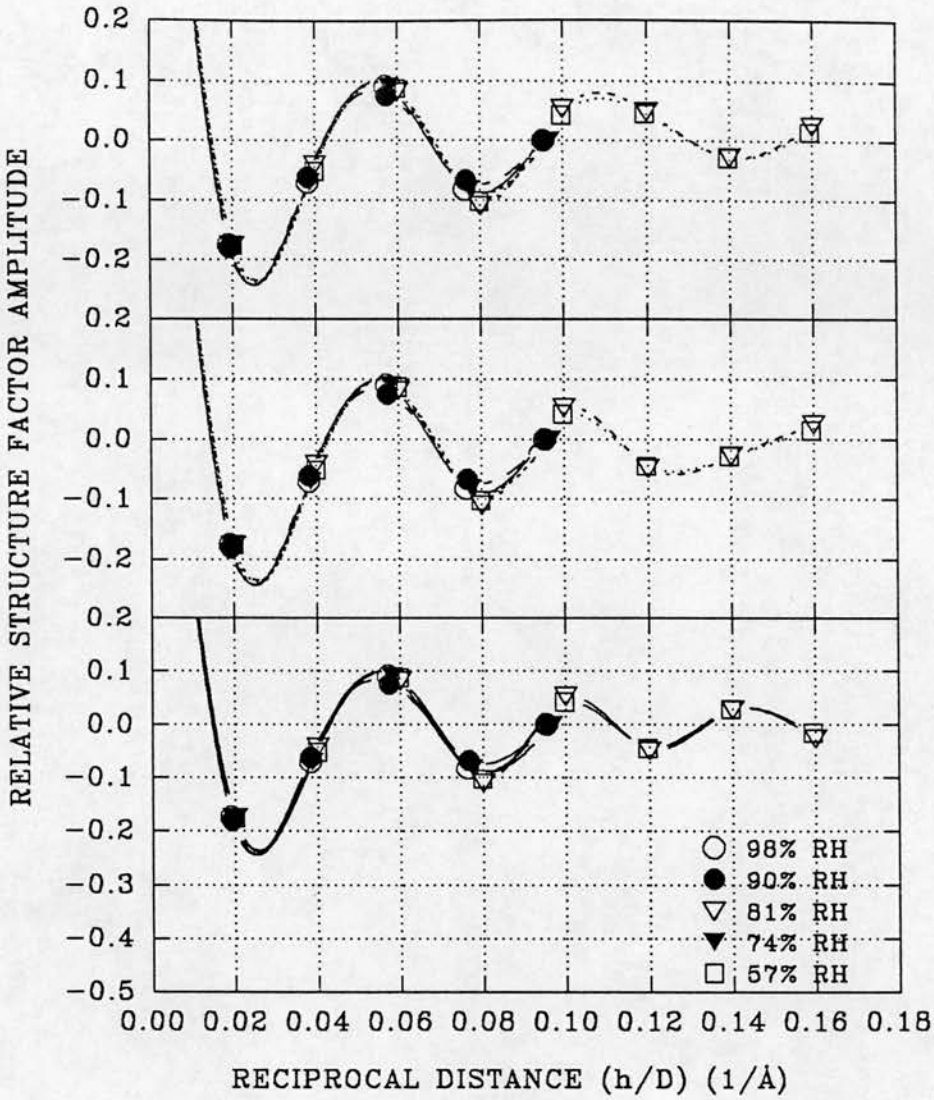

Figure 4.6 Phasing the diffraction data, collected from DOPC+ amantadine FB bilayers, using the swelling series method. Diffraction data were collected from oriented bilayer samples at 20°C and between 98% and 57% RH. Although the DOPC+ amantadine FB bilayers diffracted out to eight orders, the swelling series method has only successfully phased the first five orders. Three possible solutions to the phase assignments of the higher (6 to 8) orders are shown above. Each of phase assignment combinations shown above form plausible continuous Fourier transforms, leaving ambiguity in the higher diffraction order phase assignments.

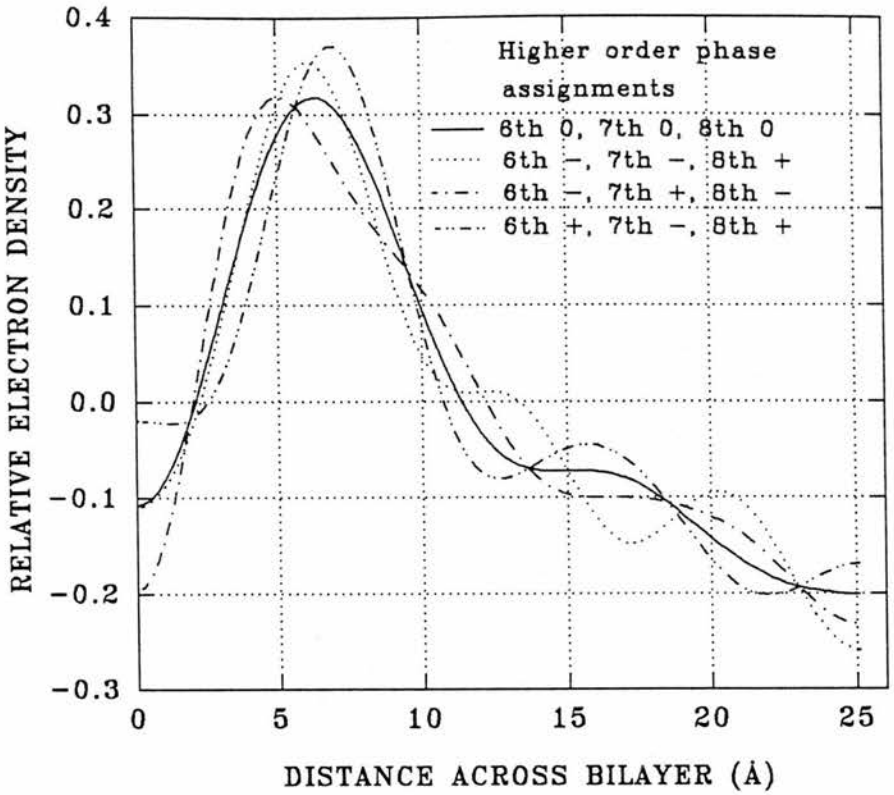

Figure 4.7 Construction of possible DOPC+amantadine FB bilayer electron density maps, using the phase assignment combinations unresolvable by the swelling series method (Figure 4.6). The diffraction data were collected out to eight orders from oriented amantadine FB bilayer samples at 20°C and between 98% and 57% RH. The swelling series method has only successfully phased the first five orders of diffraction (Figure 4.6), leaving the phases of the higher orders unresolved. The electron density maps have been constructed using either all eight orders, and the three suggested higher order phase assignments of Figure 4.6, or using only five orders of diffraction, the limit of successful phase assignment. All of the constructed electron density maps display the characteristics of phospholipid bilayers; a water layer (0Å); a phosphate headgroup (5-8Å); a lipid chain terminal methyl region characterised by low electron density (25Å). For clarity, only half of the bilayer unit is shown above. The five order structure, compared with the possible eight order structures, indicates the level of truncation error present in five order structures.

bilayer structure could be ascribed to the presence of amantadine. The DOPC+amantadine FB electron density map calculated using five orders (Figure 4.7, solid line) indicates the likely level of truncation error present in five order electron density maps due to the inability of the swelling series method to phase the higher order (6 to 8) diffraction data (up to ± 0.1 relative electron density units).

The structures of DOPC+amantadine FB bilayers at 20°C and between 98% and 57% RH have been calculated using the truncated Fourier series of five orders of diffraction (Figure 4.8). As with the pure DOPC bilayer data (Figure 4.5), the truncated DOPC+amantadine FB electron density distributions suggest that decreasing the relative humidity reduces the phospholipid headgroup spacing across the water layer (Figure 4.8). The humidity dependent reduction in the size of the water layer would account for the decrease in bilayer spacing with humidity (Figure 4.1). Making comparisons between five order structures, however, assumes that truncation errors affect all the bilayer structures to a similar degree.

4.3.4 Phasing the diffraction data collected from bilayers of DOPC containing amantadine HCl.

The DOPC+amantadine HCl bilayers diffracted to a maximum of six orders (Table 4.3) reducing the possible phase assignment combinations, compared to the eight order DOPC+amantadine FB data. Using the swelling series method, phases have been assigned to the first five orders of the DOPC+amantadine HCl diffraction data, with the phase of the sixth order remaining ambiguous (Figure 4.9). The two electron density maps constructed using the alternative sixth order phase assignments (DOPC+amantadine HCl at 20°C and 81% RH) both represent structures characteristic of phospholipid bilayers (Figure 4.10). The five order DOPC+amantadine HCl electron density map has also been constructed for comparison with the six order structures (Figure 4.10), indicating the level of truncation error that exists in five order structure (approximately ± 0.015 relative electron density units). It is possible that truncation errors greater than those

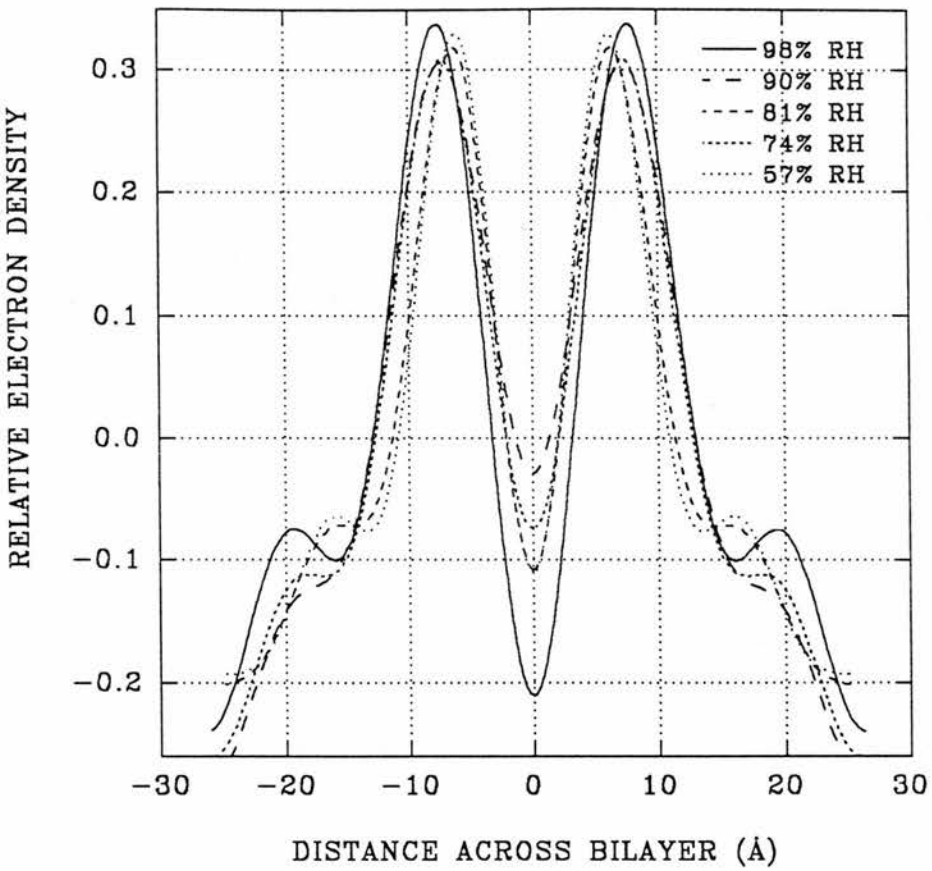

Figure 4.8 Construction of DOPC+amantadine FB bilayer electron density maps using five orders of diffraction, the limit of successful phase assignment (Figure 4.6). Although diffraction data were collected out to eight orders from the oriented bilayer samples, at 20°C and between 98% and 57% RH, electron density maps have been constructed using only five orders of diffraction, the point of successful phase assignment. The size of the water layer (0Å) decreases with the sample humidity, closing together the phosphate headgroups (±5-9Å). The electron density maps do not, however, take into account truncation errors (Figure 4.7) or data accuracy limits.

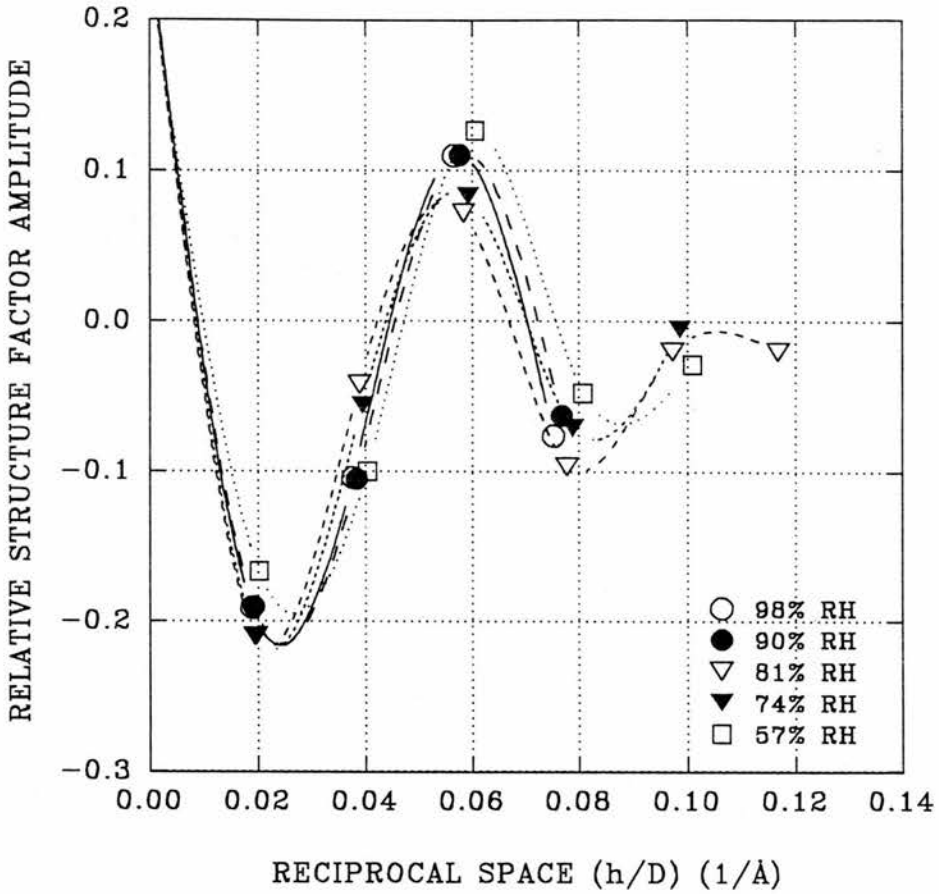

Figure 4.9 Phasing the DOPC+amantadine HCl bilayer diffraction data using the swelling series method. Diffraction data were collected from oriented bilayer samples at 20°C and between 98% and 57% RH. Although diffraction data have been collected out to six orders from the DOPC+amantadine HCl bilayer samples, the swelling series method has only successfully phased the first five orders. The two possible phase assignments of the sixth order both form plausible continuous Fourier transforms, leaving ambiguity in the sixth diffraction order phase assignment.

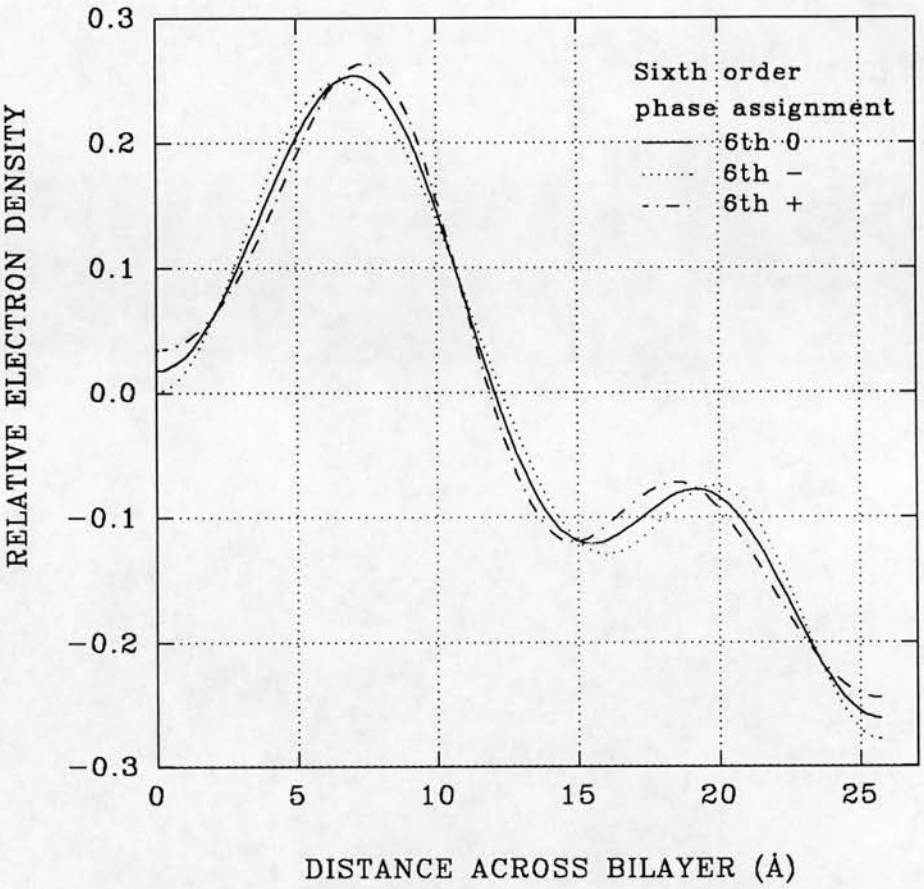

Figure 4.10 Construction of the five order and two possible six order DOPC+amantadine HCl bilayer electron density maps. Diffraction data were collected out to six orders from oriented DOPC+ amantadine HCl bilayer samples at 20°C and between 98% and 57% RH. The swelling series phase assignment method successfully phased the first five orders of diffraction (Figure 4.9), leaving the phase of the sixth order unresolved. The electron density maps have been constructed using either all six orders, with the sixth order phased both positively and negatively, or using only five orders of diffraction, the limit of successful phase assignment. All of the electron density maps display the characteristics of phospholipid bilayers; a water layer (0Å); a phosphate headgroup (6-8Å); a lipid chain terminal methyl region characterised by low electron density (25Å). For clarity, only half of the bilayer unit is shown above. Comparison of the five order and two six order structures, indicates the level of truncation error likely in the five order structure.

indicated by Figure 4.10 exist, if higher order diffraction spots exist but were undetected on film at any humidity.

The five order bilayer structures of DOPC+amantadine HCl at 20°C and between 98% and 57% RH are shown in Figure 4.11. As was the case with the pure DOPC and DOPC+amantadine FB bilayers, decreasing the humidity appears to reduce the phospholipid headgroup separation across the water layer. As per the pure DOPC and DOPC+amantadine FB data, making comparisons between the five order DOPC+amantadine HCl electron density maps assumes that the truncation error affects all the bilayer structures in a similar manner and to the same degree.

4.4 Comparison of pure DOPC bilayers with DOPC bilayers containing either amantadine FB or HCl.

In order to compare the electron density distribution of the DOPC bilayer with that of the DOPC+amantadine bilayer it is important to have some knowledge of the accuracy with which bilayer structures can be constructed. As the swelling series phase assignment method, for all three DOPC based systems, has only been successful out to five orders, truncation errors exist in the data. The accuracy and reproducibility of the diffraction data must also be considered, as observed bilayer differences on addition of drug might be of an order purely ascribable to normal sample variation. The reproducibility of a membrane sample was investigated (Chapter 3) for a pure DOPC bilayer sample at 20°C and 57% RH, the results of which in a Monte Carlo simulation program provided an estimate of the 95% confidence limits for the bilayer electron density distribution (Figure 3.3).

The confidence limits for the DOPC and DOPC+amantadine FB electron density maps at 20°C and 98% RH (Figure 4.12) were created using a Monte Carlo simulation program, five orders of diffraction and the order error estimate calculated for DOPC data (Chapter 3). The Monte Carlo simulation program calculates the upper and lower 95% confidence limits for the electron density distribution of the bilayer. The two solid lines of Figure 4.12 are the upper and lower electron density limits for the DOPC+amantadine FB bilayer, while the

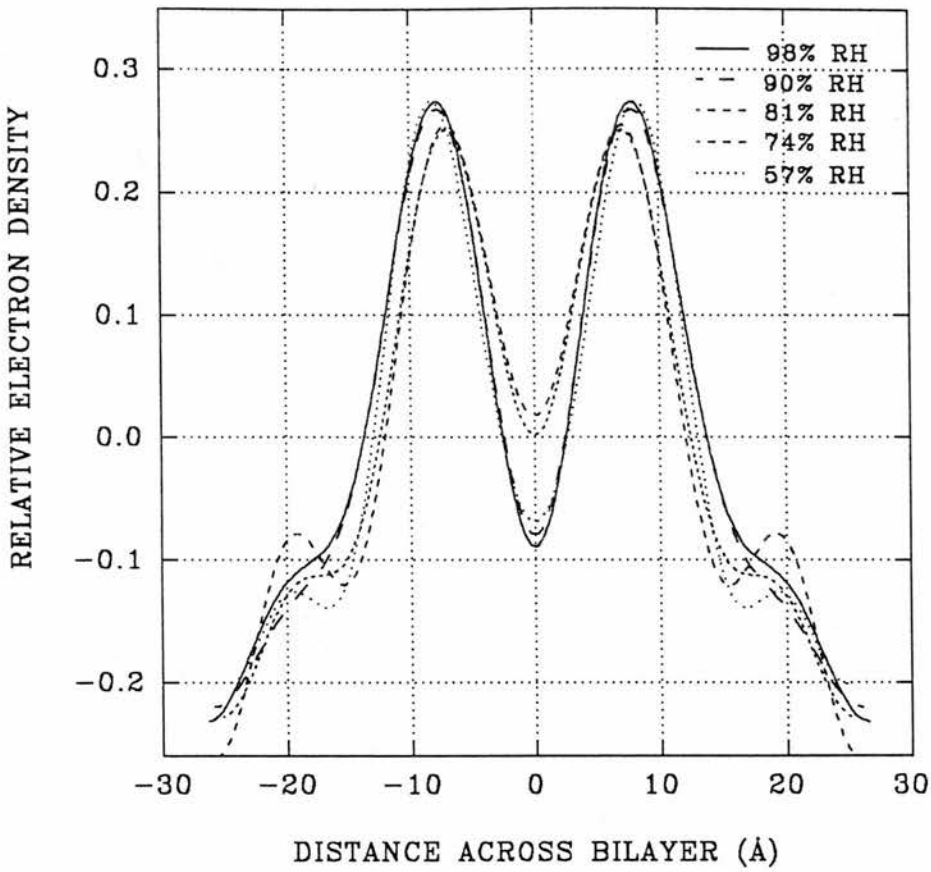

Figure 4.11 Construction of DOPC+amantadine HCl bilayer electron density maps using five orders of diffraction. The diffraction data were collected out to six orders from oriented bilayer samples at 20°C and between 98% and 57% RH. The swelling series method successfully phased the first five orders of diffraction (Figure 4.9), leaving the sixth order phase assignment unresolved. The electron density maps have, therefore, been constructed using only five orders of diffraction, the point of successful phase assignment. The maps show that the size of the water layer (0Å) decreases with the sample humidity, closing together the phosphate headgroups (±6-8Å). The electron density maps do not take into account truncation errors (Figure 4.10) or data accuracy limits.

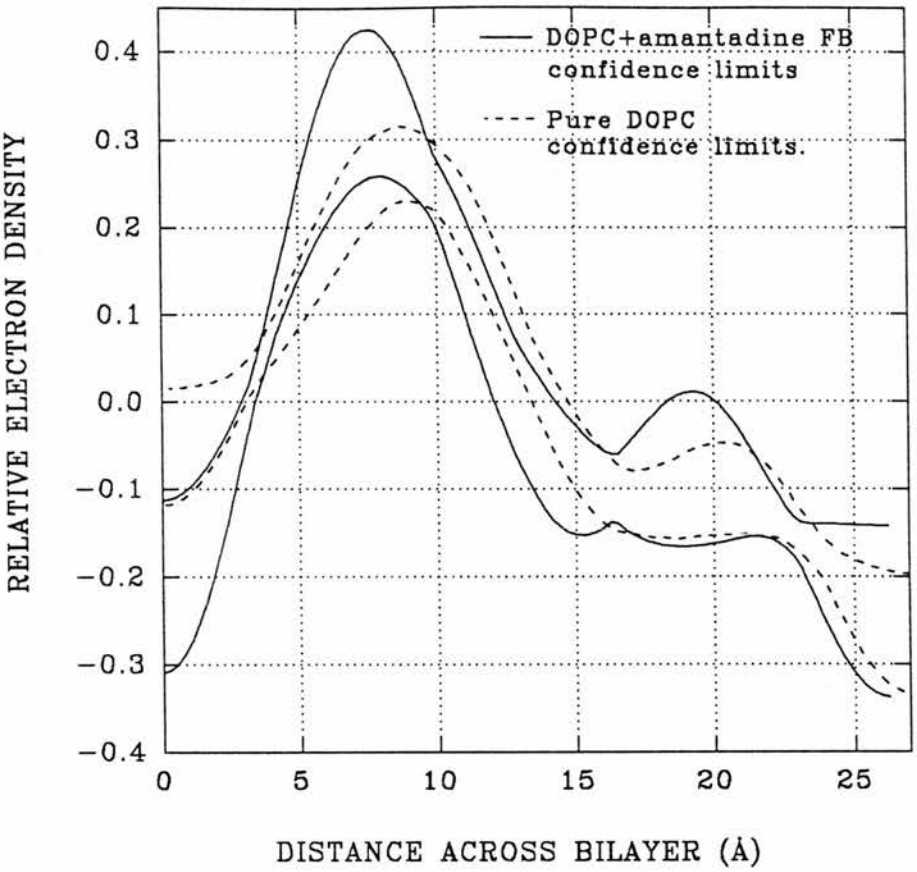

Figure 4.12 Comparison of the 95% confidence limits for the electron density distribution of DOPC and DOPC+amantadine FB bilayers at 20°C and 98% RH. Diffraction data were collected from oriented bilayer samples and phased out to five orders using the swelling series method. The 95% confidence limits were constructed using a Monte Carlo simulation program, five orders of X-ray diffraction and structure factor amplitude error limits derived from DOPC sample reproducibility experiments (Chapter 3). For clarity, only one half of the bilayer unit is shown above, where the centre of the water and lipid layers are located at 0Å and 26Å respectively. Although the two bilayer structures appear to differ significantly between 0Å and 4Å, the maps do not take into account truncation errors which might strongly influence the shape and depth of the water layer (Figures 4.4 and 4.7).

dashed lines are those of the pure DOPC bilayer. For clarity only half of the bilayer structure is shown, with the water layer and centre of the lipid layer being located at 0Å and 26Å respectively.

At first it might appear from Figure 4.12 that there is discernible difference between the DOPC and DOPC+amantadine FB bilayer (between 0-4Å), however, uncertainty in the electron density distribution due to Fourier series truncation errors are not included in the diagram. Truncation errors affect both the pure DOPC (Figure 4.4, uncertainty of ± 0.025 relative units) and the DOPC+amantadine FB bilayers (Figure 4.7, uncertainty of ± 0.1 relative units) and are potentially quite large between 0Å and 3Å, enough to eliminate any conclusions of differences between the two bilayer structures being compared. Comparison of DOPC and DOPC+amantadine FB bilayers at other humidities show the two water layer structures (0-3Å) to be indistinguishable (Figure 4.13, 57% RH data), even before truncation errors are considered. The 57% RH data indicate that there are differences in the headgroup positions (*ca* 7-10Å for DOPC and 5-7Å for DOPC+amantadine FB) between the two systems. This structural change would help to account for the alteration in bilayer spacing that occurs on addition of amantadine (FB or HCl) to DOPC (Figure 4.1). The change in headgroup position is also suggested by the 98% RH data (Figure 4.12), albeit less conclusively, as well as at intermediate humidities.

Although a change in the phosphate headgroup position is suggested, structural changes that might occur on addition of amantadine HCl to DOPC bilayers cannot be resolved using the five order diffraction data (Figure 4.14). Whilst Figure 4.14 only shows the data from bilayers at 20°C and 98% RH, data from other humidities give similarly inconclusive results about the interaction of amantadine HCl with DOPC. A comparison of the 95% confidence limits for the DOPC+amantadine FB and the DOPC+amantadine HCl electron density distributions cannot distinguish any differences between the two charge states of amantadine (Figure 4.15). Any differences in the DOPC-amantadine interaction, due to charge effects, cannot be resolved by using only five orders (truncated Fourier series) to construct electron density maps.

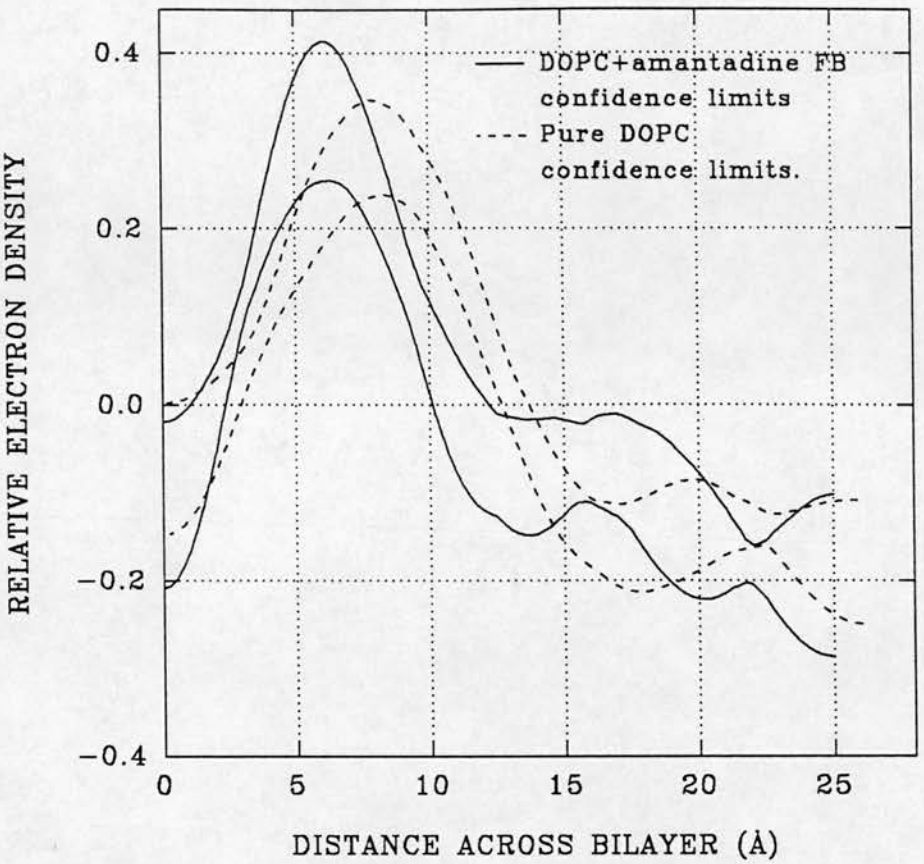

Figure 4.13 Comparison of the 95% confidence limits for the electron density distribution of DOPC and DOPC+amantadine FB bilayers at 20°C and 57% RH. Diffraction data were collected from oriented bilayer samples and phased out to five orders using the swelling series method. The 95% confidence limits were constructed using a Monte Carlo simulation program, five orders of X-ray diffraction and structure factor amplitude error limits derived from DOPC sample reproducibility experiments (Chapter 3). For clarity, only one half of the bilayer unit is shown above, where the centre of the water and lipid layers are located at 0Å and 26Å respectively. The 57% RH data indicates that there is a difference in the headgroup positions (*ca* 7-10Å for DOPC and 5-7Å for DOPC+ amantadine FB bilayers). The change in headgroup position would help to account for the change in bilayer spacing that occurs on addition of amantadine (FB or HCl) to DOPC (Figure 4.1). The change in headgroup position is also suggested by the 98% RH data (Figure 4.12), albeit less conclusively, as well as at intermediate humidities.

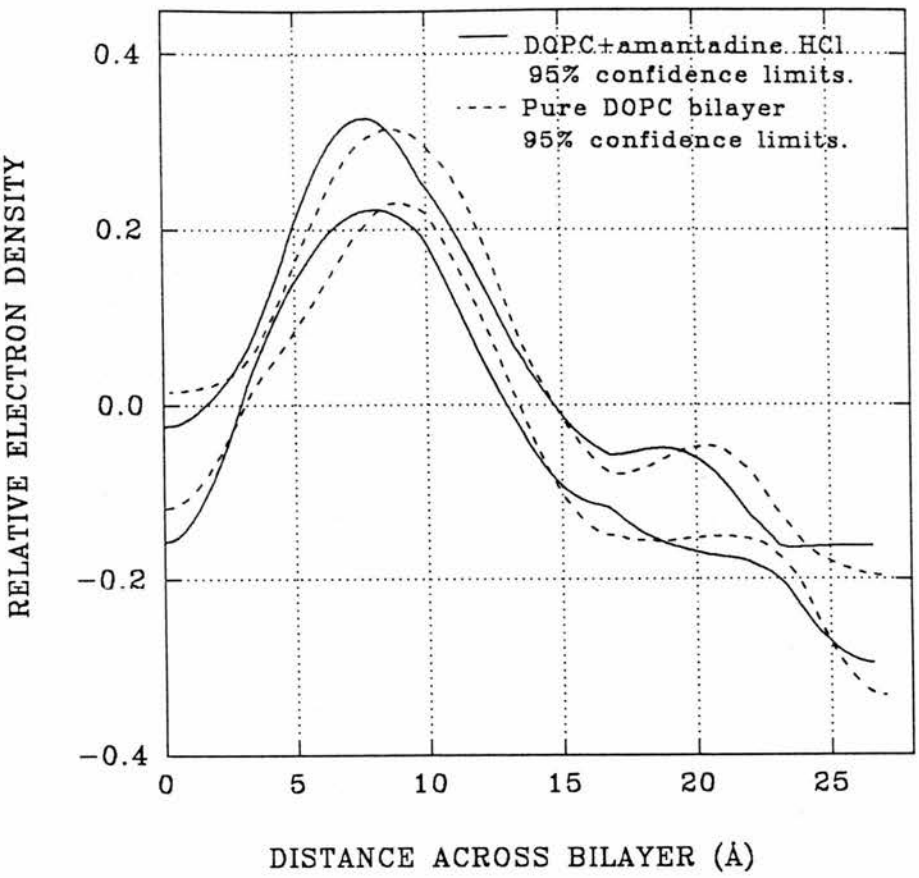

Figure 4.14 Comparison of the 95% confidence limits for the electron density distribution of DOPC and DOPC+amantadine HCl bilayers at 20°C and 98% RH. Diffraction data were collected from oriented bilayer samples at 20°C and 98% RH and phased out to five orders using the swelling series method. The 95% confidence limits were constructed using a Monte Carlo simulation program, five orders of X-ray diffraction and structure factor amplitude error limits derived from DOPC sample reproducibility experiments (Chapter 3). For clarity, only one half of the bilayer unit is shown above, where the centre of the water and lipid layers are located at 0Å and 26Å respectively. The 95% confidence limits do not indicate any differences between the two bilayer systems. Due to truncation error, any electron density distribution changes that occur, on addition of amantadine HCl to DOPC bilayers, cannot be resolved using only five orders of diffraction to construct electron density maps.

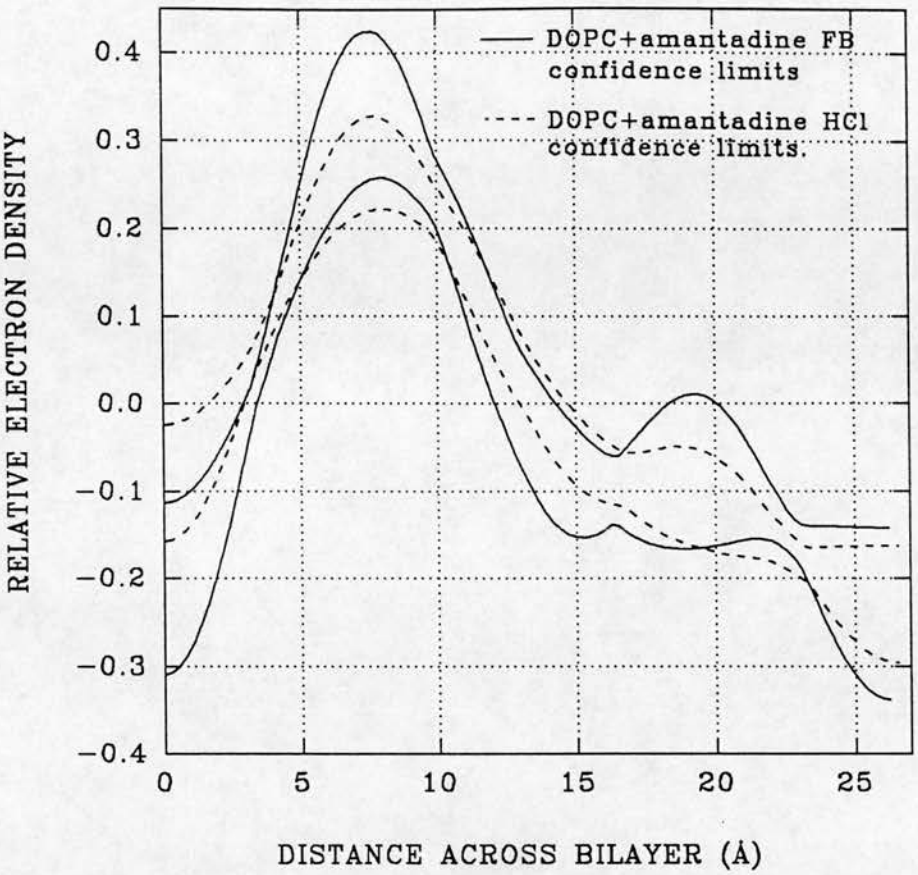

Figure 4.15 Comparison of the 95% confidence limits for the electron density distribution of DOPC+amantadine FB and DOPC+amantadine HCl bilayers at 20°C and 98% RH. Diffraction data were collected from oriented bilayer samples at 20°C and 98% RH and phased out to five orders using the swelling series method. The 95% confidence limits were constructed using a Monte Carlo simulation program, five orders of X-ray diffraction and structure factor amplitude error limits derived from DOPC sample reproducibility experiments (Chapter 3). For clarity, only one half of the bilayer unit is shown above, where the centre of the water and lipid layers are located at 0Å and 26Å respectively. Due to truncation error any electron density distribution differences between amantadine FB and amantadine HCl in DOPC bilayers cannot be resolved using only five orders of diffraction to construct electron density maps.

4.5 Discussion of the swelling series method.

The swelling series technique relies on the assumption that the bilayer structure does not change as the humidity increases. The water layer however is an integral part of the membrane structure and variations in humidity do alter the phospholipid structure (Tardieu *et al.*, 1973). Indeed, the bilayer structure changes significantly on the close approach of adjacent bilayers as the system is dehydrated (Small, 1967; LeNeveu *et al.*, 1976, 1977; Parsegian *et al.*, 1979; Lis *et al.*, 1981) and this lateral compression can cause large changes in lipid area (Parsegian and Rand, 1983; Lis *et al.*, 1982a, b). The swelling series method assumes that the continuous Fourier transform of a single structure is sampled at multiple points along its length by the collection of data at different humidities. Because the bilayer structure changes with humidity, however, each data set in a swelling series samples a different continuous Fourier transform. While the swelling series can still be effective as a phasing method, it is less reliable when large structural changes occur with humidity, or for phasing higher orders of diffraction.

4.6 Conclusions of the diffraction study.

The interaction of amantadine (FB and HCl) with DOPC bilayers at 20°C and between 98% and 57% RH has been studied. Oriented bilayer samples were studied by X-ray diffraction using the swelling series phasing method. Although the DOPC based bilayers diffracted to a maximum of eight orders, the swelling series phasing method was only able to phase unambiguously the first five orders produced by each bilayer system studied (Figures 4.3, 4.6 and 4.9). As a result of this inability to phase the higher diffraction orders, the DOPC based bilayer electron density maps all have truncation error associated with them (Figures 4.4, 4.7 and 4.10). The level of the truncation errors is such that little can be concluded from comparisons made between bilayer structures with and without amantadine present (Figures 4.12, 4.13 and 4.14). Also, any differences between the interaction

of amantadine FB and amantadine HCl with DOPC bilayers could not be determined by the diffraction study (Figure 4.15)

The bilayer thickness can be measured from the X-ray diffraction data without the need to assign phases to the data. Adding amantadine of either form to DOPC bilayers at 20°C reduced the bilayer thickness by 1-2.5Å, depending on humidity. The bilayer thickness of all three systems also decreases with relative humidity and the electron density map constructions appear to show that this decrease in thickness is attributable in part to a decrease in the phospholipid headgroup separation (Figures 4.5, 4.8 and 4.11).

It can be concluded that a change in bilayer structure occurs on addition of amantadine to the DOPC bilayer, as the bilayer thickness is reduced significantly. The process of swelling DOPC bilayers alters the bilayer structure and therefore the form of the continuous Fourier transform, reducing the ability of the swelling series method to phase higher orders. To analyse more fully the interaction between DOPC bilayers and amantadine would require the ability to phase unambiguously the diffraction data out to higher orders than has been achieved here using the swelling series method.

Chapter 5.

A study of a novel bromolipid.

5.1 Aim of studying a novel bromolipid.

To date, the only popular phasing method used in X-ray diffraction studies of membranes is the swelling series approach (Torbet and Wilkins, 1976; Franks and Leib, 1981). Isomorphous replacement, the principle method used for phasing diffraction data from protein crystals (Blundell and Johnson, 1976), has seldom been used successfully on a membrane system (Makowski and Lee, 1983). Compared with X-ray diffraction, more reliable phasing methods are available for the analysis of neutron diffraction data from membrane samples, such as H_2O/D_2O exchange (Franks and Lieb, 1979). Unlike X-rays which are diffracted by electrons, neutrons are diffracted by nuclei and, as a result, the insertion of isotopes into a membrane can significantly change the neutron diffraction pattern (the basis of the H_2O/D_2O exchange phasing method). The isotope effect, therefore, provides neutron diffraction with a phasing method which does not alter the membrane structure. Conversely, the X-ray diffraction swelling series method alters the membrane structure, thus reducing the effectiveness of this technique.

The aim of the work in this chapter was to study a novel phospholipid which might provide an alternative phasing method to the swelling series approach. A novel brominated phospholipid (bromolipid) derivative of DPPC has been synthesised (Chapter 3), where the *sn*-2 terminal methyl group of DPPC has been exchanged for a bromine atom. To characterise bilayers of the novel molecule, the bromolipid has been studied by X-ray diffraction, using the swelling series method, and by differential scanning calorimetry (DSC). It was hoped that, once characterised, the bromolipid might offer two methods of phasing diffraction data: Firstly by the bromolipid bromine atom acting as a heavy atom in isomorphous replacement experiments and secondly by the bromine atom acting as an anomalous scatterer in multiple anomalous dispersion (MAD) experiments.

Isomorphous replacement is a phasing method used extensively in protein crystallography, where a heavy atom is added into the unit cell as a 'label' (Blundell and Johnson, 1976). In a typical isomorphous replacement experiment several samples might be studied, each with different heavy atoms, or increasing amounts

of the same atom, present. As well as the presence of the heavy atom acting as a phasing agent, it can also be used to put the relative electron density scale into one of absolute density. The anomalous scattering (MAD) phasing method is still relatively new to protein crystallography (Hendrickson, 1985a, b) and has yet to be used in membrane diffraction experiments. In the MAD experiment only a single sample, containing an anomalous scattering centre, need be studied. MAD diffraction patterns are collected at different X-ray wavelengths (either side of a suitable absorption edge), with differences between the collected patterns being used as the phasing method (Hendrickson, 1991).

5.1.1 Incorporating heavy atoms into membrane structures.

The use of heavy atom methods have had limited success with biological membranes (Akers and Parsons, 1970; Harker, 1972; Blaurock, 1973), where two principle methods have been used to introduce a heavy atom into a membrane structure:

1) Label a phospholipid molecule with the heavy atom (Wiener and White, 1991; McIntosh and Holloway, 1987).
2) Attach the heavy atom to a secondary molecule that is then inserted into the membrane.

Adding bromine across a lipid chain double bond has been the main way in which bromolipids have been synthesised and studied in the past (Wiener and White, 1991; McIntosh and Holloway, 1987), especially for use in fluorescence quenching experiments (Leto *et al.*, 1980; East and Lee, 1982; Holloway *et al.*, 1982; Markello *et al.*, 1985; Everett *et al.*, 1986). This addition across a double bond method, however, creates a molecule that has a large atom attached perpendicular to the direction of the lipid chains, which could sterically hinder chain packing. Recent X-ray diffraction work has used such brominated lipids primarily to locate the bromine atom for fluorescence work, rather than as a diffraction phasing method (Wiener and White, 1991; Silvius, 1990; Yeager and Fiegenson, 1990; de Kroon *et al.*, 1990).

The second approach to placing heavy atoms inside a membrane has been that taken by McIntosh *et al.*, (1976) and Franks *et al.*, (1978), who showed that halogenated cholesterol analogues could be isomorphously exchanged with cholesterol and used to phase the signs of the lamellar reflections. Katsaras and Stinson, (1990) and Katsaras *et al.*, (1991) have placed brominated palmitic acid, brominated butylated hydroxytoluene (BHT) and brominated α-tocopherol, into DPPC bilayers with varying success. The bromine atoms, attached to the small molecules palmitic acid and α-tocopherol, tended to have a fairly wide distribution in the bilayer (9Å). The bromine atoms attached to BHT could not be located in the bilayer at all. The bromine atoms placed into the bilayer, in the labelling experiments were, however, for use as positional markers rather than as diffraction phasing agents.

5.1.2 The use of bromine as a heavy atom label.

Bromine was chosen to be the heavy atom label in the DPPC analogue because of its potential for use in both isomorphous replacement and MAD experiments. The bromine atom is extremely electron dense, having thirty five electrons in almost same volume as the nine electrons of a methyl group. The bromine atom should, therefore, be easy to locate in X-ray diffraction electron density maps. The bromine atom has a suitable absorption edge for use in MAD experiments, with an energy in the X-ray wavelength range obtainable by current synchrotron sources (*ca* 1Å wavelength, obtainable at the synchrotron radiation source (SRS), Daresbury Laboratory, Warrington, England). In addition, as the bromine atom and the methyl group have a similar atomic radius (1.85Å versus 2.0Å), exchanging the bromine atom for a phospholipid methyl group should minimise any changes in membrane structure. Bromine is also known to act neutrally in a lipid chain environment and numerous X-ray and fluorescence experiments have utilised a variety of brominated lipids without the bilayer being distorted other than by steric effects (Leto *et al.*, 1980; East and Lee, 1982; Holloway *et al.*, 1982; Markello *et al.*, 1985; Everett *et al.*, 1986).

The bromolipid bromine atom was placed at the terminal position of a lipid chain so that a layer of high electron density occurred at the centre of the bilayer, the ideal position for a label in isomorphous replacement experiments (Franks and Leib, 1981). Just one (the *sn-2* chain) of the two inequivalent lipid chains of DPPC was labelled with a bromine atom. The two lipid chains are inequivalent (Figure 1.5), as the *sn*-2 chain penetration into the bilayer is shortened by a sharp bend between C-2 and C-3 (Zaccai *et al.*, 1979). Two different populations of bromine in the bilayer would have been created if both the *sn*-1 and the *sn*-2 lipid chains of the bromolipid had been labelled.

5.2 X-ray diffraction study of DPPC and bromolipid in the gel phase.

Oriented samples of gel phase DPPC and bromolipid bilayer were studied by X-ray diffraction using the swelling series phasing method (described in Chapters 2 and 3). Swelling series data were compiled for two systems:

1) pure DPPC bilayers at 20°C and between 98% and 57% RH.
2) pure bromolipid bilayers at 20°C and between 98% and 57% RH.

Each system was studied at five different humidities (98%, 90%, 81%, 74% and 57% RH), using the sample preparation and data analysis methods described in Chapter 3.

5.3 Results of DPPC and bromolipid bilayer diffraction analysis.

Meridional diffraction data (Tables 5.1 and 5.2) were collected out to fourteen and twelve orders from DPPC and bromolipid bilayers respectively. At 20°C, both DPPC and bromolipid form bilayers in the $L_{\beta'}$ phase (Plates 5.1 and 5.2), indicated by the equilateral diffraction at [4.1Å^{-1}] (Stumpel *et al.*, 1983) due to the hydrocarbon chains being hexagonally packed (Chapman *et al.*, 1967). The [4.1Å^{-1}] equilateral diffraction angle, above the equator, provides a measure of the lipid chain tilt (Levine 1972, 1973), that can be combined with the meridional diffraction information to provide a better picture of the bilayer structure.

PLATE 5.1 The diffraction pattern collected from an oriented sample of DPPC at 20°C and 90% RH. The gel phase sample diffracted meridionally out to twelve orders. One can also see diffraction out to four orders resulting from phase separation in the sample. These diffraction spots arise from membranes in the sample with a larger bilayer thickness (D) than the bulk DPPC bilayers, possibly from bilayers at the sample/air interface.

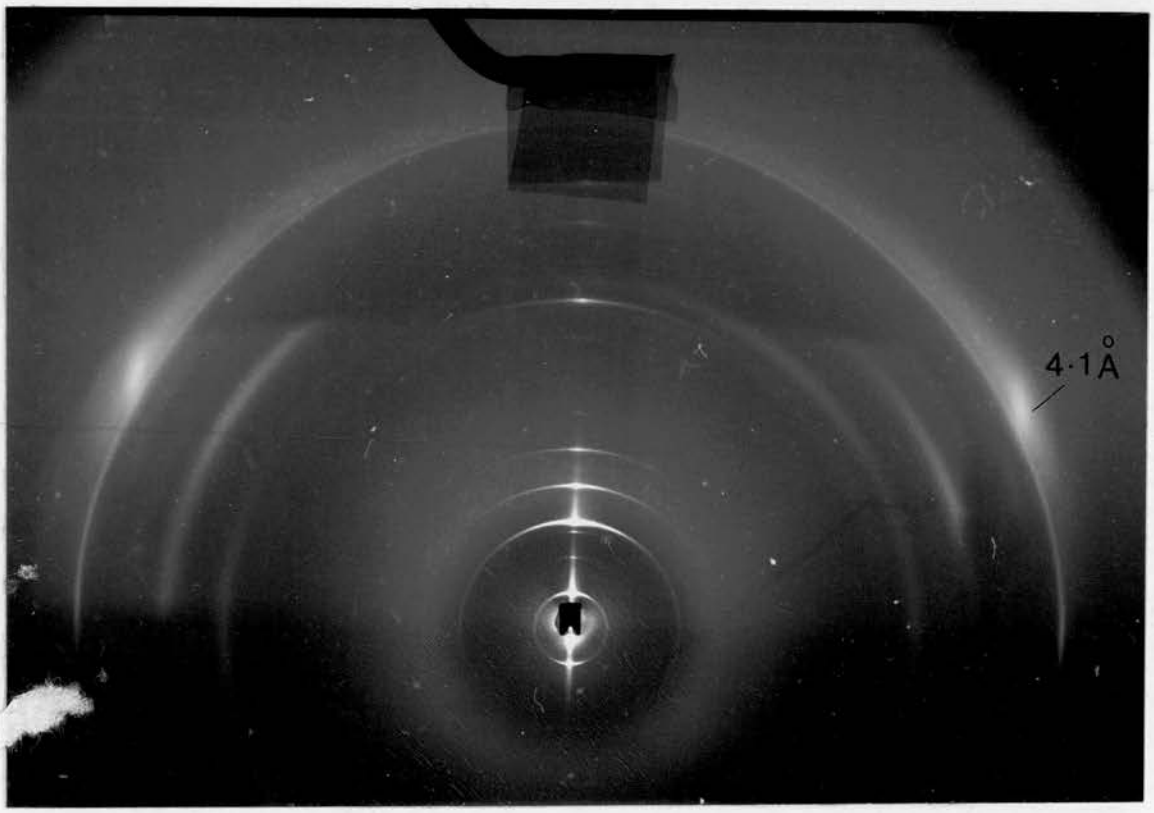

PLATE 5.2 A diffraction pattern collected from an oriented sample of bromolipid bilayers at 20°C and 90% RH. Twelve orders of meridional diffraction can be observed in the diffraction pattern. The gel ($L_{\beta'}$) phase sample also diffracted equilaterally, producing a diffuse spot at 4.1$Å^{-1}$, in agreement with that found for DPPC by Stumpel *et al.* (1983). One can also see diffraction out to four orders resulting from phase separation in the sample. These diffraction spots arise from membranes in the sample with a larger bilayer thickness than the bulk bromolipid bilayers, possibly at the sample/air interface.

Table 5.1 Diffraction data collected from gel phase DPPC bilayers.

Diffraction order	Phased structure factor amplitude diffraction data collected from DPPC bilayers at 20°C.					Variation of data (SD)
1	−0.191	−0.185	−0.189	−0.189	−0.191	2%
2	−0.082	−0.094	−0.091	−0.083	−0.070	11%
3	+0.077	+0.086	+0.081	+0.078	+0.072	7%
4	−0.151	−0.148	−0.149	−0.155	−0.160	3%
5	0	+0.025	+0.022	+0.014	+0.010	31%
6	−0.065	−0.057	−0.048	−0.066	−0.075	14%
7	−0.015	−0.034	−0.028	−0.024	−0.009	38%
8	−0.039	−0.027	−0.024	−0.037	−0.057	31%
9	−0.036	−0.036	−0.036	−0.036	−0.036	7%
10	−0.030	−0.027	−0.022	−0.028	−0.031	11%
11	+0.034	+0.021	+0.020	+0.033		36%
12		−0.033	−0.026	−0.018		
13			−0.012	−0.019		
14				−0.019		
Relative humidity	98%	90%	81%	74%	57%	
Bilayer repeat (Å)	58.0	57.9	57.7	57.5	57.1	

Table 5.2 Diffraction data collected from gel phase bromolipid bilayers.

Diffraction order	Phased structure factor amplitude diffraction data collected from bromolipid bilayers at 20°C.			
1	−0.113	−0.114	−0.117	−0.134
2	+0.034	+0.019	+0.018	+0.071
3	+0.202	+0.207	+0.210	+0.164
4	−0.107	−0.107	−0.099	−0.100
5	+0.074	+0.061	+0.052	+0.067
6	−0.031	−0.019	−0.007	−0.048
7	0	0	0	+0.022
8	+0.041	+0.020	0	+0.066
9	−0.028	−0.021	−0.023	−0.020
10	−0.025	−0.019	−0.017	0
11	+0.057	+0.030	+0.025	−0.055
12		−0.040	−0.034	
Relative humidity	98%	90%	81%	57%
Bilayer repeat (Å)	55.9	56.3	56.7	54.7

5.3.1 Estimating the error levels in the diffraction data.

Confidence limits for the distribution of electron density across a bilayer can be estimated using a Monte Carlo simulation programme (Chapter 3). An error limit estimate is, however, required for each structure factor amplitude value used to construct the electron density distribution maps. The level of error in measuring the intensity of a diffraction spot from a film was previously shown to be typically in the region of 2-6% of the magnitude of the intensity spot (Chapter 3). Data have also been presented showing the variation in the diffraction data between five 'identical' fluid phase DOPC samples (Table 3.3). While only four orders of diffraction were collected from the DOPC bilayers, these results showed that the measured intensity of a spot could vary by up to 26%. The data, however, also suggested that these large variations in the collected diffraction patterns resulted from variations in the structure of the DOPC bilayer sample, rather than the accuracy with which diffraction data can be recorded.

Diffraction data have not been collected from a standard gel phase DPPC sample enough times for structure factor error estimates to be assessed. The variation in diffraction data of a 20°C DPPC sample over the relative humidity range 98% to 57% has, however, been analysed (Table 5.1). The first four orders of diffraction obtained from the DPPC bilayers, over all humidities studied, vary considerably less than did the data collected from five 'identical' DOPC samples (Tables 5.1 and 3.3). The DPPC structure factor amplitudes varied with a standard deviation of between 3% and 38%, with the higher orders varying the most (Table 5.1). These variations in diffraction data represent an over-estimate of the diffraction data error level, as variations in diffraction data with humidity are expected.

5.3.2 Pure DPPC bilayers at 20°C.

The swelling series plot used to phase the diffraction data from DPPC bilayers, at 20°C and between 98% and 57% RH, is shown in Figure 5.1. Phases

were assigned to the diffraction data using the method of calculating continuous Fourier transforms for the data, then analysing electron density maps constructed using the chosen phases. Electron density maps of DPPC at 20°C and between 98% and 57% RH (Figure 5.2) were constructed using up to twelve orders of diffraction, if available, and the phase assignments obtained by the swelling series method (Figure 5.1). The electron density distributions are orientated so that the centre of the lipid layer is located at 0Å and the water layers are located at ±29Å.

The DPPC electron density maps locate the phosphate headgroup and ester linkage regions at ±22Å and ±17Å, respectively, from the centre of the lipid layer (0Å). Of note is the higher structural detail observable in the DPPC bilayer, which regularly diffracted to twice the number of orders than were obtained from DOPC bilayers (Chapter 4) at the same temperature. The resolution of a diffraction pattern is calculated as being the unit cell size (D) divided by the number of the highest order collected. Thus the twelve order DPPC data have a typical resolution of 58/12 = 4.8Å, compared with the DOPC bilayer data with a resolution of 7.7Å. DPPC forms bilayers in the gel ($L_{\beta'}$) phase at 20°C, whereas DOPC forms fluid (L_{α}) phase bilayers, which accordingly diffract out to fewer orders.

The DPPC electron density maps (Figure 5.2) suggest that the shape of the water layer changes only slightly with decreasing humidity and the phosphate head group separation, across the water layer, remains relatively constant. That is not to say that the head groups on the same side of the bilayer are not being pushed apart, perpendicular to the bilayer normal, by the insertion of water around the phosphatidylcholine headgroup. Previous work (Tardieu *et al.*, 1973; Torbet and Wilkins, 1976; Katsaras and Stinson, 1990; Katsaras *et al.*, 1992) has shown that raising the sample humidity increases the amount of water inserted around the lipid headgroup, thus increasing the lipid chain tilt angle and reducing the bilayer thickness. In contrast to gel phase DPPC bilayers, DOPC bilayers (Chapter 4) exhibit a general increase in bilayer size with increasing humidity as they are in the chain disordered fluid (L_{α}) phase.

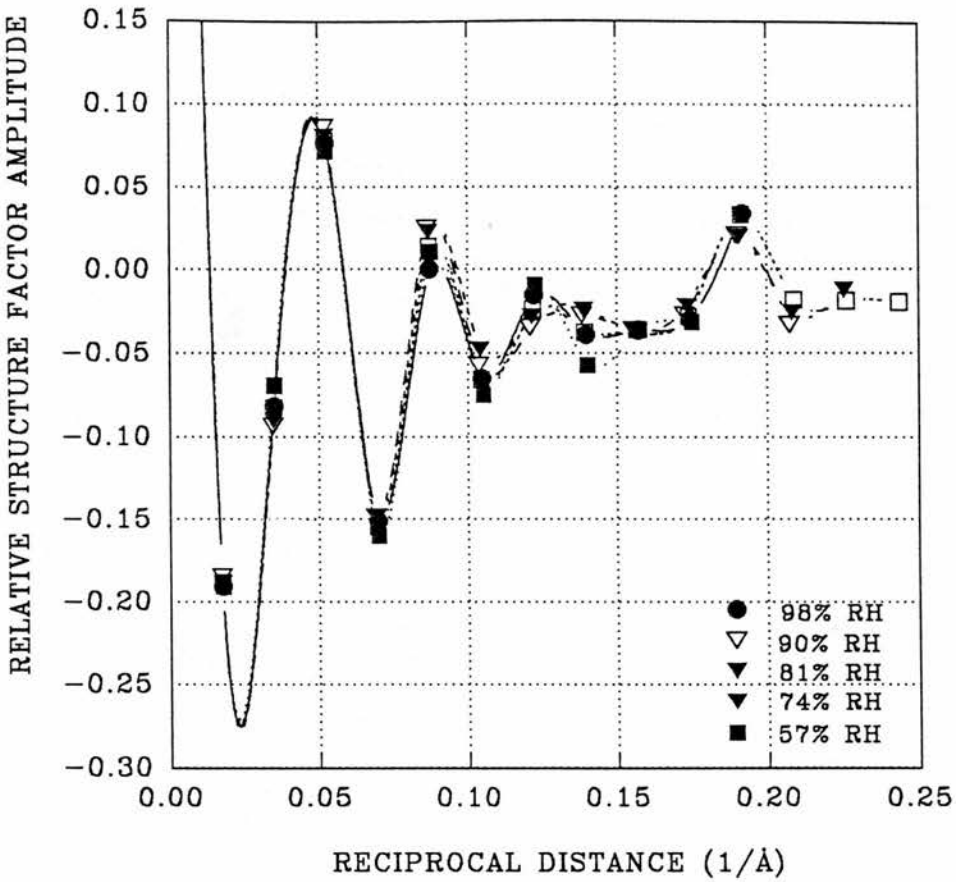

Figure 5.1 The swelling series plot used to phase the diffraction data collected from oriented DPPC bilayers at 20°C and between 98% and 57% RH. Diffraction data were collected out to fourteen orders from the DPPC bilayer samples. The symbols represent the structure factor amplitude value of each order plotted against h/D (h is the order number and D is the bilayer thickness). The plotted lines are spline curves fitted to the data, as estimates of the form of the continuous Fourier transform.

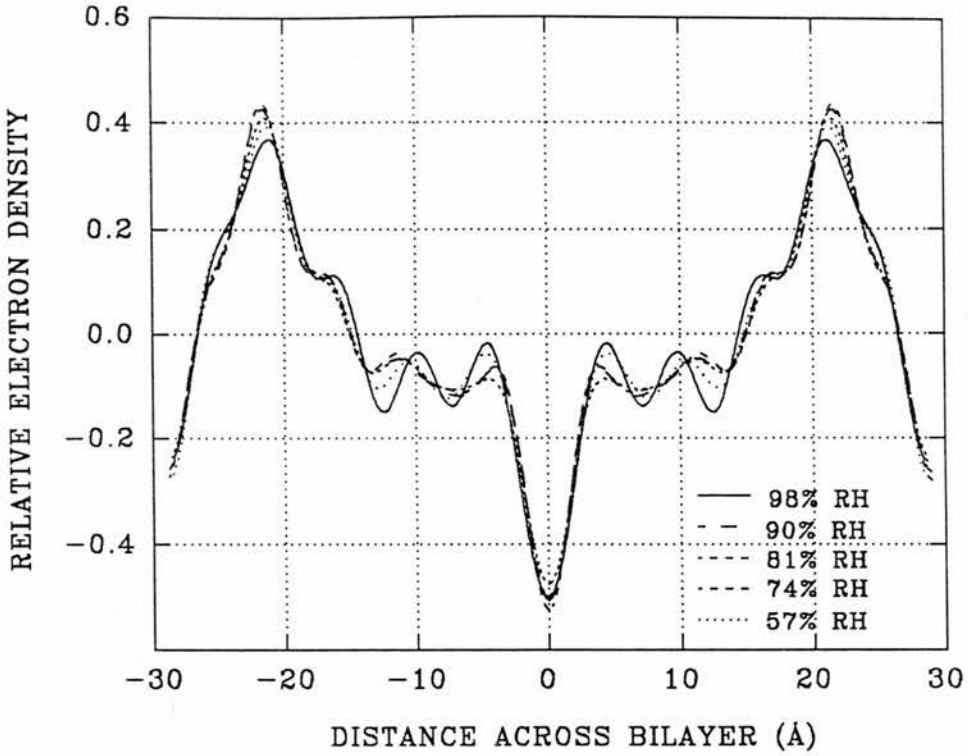

Figure 5.2 The electron density distribution maps of DPPC bilayers. Diffraction data were collected from oriented DPPC samples at 20°C and between 98% and 57% RH and phased using the swelling series method (Figure 5.1). The electron density maps were constructed using up to twelve orders of diffraction, if available, at each humidity studied. The DPPC phosphate headgroup, the ester linkage group and the lipid layer can be located at ±22Å, ±17Å and -15Å to +15Å respectively. The electron density distribution maps do not, however, take truncation or data accuracy errors into account.

The electron density maps of DPPC (Figure 5.2) were constructed using up to twelve orders of diffraction and the phase assignments generated by the swelling series method (Figure 5.1). It is the higher order phases, however, which are most difficult to phase unambiguously using the swelling series method. To judge the importance of the higher orders, DPPC electron density maps (data from DPPC at 20°C and 90% RH) have been constructed using between nine and twelve orders (Figure 5.3). The graphs show that each subsequent higher order of diffraction contributes only a small amount to the electron density map construction. The contribution of each order to the electron density map also indicates the error level that would be incurred by incorrectly phasing that order. If the phase assignment of an order were incorrect, the electron density distribution would be shifted in an equal but opposite direction from the true distribution by the inclusion of that order. Any single higher order (orders 10, 11 or 12) phase assignment error would not appear to greatly distort the calculated electron density distribution (Figure 5.3).

The 95% confidence limits for the DPPC electron density distribution were calculated by a Monte Carlo simulation program, using twelve orders of diffraction and either the variation (over all humidities studied) in diffraction data listed in Table 5.1, or a standard deviation error limit for all diffraction orders of 6% (Figure 5.4). Both structure factor amplitude error estimates produce similar 95% confidence limits for the DPPC electron density distribution, with the 6% estimate giving a slightly narrower confidence distribution. As the error limits of Table 5.1, calculated from the variation of DPPC diffraction data, are likely to represent an over-estimate, Figure 5.4 suggests that 6% is the error limit value to use for the structure factors.

5.3.3 Pure bromolipid bilayers at 20°C.

Oriented samples of the bromolipid at 20°C diffracted out to twelve meridional orders (Plate 5.2, Table 5.3). The swelling series plot used to phase the diffraction data from bromolipid bilayers, at 20°C and between 98% and 57% RH, is shown in Figure 5.5. Phases were assigned to the diffraction data using the

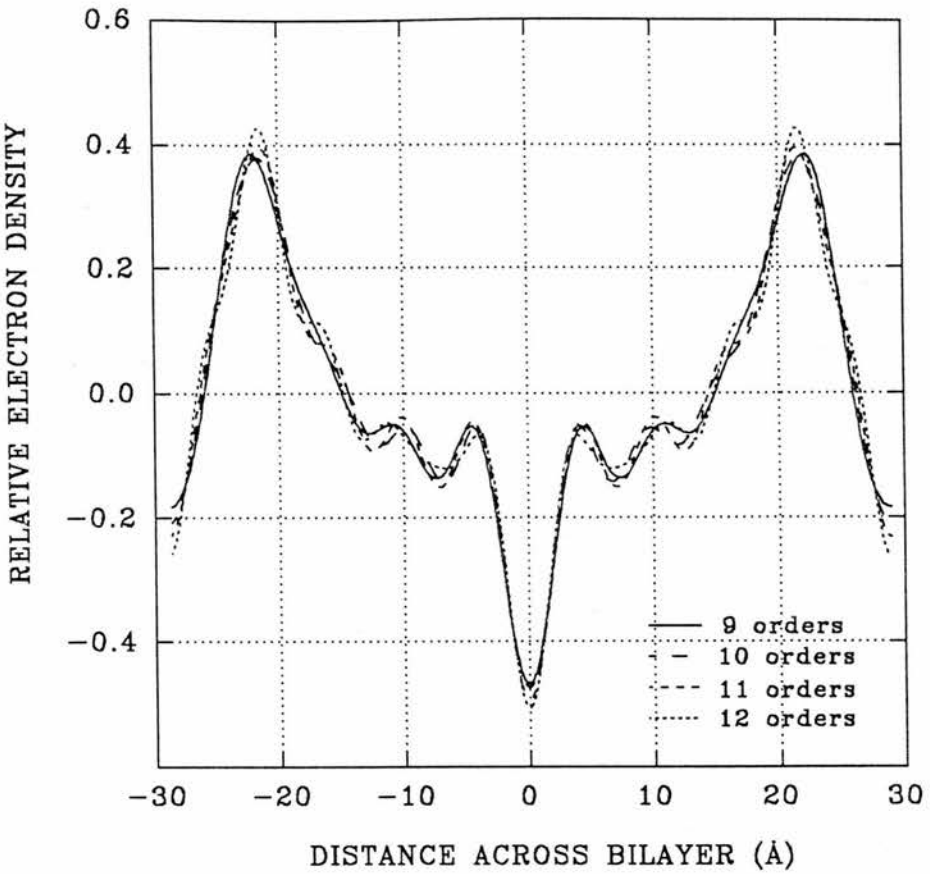

Figure 5.3 The electron density maps of DPPC bilayers constructed using a variable number of diffraction orders. Diffraction data were collected from oriented DPPC bilayers, at 20°C and between 98% and 57% RH, and phased using the swelling series method. The electron density maps of the 90% RH data were constructed using between nine and twelve orders of diffraction and the swelling series phase assignments (Figure 5.1). In all the electron density maps, the DPPC phosphate headgroup and centre of the lipid layer can be located at ±22Å and 0Å respectively. The outer orders (9-12), which are the most difficult to phase using the swelling series method, each only contribute a little to the overall electron density map construction. The incorrect phasing of one of these outer orders (9-12) would, therefore, only affect the electron density map construction to a small degree.

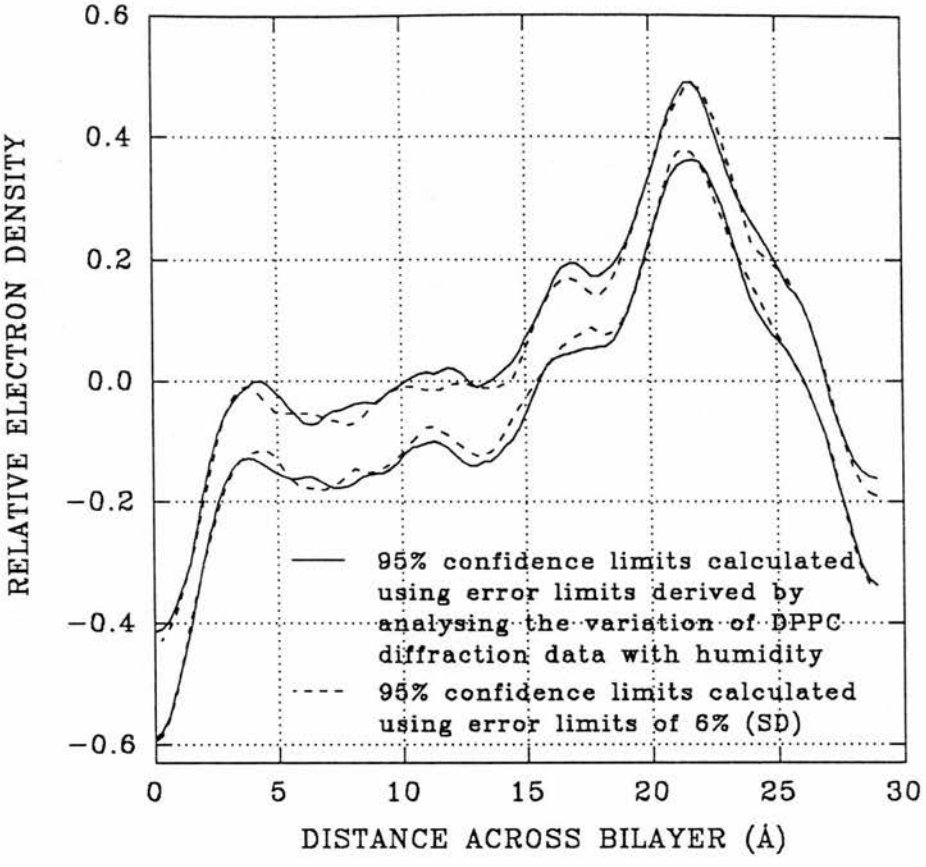

Figure 5.4 The 95% confidence limits for the DPPC bilayer electron density distribution. Only one half of the bilayer unit is shown, where the centre of the lipid and water layers are located at 0Å and 28Å, respectively. Diffraction data were collected from oriented DPPC bilayer samples at 20°C and 90% RH and phased using the swelling series method (Figure 5.1). The 95% confidence limits were calculated using a Monte Carlo simulation program and twelve orders of diffraction. Error limits for the structure factor amplitude data were either derived from the variations of the DPPC data with humidity (Table 5.1) or set at 6% (SD) for all orders. The two data error limits produce similar 95% confidence limits. The DPPC phosphate headgroups (22Å), the ester linkages (17Å) and the low electron density terminal methyl region (0Å) are all still clearly visible within the 95% confidence limit bounds.

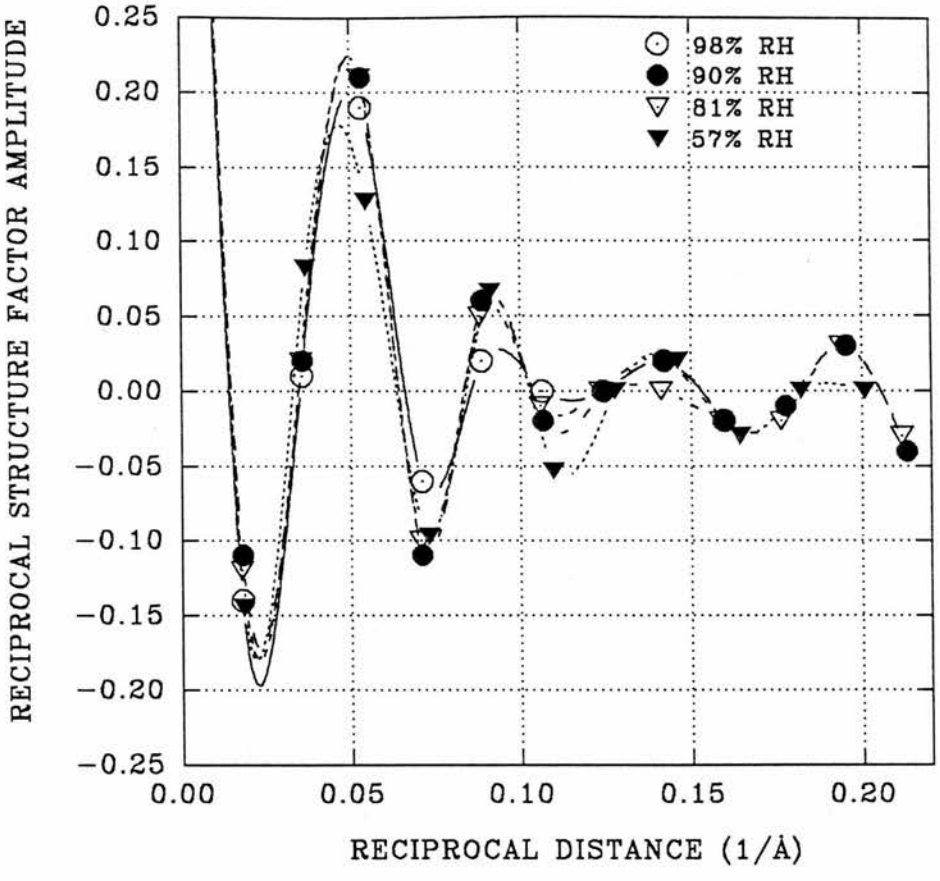

Figure 5.5 The swelling series plot used to phase the diffraction data collected from oriented bromolipid bilayers at 20°C and between 98% and 57% RH. Diffraction data were collected out to a maximum of twelve orders from the bromolipid bilayer samples. The symbols represent the structure factor amplitude of each order plotted against h/D (h is the order number and D is the bilayer thickness). The plotted lines are spline curves fitted to the data, as estimates of the form of the continuous Fourier transform. The bromolipid continuous Fourier transforms are positively shifted compared with the DPPC data (Figure 5.1), a result of the electron dense bromolipid bromine atoms being located at the centre of the lipid layer (Franks and Lieb, 1981).

method of calculating continuous Fourier transforms for the data, then constructing electron density maps using the chosen phases. The bromolipid structure factor phase assignments and bilayer repeats, calculated using Bragg's law (equation 2.2), are given in Table 5.2. In comparison with the swelling series plot for DPPC (Figure 5.1), the continuous Fourier transform fitted to the bromolipid data is shifted in the positive direction (Figure 5.5). The positive shift is a direct result of having a large scattering mass at the centre of the bilayer (Franks and Leib, 1981).

The electron density maps of bromolipid bilayers at 20°C, and between 98% and 57% RH, were constructed using up to twelve orders of diffraction and the phase assignments obtained using the swelling series method (Figure 5.6). The electron density maps locate the bromolipid phosphate headgroups and ester-linkage regions at ±21Å and ±17Å respectively from the centre of the lipid layer (0Å). The bromolipid formed bilayers that were several Angstroms thinner than the equivalent DPPC bilayers under the same conditions of temperature and humidity (Tables 5.1 and 5.2). The reduction in bilayer thickness could be attributable to several factors:

1) an increase in the lipid chain tilt angle;
2) bromolipid and DPPC bilayers hydrate to different extents;
3) interdigitation at the centre of the bilayer;
4) the bromine atom creates disorder at the centre of the lipid layer or along the lipid chain thus shortening it by the creation of *gauche* bonds;
5) impurities in the phospholipid samples alter the bilayer structure.

No impurities were detected in either the bromolipid or DPPC bilayer samples by TLC (Chapter 3) and the chain tilt angle theory can be tested by analysis of the equilateral diffraction obtained from the membrane samples.

5.3.4 Measurement of the bromolipid and DPPC lipid chain tilt angle.

The [4.2Å^{-1}] equilateral diffraction data from gel phase bilayers (Table 5.3) provide a measure of the lipid chain tilt angle (Stumpel *et al.*, 1983). Equilateral [4.2Å^{-1}] diffraction peaks were measured at between 23°±1° and 25°±1° above the

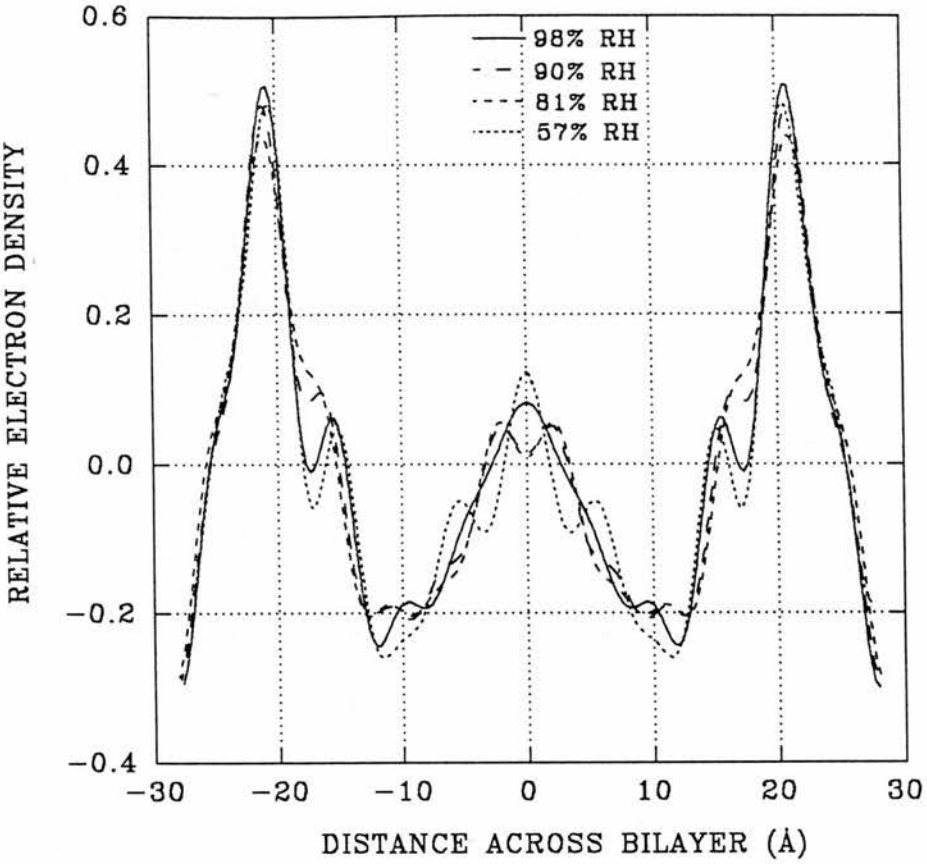

Figure 5.6 The bromolipid bilayer electron density distribution maps at 20°C. Diffraction data were collected from oriented bromolipid bilayer samples at 20°C and between 98% and 57% RH, and phased using the swelling series method (Figure 5.5). The electron density maps were constructed using up to twelve orders of diffraction at each humidity studied. The bromolipid phosphate headgroup, the ester linkage group and the centre of the lipid layer can be located at ±21Å, ±17Å and 0Å respectively. The bromolipid bromine atoms increase the electron density at the centre of the lipid layer, compared with the DPPC *sn*-2 lipid chain terminal methyl group electron density (Figure 5.2). The electron density distribution maps do not, however, take into account truncation or data accuracy errors.

equator from DPPC bilayers and between 23°±1° and 28°±1° from bromolipid bilayers. The observation that bromolipid bilayers, at 20°C, are up to 2.3Å thinner than the equivalent DPPC bilayers might be an indication of a lipid chain tilt angle difference between the two bilayer systems. The tilt angle data (Table 5.3), however, show that DPPC and bromolipid form bilayers with lipid chains packed at similar tilt angles. Assuming that DPPC lipid chains pack at an angle of ≈25° to form a lipid layer of width 30Å (Figure 5.2), the bromolipid lipid chain tilt angle would have to increase from that of DPPC to 32° to decrease the bilayer thickness by 2Å [30/cos(25)=28/cos(32)]. Clearly such a large increase in chain tilt (7°) does not occur in the bromolipid bilayer compared with the DPPC bilayer.

Table 5.3 shows the thickness of DPPC and bromolipid bilayers, the difference in the angle of the [4.2Å^{-1}] equilateral diffraction, and the difference in bilayer thickness that the chain tilt angle difference accounts for. Whilst at 90% RH the lipid chain tilt appears to account for up to 1Å of the bilayer thickness difference between DPPC and bromolipid bilayers, there appears to be no difference in the chain tilt angle between DPPC and bromolipid bilayers at 57% RH, even though the bilayer thickness difference (2.3Å) is at its greatest at this humidity. It appears therefore that factors other than the lipid chain tilt angle act to decrease the thickness of the bromolipid bilayers.

Table 5.3 Measurements of the [4.2Å^{-1}] equilateral diffraction spot angle above the equator from bromolipid and DPPC bilayer samples at 20°C.

Relative humidity	Bromolipid bilayer thickness (Å)	Bromolipid [4.2Å^{-1}] diffraction angle	DPPC bilayer thickness (Å)	DPPC [4.2Å^{-1}] diffraction angle	Decrease in a 33Å lipid layer attributed to a change in the chain tilt angle
98%	55.9	28 ±1°	57.9	25 ±1°	0.8Å of 2.0Å
90%	56.3	28 ±1°	58.0	24 ±1°	1.0Å of 1.7Å
81%	56.7	27 ±1°	57.7	25 ±1°	0.5Å of 1.0Å
74%	55.7	25 ±1°	57.5	24 ±1°	0.2Å of 1.8Å
57%	54.8	23 ±1°	57.1	23 ±1°	0.0Å of 2.3Å

5.4 Scaling the DPPC and bromolipid electron density distribution maps.

The magnitude of the zero order structure factor defines the mean scattering density (Franks and Leib, 1981). However, the zero order cannot be collected as it is lost in the main beam, making the placement of electron density on anything other than a relative scale difficult. An absolute scale for electron density maps can be achieved, but requires knowledge of the average lipid area, which is not determined from the diffraction experiment (Wiener and White, 1991). The DPPC and bromolipid electron density maps were, therefore, only placed on a relative scale. To scale the electron density maps to one another, the DPPC electron density map was multiplied by a factor which matched the height of its electron dense phosphate headgroup with that of the bromolipid (Figure 5.7). To match the headgroup peak heights, the DPPC electron density profiles, at every humidity were multiplied by a factor of 1.2. This scaling, however, presumes that the phosphate headgroups of the two phospholipids should actually produce the same peak height. As the two phospholipids only differ at the centre of the lipid layer, far removed from the headgroup, the scaling method was felt to be reasonable approach to take. Although conformational differences of the DPPC and bromolipid headgroup and glycerol backbone regions could result in the two phospholipids having distinct peak heights, the electron density maps do not suggest such a difference to exist.

5.4.1 Comparison of the DPPC and bromolipid electron density distribution maps.

Comparison of the DPPC and bromolipid electron density maps (Figure 5.7, data from bilayers at 90% RH) shows that the major difference between the two systems lies at the centre of the lipid layer, the location of the electron dense bromolipid bromine atoms. The bilayer thickness difference between the bromolipid and DPPC bilayers (56.7-54.7Å versus 58.0-57.1Å respectively, at 20°C and 98-57% RH) is *ca* 2Å. As both the DPPC and bromolipid headgroups ($\pm$22Å for DPPC and $\pm$21Å for bromolipid) are located 7Å from the centre of the water layer ($\pm$28Å for DPPC and $\pm$27Å for bromolipid), the electron density maps show that

the disparity in bilayer thickness between DPPC and bromolipid may be attributable to differences in the lipid chain layer.

The bromolipid minus DPPC difference map (Figure 5.7 [bottom], data from bilayer samples at 20°C and 90% RH) reveals a large peak of electron density, presumably the bromine atoms merging to form a single peak, at the centre of the bromolipid lipid layer. The difference map (Figure 5.7 [bottom]) does not have a level baseline, suggesting that structural differences between DPPC and bromolipid exist, a fact already highlighted by the bilayer thickness measurements.

5.4.2 Comparison of the DPPC and bromolipid bilayers 95% confidence limits.

A Monte Carlo simulation program has been applied to the diffraction data obtained from DPPC and bromolipid bilayers at 20°C and 90% RH, using a structure factor amplitude error limit of 6% for all diffraction orders (Figure 5.8). The calculated 95% confidence limits (Figure 5.8) indicate that the DPPC and bromolipid bilayers are structurally indistinguishable from the centre of the free water layer (28Å) to the ester linkage region (17Å). Major structural differences between the two bilayer systems occur over the entire lipid chain region (17Å-0Å), with the largest difference being at the centre of the lipid layer.

A Monte Carlo simulation program was used to calculate the 95% confidence limits of the bromolipid minus DPPC difference map, using the difference structure factor amplitude standard deviation of 8.5% ($8.5\% = \sqrt{[6\%^2 + 6\%^2]}$). The difference map indicates that the major difference between the bromolipid and DPPC bilayers is the existence of a large peak of electron density at the centre of the bromolipid lipid layer (–5 to +5Å). The data suggests that the bromine peak of Figure 5.9 has a height of 0.52 ±0.05 relative units.

5.5 Gaussian distribution fitting to the bromine peak

The DPPC minus bromolipid distribution at the centre of the lipid layer (Figure 5.9) is putatively the electron density of two bromine atoms (more

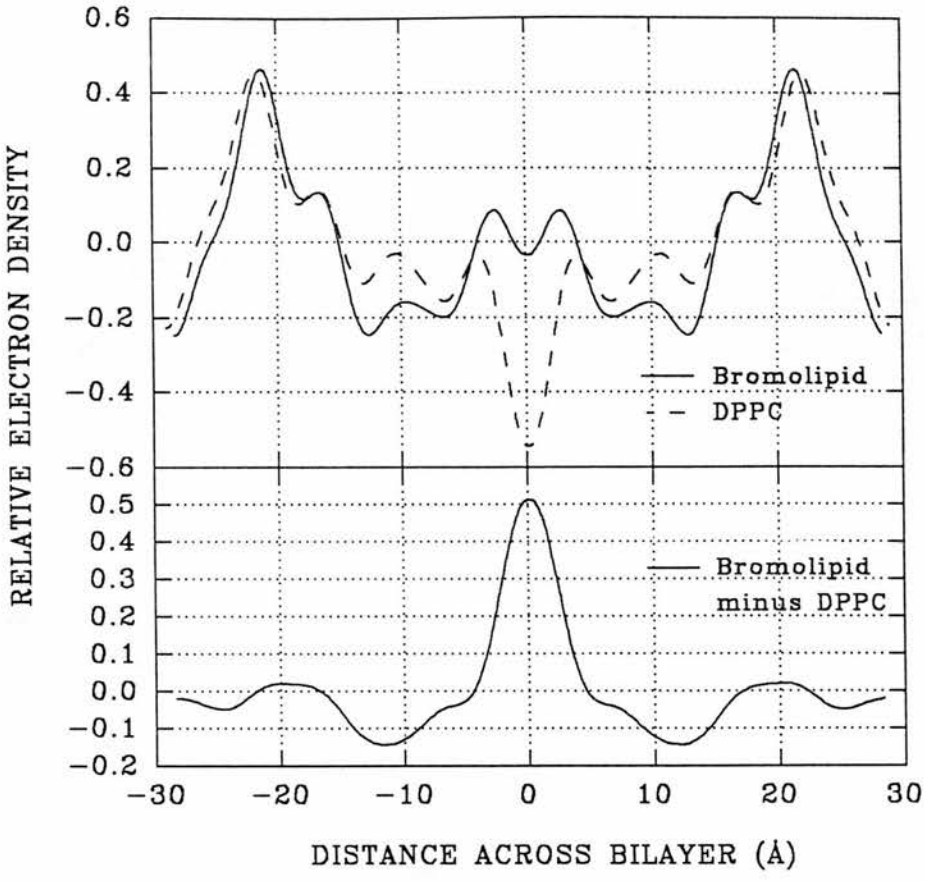

Figure 5.7 Comparison of the bromolipid and DPPC bilayer electron density maps. Each of the electron density maps (top) were constructed using twelve orders of diffraction, collected from oriented bilayer samples at 20°C and 90% RH. The two systems were scaled together by multiplying the DPPC profile by a factor of 1.2. Although the bromolipid and DPPC bilayers differ in thickness (56.3Å versus 58Å respectively), their phosphate headgroups (22-21Å) and ester linkage groups (17Å) are similarly situated. Larger structure variations occur between the two bilayer structures in the lipid layer (-15Å to+15Å). The bromolipid minus DPPC difference electron density map (bottom) highlights the presence of the electron dense bromolipid bromine atoms at the centre of the lipid layer.

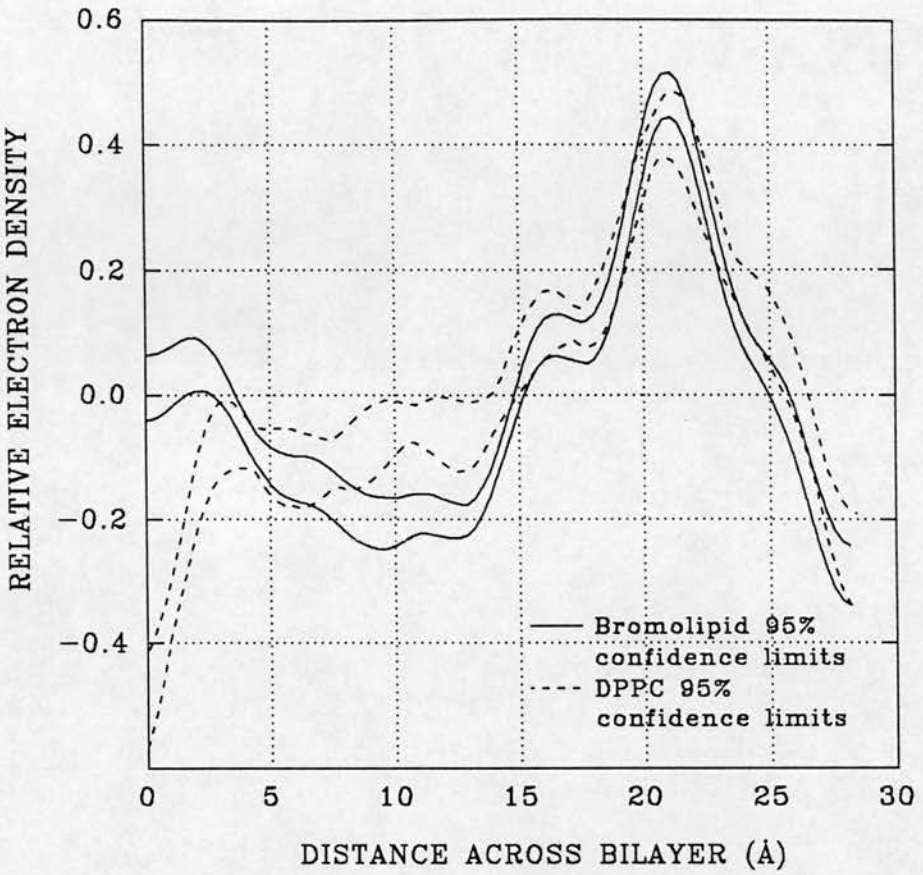

Figure 5.8 Comparison of the 95% confidence limits for the bromolipid and DPPC bilayer electron density distributions. Only one half of each bilayer unit is shown, where the centre of the lipid and water layers are located at 0Å and 27-28Å, respectively. Diffraction data, collected from oriented bilayer samples at 20°C and between 98% and 57% RH, were phased using the swelling series method. The 95% confidence limits were calculated using a Monte Carlo simulation program and twelve orders of diffraction. Error limits for the structure factor amplitude data were set at 6% (SD) for all orders. The two systems were scaled together by multiplying the DPPC profile by a factor of 1.2. The bromolipid and DPPC bilayers are indistinguishable from the centre of the water layer (27-28Å) to the ester linkages (17Å), when using the 95% confidence limit bounds. The bromolipid bromine atoms clearly increase the electron density at the centre of the lipid layer (0-4Å). There also appears to be another discernible difference in electron density (5Å to 15Å) between the bromolipid and DPPC bilayers.

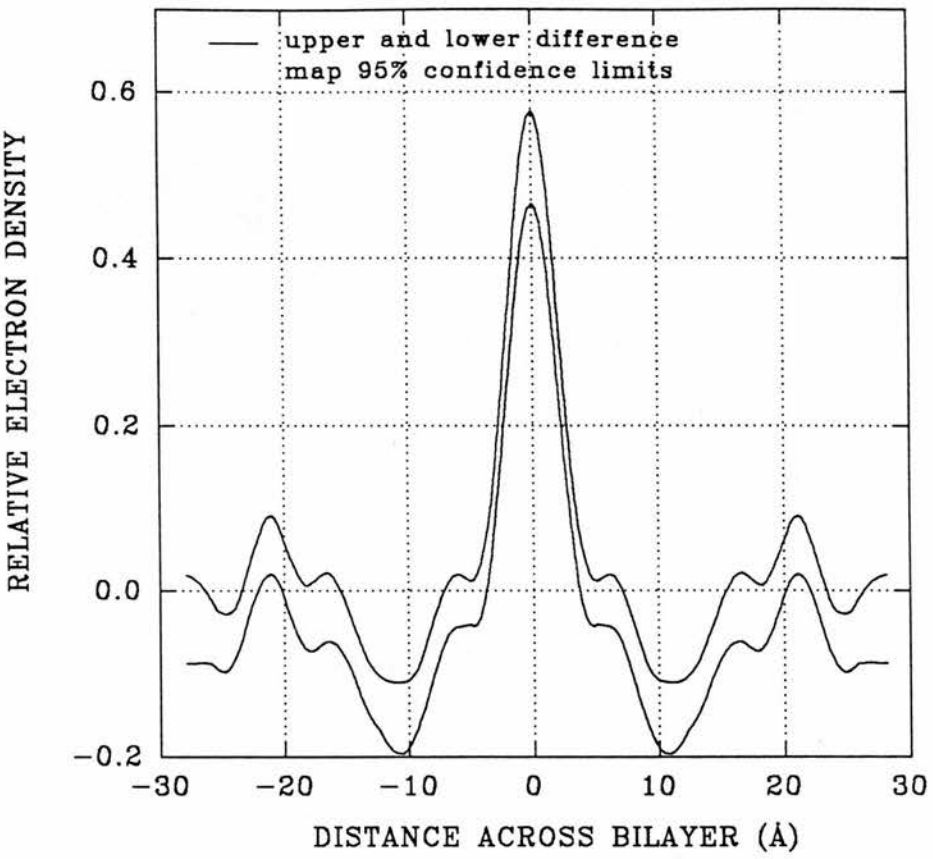

Figure 5.9 The 95% confidence limits for the bromolipid minus DPPC difference map. Diffraction data were collected from oriented bilayer samples at 20°C and 90% RH and phased using the swelling series method. Twelve orders of structure factor amplitude difference values (bromolipid minus DPPC) were used in a Monte Carlo simulation program to calculate the 95% confidence limits for the difference map electron density distribution. A structure factor amplitude difference value error limit of 8.5% (SD) was also used in the map calculation. The difference map indicates that the bromolipid bromine atoms substantially increase the electron density at the centre of the lipid layer. The bromolipid and DPPC bilayers also differ significantly in electron density between 5Å and 15Å.

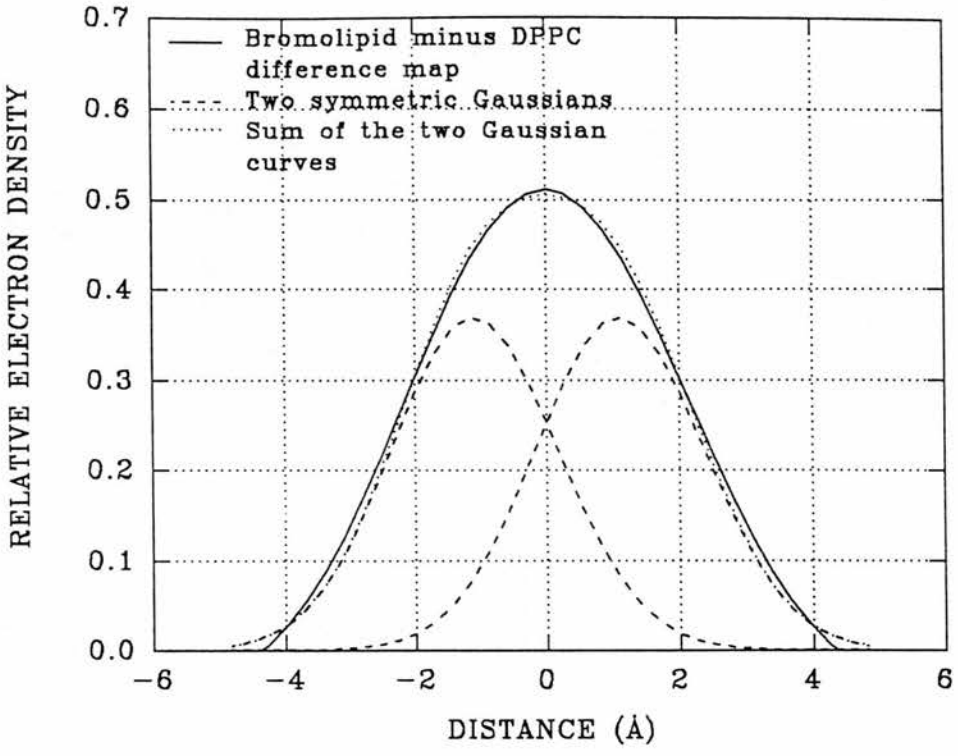

Figure 5.10 Gaussian fitting to the bromolipid minus DPPC difference map at the centre of the lipid layer. Diffraction data, collected from oriented bilayer samples at 20°C and 98% and 57% RH (90% RH data shown), were phased using the swelling series method. The difference map (-6Å to+6Å, shown above) was constructed by Fourier transforming the difference in structure factor amplitude values, between bromolipid and DPPC bilayers, out to twelve orders. Two mirror image (about 0Å) Gaussian distributions were adjusted in size, shape and position, until their combined distribution fitted the difference map electron density distribution. Assuming that the difference map profile is the result of the addition of two bromine atoms, each with a Gaussian distribution, the above graph suggests that the two bromolipid bromine atoms are separated at the centre of the lipid layer by only 2Å.

accurately the electron density of two bromolipid bromine atoms minus two DPPC methyl groups). Assuming that the subtraction peak at the centre of the lipid layer is wholly due to the overlapping electron density of two bromine atoms having a Gaussian distribution in the bilayer, the separation of the bromine atoms at the centre of the bilayer can be obtained by fitting two Gaussian distributions to the subtraction peak. Gaussian fitting to the bromolipid/DPPC subtraction data has been performed (Figure 5.10) and shows that the subtraction peak can be described by two Gaussian distributed atoms placed *ca* 2Å apart.

5.6 Differential scanning calorimetry (DSC) study of bromolipid and DPPC.

The aim of the differential scanning calorimetry (DSC) experiments was to study the thermal behaviour of the bromolipid, in comparison with DPPC. As the bromolipid was expected to be used in diffraction experiments mixed with DPPC, calorimetry experiments have also been performed on a 1:1 mixture of the two lipids. The DSC study can be divided into two sections:

1) A study of the phase nature of fully hydrated bromolipid and DPPC between 10°C and 70°C.
2) A study of the phase nature of a fully hydrated 1:1 (wt) mixture of bromolipid and DPPC between 10°C and 70°C.

DSC sample preparation and methodology are described in Chapter 3.

5.6.1 Results of DSC experiments.

Figure 5.11 shows a typical thermogram of heat flow versus temperature for pure DPPC in excess water. The main peak at 42.5°C is the lipid chain melting transition between the $P_{\beta'}$ (gel ripple) and L_{α} (fluid) phases (Chapman *et al.*, 1967). The peak at 37.3°C is the well documented $L_{\beta'}$ (gel lamellar) to $P_{\beta'}$ (gel ripple) (Rand *et al.*, 1975; Janiak *et al.*, 1976) pretransition. The peak at 26°C is an experimental artefact and can be discounted. Figure 5.12 shows the thermogram of a pure bromolipid sample in excess water. The main peak transition of bromolipid

(33.7°C) occurs nearly 9° lower than the equivalent DPPC transition. Thermograms were also collected from a 1:1 mixture of DPPC and bromolipid (Figure 5.13), showing the lipid mixture to have a main transition at 36.7°C and a pretransition peak at 31.8°C (Table 5.4).

5.6.2 Conclusions of the DSC study.

The calorimetry results (Table 5.4) show that bromolipid bilayers melt co-operatively in a similar fashion to those of DPPC, as indicated by the shape and enthalpy of the lipid chain melting peaks (42.5°C and 33.7°C for DPPC and bromolipid respectively, Figures 5.11 and 5.12). Although they differ in their main phase melting temperature, both DPPC and bromolipid bilayers melt into the L_{α} conformation with a similar enthalpy. However, the chain melting events of DPPC and bromolipid samples occur at temperatures 9° apart, suggesting that the bromolipid gel phase lipid chain packing is disrupted by the bromine/methyl exchange. The results also show that the bromolipid has a gel to ripple phase pretransition of a much smaller enthalpy than DPPC. Both DPPC and bromolipid bilayers below the pretransition temperature form $L_{\beta'}$ phase bilayers, verified by the X-ray diffraction work, but the bromolipid chains incorporating a bromine atom are packing in a way possibly hindering $P_{\beta'}$ phase formation.

Table 5.4 DPPC, bromolipid and 1:1 (DPPC:bromolipid) mixture differential scanning calorimetry data.

Lipid /Lipid mixture	Pretransition temperature (°C)	Main transition temperature (°C)	Enthalpy of main transition (KJ/mol)	Enthalpy of pretransition (KJ/mol)
DPPC in excess water	37.2 ±0.2	42.5 ±0.2	38.2 ±2	5.8 ±0.3
bromolipid in excess water	30.5 ±0.2	33.7 ±0.4	43.5 ±2	small
1:1 (wt) mixture of DPPC and bromolipid	31.8 ±0.2	36.7 ±0.1	36.8 ±2	1.8 ±0.2

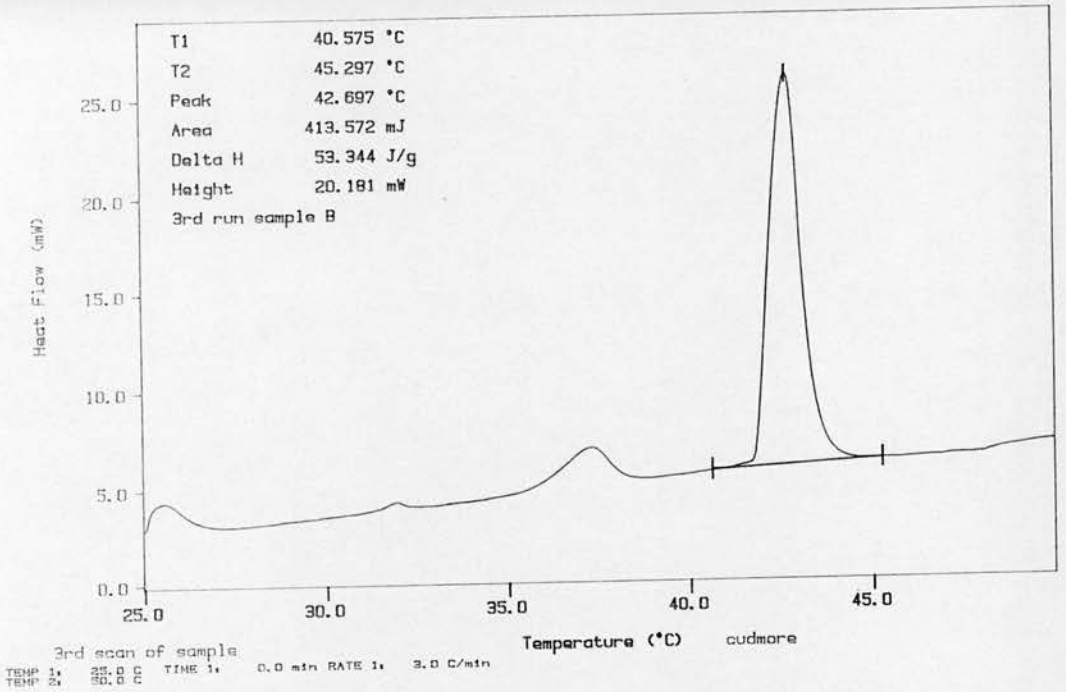

Figure 5.11 DSC plot of fully hydrated DPPC. The plot shows the main phase $P_{\beta'}$–L_{α} transition occurring at 42.7°C and the $L_{\beta'}$–$P_{\beta'}$ pretransition at 37.3°C. The small peak at *ca* 32°C has not been previously reported for DPPC, and has been taken to be an experimental artifact. A chloroform solution of DPPC (20mg/ml) was dried down in a rotary evaporator, then washed twice with acetone, before finally being dried down in a rotary evaporator to a solid. The dry sample was then placed in a 50µl volume platinum pan and the total mass of lipid weighed using a four point balance. Water (5.7 µl water/mg) was injected by syringe into the pan containing the dried lipid sample. A reference pan containing only water was also prepared for the experiments. Pan lids were sealed onto the sample pans by cold welding using a Perkin Elmer sealing press. Experiments were carried out using a Perkin Elmer DSC 7 machine with a Perkin Elmer Tac 7/7 instrument controller. Samples were loaded into the calorimeter and cycled from 10°C to 70°C, to anneal and homogenise the sample. The sample was then allowed to equilibrate at 10°C for 30 minutes before an experimental run from 10°C to 70°C was recorded.

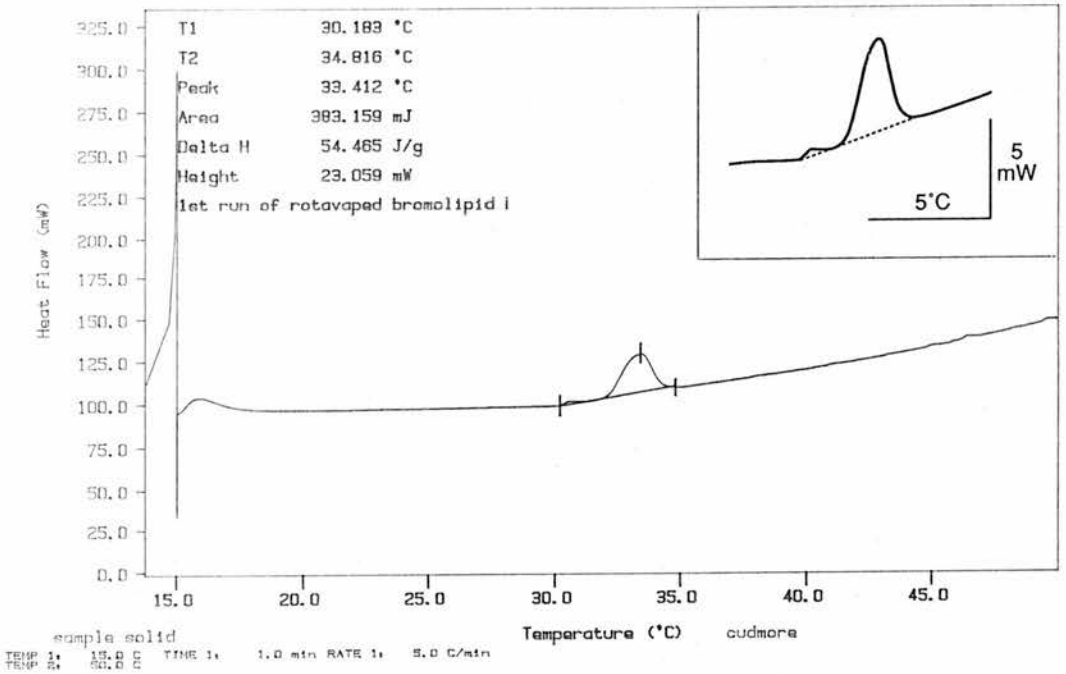

Figure 5.12 DSC plot of fully hydrated bromolipid. The main $P_{\beta'}$–L_{α} phase transition is at 33.4°C. The insert (top right of plot) is a magnification of the plot to show the presence of the pretransition at 30.5°C. A chloroform solution of the bromolipid (20mg/ml) was dried down in a rotary evaporator, then washed twice with acetone, before finally being dried down in a rotary evaporator to a solid. The dry sample was then placed in a 50µl volume platinum pan and the total mass of lipid weighed using a four point balance. Water (5.7 µl water/mg) was injected by syringe into the pan containing the dried lipid sample. A reference pan containing only water was also prepared for the experiments. Pan lids were sealed onto the sample pans by cold welding using a Perkin Elmer sealing press. Experiments were carried out using a Perkin Elmer DSC 7 machine with a Perkin Elmer Tac 7/7 instrument controller. Samples were loaded into the calorimeter and cycled from 10°C to 70°C, to anneal and homogenise the sample. The sample was then allowed to equilibrate at 10°C for 30 minutes before an experimental run from 10°C to 70°C was recorded.

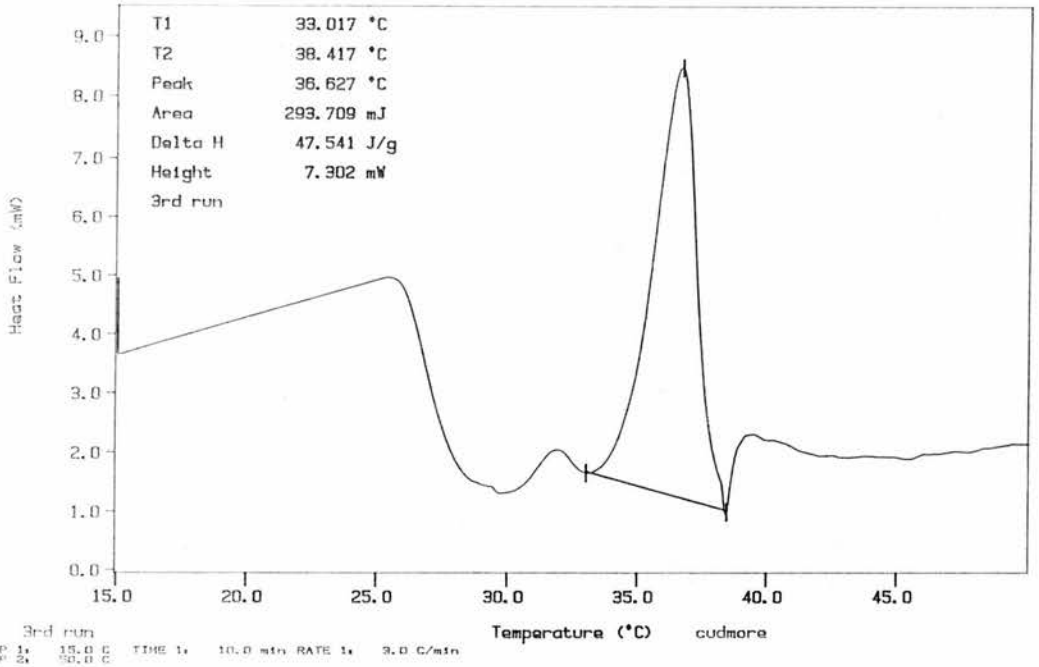

Figure 5.13 DSC plot of a fully hydrated 1:1 (mol:mol) mixture of DPPC and bromolipid. Against an uneven background can be seen the gel to ripple ($L_{\beta'}$–$P_{\beta'}$) and ripple to fluid ($P_{\beta'}$–L_{α}) phase transitions. The $P_{\beta'}$–L_{α} (36.6°C) and $L_{\beta'}$–$P_{\beta'}$ (31.8°C) transitions of the 1:1 mixture bilayers occur at temperatures intermediate between those found for DPPC and bromolipid bilayers. A chloroform solution of a 1:1 mix of DPPC and bromolipid (20mg/ml) was dried down in a rotary evaporator, then washed twice with acetone, before finally being dried down in a rotary evaporator to a solid. The dry sample was then placed in a 50µl volume platinum pan and the total mass of lipid weighed using a four point balance. Water (5.7 µl water/mg) was injected by syringe into the pan containing the dried lipid sample. A reference pan containing only water was also prepared for the experiments. Pan lids were sealed onto the sample pans by cold welding using a Perkin Elmer sealing press. Experiments were carried out using a Perkin Elmer DSC 7 machine with a Perkin Elmer Tac 7/7 instrument controller. Samples were loaded into the calorimeter and cycled from 10°C to 70°C, to anneal and homogenise the sample. The samples were then allowed to equilibrate at 10°C for 30 minutes before an experimental run from 10°C to 70°C was recorded.

A 1:1 bilayer mixture of DPPC and bromolipid had a main phase transition temperature that was intermediate between those of the pure species. The bromolipid bromine atoms, at a lower bilayer concentration, have a less disruptive effect on the bilayer packing in the mixed phospholipid bilayer, shown by the increase in size of the pretransition peak and the increase in phase melting temperatures.

5.7 Discussion of the bromolipid study.

X-ray diffraction patterns were collected from both oriented bromolipid and DPPC samples at 20°C and between 98% and 57% RH. The diffraction data were phased using the swelling series phasing method (Figures 5.1 and 5.5). Electron density map construction has shown that the bromolipid forms bilayers of a similar, but not identical, structure to those of DPPC (Figures 5.7 and 5.8). The major difference between bromolipid and DPPC bilayers is the presence of an electron dense region at the centre of the bromolipid lipid layer, presumably the bromine atom location in the bilayer. The two systems, however, also differ significantly across the entire lipid layer length (0 to 15Å, Figure 5.8).

Both DPPC and bromolipid form gel $L_{\beta'}$ phase bilayers at 20°C (Plates 5.1 and 5.2). The two species form bilayers that differ in thickness by 1-2.3Å at 20°C (Table 5.3), depending on humidity. Whilst the tilt angle data accounts for some of the difference in bilayer thickness between DPPC and bromolipid in all but the 57% RH bilayers, the bromolipid chain tilt does not increase by enough at any humidity to wholly account for the bilayer thickness differences. It appears therefore that factors other than chain tilt angle decrease the bromolipid bilayer thickness.

The bromine atoms of opposing bromolipid molecules in a bilayer structure have been estimated as being *ca* 2Å apart by Gaussian fitting to electron density map subtractions (Figure 5.10). As these *sn-2* chain terminals are so close in space, this would suggest that the *sn-1* chains, which penetrate deeper into the lipid layer for symmetric chain phospholipids (Zaccai *et al.*, 1979) must either interdigitate at the centre of the lipid layer or be distorted from their DPPC conformation (Figure

5.14). Whilst interdigitation of lipid chains has previously been described and characterised (Shah *et al.*, 1990; Huang and Mason, 1986; Mattai *et al.*, 1987) and would be a possible mechanism of reducing the bilayer thickness, a disorder at the centre of the lipid layer might be the more likely explanation.

The decrease in bilayer thickness of 1Å to 2.3Å represents only a change of 0.5-1.15Å per bromolipid molecule on either side of the membrane leaflet, less than the length of a single carbon-carbon bond. While the decrease in bilayer thickness is significant, i.e. some change has definitely happened, it does not necessarily represent a large distortion of the DPPC structure. The bromolipid has been synthesised for use in X-ray diffraction studies, primarily in mixtures with DPPC. In such mixtures, the bromolipid would be expected to have an even smaller disruptive effect on bilayer structure. The calorimetry results (Table 5.4) show that mixing bromolipid one to one with DPPC produces a bilayer with physical properties that approach those of pure DPPC. As the quantities of bromolipid required to be introduced into a DPPC bilayer for a 'labelling' effect in X-ray experiments may be quite small, it would have been useful to obtain calorimetry data from DPPC bilayers containing only small amounts of bromolipid.

Although designed as a symmetric chain analogue, the bromolipid is a mixed-chain phospholipid, as the *sn-1* and *sn-2* lipid chains differ in composition. While most investigations of phospholipid systems examine phospholipids of identical chain composition, more recently mixed-chain lipids have been studied (Keough and Davis, 1979; Stumpel *et al.*, 1981, 1983; Mason *et al.*, 1981 a, b, 1983; Huang *et al.*, 1983; Huang and Levin, 1983; McIntosh *et al.*, 1984; Lewis *et al.*, 1984; Tummler *et al.*, 1984; Hui *et al.*, 1984; Serrallach *et al.*, 1984). Even symmetric chain phospholipids form structures where the chains are conformationally inequivalent. The observed phospholipid chain length difference is related to the conformational inequivalence of the two acyl chains (Hitchcock *et al.*, 1974; Elder *et al.*, 1977; Pearson and Pascher, 1979). Neutron diffraction (Buldt *et al.*, 1979; Zaccai *et al.*, 1979) has established that the *sn-1* chain of gel phase DPPC penetrates deeper into the bilayer than the *sn-2* chain by approximately 1.5 carbon-carbon bond lengths, as the initial segment of the *sn-2* lipid chain lies

perpendicular to the *sn-1* chain. The difference in observed chain length becomes more pronounced as the length of the *sn-2* chain is reduced in length (Mattai *et al.*, 1987). To maximise van der Waals contacts in these gel phase bilayers, there must be interdigitation of the acyl chains across the centre of the bilayer (Chen and Sturtevant, 1981; Mason *et al.*, 1981b; Huang *et al.*, 1983; Hui *et al.*, 1984). In the absence of interdigitation, an energetically unfavourable chain packing situation would occur, with voids created toward the terminal methyl groups.

Figure 5.14 is a diagrammatic view of the centre of the bromolipid bilayer. The bromolipid bromine atoms have been estimated as being 2Å apart by Gaussian fitting to difference map data (Figure 5.10). If the bromolipid were structurally similar to DPPC at the centre of the bilayer, then the *sn-1* palmitoyl chains would penetrate approximately 2Å deeper into the centre of the bilayer than the bromine atoms, resulting in the palmitoyl chains interdigitating by *ca* 1Å. It can therefore be concluded that bromolipid is not identical to DPPC at the centre of the bilayer. The clashing of lipid chains at the centre of the lipid layer, which must result in deviation from the structure of DPPC, could either result in interdigitation or lipid chain disordering.

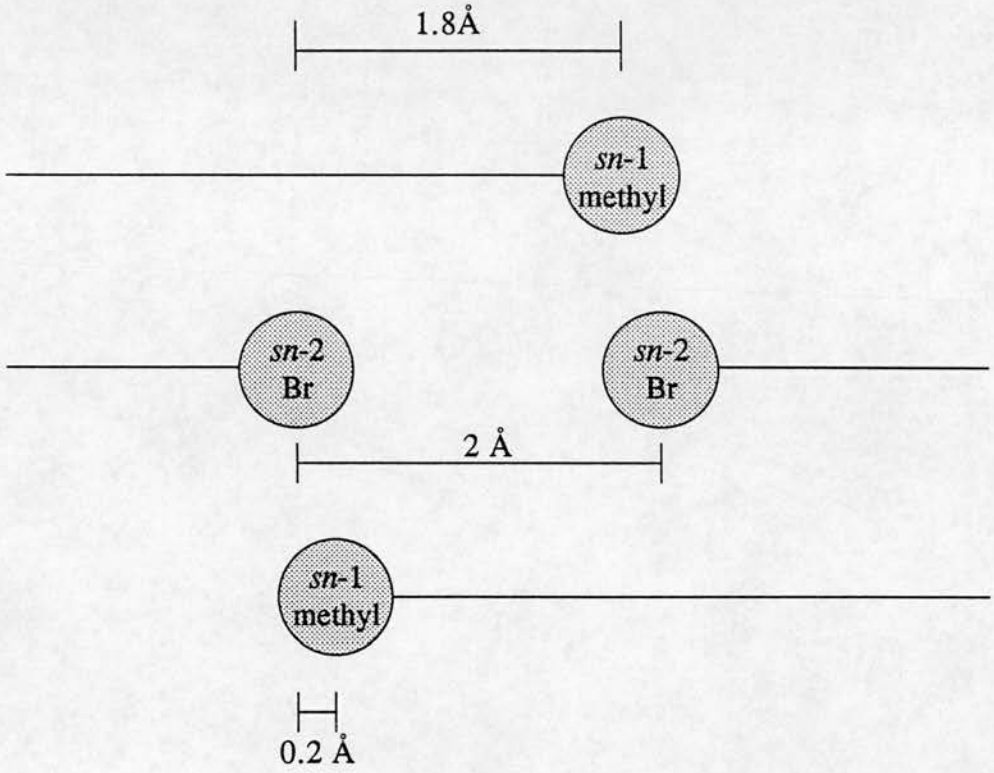

Figure 5.14 Illustration of events at the centre of the bromolipid lipid layer suggested by the X-ray diffraction study. The *sn*-1 terminus of DPPC has previously been estimated as being 1.8Å apart from the *sn*-2 terminus (Zaccai *et al.*, 1979). The bromine atom of bromolipid clearly marks the position of the *sn*-2 terminus. Gaussian fitting to the X-ray diffraction data suggests that the bromine atoms of opposing bromolipid molecules in a bilayer are *ca* 2Å apart. The *sn*-1 methyl groups of bromolipid would then have to interdigitate by 1.6Å to be the same distance away from the bromine atoms that the DPPC *sn*-1 and *sn*-2 groups have been found to be apart. The diagram suggests that the bromolipid must differ from DPPC at the centre of the lipid layer, with the bromolipid *sn*-1 palmitoyl chains being interdigitated or the lipid chains being disordered.

Chapter 6.

The use of bromolipid in isomorphous replacement experiments.

6.1 X-ray diffraction study of mixtures of DPPC and bromolipid.

A novel brominated structural analogue of DPPC, the bromolipid, has been synthesised (Chapter 3) and studied by X-ray diffraction and DSC (Chapter 5). The diffraction and calorimetry studies have shown that the pure bromolipid and DPPC differ in their bilayer conformation. A study of the bromolipid as mixtures with DPPC was carried out with several objectives:

1) to see if the DPPC:bromolipid mixture bilayer structure approaches that of the pure DPPC structure;
2) to use the DPPC:bromolipid mixture bilayer data to help elucidate conformational differences between pure bromolipid and DPPC bilayer structures;
3) to see if the bromolipid can act as a phasing agent in isomorphous replacement experiments.

The bromolipid, used as a phasing agent, would only be expected to make up a small proportion of the total lipid present in the membrane under study. Therefore, irrespective of the pure bromolipid structure, if the bromolipid is structurally similar to DPPC when mixed with DPPC (or only differs in a small and predictable manner) then it might be suitable for use as a phasing agent. Three different DPPC:bromolipid mixture ratios (1:1, 7:2 and 4:1) have been studied by X-ray diffraction and the swelling series method (Franks and Leib, 1981; Torbet and Wilkins, 1976). The two lipid mixture ratios which are dominated by DPPC (7:2 and 4:1) were chosen to be of a similar composition so that the sensitivity of the DPPC X-ray diffraction patterns to the presence of the bromolipid could be assessed. The mixture bilayers were studied as oriented samples at 20°C and between 98% and 57% RH.

6.1.1 Swelling series data from the DPPC:bromolipid mixture bilayers.

Meridional diffraction data were collected out to a maximum of twelve orders from the 1:1 DPPC:bromolipid mixture bilayers. A maximum of nine orders

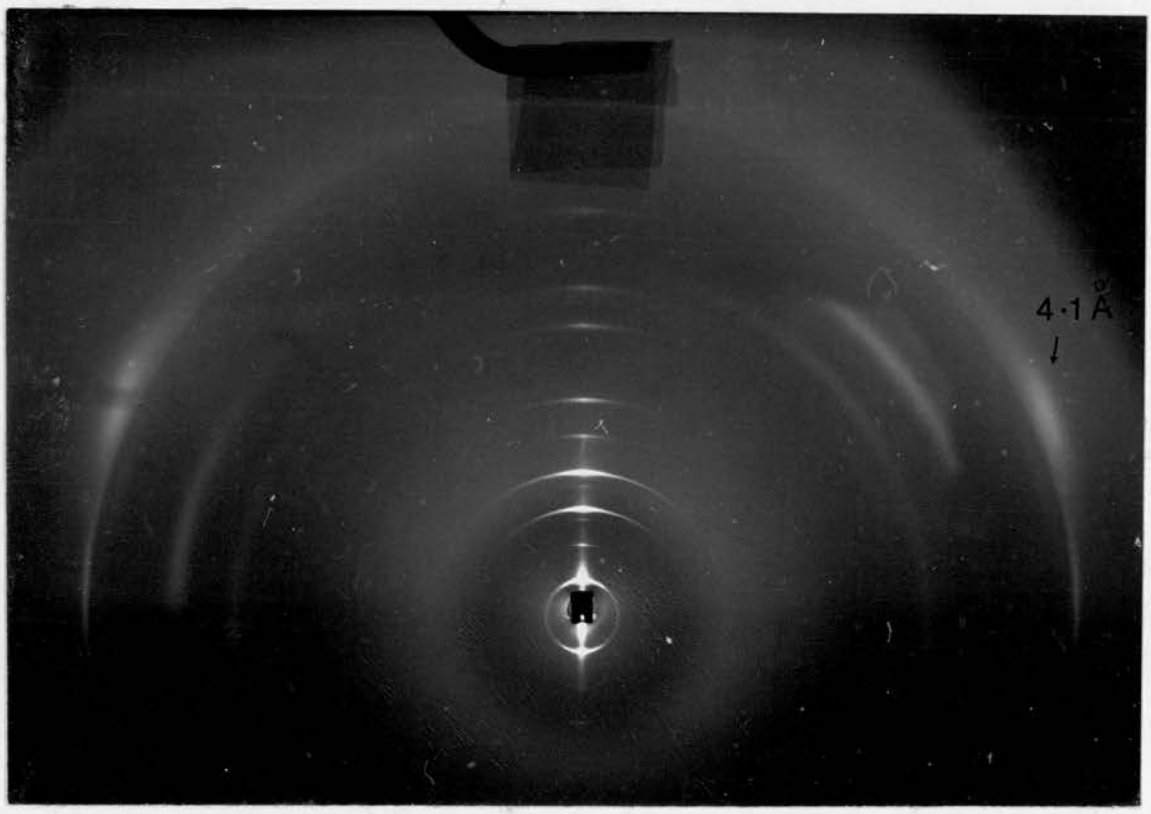

PLATE 6.1 The diffraction pattern collected from an oriented sample of a 1:1 mixture of DPPC and bromolipid at 20°C and 57% RH. Eleven meridional orders of diffraction can be seen on the plate, along with a diffraction spot at 4.1Å^{-1}. The 4.1Å^{-1} diffraction spot indicates that the mixture bilayers form the chain tilted gel ($L_{\beta'}$) phase.

Table 6.1 Diffraction data for the 1:1 DPPC:bromolipid mixture bilayer system.

Order number	Phased structure factor data				
1	–0.159	–0.149	–0.147	–0.143	–0.160
2	–0.029	–0.034	–0.044	–0.040	–0.025
3	+0.118	+0.122	+0.136	+0.134	+0.112
4	–0.109	–0.126	–0.121	–0.121	–0.110
5	+0.021	+0.028	+0.027	+0.025	+0.035
6	–0.033	–0.044	–0.037	–0.032	–0.052
7	0	+0.015	+0.012	0	0
8	+0.027	+0.037	+0.024	+0.018	+0.044
9	–0.032	–0.025	–0.025	–0.037	–0.039
10	0	–0.027	0	–0.011	–0.012
11	+0.060	+0.043	+0.030	+0.020	+0.037
12		+0.041			
Relative humidity	98%	90%	81%	74%	57%
Bilayer thickness (Å)	57.0±0.2	56.8±0.2	56.9±0.2	56.7±0.2	56.5±0.2
[4.2Å^{-1}] diffraction angle	26° ±1°	24° ±1°			24° ±1°

Table 6.2 Diffraction data for the 7:2 DPPC:bromolipid mixture bilayer system.

Order number	Phased structure factor data		
1	–0.191	–0.191	–0.202
2	–0.085	–0.073	–0.054
3	+0.121	+0.121	+0.109
4	–0.112	–0.125	–0.112
5	0	0	0
6	–0.028	–0.047	–0.029
7	–0.022	–0.040	0
8	0	0	–0.017
9	–0.024	–0.025	–0.030
Relative humidity	98%	90%	74%
Bilayer thickness (Å)	58.0±0.2	58.0±0.2	58.0±0.2

Table 6.3 Diffraction data for the 4:1 DPPC:bromolipid mixture bilayer system.

Order number	Phased structure factor data		
1	–0.198	–0.185	–0.185
2	–0.084	–0.092	–0.098
3	+0.077	+0.109	+0.109
4	–0.098	–0.140	–0.142
5	0	+0.026	+0.022
6	–0.034	–0.036	–0.035
7	–0.036	–0.037	–0.028
8	0	0	0
9	–0.030	–0.036	–0.030
Relative humidity	98%	90%	74%
Bilayer thickness (Å)	58.7±0.2	58.2±0.2	58.0±0.2

were collected from the 7:2 and 4:1 DPPC:bromolipid mixture bilayer systems. Plate 6.1 shows a typical diffraction pattern collected from the 1:1 mixture bilayers, with eleven meridional orders and a 4.1Å^{-1} equilateral spot indicative of phospholipids in the $L_{\beta'}$ tilted lipid chain phase (Chapman *et al.*, 1967; Levine 1972, 1973). The meridional diffraction spacing and Bragg's law (equation 2.2) were used, without phase information, to calculate the bilayer repeat distances (D) for the mixture bilayers (Tables 6.1, 6.2 and 6.3). The 1:1 mixture bilayers have a bilayer thickness that ranges between 57.0Å and 56.5Å, depending on humidity, which are intermediate between those measured from the two pure species (56.7-55.2Å and 58.0-57.0Å for bromolipid and DPPC respectively). The bilayer thickness measurements from the 7:2 (58.0Å) and 4:1 (58.0-58.7Å) DPPC:bromolipid mixture bilayers (Tables 6.2 and 6.3) are comparable to those measured from pure DPPC bilayers (57.5 to 58.0Å).

Except for the seventh order, the swelling series method assigned the same phases to the 1:1 mixture diffraction data that were assigned to the pure DPPC bilayer data (Figures 6.1 and 5.1). The second order, assigned a positive phase in the pure bromolipid data (Figure 5.5), changes to a negative phase in the 1:1 mixture bilayer data. Although the 7:2 DPPC:bromolipid mixture has a slightly

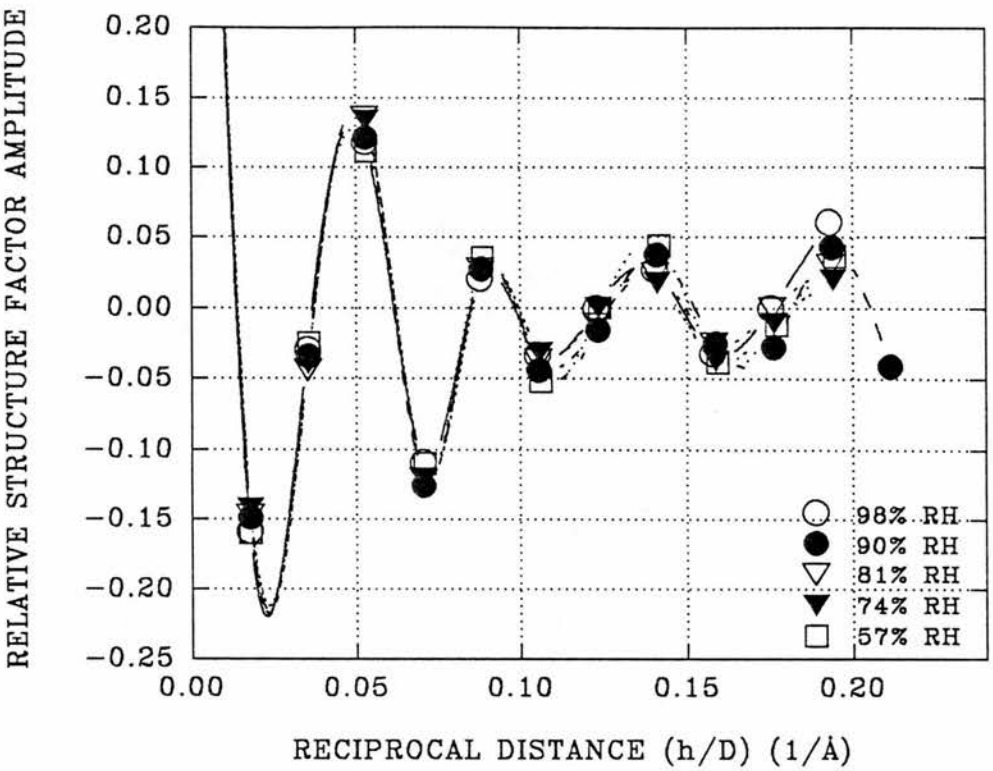

Figure 6.1 The swelling series plot used to phase the diffraction data collected from 1:1 (DPPC:bromolipid) mixture bilayers. Diffraction data were collected out to twelve orders from oriented bilayer samples, at 20°C and between 98% and 57% RH. The symbols represent the structure factor amplitude of each diffraction order plotted against h/D (h is the order number and D is the bilayer thickness). The plotted lines are spline curves fitted to the data, as estimates of the form of the continuous Fourier transform.

higher bromolipid concentration than the 4:1 mixture, the diffraction data collected from both of these bilayer systems were similar (Tables 6.2 and 6.3) and have both been allocated the same phases that were assigned to the pure DPPC bilayer data (Figures 6.2, 6.3 and 5.1). The eighth order of the 7:2 and 4:1 mixture bilayer data, which was assigned a positive phase for both the pure bromolipid and 1:1 mixture bilayer data (Figures 5.5 and 6.1), were either recorded as zero values, or assigned a negative phase (Figures 6.2 and 6.3).

6.2 Electron density map construction using the mixture bilayer diffraction data.

Electron density maps of 1:1 DPPC:bromolipid bilayers were constructed using up to twelve orders of diffraction (Figure 6.4). The maps locate the 1:1 lipid mixture phosphate headgroups and ester linkage regions at ±21Å and ±17Å respectively from the centre of the lipid layer (0Å). Electron density maps of both 7:2 and 4:1 DPPC:bromolipid mixture bilayers were also constructed, using only nine orders of diffraction (Figures 6.5 and 6.6). The electron density maps locate both the 7:2 and 4:1 DPPC:bromolipid mixture bilayer phosphate headgroups at ±22Å from the centre of the low electron density lipid layer (0Å). The ester-linkage region is more difficult to locate in these electron density maps (Figures 6.5 and 6.6), compared with the 17Å peak in the 1:1 mixture bilayer (Figure 6.4).

6.2.1 Scaling the DPPC and bromolipid mixture electron density distribution maps.

The DPPC and bromolipid electron density maps were only placed on a relative scale (Section 5.4). To scale the electron density maps to one another, the DPPC electron density map was multiplied by a factor which matched the height of its electron dense phosphate headgroup with that of the bromolipid (Figure 5.7). To match the headgroup peak heights, the DPPC electron density profiles were multiplied by a factor of 1.2.

The mixture bilayers were also scaled to the bromolipid data by matching up the phosphate peak heights. The scaling took the form of multiplying the 1:1

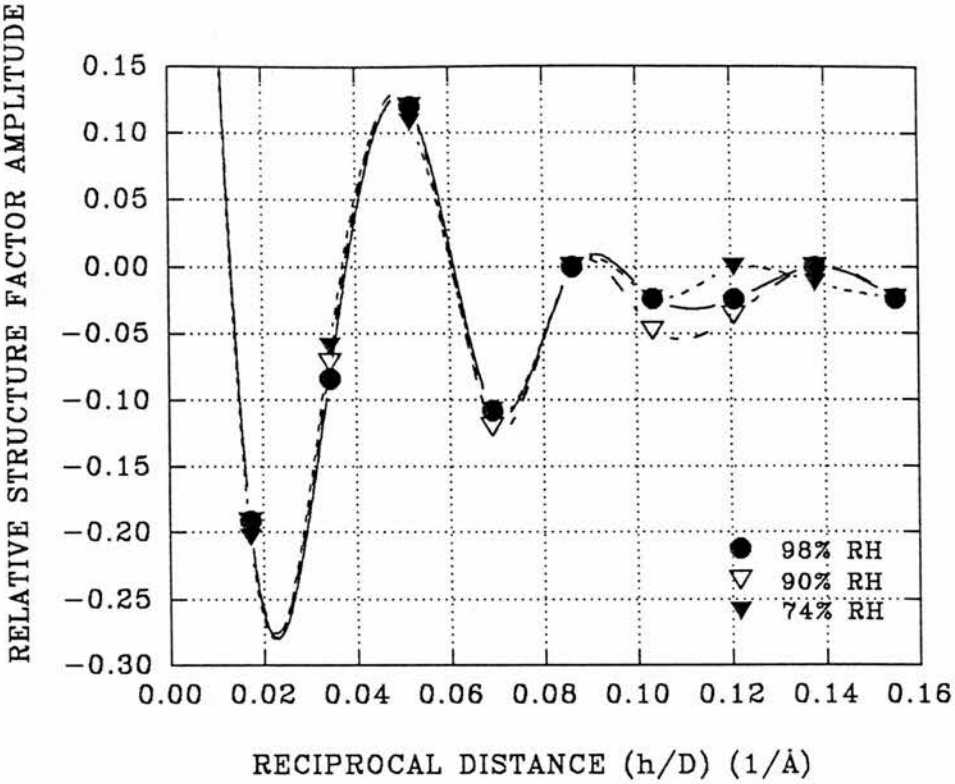

Figure 6.2 The swelling series plot used to phase the diffraction data collected from 7:2 (DPPC:bromolipid) mixture bilayers. Diffraction data were collected out to nine orders from oriented bilayer samples, at 20°C and either 98%, 90% or 74% RH. The swelling series has assigned the same phases to the 7:2 mixture bilayer data as those assigned to the pure DPPC bilayer data (Figure 5.1). The symbols represent the structure factor amplitude of each order plotted against h/D (h is the order number and D is the bilayer thickness). The plotted lines are spline curves fitted to the data, as estimates of the form of the continuous Fourier transform.

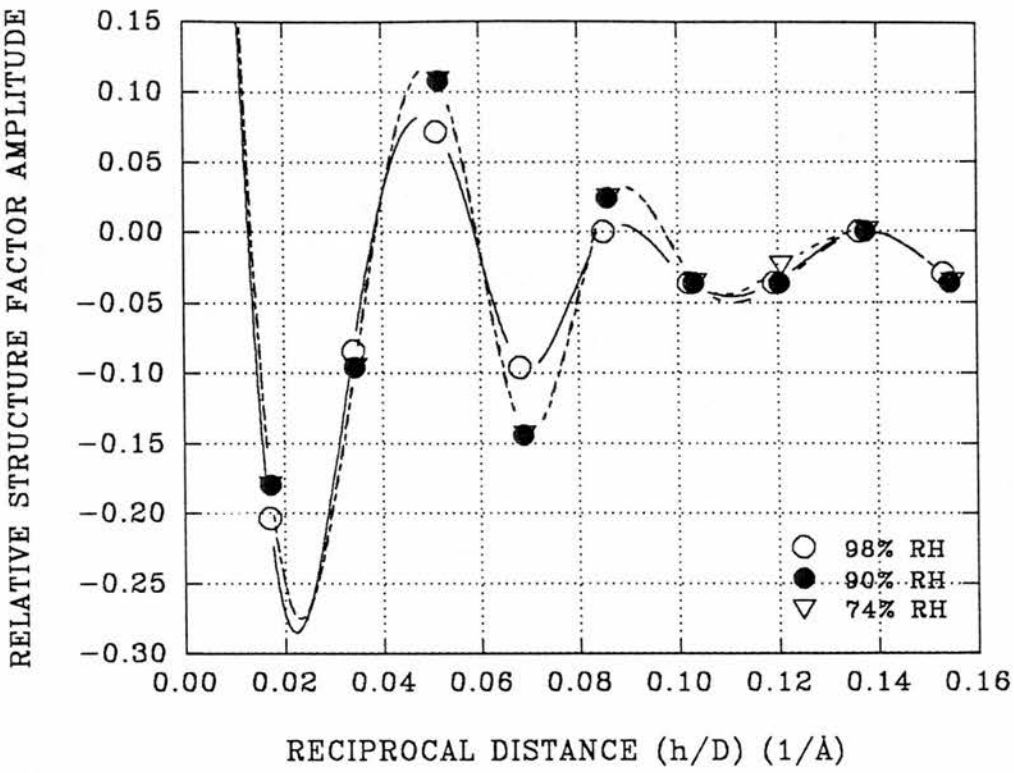

Figure 6.3 The swelling series method plot used to phase the diffraction data collected from 4:1 (DPPC:bromolipid) mixture bilayers. Diffraction data were collected out to nine orders from oriented bilayer samples, at 20°C and either 98%, 90% or 74% RH. The swelling series has assigned the same phases to the 4:1 mixture bilayer data that were assigned to both the 7:2 mixture bilayer (Figure 6.2) and the pure DPPC bilayer data (Figure 5.1). The symbols represent the structure factor amplitude of each order plotted against h/D (h is the order number and D is the bilayer thickness). The plotted lines are spline curves fitted to the data, as estimates of the form of the continuous Fourier transform.

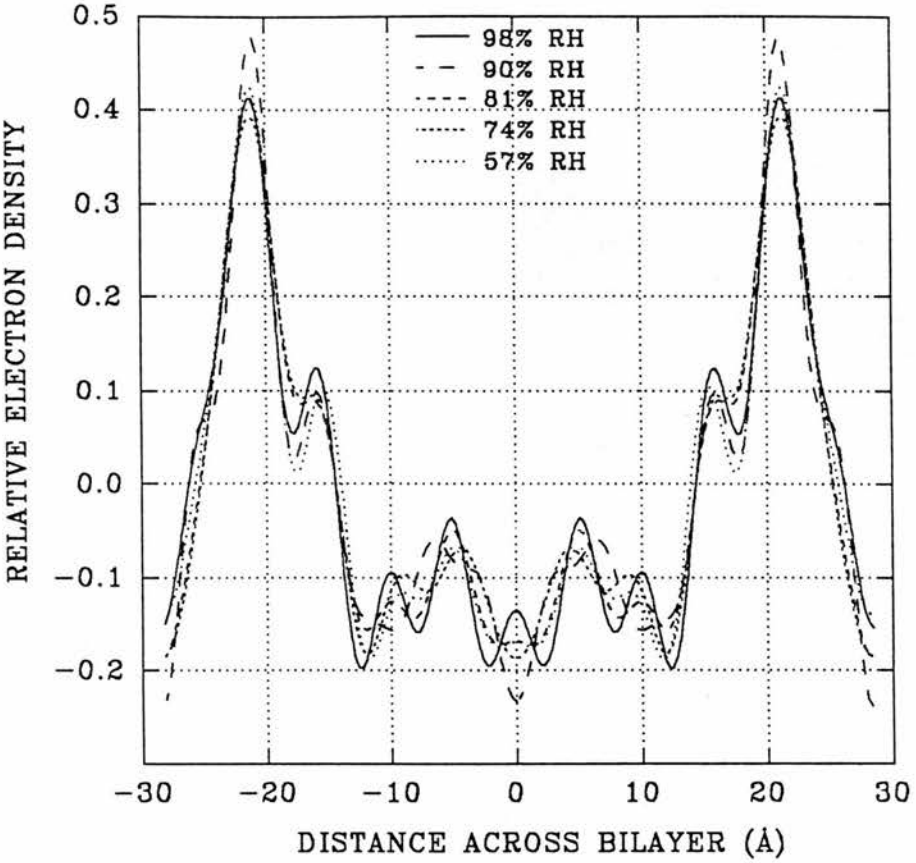

Figure 6.4 The electron density distribution maps of 1:1 (DPPC:bromolipid) mixture bilayers. The electron density maps were constructed using up to twelve orders of diffraction collected from oriented samples at 20°C and between 98% and 57% RH and phased using the swelling series method (Figure 6.1). The DPPC phosphate headgroup, the ester linkage group and the lipid layer can be located at ±21Å, ±17Å and -15Å to +15Å respectively. The electron density distribution maps do not, however, take truncation or data accuracy errors into account.

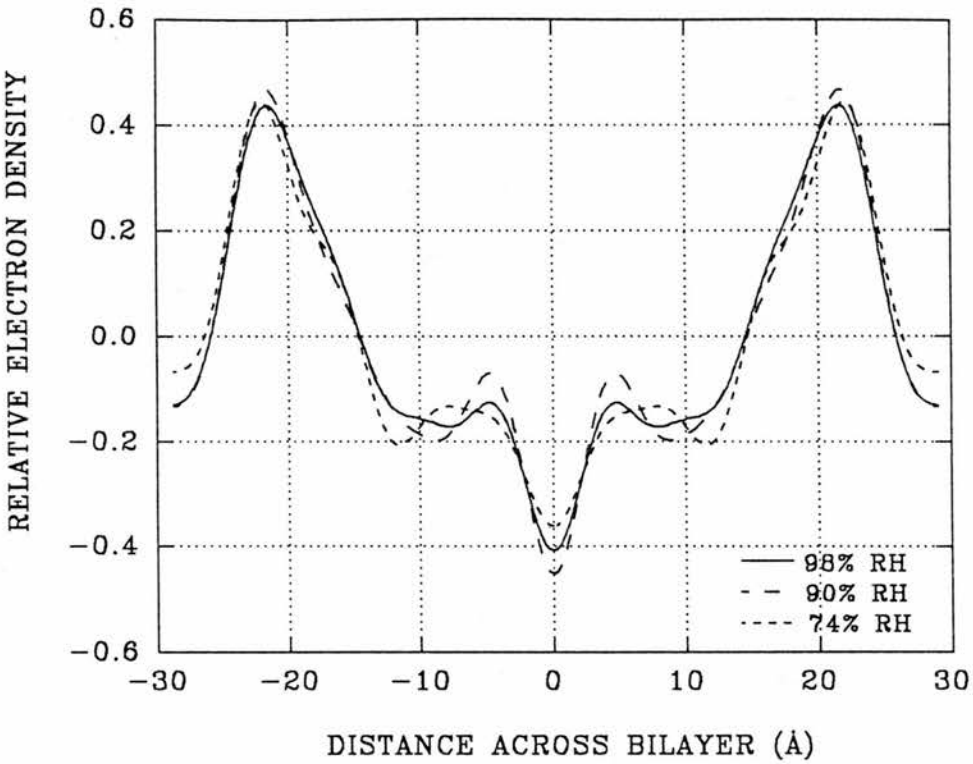

Figure 6.5 The electron density distribution maps of 7:2 (DPPC:bromolipid) mixture bilayers. The electron density maps were constructed using nine orders of diffraction, collected from oriented samples at 20°C and either 98%, 90% or 57% RH, and phased using the swelling series method (Figure 6.2). The DPPC phosphate headgroup and the lipid layer can be located at ±22Å and -15Å to +15Å respectively. The ester-linkage group, locatable at ±17Å in the twelve order 1:1 mixture bilayer maps (Figure 6.4), is less obvious. The electron density distribution maps do not take into account truncation or data accuracy errors.

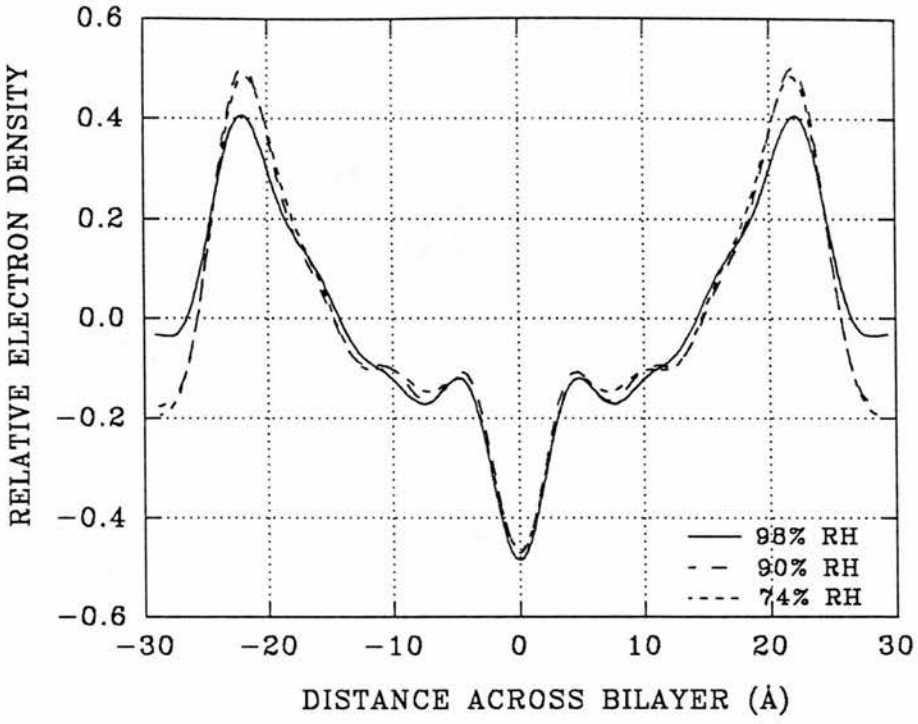

Figure 6.6 The electron density distribution maps of 4:1 (DPPC:bromolipid) mixture bilayers. The electron density maps were constructed using nine orders of diffraction, collected from oriented samples at 20°C and either 98%, 90% or 57% RH, and phased using the swelling series method (Figure 6.3). The DPPC phosphate headgroup and the lipid layer can be located at ±22Å and -15Å to +15Å respectively. The ester-linkage group, located at ±17Å in the twelve order 1:1 mixture bilayers (Figure 6.4), is less obvious. The electron density distribution maps do not take into account truncation or data accuracy errors.

mixture profiles by a factor of 1.1 and both the 7:2 and 4:1 mixture bilayers by a factor of 1.2 (the same factor applied to pure DPPC). The scaling factor required to match the phosphate peak heights, therefore, appears to relate to the concentration of bromolipid in the bilayer.

6.2.2 Comparison of pure DPPC, 1:1 mixture and pure bromolipid bilayers.

The electron density profiles of pure DPPC, 1:1 mixture and bromolipid bilayers at 20°C and 90% RH, all constructed using twelve orders of diffraction, are compared in Figure 6.7. The maps of the three systems show a progression from a pure bromolipid to a pure DPPC bilayer structure (Figure 6.7), where the lipid chain terminal region (−5 to +5Å) electron density increases markedly with the proportion of bromolipid in the bilayer. Increasing the bromolipid concentration, to form a 1:1 mixture, significantly decreases the DPPC bilayer thickness (Table 6.4). There appears, however, to be little variation in the phosphate headgroup separation, across the water layer, compared with the difference in bilayer thickness between the three systems (the two pure species and the 1:1 mixture). The variation in bilayer thickness appears to be attributable to a decrease in the lipid layer, rather than the water layer, thickness.

Table 6.4 Comparison of electron density data for DPPC, bromolipid and the 1:1 mixture at 20°C and 90% RH. Twelve orders of diffraction were used to construct the electron density distribution maps.

Lipid / lipid mixture	Bilayer Thickness (Å)	Phosphate group separation, across the water layer (Å)
bromolipid	56.3 ±0.2	13.8 ±0.2
1:1 mix	56.8 ±0.2	14.1 ±0.2
7:2 mix	58.1 ±0.2	14.0 ±0.2
4:1 mix	58.2 ±0.2	14.0 ±0.2
DPPC	58.0 ±0.2	14.1 ±0.2

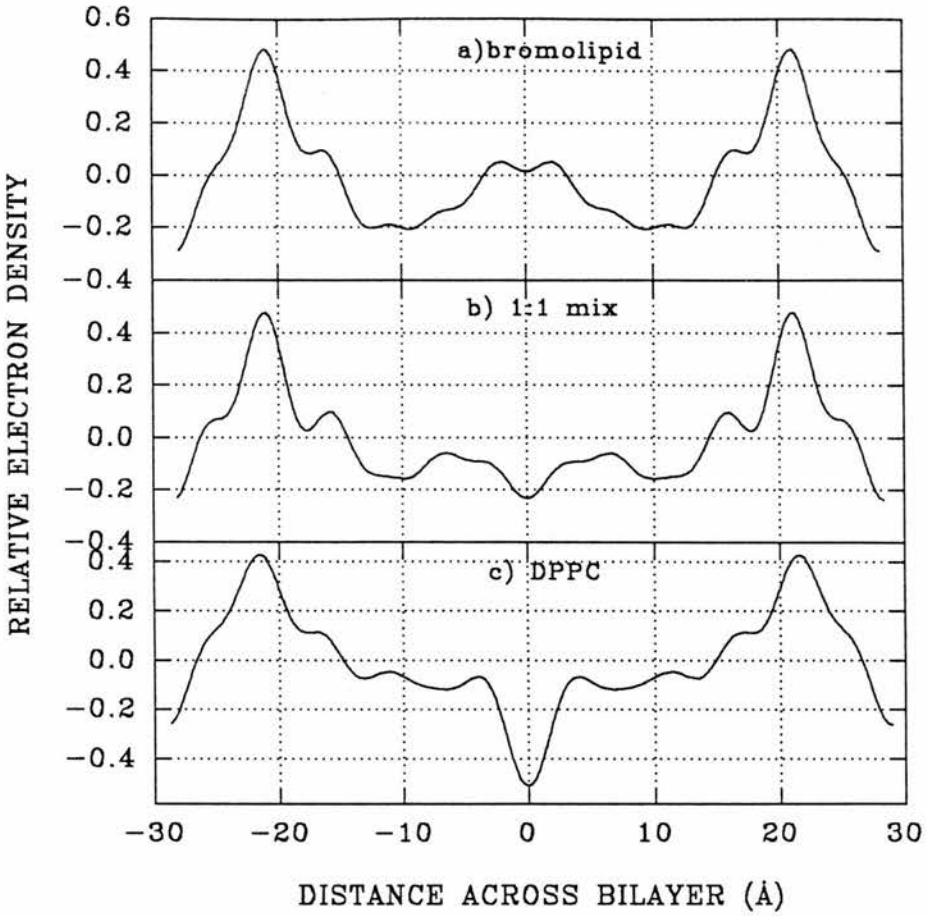

Figure 6.7 Comparison of the bromolipid (top), 1:1 mixture (middle) and DPPC (bottom) bilayer electron density distribution maps. The electron density maps were all constructed using twelve orders of diffraction, collected from oriented samples at 20°C and 90% RH and phased using the swelling series method. The 1:1 mixture and pure DPPC maps were scaled to the pure bromolipid map by multiplying the profiles by a factor of 1.1 and 1.2 respectively. The three electron density maps show a progression from a pure DPPC to a pure bromolipid bilayer, where the electron density at the centre of the lipid layer increases with the bromolipid concentration. The electron density distribution maps do not take into account experimental errors.

6.2.3 Comparison of 7:2 mixture, 4:1 mixture and pure DPPC bilayers.

The electron density maps of 7:2 and 4:1 DPPC:bromolipid mixture bilayers and pure DPPC bilayers (Figure 6.8) have all been constructed using nine orders of diffraction. The level of truncation error introduced into the DPPC bilayer structure from using only nine orders of diffraction to construct electron density maps is indicated in Figure 5.3. The electron density maps of Figure 6.8 suggest that a small quantity of bromolipid in a DPPC bilayer increases the electron density at the centre of the lipid layer, but also decreases the electron density at $\pm$10Å. The electron density increase is presumably attributable to the insertion of bromine atoms into the centre of the lipid bilayer, whilst the decrease in electron density, at $\pm$10Å, has an unknown origin.

6.3 The 95% confidence limits of the mixture bilayer electron density maps.

The 95% confidence limits for the electron density distribution across the mixture (1:1, 7:2 and 4:1) bilayers have been estimated by a Monte Carlo simulation programme. The confidence limits were calculated using a standard deviation error limit estimate of $\pm$ 6% for all structure factor amplitude orders. Comparing the 95% confidence limits for the 1:1 mixture bilayer with those of pure DPPC bilayers (Figure 6.9) shows that there are significant differences between the two systems at $\pm$10Å (the lipid chain layer), $\pm$18Å (the ester linkage region) and 0Å (the centre of the lipid layer). Any apparent distinctions between the two systems across the headgroup region ($\pm$20-24Å) are due to there being a difference in bilayer thickness and all measurements being made relative to the centre of the lipid layer.

Comparing the 95% confidence limits of the 4:1 and 7:2 mixture bilayer systems with the pure DPPC system (Figure 6.10) shows that the addition of a small quantity of bromolipid to DPPC appears to increase the bilayer electron density at the centre of the lipid layer (0Å), although not significantly for the 4:1 bilayer when using a structure factor amplitude error limit of 6%. The 95%

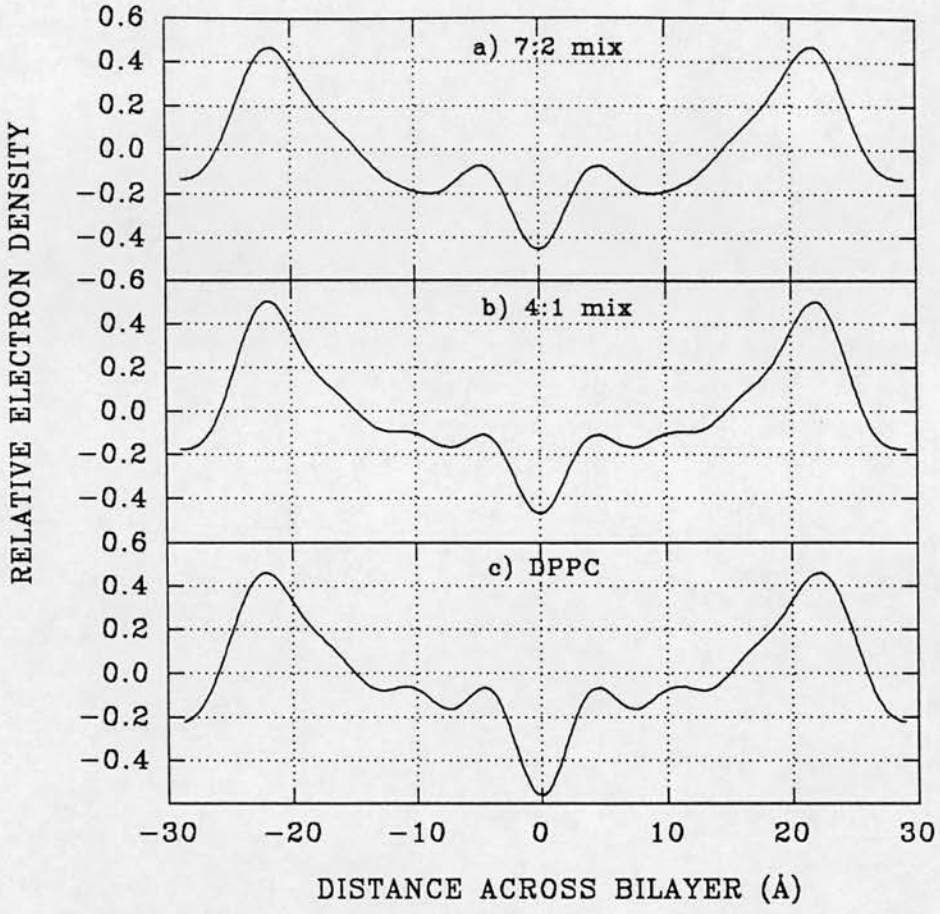

Figure 6.8 Comparison of the 7:1 (top), 4:1 mixture (middle) and pure DPPC (bottom) electron density maps. The electron density maps were all constructed using nine orders of diffraction, collected from oriented samples at 20°C and 90% RH and phased using the swelling series method. Each of the profiles were scaled to that of pure bromolipid by multiplication to match phosphate peak heights, by a factor of 1.2. Using nine orders of diffraction, the maximum available for the 4:1 and 7:2 mixture samples, introduces truncation error into the pure DPPC structure (Figure 5.3), if not all three of the structures shown above. Adding a small quantity of bromolipid to the DPPC bilayer increases the electron density at the centre of the lipid layer (0Å). There also appears, however, to be a decrease in electron density at $\pm$10Å as the bromolipid concentration increases. The electron density distribution maps do not take data accuracy errors into account.

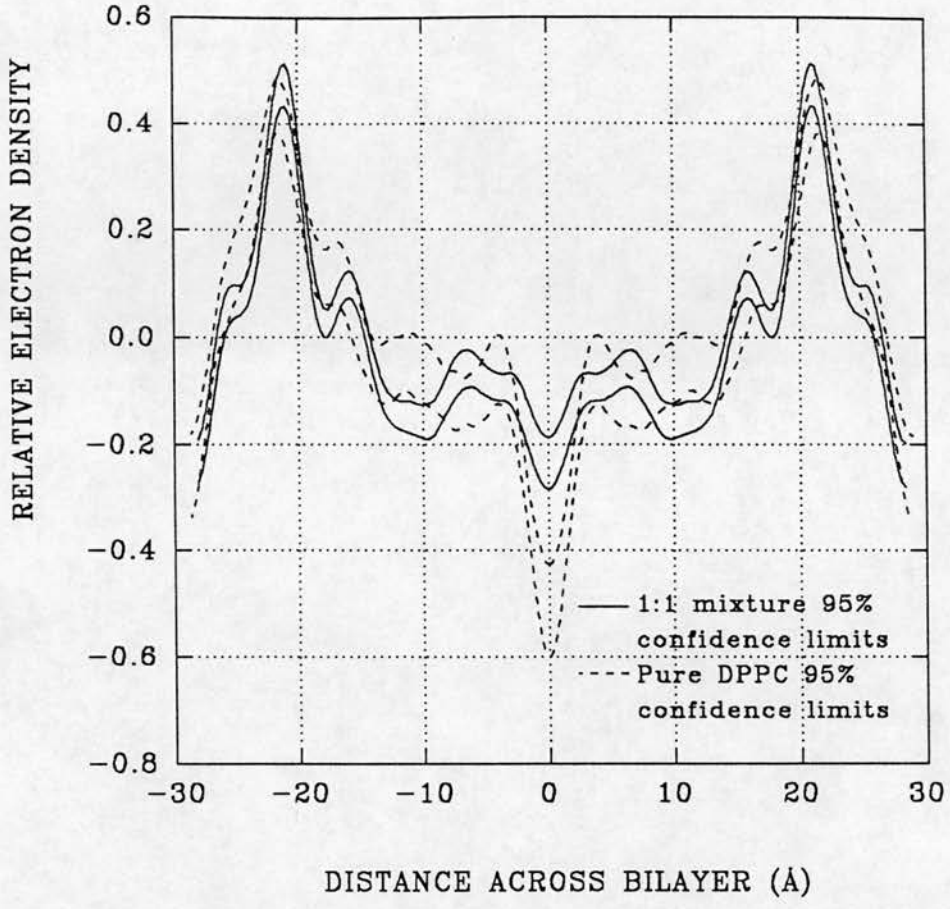

Figure 6.9 Comparison of the 1:1 (DPPC:bromolipid) mixture and pure DPPC 95% confidence limits for the electron density distribution across the bilayer. Diffraction data were collected from oriented bilayer samples at 20°C and 90% RH and phased using the swelling series method. The 95% confidence limits, for the electron density distribution across the bilayer, were calculated using a Monte Carlo simulation program and twelve orders of diffraction. Error limits for the structure factor amplitude data were set at 6% (SD) for all orders. The 1:1 mixture and pure DPPC maps were scaled to the pure bromolipid map by multiplying the profiles by a factor of 1.1 and 1.2 respectively. The comparison shows that the addition of bromolipid to DPPC, to form a 1:1 mixture, significantly increases the electron density at the centre of the lipid layer (0Å). Other significant differences between the two bilayer systems, at $\pm$10Å and $\pm$18Å, also exist however.

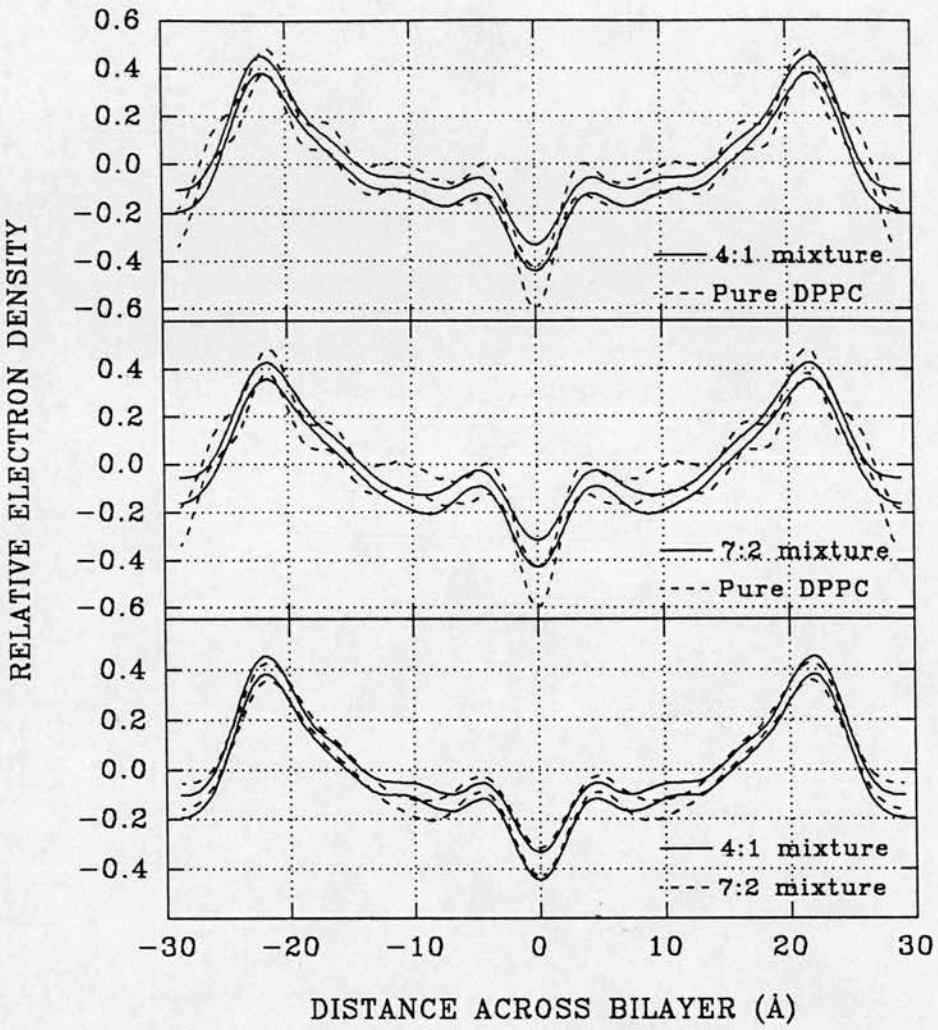

Figure 6.10 Comparison of the 95% confidence limits for the 4:1 mixture, 7:2 mixture and the pure DPPC bilayer electron density distributions. Diffraction data were collected from oriented bilayer samples, at 20°C and 90% RH, and phased using the swelling series method. The 95% confidence limits for the electron density distribution across the bilayer were calculated using a Monte Carlo simulation program and twelve orders of diffraction. Error limits for the structure factor amplitude data were set at 6% (SD) for all orders. Each of the profiles were scaled to that of pure bromolipid by multiplication to match phosphate peak heights, by a factor of 1.2. The 4:1 and 7:2 map comparisons with DPPC (top and middle) shows that the addition of a small quantity of bromolipid to DPPC appears to increase the bilayer electron density at the centre of the lipid layer (0Å), although not significantly in the case of the 4:1 mixture bilayer. The 4:1 and 7:2 mixture map comparison (bottom) shows that the two bilayer systems only differ significantly at ±10Å. The origin of this structural difference is unknown.

confidence limits for the distribution of electron density in the 4:1 and 7:2 mixture bilayers (Figure 6.10, bottom) suggests that the small increase in bromolipid concentration, from the 4:1 to 7:2 lipid ratio, reduces the electron density at 10Å, without significantly increasing the electron density at 0Å.

6.4 Electron density difference maps.

Difference maps have been constructed to analyse the pure DPPC, lipid mixture (1:1, 7:2 and 4:1) and bromolipid bilayer structures (Figures 6.11 and 6.12). The bromolipid minus 1:1 DPPC:bromolipid mixture difference map (Figure 6.11 (a)) has a large peak in electron density at 0Å, due to the increase in bromine atom concentration. The decrease in electron density along the lipid chain layer (4-15Å) that was shown to be a difference between pure bromolipid and pure DPPC bilayers (Figure 5.8), is also evident between the pure bromolipid and 1:1 mixture bilayers. The bilayer thickness difference between bromolipid and 1:1 mixture bilayers is approximately 0.5Å (Table 6.1 and 5.2). The difference map baseline oscillates around zero electron density, and may be due to a combination of scaling, truncation, changes in bilayer thickness and experimental errors.

The 1:1 lipid mixture minus pure DPPC bilayer difference map (Figure 6.11 (b)) reveals a sharp electron density peak at the centre of the lipid layer due to the bromolipid bromine atoms. Calculating the electron density distribution confidence limits (Figure 6.9) showed that the 1:1 mixture and DPPC bilayer systems differed at 0Å, $\pm$10Å, and $\pm$18Å, all regions highlighted in the difference map. The large oscillations of the difference map baseline, between 5 and 28Å, may also arise due to the large difference in bilayer thickness between the pure DPPC and 1:1 DPPC:bromolipid bilayers (1.2Å at 20°C and 90% RH). The 1:1 mixture minus DPPC and the bromolipid minus 1:1 mixture difference maps both have an electron density peak at 0Å of a similar magnitude (0.25 versus 0.27 relative electron density units), which are presumably due to similar increases in bromine concentration.

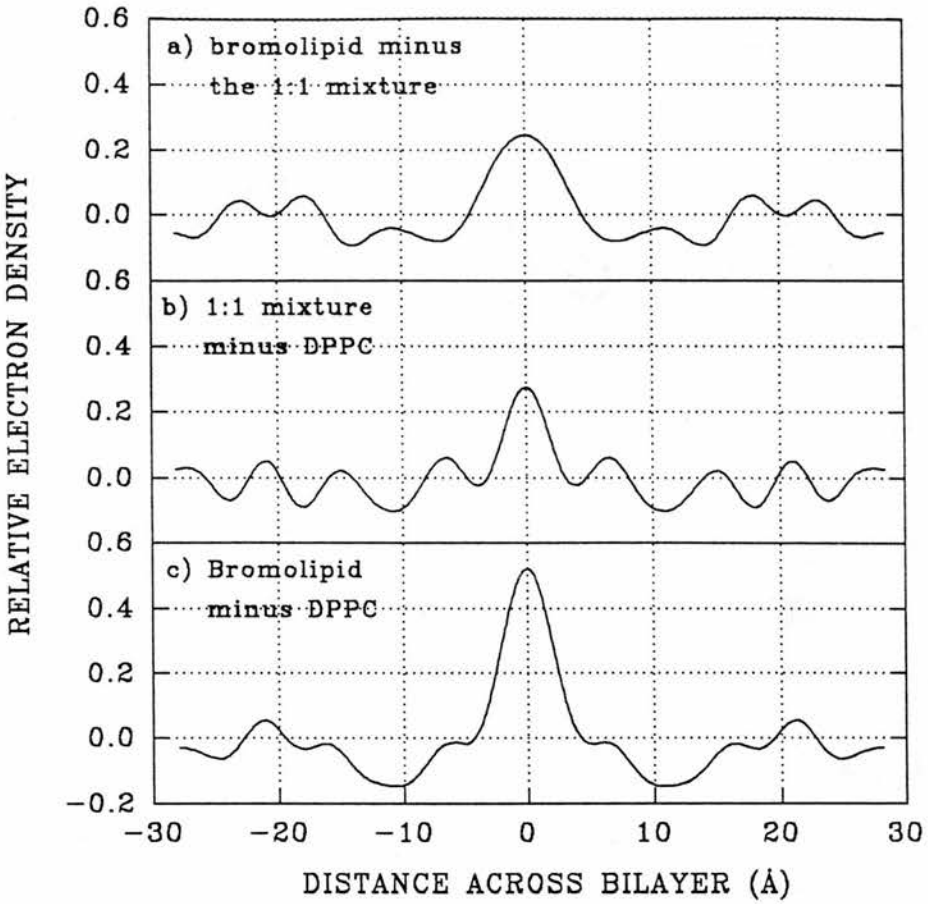

Figure 6.11 Electron density difference maps of a) bromolipid minus 1:1 (DPPC:bromolipid) mixture, b) 1:1 (DPPC:bromolipid) mixture minus DPPC and c) bromolipid minus DPPC. The maps were created using twelve orders of diffraction that were collected from bilayer samples at 20°C and 90% RH. The difference profiles show that the major effect of adding bromolipid to DPPC is to increase the electron density at the centre of the lipid layer.

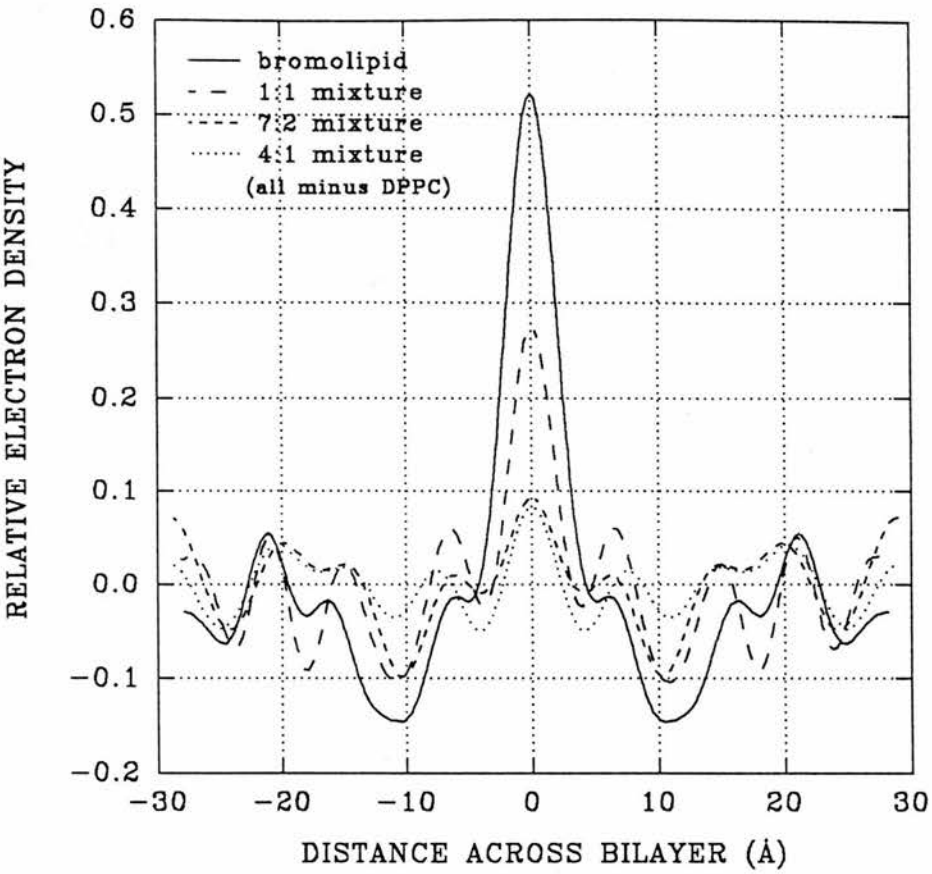

Figure 6.12 Comparison of the pure bromolipid minus DPPC and the three DPPC:bromolipid (1:1, 7:2 and 4:1) mixture minus DPPC electron density difference maps. All the data shown were collected from bilayers at 20°C and 90% RH. The graph shows that increasing the bromine atom concentration in the bilayer increases the electron density at the centre of the lipid layer (0Å). Increasing the bromine atom concentration also appears, however, to decrease the electron density at ±10Å.

The pure bromolipid minus DPPC difference map (Figure 6.11 (c)) shows that the main difference feature between pure DPPC and pure bromolipid bilayers is the increase in electron density at the centre of the lipid layer. Another feature of the bromolipid minus DPPC difference map is the decrease in electron density, centred at $\pm$10Å, in the lipid chain region. A reduction in electron density could result from a reduction in lipid chain tilt, which would also increase the bromolipid bilayer thickness (which is not the case). The chain tilt angle observed in the 1:1 mixture data does not markedly differ from the pure DPPC or bromolipid measured chain tilt angles (Tables 6.1 and 5.4).

All three difference maps of Figure 6.11, show a single peak at the centre of the lipid layer, attributable to the two bromine atoms, suggesting that the bromine atoms are close together in space (*ca* 2Å in the pure bromolipid bilayer). The difference map of bromolipid minus 1:1 (Figure 6.11 (a)) has a wider bromine difference peak than that of the 1:1 minus DPPC difference map (Figure 6.11 (b)). It may be that the more bromolipid there is present in the bilayer the more disordered the chain terminal packing becomes, widening the bromine atom distribution. Also, as the bromolipid concentration increases, the smaller the bilayer thickness gets and the closer would the *sn*-1 and *sn*-2 lipid chain terminals become in space, making an ordered structure at the centre of the bilayer less likely. Chain terminal methyl groups, being sterically large, pack unfavourably next to similar methyl groups of opposing molecules in the bilayer (Zaccai *et al.*, 1979), preferring to pack next to the smaller methylene groups.

The bromolipid and DPPC:bromolipid mixture minus DPPC difference maps have all been superimposed to form one diagram (Figure 6.12). The size of the difference peak at the centre of the lipid layer increases with the concentration of bromolipid in the bilayer, strengthening the evidence that the subtraction peak is attributed to bromine atoms at the centre of the lipid layer. The difference map trough at $\pm$10Å also appears to relate to the concentration of bromolipid in the bilayer, with the region decreasing in electron density as the bromolipid concentration increases. Comparison of the DPPC and bromolipid mixture electron

density maps suggests that other features of the difference maps, such as the trough at ±25Å, are merely artefacts of the subtraction method.

Confidence limits for the difference maps of Figure 6.12 (Figures 5.9 and 6.13) were calculated using a Monte Carlo simulation program and structure factor amplitude error limits of 6% (SD). The maps reinforce the observation of the growth of the bromine peak at 0Å and the decrease in electron density at ±10Å, as the bromolipid concentration increases. The confidence limits have been used to measure the heights and accuracy of the putative bromine peak in the difference maps of Figure 6.12. The bromine peak height versus bromine atom concentration (Figure 6.14) plots almost as a straight line, strongly suggesting a link between the two.

6.5 Variation of structure factor amplitude data on exchange of bromolipid for DPPC in the bilayer.

The general trend that increasing the proportion of bromolipid in a bilayer positively shifts the continuous Fourier transform is demonstrated in Figure 6.15. To observe a uniform positive shift across all orders would require there to be a single bromine atom of point width at the centre of the bilayer, which is not the case here. The bromolipid bilayer has two finite width (1.85Å) bromine atoms which are located approximately 1Å either side of the centre of the lipid layer. The structure factor amplitude data is also affected by changes in bilayer structure and in particular by variations in the bilayer thickness, which accompanies the addition of bromolipid to DPPC bilayers. This is seen as an alteration in the sampling, in reciprocal space, of the continuous Fourier transform.

In general, the bromolipid bilayer continuous Fourier transform is positively shifted compared with the DPPC/DPPC:bromolipid mixture bilayer continuous Fourier transforms (Figure 6.15). The effect that adding bromolipid to a bilayer has on the structure factor amplitude data can be used as a phasing method. From the intensity change that occurs on the addition of bromolipid, it should be possible to ascertain the original amplitude phases of an unknown sample's diffraction.

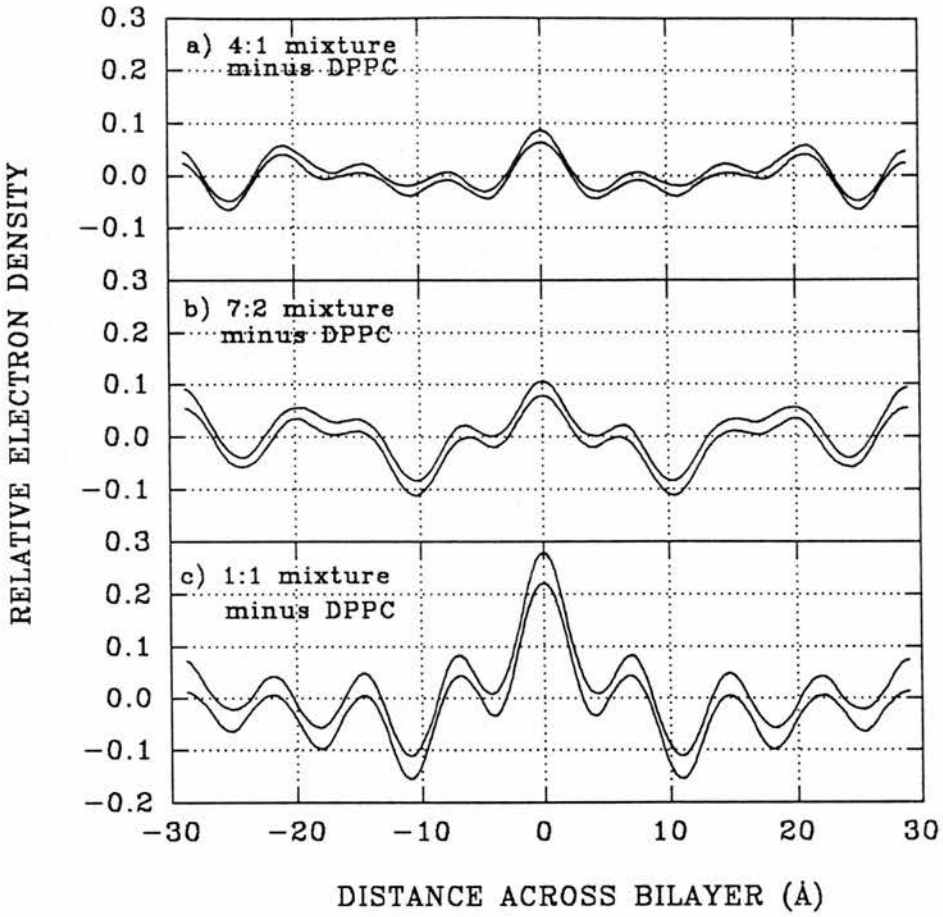

Figure 6.13 The 95% confidence limits for a) 4:1 mixture minus DPPC, b) 7:2 mixture minus DPPC and c) 1:1 mixture minus DPPC electron density difference distributions. Diffraction data were collected from oriented bilayer samples at 20°C and 90% RH and phased using the swelling series method. The 95% confidence limits for the electron density distribution across the bilayer were calculated using a Monte Carlo simulation program and either nine (graphs a, b) or twelve (graph c) orders of diffraction. Error limits for the structure factor amplitude difference data were set at 8.5% (SD) for all orders. The equivalent bromolipid minus DPPC difference map is shown in Figure 5.9. The graphs show that increasing the bromine atom concentration in the bilayer increases the electron density at the centre of the lipid layer (0Å). Increasing the bromine atom concentration also appears, however, to decrease the electron density at ±10Å.

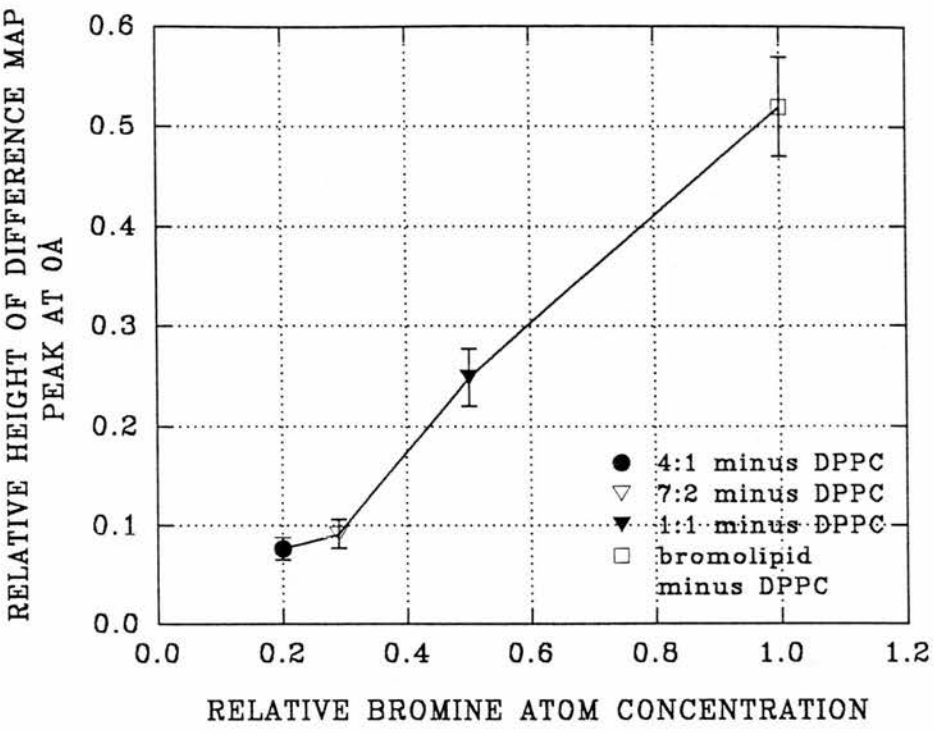

Figure 6.14 A plot of the bilayer bromine atom concentration versus the bromine atom difference map peak height. Diffraction data were collected from oriented bilayer samples at 20°C and 90% RH and phased using the swelling series method. Difference maps were constructed by Fourier transforming either the bromolipid minus DPPC or DPPC:bromolipid (1:1, 7:2 and 4:1) mixture structure factor amplitude difference data. Bromine atom peak error bar values were obtained using a Monte Carlo simulation program to estimate the 95% confidence limits for the bilayer electron density distributions. The putative bromine atom peak height plots almost as a straight line against bromine atom concentration, strengthening the claim that the 0Å peak represents the bromolipid bromine atom location.

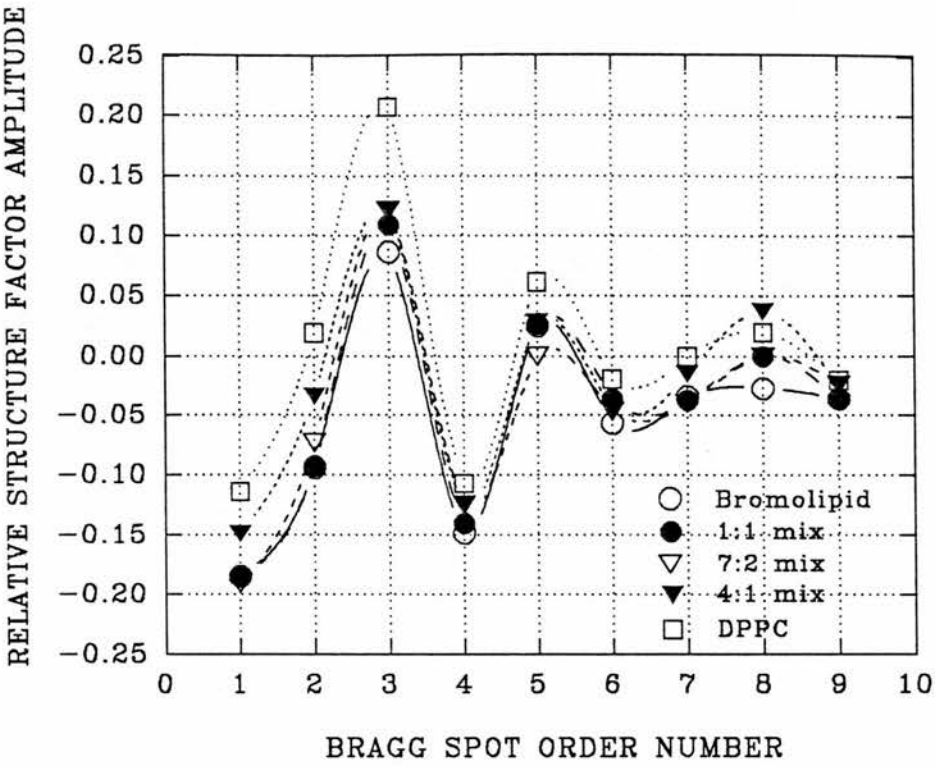

Figure 6.15 A plot of the pure DPPC, DPPC:bromolipid (1:1, 7:2 and 4:1) mixtures and pure bromolipid structure factor amplitude data. The diffraction data were collected from oriented bilayer samples at 20°C and 90% RH. The plot shows that there is a relationship between the bromolipid bilayer concentration and the structure factor amplitude data. Increasing the bromolipid concentration tends to shift the structure factor amplitude values in the positive direction.

Table 6.5 indicates the difference in diffraction data between bromolipid, and DPPC:bromolipid mixture, bilayers and pure DPPC bilayers (nine orders, collected at 90% RH). Adding the bromolipid to DPPC bilayers generally shifts the structure factor amplitude values in the positive direction. The greater the increase in bromolipid concentration, the greater is the shift in the diffraction data. It is, however, a change in order intensity, not amplitude, that is observed on the diffraction patterns which is dependant on the original diffraction phase. For example, a negative phase amplitude order that is positively shifted on addition of bromolipid would result in the observed diffraction intensity decreasing in magnitude. Conversely, a positive phase amplitude order that is positively shifted on addition of bromolipid would increase the observed magnitude of diffraction intensity. The described decrease in intensity may not hold true, however, if a positively shifted negative phase changes phase. The positively shifted negative phase, which might be expected to get smaller, may either get smaller or larger in intensity, depending on the original size of the amplitude and magnitude of the positive shift.

Table 6.5 Changes in the structure factor amplitude data as the bromolipid concentration in the bilayer increases.

	Difference structure factor amplitudes out to nine orders for bromolipid (and mixtures) minus DPPC. The data, collected at 20°C and 90% RH, has an error limit of ±8.5%.			
Diffraction order	4:1 minus DPPC	7:2 minus DPPC	1:1 minus DPPC	bromolipid minus DPPC
1	0.000	–0.006	+0.036	+0.071
2	+0.002	+0.021	+0.060	+0.113
3	+0.023	+0.035	+0.036	+0.121
4	+0.008	+0.023	+0.022	+0.041
5	+0.001	–0.025	+0.003	+0.036
6	+0.021	+0.010	+0.013	+0.038
7	–0.003	–0.006	+0.049	+0.034
8	+0.027	+0.027	+0.064	+0.047
9	0.000	+0.011	+0.011	+0.015

6.6 Conclusions of DPPC:bromolipid mixture study.

In summary, the bromolipid has been studied in three different bilayer mixtures with DPPC (4:1, 7:2 and 1:1) by X-ray diffraction. Both the 4:1 and 7:2 DPPC:bromolipid mixture bilayers have a bilayer thickness similar to that measured from pure DPPC bilayers (Table 6.4). The 1:1 mixture bilayers have a bilayer thickness that is closer in magnitude to that of pure bromolipid than pure DPPC bilayers. The swelling series was used to phase the mixture bilayer diffraction data (Figures 7.1, 7.2 and 7.3). Both the 4:1 and 7:2 DPPC:bromolipid mixture bilayer data were assigned the same phases that were assigned to the pure DPPC bilayer data, supporting the validity of the phase assignments. Increasing the bromolipid concentration in the bilayer generally causes a positive shift the structure factor amplitude values (Figure 6.15, Table 6.5). The positive shift is highlighted by the change in phases (negative to positive), and appearance of zero values, of certain order numbers as the bromolipid concentration increases. For example, the eighth order, assigned a negative phase in the pure DPPC data, was either phased negative or appeared as a zero value in the 4:1 and 7:2 mixture data and was assigned a positive phase in the 1:1 mixture and pure bromolipid bilayer data (Figures 6.1 and 5.5). The second order, assigned a negative phase in the 1:1 mixture data, changes to a positive phase in the pure bromolipid bilayer data (Figure 5.5).

Mixture bilayer (1:1, 7:2 and 4:1 DPPC:bromolipid) electron density maps (Figures 6.4, 6.5 and 6.6) show that the phospholipid headgroup position ($\pm$21-22Å) varies little with either humidity or, unlike the bilayer thickness, bromolipid concentration (Table 6.4). As the bromolipid concentration in the bilayer increases, a growth in electron density at the centre of the lipid layer appears in the bilayer profiles (Figure 6.7). Confidence limits (95%) calculated for the electron density distributions reinforce the observation of a growth in electron density at 0Å as the bromolipid concentration increases (Figures 6.9 and 6.10). The 95% confidence limits also indicate that a significant decrease in electron density occurs, centred at $\pm$10Å, as the bromolipid concentration increases (Figure 6.10, middle). Electron density difference maps also highlight both the growth of the bromine atom peak at

0Å and the decrease in electron density at $\pm$10Å as the bromolipid concentration in the bilayer increases (Figures 6.12, 6.13 and 6.14).

Generally, adding bromolipid to DPPC bilayers shifts the structure factor amplitude values in the positive direction (orders 1 to 9, Table 6.5). The shift in the diffraction data can be used as a phasing method, as changes in observed intensity are dependent on the original phase of the order. The bromolipid method of data phasing has the potential to be more conclusive than the swelling series method. Not only will the diffraction data of a bilayer sample vary in a predictable way with bromolipid concentration, that allows the data to be phased, but the reconstructed electron density maps will also show a bromine atom peak of a predictable size and position in the bilayer.

Chapter 7.

Bromolipid and DPPC in the fluid (L_α) phase.

7.1 Studying the bromolipid and DPPC in the fluid (L_α) phase.

Fluid (L_α) phase bilayers of the bromolipid and DPPC were studied by X-ray diffraction and the swelling series method. The aim of the study was to see whether structural differences that exist between the gel phase bilayers (Chapter 5) also exist in the fluid phase. The study also investigated the potential of using the bromolipid as a phasing agent in fluid phase bilayers.

7.2 Diffraction data from fluid phase DPPC bilayers.

Oriented DPPC bilayers were studied by X-ray diffraction at either 46°C, 50°C or 53°C, and between 98% and 57% RH. Plate 7.1 shows a typical fluid phase diffraction pattern collected from DPPC bilayers in which eight meridional orders of diffraction are clearly visible. The DPPC bilayer thickness was calculated using Bragg's law (equation 2.2) and the meridional diffraction spacing, at each temperature and humidity studied (Table 7.1). Sharp differences in bilayer thickness resulting from a small adjustment in environmental conditions, such as temperature or humidity, may indicate the occurrence of a phase change (Luzzati, 1968). The bilayer thickness results show that the phase adopted by DPPC was dependent on the sample humidity as well as the temperature (Table 7.1). The thickness of the gel phase DPPC bilayers (Table 7.1, 56.2-57.2Å bilayers) decreases markedly when the phospholipids adopt the fluid phase conformation (Table 7.1, 51.5Å to 53.9Å bilayers). These results are in line with the previous observation that increasing the content of water in the bilayer decreases the phospholipid phase melting temperature (Chapman *et al.*, 1967).

A maximum of eight orders were collected from the fluid phase DPPC bilayer samples, compared with up to fourteen collected from gel phase bilayers (Figure 5.1). The fluid phase DPPC diffraction were phased using the swelling series method (Figure 7.1). The phases independently assigned to the fluid phase DPPC data using the swelling series method are identical to those assigned to the gel phase bilayer data (Tables 7.1 and 5.1), supporting their assignment.

PLATE 7.1 The diffraction pattern collected from pure DPPC bilayers in the fluid (L_α) phase. The pattern was collected from an oriented DPPC sample at 53°C and 74% RH. Eight orders of diffraction are clearly visible on the film.

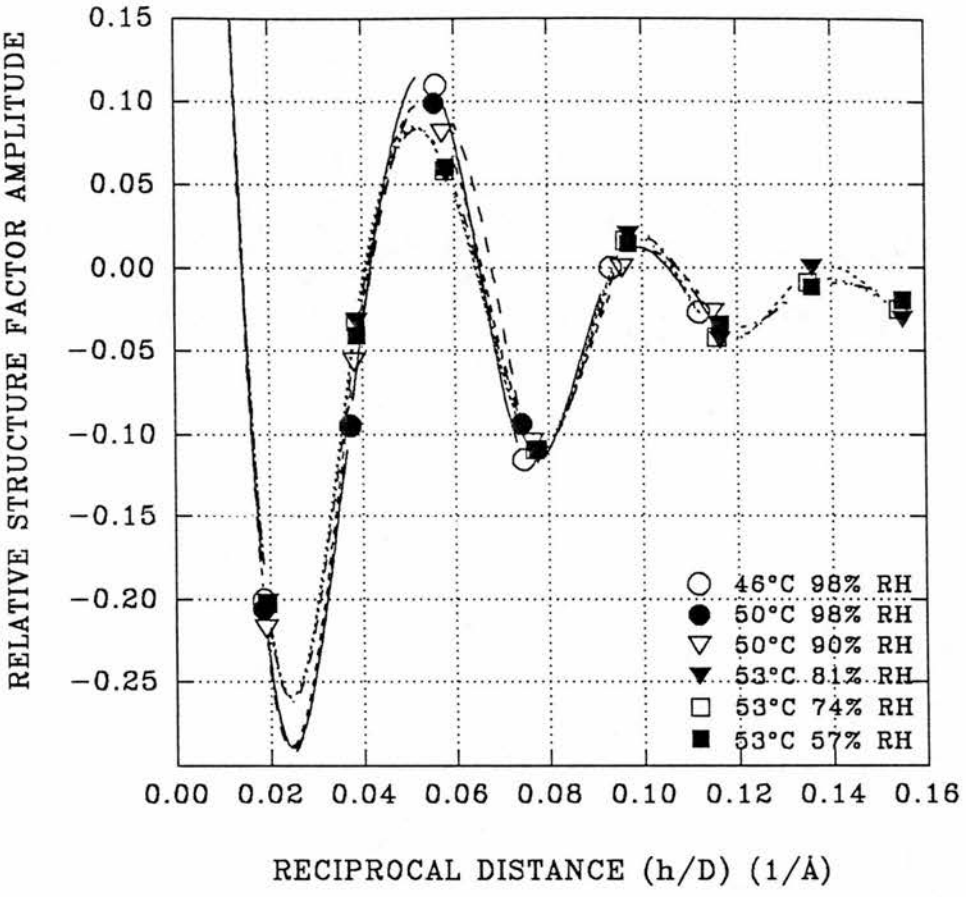

Figure 7.1 The swelling series plot used to phase the diffraction data collected from fluid phase bilayers of pure DPPC. The diffraction data were collected from oriented DPPC bilayers at either 46°C, 50°C or 53°C and between 98% and 57% RH. A maximum of eight orders were collected from the fluid phase DPPC bilayer samples. The symbols represent the structure factor amplitude of each order plotted against h/D (h is the order number and D is the bilayer thickness). The plotted lines are spline curves fitted to the data, as estimates of the form of the continuous Fourier transform.

Table 7.1 Variation of the DPPC bilayer thickness with humidity and temperature.

Relative humidity	Bilayer thickness at 46.0°C (Å)	Bilayer thickness at 50.0°C (Å)	Bilayer thickness at 53.0°C (Å)
98%	53.9	52.4	52.2
90%	57.2	52.2	-
81%	-	56.5	51.6
74%	-	56.2	51.8
57%	56.8	56.6	51.5

7.2.1 Electron density maps of fluid (L_α) phase DPPC bilayers.

Electron density maps of fluid (L_α) phase DPPC bilayers at 46°C, 50°C and 53°C (Figure 7.2) were constructed using the maximum number of diffraction orders available (Table 7.2). The maps locate the fluid phase DPPC phosphate headgroups at ±20Å from the centre of the lipid layer. The fluid phase DPPC phosphate to phosphate headgroup distance, across the lipid layer, is therefore *ca* 4Å shorter than that measured from the gel phase bilayers at 20°C (40Å versus 44Å, Figures 5.2 and 7.2). Lipid chain carbon-carbon bonds, that are in the *trans* form in gel phase bilayers, can adopt a *gauche* bond conformation in the fluid phase bilayers, substantially reducing the width of the lipid layer.

More orders of diffraction were collected from fluid phase DPPC bilayers at 53°C (8 orders) than at 46°C or 50°C (6 orders), a fact reflected by the higher resolution diffraction patterns obtained at 53°C (Plate 7.2). The effect of higher orders (5-8) on the calculation of the DPPC electron density distribution has been assessed by calculating electron density maps using between five and eight orders of diffraction (Figure 7.3, data for DPPC at 53°C and 74% RH). The five order electron density map agrees well with the higher resolution eight order map. With increasing orders used to construct the maps, little change is seen in the position of the DPPC phosphate group at ±20Å, in contrast to the lipid layer region which becomes less rounded in shape. The electron density maps constructed using a truncated Fourier series (less than the maximum number of orders) give an

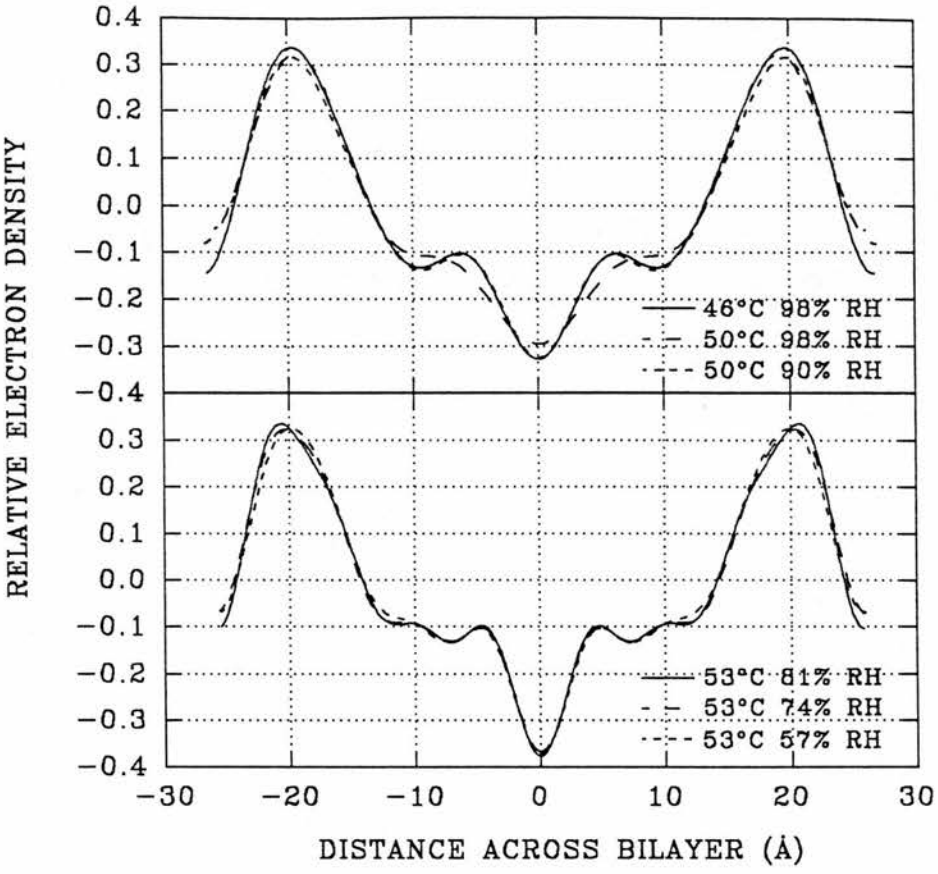

Figure 7.2 The electron density distribution maps of fluid phase DPPC bilayers. Diffraction data were collected from oriented bilayer samples, at 46°C, 50°C and 53°C and between 98% and 57% RH, and phased using the swelling series method (Figure 7.1). The centre of the water layer, phosphate headgroups and centre of the lipid layer can be located at ±25Å, ±20Å and 0Å respectively.

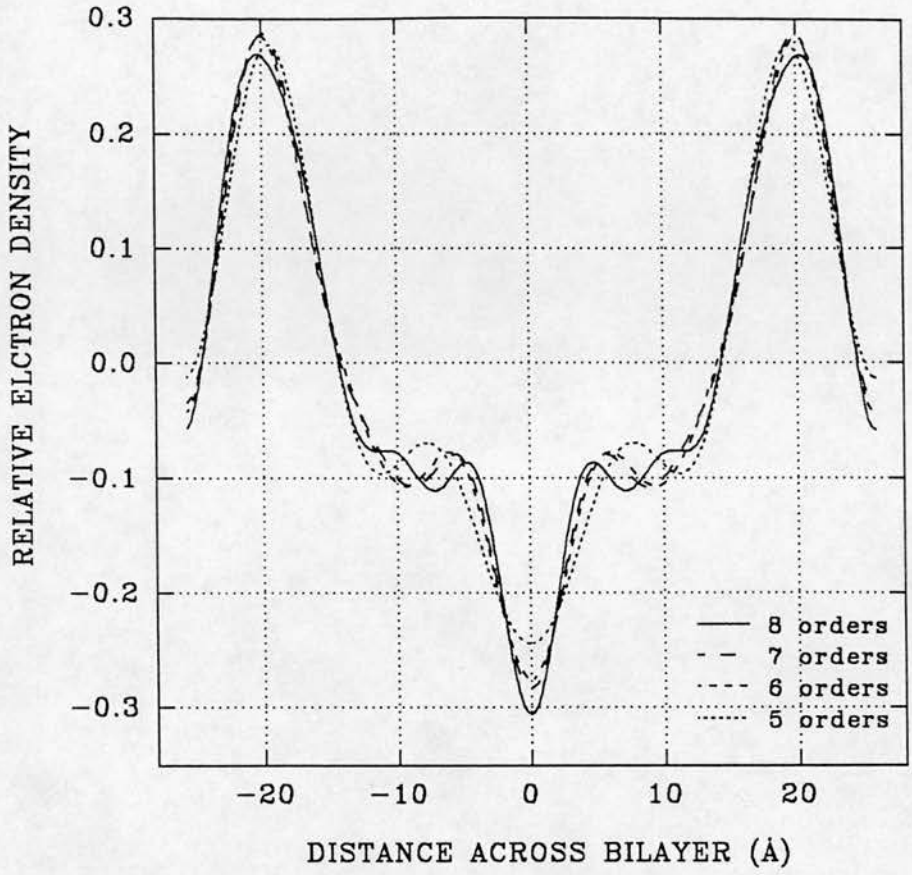

Figure 7.3 The construction of fluid phase DPPC bilayer electron density maps, using a variable number of diffraction orders. The maps were constructed using between five and eight of the diffraction orders collected from DPPC (53°C and 74% RH) and phased using the swelling series method (Figure 7.1). The graphs indicate the effect that increasing orders of diffraction have on the electron density map construction. Comparison of the graphs also indicates the level of truncation error present in electron density maps constructed using less than the maximum available orders. The level of error that would be introduced into a bilayer structure by the incorrect phasing of an order, i.e. double the effect of not using that order in the construction, can also be determined from the maps. Comparison of the maps shows that the position of the DPPC phosphate headgroup (±20Å) only varies slightly with the number of orders used, with greater variation occurring in the lipid layer (−15Å to +15Å).

indication of the level of error that would result from an incorrect phase assignment to the data. For example, the difference between the electron density maps constructed using six orders versus five orders is equal to half the error of incorrectly phasing the sixth order. However, the higher order (5-8) structure factor values are small in size (Table 7.2), and a large error would only be introduced into the electron density map construction by multiple incorrect phase assignments.

Table 7.2 Diffraction data from fluid phase DPPC bilayers.

Diffraction order	Structure factor amplitude					
1	–0.200	–0.206	–0.218	–0.201	–0.202	–0.201
2	–0.095	–0.095	–0.056	–0.033	–0.033	–0.041
3	+0.109	+0.100	+0.080	+0.056	+0.058	+0.061
4	–0.115	–0.094	–0.104	–0.112	–0.109	–0.109
5	0		0	+0.020	+0.017	+0.014
6	–0.026		–0.026	–0.044	–0.034	–0.034
7				0	–0.009	–0.011
8				–0.032	–0.025	–0.020
Temperature	46°C	50°C	50°C	53°C	53°C	53°C
Relative humidity	98%	98%	90%	81%	74%	57%
Bilayer Repeat (Å)	53.9	52.4	52.2	51.6	51.8	51.5

7.3 Diffraction data from fluid phase Bromolipid bilayers.

Oriented bromolipid bilayers were studied by X-ray diffraction, at either 46°C or 53°C and between 98% and 57% RH. Plate 7.2 shows a typical fluid phase diffraction pattern collected from bromolipid bilayers in which six meridional orders of diffraction are clearly visible. At 46°C, and 98% to 57% RH, the bromolipid formed fluid phase bilayers, in contrast to DPPC which only formed fluid phase bilayers at 46°C and 98% RH. This finding is in agreement with the calorimetry study (Chapter 3), which has shown that bromolipid has a lower gel to fluid phase transition temperature than DPPC.

PLATE 7.2 The diffraction pattern collected from pure bromolipid bilayers in the fluid (L_α) phase. The pattern was collected from an oriented bromolipid sample at 46°C and 74% RH. Six orders of diffraction are clearly visible on the film.

Eight orders of diffraction were collected from the fluid phase bromolipid bilayers at 46°C (Table 7.3) compared with twelve at 20°C (Table 5.2). The collection of only five orders at 53°C may either be due to the continuous Fourier transform sampling genuine zero amplitude values at 53°C, as the higher orders measured at 46°C are all small in magnitude, or due to increased disorder in the bilayer sample. The swelling series method was used to assign phases to the bromolipid diffraction data (Figure 7.4). The phases assigned to the fluid phase bromolipid bilayers (Tables 7.3 and 7.4) match those assigned to the gel phase data (Table 5.2), supporting their validity.

7.3.1 Electron density maps of fluid (L_α) phase bromolipid bilayers.

Electron density distribution maps of fluid phase bromolipid bilayers were constructed using the maximum number of orders available for each data set and the swelling series phase assignments (Figure 7.5). Like DPPC, fluid phase bromolipid bilayers have a smaller bilayer thickness than gel phase bilayers (50.1-48.5Å versus 56.7-54.7Å), as a result of the bilayers passing through the gel to fluid phase transition, and disordering in the bilayer structure, with increasing temperature. Decreasing the sample humidity at both 46°C and 53°C decreases the fluid phase bromolipid bilayer thickness (Table 7.3), indicating dehydration of the bilayer water layer. The electron density maps (Figure 7.5) locate the bromolipid phosphate groups at $\pm$19Å at 46°C and $\pm$18Å at 53°C, which are 4Å closer, across the lipid layer, at 46°C than at 20°C (38Å versus 42Å, Figures 7.5 and 5.5). A similar decrease in phosphate separation was found between DPPC bilayers at 46°C and 20°C (Figures 5.2 and 7.2).

The effects of truncation error on the bromolipid electron density map construction have been estimated using a data set containing eight orders (bromolipid at 46°C and 57% RH). Bromolipid electron density maps were calculated using between five and eight orders of diffraction i.e. constructed using a truncated Fourier series (Figure 7.6). The generated electron density maps all depict similar structures, where the bromolipid phosphate headgroup at $\pm$19Å varies only slightly in shape and position. The lipid layer (−15 to +15Å), in

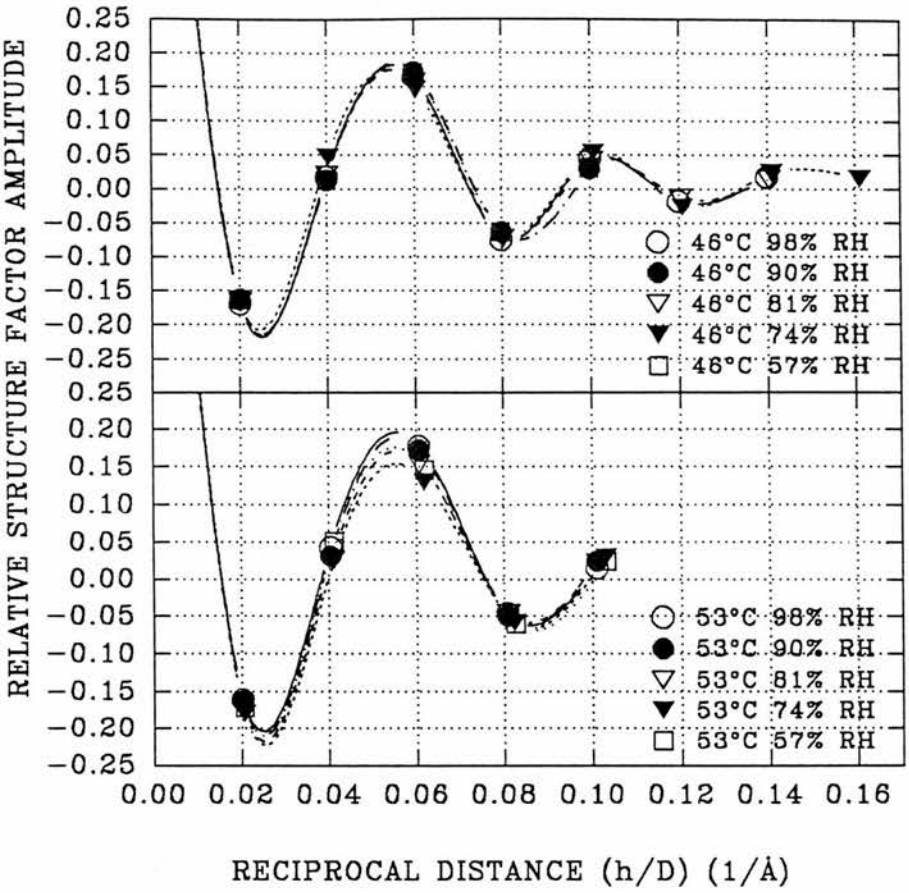

Figure 7.4 The swelling series plot used to phase the diffraction data collected from fluid phase bromolipid bilayers. The diffraction data were collected from oriented bilayer samples at either 46°C (top) or 53°C (bottom) and between 98% and 57% RH. A maximum of eight orders of diffraction were collected from the fluid phase bromolipid samples. The symbols represent the structure factor amplitude of each order plotted against h/D (h is the order number and D is the bilayer thickness). The plotted lines are spline curves fitted to the data, as estimates of the form of the continuous Fourier transform.

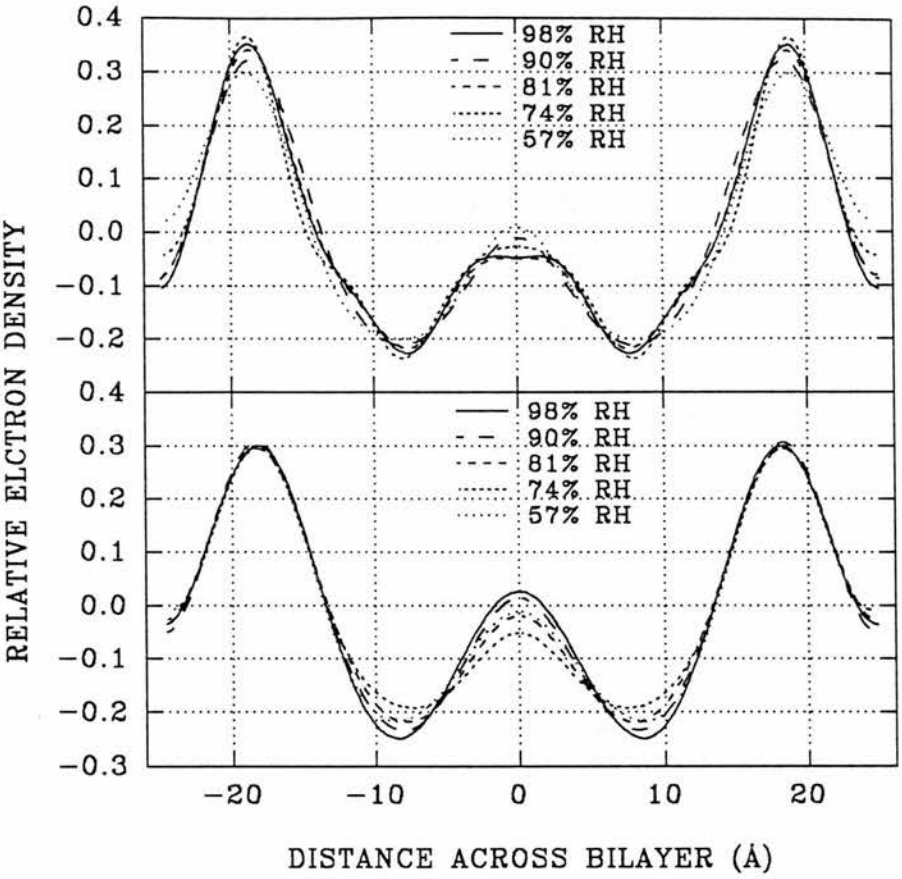

Figure 7.5 The electron density distribution maps of fluid phase bromolipid bilayers at 46°C (top) and 53°C (bottom). Diffraction data were collected from oriented bilayer samples, at 46°C and 53°C and between 98% and 57% RH, and phased using the swelling series method (Figure 7.4). The centre of the water layer, phosphate headgroups and centre of the lipid layer can be located at ±24Å, ±19-18Å and 0Å respectively. The bromolipid bromine atoms form an electron dense peak at -5Å to +5Å.

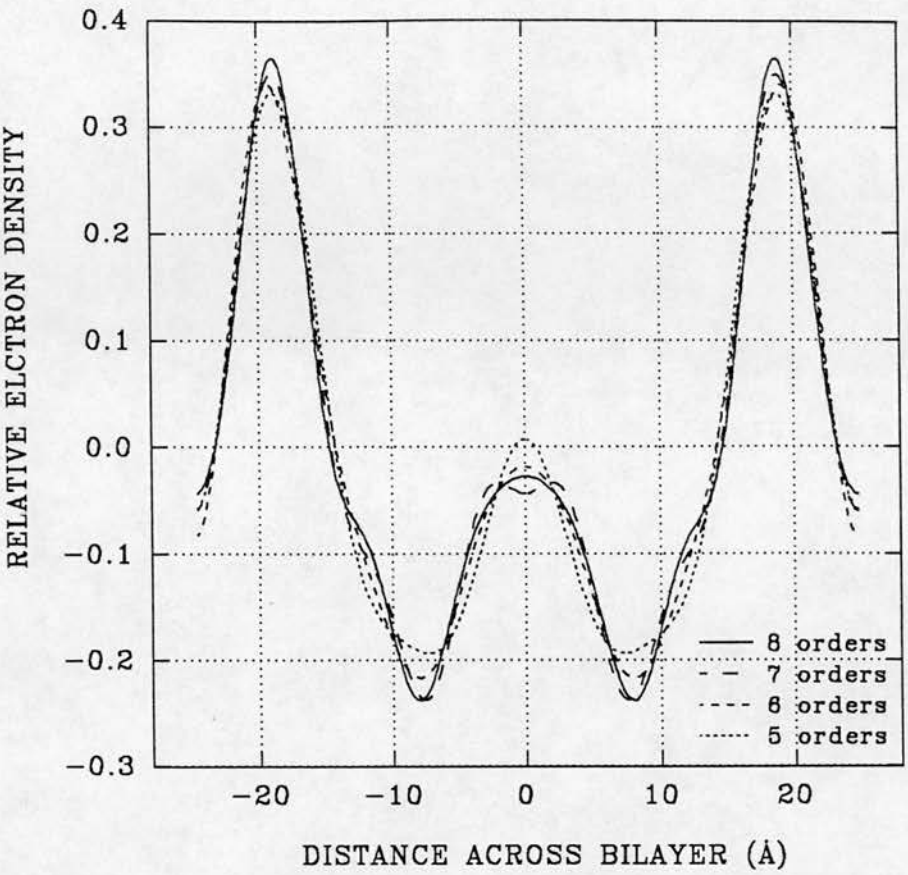

Figure 7.6 Fluid phase bromolipid bilayer electron density maps, constructed using a variable number of diffraction orders. The diffraction data were collected from oriented bilayer samples, at 46°C and 74% RH, and phased using the swelling series method (Figure 7.4). The electron density maps of the 57% RH data have been constructed using either five, six, seven or eight orders of diffraction. The graph indicates the effect that increasing orders of diffraction have on the electron density map construction. The graph also indicates the level of truncation error present in electron density maps constructed using less than the maximum available orders and the level of error that would be introduced into the bilayer structure by the incorrect phasing of an order, i.e. double the effect of not using that order in the construction. The position of the bromolipid phosphate headgroup (19Å) only varies slightly, depending on the number of orders used, with greater variation occurring in the lipid layer (−15Å to +15Å).

Table 7.3 Bromolipid diffraction data at 46°C.

Diffraction order	Phased structure factor amplitude data collected from bromolipid bilayers at 53°C				
1	−0.163	−0.163	−0.167	−0.167	−0.172
2	+0.018	+0.013	+0.020	+0.047	+0.070
3	+0.164	+0.172	+0.156	+0.146	+0.128
4	−0.076	−0.063	−0.073	−0.072	−0.055
5	+0.046	+0.031	+0.042	+0.054	+0.038
6	−0.019		−0.013	−0.026	
7	+0.018		+0.015	+0.025	
8				+0.016	
Relative humidity	98%	90%	81%	74%	57%
Bilayer Repeat (Å)	50.1	50.1	49.9	49.7	49.3

Table 7.4 Bromolipid diffraction data at 53°C.

	Phased structure factor amplitude data collected from bromolipid bilayers at 53°C				
1	−0.161	−0.164	−0.172	−0.180	−0.172
2	+0.043	+0.031	+0.023	+0.026	+0.051
3	+0.177	+0.172	+0.154	+0.129	+0.146
4	−0.047	−0.050	−0.047	−0.056	−0.060
5	+0.015	+0.024	+0.022	+0.029	+0.024
Relative humidity	98%	90%	81%	74%	57%
Bilayer Repeat (Å)	49.6	49.6	49.4	48.6	48.5

particular the bromine atom peak (0Å) at the centre of the lipid layer, varies more with the number of diffraction orders used. The higher order (6-8) structure factors of the bromolipid have small values and therefore only contribute a small amount to the electron density map construction. Fluid phase bromolipid bilayers at 53°C only diffracted out to five orders, compared with eight orders at 46°C. If the higher orders (6-8) are not genuine zero values, the level of truncation errors that might be present in the five order structures of bromolipid at 53°C (Figure 7.5, Bottom) can be estimated by comparing the five and eight order structures of Figure 7.6.

7.4 Comparison of bromolipid and DPPC bilayers.

Both the fluid and the gel phase DPPC and bromolipid electron density maps were only placed on a relative scale. To scale the electron density maps to one another, the DPPC electron density map was multiplied by a factor which matched the height of its electron dense phosphate headgroup with that of the bromolipid (Figure 5.7). To match the headgroup peak heights, the fluid phase DPPC electron density profiles were multiplied by a factor of 1.2, the same multiplication factor used in the gel phase (Section 5.4).

Fluid phase DPPC bilayers were consistently thicker than those formed by bromolipid. The difference in bilayer thickness of the fluid phase bilayers (2.2-3.8Å) is wider than that found between the gel phase bilayers (Tables 7.2, 7.3, 5.1 and 5.2). The electron density profiles of DPPC and bromolipid have been compared at both 46°C and 53°C (Figure 7.7), showing that at both temperatures the two bilayer structures differ mainly in the lipid chain region, between -10Å and +10Å. The bromolipid bilayer electron density is greater between –4Å and +4Å (due to bromine atoms) but lesser between ±4-12Å (along the lipid chain layer).

The electron density maps compared in Figures 7.7 were constructed using various numbers of orders (bromolipid at 46°C and 53°C used seven and five orders respectively, DPPC at 46°C and 53°C used six and eight orders respectively). Although all the electron density maps were constructed using the maximum number of orders available, the electron density map comparisons may therefore be between structures containing truncation error, similar to that demonstrated in Figures 7.3 and 7.6. The truncation errors involved, however, would be unlikely to be large enough to discount the differences observed between the DPPC and bromolipid structures.

7.5 Estimating the confidence limits of the electron density maps.

The 95% confidence limits for the electron density distribution across the fluid phase bromolipid and DPPC bilayers have been estimated using a Monte Carlo

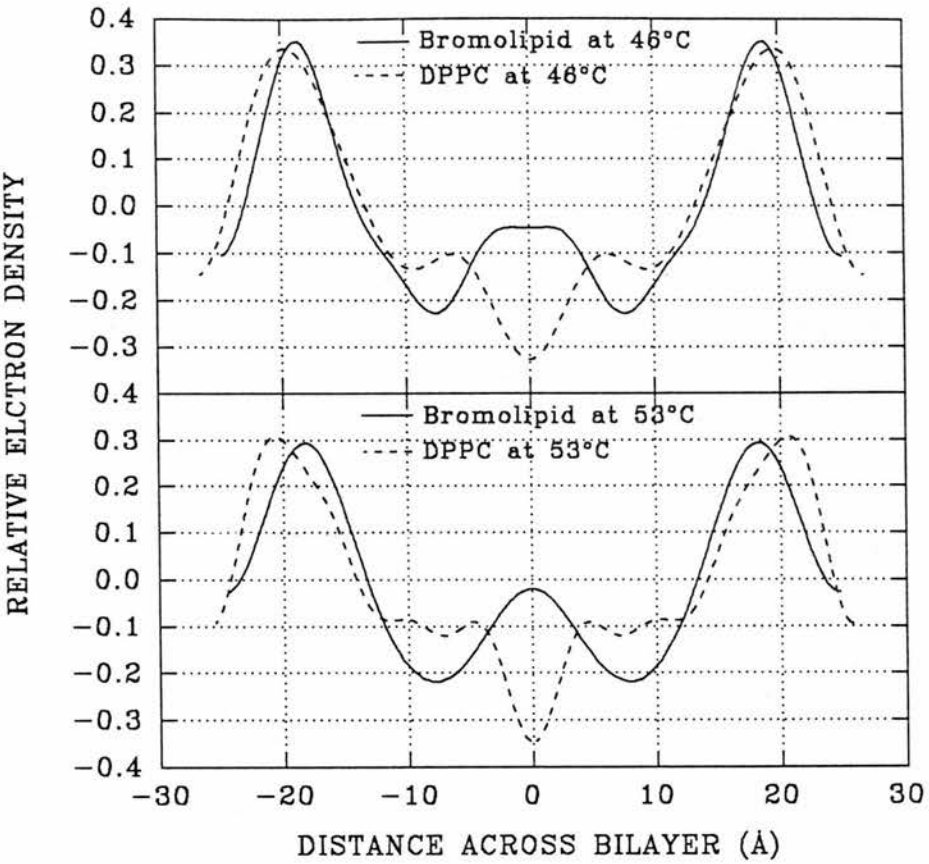

Figure 7.7 Comparison of the fluid phase bromolipid and DPPC bilayer electron density maps, at either 46°C and 98% RH (top) or 53°C and 81% RH (bottom). Diffraction data were collected from oriented bilayer samples and phased using the swelling series method. The 46°C bromolipid and DPPC electron density maps were constructed using seven and six orders respectively and 53°C maps using five and eight orders respectively. At both temperatures, the two bilayer structures were scaled to one another by multiplying the DPPC profile by a factor of 1.2. The phospholipid phosphate headgroups and the centre of the lipid layer can be located at ±18-22Å and 0Å respectively. The DPPC and bromolipid structures differ, at 46°C and 53°C, both in their bilayer thickness and their electron density between -10 and +10Å.

simulation program with a structure factor amplitude error level of 6% for each order. Comparison of the 95% confidence limits for DPPC and bromolipid bilayers (Figure 7.8, 46°C and 98% RH data) shows that the two bilayer structures differ significantly over the majority of the lipid chain layer (−10Å to +10Å). In contrast, the DPPC and bromolipid headgroups (±18-20Å) are similar in shape and size.

The 95% confidence limits for the bromolipid minus DPPC electron density difference map have also been calculated (Figure 7.9, 46°C and 98% RH data), using a difference structure factor amplitude error limit of 8.5% (equivalent to structure factor limit of 6% as $\sqrt{((6)^2+(6)^2)}=8.5$). The 95% confidence limits suggest that the difference map bromine peak has a height of 0.30 ±0.04 relative units and a width of 9.0Å±0.5Å. The accuracy of the bromine atom difference peak (Figure 7.9, peak centred at 0Å) is limited by both truncation errors and the accuracy with which diffraction data can be measured. Whilst the calculation of 95% confidence limits attempts to estimate the effect of diffraction data accuracy, truncation error can significantly alter both the DPPC and the bromolipid electron density maps at the centre of the lipid layer (Figures 7.3 and 7.6). Gaussian distribution fitting, to estimate the size and separation of the two bromine atoms at the centre of the bilayer, has not been undertaken, as the results would be of limited value.

7.6 Direction and size of change, of structure factor amplitudes, on exchanging bromolipid for DPPC in fluid phase bilayers.

The difference between bromolipid and DPPC diffraction data at 46°C and 98% RH are summarised in Table 7.5. As was the case for gel phase bilayers, the fluid phase structure factor amplitude values (orders 1-6, Table 7.5) shift in the positive direction, on exchanging DPPC for bromolipid. The predictable change in diffraction data, on adding bromolipid to fluid phase bilayers, should allow the bromolipid to act as an isomorphous replacement phasing agent in fluid phase bilayers. The change in diffraction intensity, on exchanging the bromolipid for DPPC, of each order can be used to assign phases, i.e. if the order intensity gets

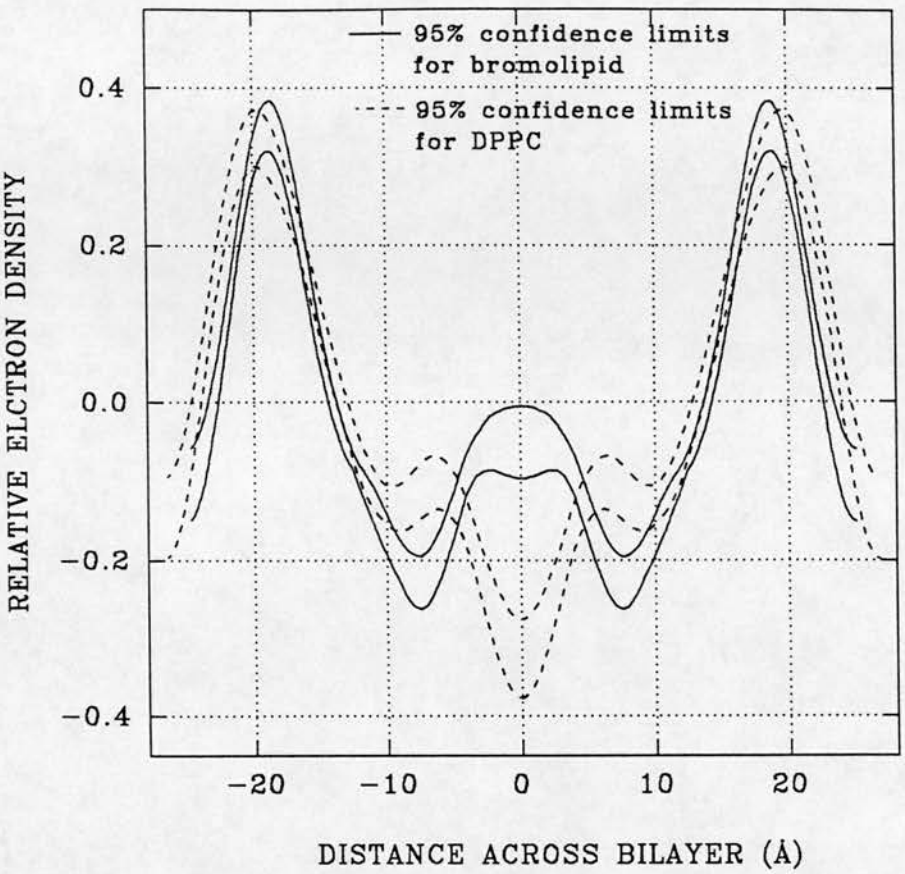

Figure 7.8 Comparison of the 95% confidence limits for the fluid phase bromolipid and DPPC electron density distributions across the bilayer. Diffraction data were collected from oriented bilayer samples, at 46°C and 98%, and phased using the swelling series method. The 95% confidence limits were calculated using a Monte Carlo simulation program, using seven and six orders of diffraction for bromolipid and DPPC respectively, with a structure factor amplitude error limit of 6% (SD) for all orders. The two bilayer structures were scaled to one another by multiplying the DPPC profile limits by a factor of 1.2. The bromolipid and DPPC headgroups ($\pm$18-20Å) are of a similar shape and size, although the DPPC headgroup appears to have a slightly wider distribution. The bromolipid bromine atoms, however, clearly increase the electron density at the centre of the lipid layer (0-4Å). There also appears to be another discernible difference, at 5-10Å, between the bromolipid and DPPC bilayers.

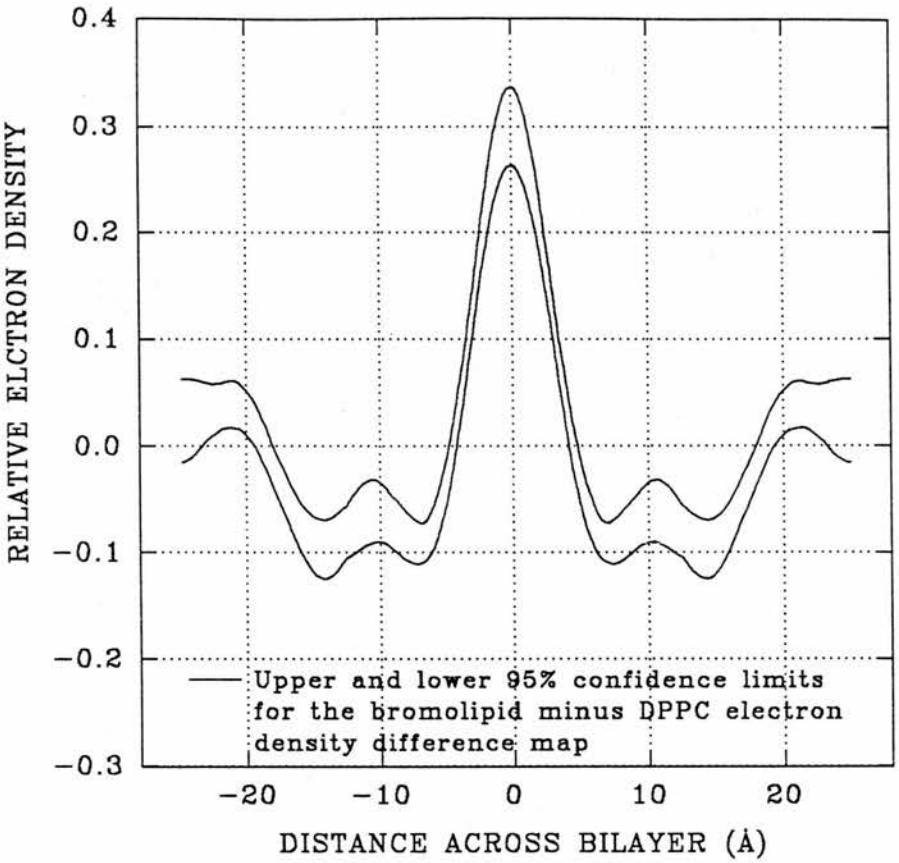

Figure 7.9 The 95% confidence limits calculated for the bromolipid minus DPPC electron density difference map. Diffraction data were collected from oriented bilayer samples, at 46°C and 98% RH, and phased using the swelling series method. The 95% confidence limits were calculated using a Monte Carlo simulation program, six orders of difference structure factor values, and an error limit of 8.5% (SD) for all difference orders. The 95% confidence limits suggest that the bromine peak has a height of 0.30±0.04 relative units and a width of 9.0±0.5Å. The 95% confidence limits do not, however, take into account possible errors from truncation effects, or incorrect phase assignment.

smaller on addition of bromolipid then the original DPPC bilayer phase was negative and vice versa.

As well as the changes in diffraction intensity on replacing DPPC with bromolipid, Table 7.5 shows the phases that would be assigned to the DPPC data (from analysing diffraction pattern changes on addition of bromolipid). The phase assignments to the DPPC data match those obtained from the swelling series method (Figure 7.1), suggesting that the bromolipid has indeed the potential to be used as a phasing agent in fluid phase bilayers.

Table 7.5 Structure factor amplitude data differences between fluid phase bromolipid and DPPC bilayers.

Diffraction order	Structure factor amplitude difference at 46°C and 98% RH	Direction of intensity change on adding bromolipid to DPPC	Suggested phase assignment to DPPC data suggested by intensity change
1	+0.037 ±0.006	smaller	–
2	+0.113 ±0.019	smaller	–
3	+0.055 ±0.009	bigger	+
4	+0.039 ±0.007	smaller	–
5	+0.046 ±0.008	bigger	+
6	+0.007 ±0.001	smaller	–

7.7 Conclusions of bromolipid in the fluid phase.

X-ray diffraction patterns were collected from fluid phase DPPC and bromolipid bilayer samples at 46°C, 50°C and 53°C and between 98% and 57% RH. The diffraction data of each phospholipid were phased using the swelling series method (Figures 7.1 and 7.4). The difference in bilayer thickness, between gel phase DPPC and bromolipid bilayers (1 to 2.3Å at 20°C), also exists in the fluid phase (3.8Å at 46°C and 2.2 to 3.2Å at 53°C). Raising the DPPC and bromolipid bilayer systems above the chain melting temperature did not abolish the thickness difference, that cannot therefore be ascribed to a chain tilt effect, as fluid phase lipids chains are untilted.

The phased diffraction data were used to construct bromolipid and DPPC electron density maps (Figures 7.2 and 7.5). Comparison of these profiles (Figure 7.7) locates the major difference between the two systems as being an electron dense peak (the bromine atoms) at the centre of the lipid layer. Whilst the bromolipid and DPPC headgroups appear to be similar, there are discernible differences between the two bilayer structures along the length of the lipid chain layer (-10Å to+10Å, Figures 7.7 and 7.8). Similar differences were also found to exist between the gel phase bromolipid and DPPC bilayers, centred at $\pm$10Å (Figures 5.7 and 5.8). In spite of the structural differences induced by the bromolipid, the diffraction data (Table 7.5) suggest that the exchange of the bromolipid for DPPC can still be used as an isomorphous replacement phasing method.

Chapter 8.

Summary of the thesis.

8.1 The interaction of amantadine FB and HCl with fluid phase DOPC bilayers.

The interaction of the small drug molecule amantadine (Figure 3.4) with fluid phase DOPC bilayers was studied by X-ray diffraction and the swelling series method. To establish whether the charge state of amantadine affects the drug-membrane interaction, amantadine was studied in both the FB and HCl forms. Swelling series data were compiled for three different systems:

1) Pure DOPC bilayers at 20°C and between 98% and 57% RH.
2) DOPC plus amantadine FB bilayers at 20°C and between 98% and 57% RH.
3) DOPC plus amantadine HCl bilayers at 20°C and between 98% and 57% RH.

Adding amantadine of either form to DOPC reduced the bilayer thickness by between 1Å and 2.5Å, depending on the humidity of the sample (Figure 4.1). Although the DOPC based bilayers diffracted to a maximum of eight orders, the swelling series method was only able to phase the first five orders of diffraction (Figures 4.3, 4.6 and 4.9). DOPC based bilayer electron density maps could, therefore, only be constructed using five orders of diffraction, the limit of phase assignment. The five order electron density maps, therefore, all have an associated truncation error (Figures 4.4, 4.7 and 4.10). The level of error in the bilayer structures means that little can be concluded from comparisons made between the bilayer structures with and without amantadine present (Figures 4.12, 4.13 and 4.14), or between the two charge states of amantadine (Figure 4.15).

The DOPC bilayer structure and, therefore, the form of the continuous Fourier transform sampled during the diffraction process, altered significantly with humidity. As the continuous Fourier transform changed with the humidity, the ability of the swelling series method to assign phases to the higher orders was diminished. A more complete analysis of the interaction of amantadine with DOPC bilayers would require the diffraction data to be phased out to higher orders than has been achieved here using the swelling series method.

8.2 Studies of bromolipid and DPPC bilayers by X-ray diffraction.

A bromolipid was synthesised and studied, primarily by X-ray diffraction, as a phospholipid molecule labelled with a bromine atom might provide an alternative phasing method to the swelling series approach. The bromolipid is a novel phospholipid derivative, where the *sn*-2 palmitoyl chain terminal methyl group of DPPC has been exchanged for a bromine atom. The bromolipid offers two methods of phasing diffraction data: firstly by the bromolipid bromine atom acting as a heavy atom in isomorphous replacement experiments, or secondly by the bromine atom acting as an anomalous scatterer in multiple anomalous dispersion (MAD) experiments. The bromolipid and DPPC were studied and compared in three different bilayer forms:

1) Pure DPPC and bromolipid bilayers in the gel ($L_{\beta'}$) phase, at 20°C and between 98% and 57% RH (Chapter 5).
2) Three different DPPC:bromolipid mixture (1:1, 7:2 and 4:1) bilayers in the gel ($L_{\beta'}$) phase, at 20°C and between 98% and 57% RH (Chapter 6).
3) Pure DPPC and bromolipid bilayers in the fluid (L_{α}) phase, at either 46°C, 50°C or 53°C and between 98% and 57% RH (Chapter 7).

Calorimetric (DSC) experiments were also performed on samples of DPPC, bromolipid and a 1:1 mixture of the two phospholipids (Chapter 5).

8.2.1 Study of DPPC and bromolipid bilayers in the gel ($L_{\beta'}$) phase.

X-ray diffraction patterns were collected from the gel phase DPPC and bromolipid bilayers out to fourteen and twelve orders, respectively (Tables 5.1 and 5.2). Both DPPC and bromolipid formed gel ($L_{\beta'}$) phase bilayers at 20°C and between 98% and 57% RH (Plates 5.1 and 5.2). The two phospholipids formed bilayers that differed in thickness by 1 to 2.3Å (Table 5.3), depending on humidity. The gel phase DPPC and bromolipid diffraction data were phased using the swelling series methods (Figures 5.1 and 5.5). Electron density map construction has shown that the bromolipid forms bilayers of a similar, but not identical, structure to those

of DPPC (Figures 5.7 and 5.8), with the major difference being the presence of an electron dense region at the centre of the bromolipid lipid layer. The bromine atoms, linked to the *sn*-2 lipid chain of bromolipid, would account for this electron density peak at the centre of the lipid layer. The bromolipid and DPPC bilayers, however, differ significantly across the entire lipid layer (0 to 15Å, Figure 5.8), showing the bromolipid not to be isomorphous with DPPC.

The bromolipid was synthesised for use in X-ray diffraction studies, primarily in mixtures with DPPC. The disruptive effect of bromolipid on the DPPC bilayer structure should decrease with the concentration of the bromolipid in the bilayer. Calorimetry (DSC) results (Table 5.4) show that mixing bromolipid 1:1 with DPPC produces a bilayer with physical properties that approach those of pure DPPC.

8.2.2 Study of mixture bilayers of DPPC and bromolipid.

Three different DPPC:bromolipid mixture ratios (1:1, 7:2 and 4:1) were studied by X-ray diffraction and the swelling series method. Both the 4:1 and 7:2 DPPC:bromolipid mixture bilayers were found to have a bilayer thickness similar to that of pure DPPC bilayers (Table 6.4). The 1:1 DPPC:bromolipid mixture formed bilayers with a thickness that was closer in magnitude to that of pure bromolipid than pure DPPC bilayers (Table 6.4). The swelling series method assigned the same phases to both the 4:1 and 7:2 DPPC:bromolipid mixture bilayer data that had previously been assigned to the pure DPPC bilayer data, supporting their validity (Figures 5.1, 7.2 and 7.3).

The electron density maps of the mixture bilayers (Figures 6.4, 6.5 and 6.6) show that the phospholipid headgroup position ($\pm$21-22Å) varies little with either humidity or, unlike the bilayer thickness, bromolipid concentration (Table 6.4). As the bromolipid concentration in the bilayer increased, a growth in electron density at the centre of the lipid layer was observed (Figure 6.7, 6.14). Confidence limits (95%) calculated for the electron density distributions reinforced the observation of an electron density peak at 0Å, due to the bromolipid (Figures 6.9 and 6.10). The

confidence limits also indicated that a significant decrease in electron density occurred, centred at ±10Å, as the bromolipid concentration increased (Figure 6.10, middle). Electron density difference maps also highlighted both the growth of the bromine atom peak at 0Å and the decrease in electron density at ±10Å as the bromolipid concentration in the bilayer increased (Figures 6.12, 6.13 and 6.14).

In general, the addition of bromolipid to the DPPC bilayer shifted the structure factor amplitude data in the positive direction (Figure 6.15, Table 6.5). This shift in the diffraction data can be used as a phasing method, as changes in the magnitude of the observed intensity are dependent on the original phase of the order. The bromolipid method of data phasing has the potential to be more conclusive than the swelling series method. Not only will the diffraction data of a bilayer sample vary in a predictable way with bromolipid concentration, that allows the data to be phased, but the reconstructed electron density maps must also show a bromine atom peak of a predictable size and position in the bilayer.

8.2.3 Study of DPPC and bromolipid bilayers in the fluid (L_α) phase.

Fluid (L_α) phase bilayers of the bromolipid and DPPC were also studied by X-ray diffraction and the swelling series method, with the aim of investigating the potential use of the bromolipid as a phasing agent in fluid phase bilayers. X-ray diffraction patterns were collected from oriented bilayer samples and phased using the swelling series method (Figures 7.1 and 7.4). Raising the bromolipid and DPPC bilayer systems above the chain melting temperature did not abolish the bilayer thickness difference between the two. The difference in the thickness could not be ascribed to a chain tilt effect, as fluid phase lipids chains are untilted. Comparison of the fluid phase DPPC and bromolipid electron density maps (Figure 7.7) located the electron dense bromolipid bromine atoms at the centre of the lipid layer. Whilst the bromolipid and DPPC headgroups appeared to have a similar structure, there was a discernible difference between the two bilayer structures along the length of the lipid chain layer (-10Å to +10Å, Figures 7.7 and 7.8). A similar difference was also found between gel phase bromolipid and DPPC bilayers, centred at ±10Å

(Figures 5.7 and 5.8). In spite of the structural differences between the bromolipid and DPPC bilayers, the diffraction data (Table 7.5) suggested that the bromolipid could be used as an isomorphous replacement phasing agent.

8.2.4 Lipid layer differences between DPPC and the bromolipid.

The DPPC and bromolipid bilayers differ by approximately 1Å-2Å in the gel phase (Tables 5.1 and 5.2) and by 2Å-4Å in the fluid phase (Tables 7.2, 7.3 and 7.4). The bilayer thickness difference is attributable to a change in the lipid layer width (Table 6.4), rather than a difference in headgroup conformation. The observed decrease in lipid layer thickness is not, however, due to a change in the lipid chain tilt angle (Table 5.3), a fact highlighted by the thickness difference existing in the fluid (L_α) phase. Comparison of pure DPPC and pure bromolipid bilayers shows that the two structures differ significantly across the entire lipid layer in both the gel (Figure 5.8) and fluid phases (Figure 7.7), with the bromolipid lipid layer having a lower relative electron density than that of DPPC (excluding the bromine atom peak). Both the DPPC:bromolipid mixture bilayer lipid layer relative electron density (centred at $\pm$10Å) and thickness decrease with increasing concentration of bromolipid in the bilayer (Figures 6.9 and 6.10). The DPPC and bromolipid lipid chains, therefore, differ in their conformation, a fact highlighted by their differing lipid layer widths and relative electron densities. One possible explanation for the observed differences might be that the heavy bromine atom disrupts the lipid chain packing, increasing the spacing between the lipid chains and decreasing the average density of the lipid layer.

8.2.5 The bromolipid as a phasing agent.

The synthesis of the bromolipid molecule has allowed electron dense bromine atoms to be inserted into a bilayer structure. The X-ray diffraction study has located the bromine atoms at the centre of the lipid layer, a result consistent with the bromine atoms having been attached to the *sn*-2 lipid chain terminus of a

phospholipid. The ability to place heavy atoms at a specific site in a membrane structure allows diffraction data to be phased by the isomorphous replacement technique. Structural changes that occurred on the addition of bromolipid to DPPC, such as the decrease in bilayer thickness, do not exclude the use of the bromolipid in isomorphous replacement experiments, as the changes appear to be continuous and predictable. The bromolipid may also offer a new phasing approach to membrane diffraction in the form of MAD experiments. Neither the concentration of bromolipid in the bilayer nor the structure of the bilayer would need to change during a MAD experiment, thus increasing the certainty of the phasing process.

Bibliography

Akers, C. K. and Parsons, D. F. (1970) Biophys. J. 10, 116-136.

Alecio, M. R., Miller, A. and Watts, A. (1985) Biochim. Biophys. Acta. 815, 139-142.

Anderson, J. M., Balda, M. S. and Fanning, A. S. (1993) Curr. Opin. Cell Biol. 5, 772-778.

Anderson, O. S. and Fuchs, M. (1975) Biophys. J. 15, 795-830.

Bach, D. (1983) In: Biomembrane structure and function, Chapter 1, 1-42, (Ed Chapman, D) The Macmillan Press Limited.

Bainton, D. (1981) J. Cell. Biol. 91, 66-76.

Bartles, J. R., Braiterman, L. and Hubbard, A. (1985) J. Cell Biol. 100, 1126-1138.

Bechinger, B. and Seelig, J. (1991) Chem. Phys. Lipids. 58, 1-5.

Belshe, R. B. and Hay, A. J. (1989) J. Resp. Dis. (supple), 52-61.

Bereiter-Hahn, J. (1990) Int. Rev. Cytol. 122, 1-63.

Bijvoet, J. M. (1949) Proc. Acad. Sci. Amst. B52, 313-314.

Bishop, W. R. and Bell, R. M. (1985) Cell 42, 51-60.

Blaurock, A. E. (1973) Biophys. J. 13, 1261-1262.

Blundell, T. L. and Johnson, L. N. (1976) Protein Crystallography, Academic Press, New York.

Bollen, I. C. and Higgins, J. A. (1980) Biochem. J. 189, 475-480.

Bradshaw, R. A. (1989) Trends Biochem. Sci. 14, 276-279.

Bragg, W. L. and Perutz, M. F. (1952) Proc. R. Soc. A. 213, 425-435.

Brockerhoff, H., Zingoni, J. and Brockerhoff, S. (1990) Neurochem. Int. 17, 15-19.

Browning, J. L. (1981) In: Liposomes: From physical structure to therapeutic applications (Ed Knight), 189-242, Elsevier North Holland Biomedical Press.

Buldt, G., Gally, H. U., Seelig, J. and Zaccai, G. (1979) J. Mol. Biol. 134, 673-691.

Caffrey, M., Fanger, G., Magin, R. L. and Zhang, J. (1990) Biophys. J. 58, 677-686.

Cantley, L. C. (1981) Curr. Topics. Bioenerget. 11, 201-237.

Casal, H. L. and McElhaney, R. N. (1990) Biochemistry 29, 5423-5427.

Cater, B. A., Chapman, D., Hawes, S. and Saville, J. (1974) Biochim. Biophys. Acta. 363, 54-69.

Ceve, G and Marsh, D. (1987) In: Phospholipid bilayers: Physical principles and models, Wiley, New York.

Chapman, D. and Chen, S. (1972) Chem. Phys. Lipids. 8, 318-326.

Chapman, D., Peel, W. E., Kingston, B. and Lilley, T. H. (1977) Biochim. Biophys. Acta. 464, 260-275.

Chapman, D., Urbina, J. and Keough, K. M. (1974) J. Biol. Chem. 249, 2512-2521.

Chapman, D., Williams, R. M. and Ladbrooke, B. D. (1967) Chem. Phys. Lipids. 1, 445-475.

Chapman, J. R. (1993) In: Practical organic mass spectrometry, 2nd Edition, J. Wiley and Sons, New York.

Cheetham, J. J. and Epand, R. M. (1987) Biosci. Rep. 7, 225-230.

Chen, S. C. and Sturtevant, J. M. (1981) Biochemistry 20, 713-718.

Chen, S. C., Sturtevant, J. M. and Gaffeny, B. J. (1980) Proc. Natl. Acad. Sci. U.S.A. 77, 5060-5063.

Crain, R. C. and Marinetti, G. V. (1979) Biochemistry 18, 2407-2414.

Cullis, P. R. and de Kruijff, B. (1979) Biochim. Biophys. Acta. 559, 399-420.

Da Silva, P. P. and Kachar, B. (1982) Cell 28, 441-450.

Danielli, J. F. and Davson, H. (1934) J. Cell Comp. Physiol. 5, 495

Darke, A., Finer, E. G., Flook, A. G. and Philips, M. C. (1972) J. Mol. Biol. 63, 265-279.

Datta, G., Parvathanathan, P. S., Rao, U. R. and Deniz, K. U. (1992) Physiol. Chem. Phys. Med. NMR. 24 (1), 51-61.

Davey, J., Hurtley, S. and Warren, G. (1985) Cell, 43, 643-652.

de Duve, C. (1975) Science 189, 186-194.

de Kroon, A. I. P. M., Soekarjo, M. W., de Gier, J. and de Kruijff, B. (1990) Biochemistry 29, 8229-8240.

de Kruijff, B., Cullis, P. R., Verkleij, A. J., Hope, M. J., Van Echteld, C. J. A. and Taraschi, T. F. (1984) In: The enzymes of biological membranes (Ed Martinosi, A) Plenum Press, New York.

de Kruijff, B., Cullis, P. R., Verkleij, A. J., Hope, M. J., Van Echteld, C. J. A., Taraschi, T. F., Van Hoogeevest, P., Killian, J. A., Rietveld, A. and Van der Steen, A. T. M. (1985) In: Progress in protein-lipid interactions (Ed Watts, A. and de Pont, J. J) Chapter 3, Elsevier science Publishers B. V.

Dickinson, R., Franks, N. P. and Leib, W. R. (1993) Biophys. J. 64, 1264-1271.

Duff, K. C. (1993) Ph.D. dissertation, University of Edinburgh, Scotland.

Duff, K. C. and Ashley, R. H. (1992) Virology 190, 485-489.

Duff, K. C., Cudmore, A. J. and Bradshaw, J. P. (1993) Biochim. Biophys. Acta. 1145, 149-156.

East, J. M. and Lee, A. G. (1982) Biochemistry 21, 4144-4151.

Elder, M., Hitchcock, P. B., Mason, R. and Shipley, G. G. (1977) Proc. R. Soc. Lond. A 354, 157-170.

Evans, W. H. (1977) Trends Biochem. Sci. 2, 169.

Evans, W. H. and Graham, J. M. (1989) In: membrane structure and function (Ed Rickwood, D) IRL Press at Oxford University Press.

Everett, J., Zlotnick, A., Tennyson, J. and Holloway, P. W. (1986) J. Biol. Chem. 261, 6725-6729.

Farquhar, M. and Palade, G. (1981) J. Cell Biol. 91, 77-103.

Fedson, D. S. (1987) Am. J. Med. 82 (Suppl 6A), 42-45.

Fields, B. N. (1985) In: Virology, Ch 4, Raven Press, New York.

Finean, J. B., Coleman, R. and Michell, R. H. (1984) In: Membranes and their cellular functions, 3rd Edition, Blackwell.

Flewelling, R. F. and Hubbell, W. L. (1986) Biophys. J. 49, 531-540.

Forbes, D. J. (1992) Curr. Opin. Cell Biol. 4, 637-645.

Franke, W. W., Scheer, U., Krohne, G. and Jarasch, E. D. (1981) J. Cell. Biol. 91, 31-50.

Franklin, C. J. and Cafiso D. S. (1993) Biophys. J. 65, 289-299.

Franks, N. P. and Leib, W. R. (1979) J. Mol. Biol. 133, 469-500.

Franks, N. P. and Leib, W. R. (1981) In: Liposomes: From physical structure to therapeutic applications (Ed Knight) Elsevier North Holland Biomedical Press.

Franks, N. P. and Levine, Y. K. (1981) Mol. Biol. Biochem. Biophys. 31, 438-487.

Franks, N. P., Arunachalam, T. and Caspi, E. (1978) Nature 276, 530-532.

Fuldner, H. H. (1981) Biochemistry 20, 5707-5710.

Gaber, B. P., Yager, P. and Peticolas, W. L. (1978) Biophys. J. 24, 677-688.

Gawrisch, K., Ruston, D., Zimmerberg, J., Parsegian, V. A., Rand, R. P. and Fuller, N. (1992) Biophys. J. 63, 1213-1223.

Gilman, A. G., Rall, T. W., Nies, A. S. and Taylor, P. (1990) In: The pharmaceutical basis of therapeutics, 8th edition, 472-473, Pergamon Press, New York.

Griffin, R. G., Powers, L. and Pershan, P. S. (1978) Biochemistry 17, 2718-2722.

Griffing, L. R. (1991) J. Electron Microsc. Tech. 17, 179-199.

Hakomori, S. (1986) Sci. Am. 254 (5), 44-53.

Handbook of Chemistry and Physics (Ed Weast, R. C) 67th edition, CRC Press (1986-1987), E-42.

Hargreaves, A. (1946) Nature 158, 620-621.

Harker, A. (1972) Biophys. J. 12, 1285-1295.

Hauser, H., Pascher, I. and Sundell, S. (1980) J. Mol. Biol. 137, 249-264.

Hauser, H., Phillips, M. C., Levine, B. A. and Williams, R. J. P. (1975) Eur. J. Biochem. 58, 133-144.

Hay, A. J. (1989) In: concepts in viral pathogenesis, Vol. 3, 561-567, Springr-Verlag, New York.

Haydon, D. A. and Hladky, S. B. (1972) Q. Rev. Biophys 5, 187-192.

Helenius, A., Mellman, Wall, D. and Hubbard, A. (1983) Trends Biochem. Sci. 8, 245-250.

Hendrickson, W. A. (1985a) In: Crystallography in molecular biology (Ed Moras, D. and Drenth, J) NATO ASI series A: Life sciences, Vol 126, 81- 87.

Hendrickson, W. A. (1985b) Methods. Enzymol. Vol 115, 41-55.

Hendrickson, W. A. (1991) Science 254, 51-58.

Hendrickson, W. A. and Teeter, M. M. (1981) Nature 290, 107-113.

Higgins, J. A. and Evans, W. H. (1978) Biochem. J. 174, 563-567.

Hirano, H., Parkhouse, B., Nicholson, G. L., Lennox, E. S. and Singer, S. J. (1972) Proc. Natl. Acad. Sci., U.S.A., 69, 2945.

Hitchcock, P. B., Mason, R., Thomas, K. M. and Shipley, G. G. (1974) Proc. Natl. Acad. Sci., U.S.A. 71, 3036-3040.

Hladky, S. B. and Haydon, D. A. (1983) Biochim. Biophys. Acta. 318, 464-468.

Hokin, L. E. (1976) Trends Biochem. Sci., 1, 233.

Holloway, P. W., Markello, T. C. and Leto, T. L. (1982) Biophys. J. 57, 63-64.

Honig, B. H., Hubbell, W. L. and Flewelling, R. F. (1986) Annu. Rev. Biophys. Biophys. Chem. 15, 163-193.

Huang, C. and Levin, I. W. (1983) J. Phys. Chem. 87, 1509-1513.

Huang, C. H. and Mason, J. T. (1986) Biochim. Biophys. Acta. 864, 423-470.

Huang, C., Mason, J. T. and Levin, I. W. (1983) Biochemistry 22, 2775-2780.

Hui, S. W. and Huang, C. H. (1986) Biochemistry 25, 1330-1335.

Hui, S. W., Mason, J. T. and Huang, C. (1984) Biochemistry 23, 5570-5577.

Janiak, M. J., Small, D. M. and Shipley, G. G. (1976), Biochemistry, 15, 4575-4580.

Katsaras, J. and Stintson, R. H. (1990) Biophys. J. 57, 649-655.

Katsaras, J., Stinson, R. H., Davis, J. H. and Kendall, E. J. (1991) Biophys. J. 59, 645-653.

Katsaras, J., Yang, D. and Epand, R. M. (1992) Biophys. J. 63, 1170-1175.

Keough, K. M. W. and Davis, P. J. (1979) Biochemistry 18, 1453-1459.

Kornfeld, S. and Mellman, I. (1989) Annu. Rev. Cell Biol. 5, 483-525.

Kratky, O. (1967) In: Small angle scattering (Ed Brumberger, H), 63-120. New York, Gordon and Breach.

Kregenow, F. M. (1981) Annu. Rev. Physiol, 43, 643-652.

Ladbrooke, B. D., Williams, R. M. and Chapman, D. (1968) Biochim. Biophys. Acta. 150, 333.

Lake, J. A. (1981) Sci. Am. 245, 84-97.

Lamb, R. A., Zebedee, S. and Richardson, C. (1985) Cell 40, 627-633.

Lanoue, K. F. and Schoolwerth, A. C. (1979) Annu. Rev. Biochem. 48, 871-922.

LeBlanc, O. H. (1969) Biochim. Biophys. Acta. 193, 350-360.

LeBlanc, O. H. (1970) Biophys. J. 14, 94a.

Leiberman, Y. A. and Topaly, V. P. (1969) Biophysics 14, 477-487.

Lenaz, G. (1977) In: Membrane proteins and their interactions with lipids, Vol 1, 47-149, (Ed Capaldi, R. A) Marcel Dekker, New York.

LeNeveu, D. M., Rand, R. P. and Parsegian, V. A. (1976) Nature 259, 601-603.

LeNeveu, D. M., Rand, R. P., Gingell, D. and Parsegian, V. A. (1977) Biophys. J. 18, 209-230.

Lesslauer, W., Cain, J. E. and Blasie, J. K. (1972) Proc. Natl. Acad. Sci. U.S.A. 69, 1499.

Leto, T. L., Roseman, M. A. and Holloway, P. W. (1980) Biochemistry 19, 1911-1916.

Levine, Y. and Wilkins, M. H. F. (1971) Nature 230, 69-72.

Levine, Y. K. (1972) Prog. Biophys. Mol. Biol. 24, 3-74.

Levine, Y. K. (1973) Prog. Surf. Sci. 3, 279-352.

Lewis, B. A., Das Gupta, S. K. and Griffin, R. G. (1984) Biochemistry 23, 1988-1993.

Lis, L. J., Lis, W. T., Parsegian, V. A. and Rand, R. P. (1981) Biochemistry 20, 1771-1777.

Lis, L. J., McAllister, M., Fuller, N., Rand, R. P. and Parsegian, V. A. (1982a) Biophys. J. 37, 657-666.

Lis, L. J., McAllister, M., Fuller, N., Rand, R. P. and Parsegian, V. A. (1982b) Biophys. J. 37, 667-672.

Luria, S. E., Darnell, J. E., Baltimore, D. and Campbell, A. (1978) In: General Virology, 3rd edition, Wiley.

Luzzati, V. (1960) Acta. Crystallogr. 13, 939-345.

Luzzati, V. (1968) In: Biological Membranes (Ed Chapman, D) Academic Press Inc. (London) Ltd.

Luzzati, V., Mustacchi, H., Skoulios, A. E. and Husson, F. (1960) Acta. Crystallogr. 13, 660.

Luzzati, V., Tardieu, A. and Taupin, D. (1972) J. Mol. Biol, 64, 269-286.

Makowski, L. and Li, J. (1983) In: Biomembrane structure and function, Chapter 2, 58-59, (Ed Chapman, D) The Macmillan Press Limited.

Margulis, L. and Schwartz, K. V. (1982) Five Kingdoms. W. H. Freeman and Company. Electron micrographs and diagrams of representative cells from the principle groups of prokaryotes, eukaryotic microorganisms, plants and animals.

Markello, T., Zlotnick, A., Everett, J., Tennyson, J. and Holloway, P. (1985) Biochemistry 24, 2895-2901.

Martin, K. and Helenius, A. (1991) Cell 67, 117-130.

Mason, J. T. and Huang, C. (1981) Lipids 16, 604-608.

Mason, J. T., Broccoli, A. V. and Huang, C. (1981a) Anal. Biochem. 113, 96-101.

Mason, J. T., Huang, C. and Biltonen, R. L. (1981b) Biochemistry 20, 6086-6092.

Mattai, J., Sripada, P. K. and Shipley, G. G. (1987) Biochemistry 26, 3287-3297.

McIntosh, T. J. and Holloway, P. W. (1987) Biochemistry 26, 1783-1788.

McIntosh, T. J., Simon, S. A., Ellington, J. C. and Porter, N. A. (1984) Biochemistry 23, 4038-4044.

McIntosh, T. J., Wallbillig, R. C. and Robertson, J. D. (1976) Biochim. Biophys. Acta. 448, 15-33.

McLaughlin, S. (1977) In: current topics in membranes and transport. Vol. 9. (Ed Bronner, F. and Kleinzeller, A) Academic Press, New York, 71-144.

Mendelsohn, R., Davies, M. A., Brauner, J. W., Schuster, H. F. and Dluhy, R. A. (1989) Biochemistry 28, 8934-8939.

Monto, A. S. (1983) Am. Fam. Physician 28, 165-169.

Moody, M. F. (1963) Science 142, 1173-1174.

Moody, M. F. (1975) Acta. Crystallogr. A31, 8-15.

Mueckler, M., Caruso, C., Baldwin, S. A., Panico, M., Blench, I., Morris, H. R., Allard, W. J., Lienhard, G. E. and Lodish, H. F. (1985) Science 229, 941-945.

Nagle, J. F. (1980) Annu. Rev. Phys. Chem. 31, 157-195.

Nagle, J. F. and Wiener, M. C. (1989) Biophys. J. 55, 309-313.

New, R. R. C. (1990) In: Liposomes, A practical approach. (Ed New, R) Chapter 3, 109-112.

Nicholson, K. G. and Wiselka, M. J. (1991) Br. Med. J. 302, 425-426.

Nillson, A., Holmgren, A. and Lindblom, G. (1991) Biochemistry, 30, 2126-2133.

Nillson, O. S. and Dallner, G. (1977) Biochim. Biophys. Acta. 464, 453-458.

Novikoff, A. (1976) Proc. Natl. Acad. Sci U.S.A. 73, 2781-2787.

Obeso, J. A. and Martinez-Lage, J. M. (1987) In: The handbook of Parkinson's disease (Ed Koller, W. C), 312-316, Marcel Dekker, New York.

Okamura, E., Umemura, J. and Takenaka, T. (1990) Biochim. Biophys. Acta. 1025, 94-98.

Okhuma, S., Moriyama, Y., Takano, T. (1982) Proc. Natl. Acad. Sci. USA. 79, 2758-2762.

Oxford, J. S. and Galbraith, A. (1980) Pharmacol. Ther. 11, 182-262.

Parsegian, V. A. and Rand, R. P. (1983) Ann. N.Y. Acad. Sci. 416, 1-9.

Parsegian, V. A., Fuller, N. and Rand, R. P. (1979) Proc. Natl. Acad. Sci. U.S.A. 76, 2750-2754.

Pearson, R. H. and Pascher, I. (1979) Nature 281, 499-501.

Pedersen, P. L. and Carafoli, E. (1987) Trends Biochem. Sci. 12, 146-150 and 186-189.

Perret, B., Chap, H. J. and Douste-Blazy, L. (1979) Biochim. Biophys. Acta. 556, 434-446.

Perutz, M. F. (1954) Proc. R. Soc. A., 225, 264.

Philips, M. C., Williams, R. M. and Chapman, D. (1969) Chem. Phy. Lipids 3, 234.

Phonphok, Y. and Rosenthal, K. S. (1991) FEBS Lett. 281, 188-190.

Post, J. A., Langer, G. A., Op den Kamp, J. A. F. and Verkleij, A. J. (1988) Biochim. Biophys. Acta. 943, 256-266.

Press, W. H., Flannery, B. P., Teukolsky, S. A. and Vetterling, W. T. (1989) In: Numerical Recipes: The art of scientific computing, 529 -538, Cambridge University Press, Cambridge.

Quinn, P. J. (1976) The Molecular Biology of Cell Membranes. University Park Press.

Rand, R. P., Chapman, D. and Larsson, K. (1975) Biophys. J. 15, 1117-1124.

Renooij, W., Van Golde, L. M. G., Zwaal, R. F. A. and Van Deenen, L. L. M. (1976) Eur. J. Biochem. 61, 53-58.

Rose, M. E. and Johnstone, R. A. W. (1982) In: Mass spectrometry for chemists and biochemists, Cambridge University Press, Cambridge.

Ruben, F. L. (1987) Am. J. Med. 82 (Suppl 6A), 31-34.
Sansom, M. S. P. and Kerr, I. D. (1993) Protein Eng. 6, 65-74.
Scherer, P. G. and Seelig, J. (1989) Biochemistry 28, 7720-7728.
Schlessinger, J. and Ullrich, A. (1992) Neuron 9, 383-391.
Schneeberger, E. E. and Lynch R. D. (1992) Am. J. Physiol 262, 647-661.
Seddon, J. M. (1990) Biochim. Biophys. Acta. 1031, 1-69.
Seelig, J. and Seelig, A. (1980) Q. Rev. Biophys. 13, 19-61.
Selinger, Z. and Lapidot, Y. (1966) J. Lipid. Res. 7, 174.
Serrallach, E. N., de Haas, G. H. and Shipley, G. G. (1984) Biochemistry 23, 713-720.
Shah, J., Sripada, P. K. and Shipley, G. G. (1990) Biochemistry 29, 4254-4262.
Shinooka, T., Shibata, A. and Terada, M. (1992) J. Mol. Biol. 103, 421-431.
Silvius, J. R. (1990) Biochemistry 29, 2930-2938.
Simons, K. and Fuller, S. D. (1985) Annu. Rev. Cell Biol. 1, 243-288.
Singer, S. J. and Nicholson, G. L. (1972) Science. 174, 720-731.
Sjolund, M., Rilfors, L. and Lindblom, G. (1989) Biochemistry 28, 1323-1329.
Skehel, J. J., Bayley, P. M., Brown, E. B., Martin, S. R., Waterfield, M. D., White, J. M., Wilson, I. A. and Wiley, D. C. (1982) Proc. Natl. Acad. Sci. USA. 79, 968-972.
Small, D. M. (1967) J. Lipid. Res. 8, 551-557.
Smith, I. C., Auger, M. and Jarrell, H. C. (1991) Ann. NY. Acad. Sci. 625, 668-684.
Srere, P. A. (1982) Trends Biochem. Sci. 7, 375-378.
Steim, J. M. (1974) Methods in Enzymology, Vol 32, 263-272.
Stumpel, J., Eibl, H. and Nicksch, A. (1983) Biochim. Biophys. Acta. 727, 246-254.
Stumpel, J., Nicksch, A. and Eibl, H. (1981) Biochemistry 20, 662-665.
Sugrue, R. J. and Hay, A. J. (1991) Virology 180, 617-624.
Sugrue, R. J., Bahadur, G., Zambon, M. C., Hall-smith, M., Douglas, A. R. and Hay, A. J. (1990) EMBO. J. 9, 3469-3476.
Sweadner, K. J. and Goldin, S. M. (1980) N. Engl. J. Med. 302, 777-783.
Taiz, L. and Zeiger, E. (1991) In: Plant Physiology, 229-233, Benjamin/Cummins, Redwood City, California.
Tardieu, A., Luzzati, V. and Reman, F. C. (1973) J. Mol. Biol. 75, 711-733.
Tate, M. W. and Gruner, S. M. (1989) Biochemistry 28, 4245-4253.
Thorens, B., Charron, M. J. and Lodish, H. F. (1990) Diabetes Care 13, 209-218.
Tolbert, N. E. and Essner, E. (1981) J. Cell. Biol 91, 271-283.

Torbet, J. and Wilkins, M. H. F. (1976) J. Theor. Biol, 62, 447-458.

Tummler, B., Herrmann, U., Maass, G. and Eibl, H. (1984) Biochemistry 23, 4068-4074.

Turner, D. C. and Gruner, S. M. (1992) Biochemistry, 31, 1340-1355.

Ullrich, A., Bell, J. R., Chen, E. Y., Herrera, R., Petruzzelli, L. M., Dull, T. J., Coussens, L., Liao, Y.-C., Tsubokawa, M., Mason, A., Seeburg, P. H., Grunfeld, C., Rosen, O. M. and Ramachandran, J. (1985) Nature 313, 756-761.

Unwin, N. and Henderson, R. (1984) Sci. Am. 250 (2), 78-94.

Velski, Z., Salsbury, N. J. and Chapman, D. (1969) Biochim. Biophys. Acta. 183, 434-446.

Wallach, D. F. H. and Zahler, P. H. (1966) Proc. Natl. Acad. Sci., U.S.A., 56, 1552.

Watts, C. and Marsh, M. (1992) J. Cell Sci. 103, 1-8.

Wiener, M. C. and White, S. H. (1991) Biochemistry 30, 6997-7008.

Wilkins, M. H. F. (1972) Ann. New. York. Acad. Sci. 195, 291.

Worcester, D. L. and Franks, N. P. (1976) J. Mol. Biol. 100, 359-378.

Worthington, C. R, King, G. I. and McIntosh, T. J. (1973) Biophys. J. 13, 480-494.

Yeager, M. D. and Fiegenson, G. W. (1990) Biochemistry 29, 4380-4392.

Yeagle, P. L. (1985) Biochim. Biophys. Acta. 822, 267-288.

Zaccai, G., Buldt, G., Seelig, A. and Seelig, J. (1979) J. Mol. Biol. 134, 693-706.

Zachowski, A. (1993) Biochem. J. 294, 1-14.

Zebedee, S. and Lamb, R. A. (1988) J. Virol. 62, 2762-2772.

Zheng, C. and Vanderkooi, G. (1992) Biophys. J. 63, 935-941.

APPENDIX

PUBLISHED PAPERS RESULTING FROM WORK PRESENTED IN THIS THESIS

Biochimica et Biophysica Acta, 1145 (1993) 149–156

BBAMEM 75860

The location of amantadine hydrochloride and free base within phospholipid multilayers: a neutron and X-ray diffraction study

K.C. Duff [a], A.J. Cudmore [a] and J.P. Bradshaw [a,b]

[a] *Department of Biochemistry, University of Edinburgh, Edinburgh (UK) and* [b] *Department of Preclinical Veterinary Sciences, University of Edinburgh, Edinburgh (UK)*

(Received 6 May 1992)
(Revised manuscript received 19 October 1992)

Key words: Amantadine free base; Amantadine hydrochloride; Phospholipid multilayer; X-ray diffraction; NMR, ^{2}H-

Concomitant neutron and X-ray studies were undertaken in order to locate accurately the anti-influenza and Parkinson's disease drug amantadine in multilayers of 1,2-dioleoyl-*sn*-glycero-3-phosphocholine. The X-ray data were phased using the swelling series method and the neutron data were phased using D_2O/H_2O exchange and a variation of the isomorphous replacement technique. The sets of data complement each other and reveal two populations of amantadine within the bilayer. One site is close to the bilayer surface, the other is much deeper. The majority of the amantadine occupies the surface site. The relative occupancy, but not the position, of the two locations appears to be dependent upon the initial protonation state of the drug. No evidence of bilayer perturbation was observed with either the protonated or the deprotonated forms of amantadine.

Introduction

Amantadine (1-aminoadamantane hydrochloride) is licensed for the prophylaxis of influenza A infection and for treatment of both influenza and Parkinson's disease [1,2]. In the case of influenza, the efficacy of amantadine is postulated to involve interruption of viral-host cell membrane fusion and/or interference in haemagglutinin maturation [3,4]. The mechanism of action of amantadine in Parkinson's disease is probably related to its ability to increase presynaptic synthesis and release of dopamine. This effect is potentiated by the drug inhibiting dopamine reuptake [5]. These therapeutic processes are thought to include the involvement of the hydrophobic, lipophilic properties of the molecule [6].

Amantadine studies undertaken so far have been wide-ranging, including its effect on influenza infection and, more recently, its specific molecular effect on the viral protein which is implicated in this drug-induced prophylaxis, namely M2 [7]. A recent study has examined the role of amantadine in the stabilisation of clathrin-coated membrane vesicles, similar to those formed upon initial viral penetration by influenza, Semliki Forest and vesicular stomatitus virus [6]. However, other authors have reported that, although tromantadine (an amantadine derivative: *N*-1-adamantyl-*N*-[2-(dimethylamino)ethoxy]acetamide hydrochloride) appears to stabilise phospholipid bilayers, amantadine itself slightly lowers the temperature of the bilayer to hexagonal phase transition. Also, NMR studies have shown that amantadine is perturbing to the organisation and motional properties of phospholipids in the bilayer phase [8]. These results indicate an amantadine-mediated increase in disorder. It can therefore be seen that a certain degree of ambiguity exists in the available data.

As a prerequisite of further mechanistic studies of amantadine, we have undertaken a series of experiments to investigate the location of the drug within bilayers of 1,2-dioleoyl-*sn*-glycero-3-phosphocholine (DOPC). To reduce possible ambiguity in the results a single lipid species was used, DOPC being the most physiologically representative. We have also examined any differences between amantadine hydrochloride (HCl) and amantadine in its free base form (FB).

This report describes the use of a specific deuterium labelling technique to locate amantadine in synthetic multilayer membranes using neutron diffraction. These

Correspondence to: J.P. Bradshaw, Department of Biochemistry, University of Edinburgh, Hugh Robson Building, George Square, Edinburgh, EH8 9XK, UK.

Abbreviations: amantadine FB, 1-amino adamantane free base; amantadine HCl, 1-amino adamantane hydrochloride; DOPC, 1,2-dioleoyl-*sn*-glycero-3-phosphocholine; DOPE, 1,2-dioleoyl-*sn*-glycero-3-phosphoethanolamine; NMR, nuclear magnetic resonance spectroscopy; rh, relative humidity.

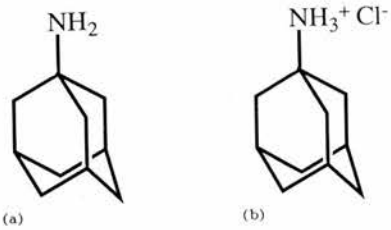

Fig. 1. The two forms of 1-aminoadamantane used in this study: (a) amantadine free base, (b) amantadine hydrochloride.

results are both quantitatively and qualitatively supported by a concomitant X-ray diffraction study using unlabelled amantadine.

Materials and Methods

1,2-Dioleoyl-*sn*-glycero-3-phosphocholine (DOPC) was purchased from Sigma (Fancy Road, Poole, UK) and confirmed to be a single species by thin-layer chromatography. Amantadine was obtained from the same source in both free base and hydrochloride forms (Fig. 1). Deuterated amantadine FB was obtained from Dr. M.R. Alecio of the Shell Research Centre (Sittingbourne, Kent, UK).

X-ray diffraction

Oriented phospholipid bilayer stacks were prepared as follows. Samples comprising 5 mg of DOPC with or without 5% (mol) amantadine were dissolved in methanol and applied to a curved glass support of approx. 1 cm^2 area. The solvent was allowed to evaporate before the slide was dried in vacuo for 2 h. Subsequently, the samples were hydrated for at least 2 h at 20°C and 100% humidity. Once fully hydrated, the samples were transferred to the sample cell of the X-ray camera.

For at least 1 h before and subsequently throughout the diffraction experiment, the samples were held in a purpose built environmental cell which allowed the temperature and humidity of the sample to be controlled. Temperature control was achieved by circulating water from a thermostat bath through tubes in the brass walls of the cell; all samples were run at 20°C at which DOPC adopts the L_α-phase. The humidity, and therefore the bilayer spacing, was controlled by passing air through containers of saturated salt solutions and then through the sample cell. Saturated solutions of $ZnSO_4$ (90% rh), KCl (81% rh), NaCl (74% rh) and NaBr (57% rh) were used in addition to distilled water (98% rh).

In the camera used to produce the diffraction patterns, 0.3 mm collimated, Nickel filtered copper K_α radiation of 1.54 Å from a Marconi-Elliot GX-13 rotating anode X-ray generator was scattered by the sample onto a pack of four 130 × 180 mm Agfa-Gevaert Osray X-ray films positioned 175 mm from the sample. The diffracted beam path was evacuated to reduce background noise from air-scattered radiation. To record the complete range of intensities without exceeding the films' dynamic range, each sample was exposed twice, typically for 20 h followed by a separate 4 min exposure. The developed films were scanned on a Joyce Loebl Chromoscan 3 microdensitometer.

Neutron diffraction

Sample preparation was essentially the same as described for the X-ray experiments, with the exception that each sample was 20 mg in weight and prepared on a quartz microscope slide. D_2O/H_2O exchange was achieved by dehydrating the samples in vacuo before re-equilibration over the new solvent.

Neutron diffraction data were collected using the D16 instrument at the Institut Max von Laue - Paul Langevin, Grenoble, France. After rehydration the quartz slide bearing its oriented multi-bilayer phospholipid sample was placed in the temperature controlled cell of the instrument along with water baths containing either D_2O or H_2O where it was allowed a further period of equilibration of 0.5–1 h. During this period the equilibration process was monitored by recording the angular position of the third or fourth order of lamellar diffraction which increased as the multilayers dehydrated and decreased as they took up water from the atmosphere. Each sample was judged to have achieved equilibrium when there was no further shift in the position of the Bragg peaks and the calculated lamellar repeat distance was that predicted for the experimental conditions by previous X-ray work. Any sample which did not fulfil both of these criteria was discarded. Each recorded diffraction pattern consisted of at least eight well defined orders. The mosaic spread of each sample was determined using the D16 software.

X-ray data analysis

The background scattering level was estimated by measuring the optical density of each X-ray film in the region immediately adjacent to a diffraction peak and interpolating across its base. Any peaks in which the dynamic range of the film had been exceeded were ignored. After integration of the diffracted intensities the films were scaled together using overlapping peaks and averaged to obtain the final set of intensities. A Lorentz factor was applied to take into account the spreading of the intensity in reciprocal space and the sampling of the peaks by the Ewald sphere. The diffraction peaks were discrete and well defined and were restricted to the meridional region of the film. In such situations, the Lorentz factor takes the form of $\sin(2\theta_h)$, where θ is the Bragg angle and h the order of diffraction. A further correction was applied for absorption of the incident and diffracted beams by the

lipid film [9]. Data sets of Bragg intensities (I_h) were scaled to each other using the expression:

$$\Sigma I_h = D/D_{\min}$$

where D is the Bragg spacing (bilayer repeat distance) and $D_{\min}$ represents the minimum Bragg spacing of a series run at different humidities.

D for each sample was determined using the Bragg equation. The instrument offset angle for each sample was calculated by iterative least squares regression of this equation over all observed orders of diffraction.

Neutron data analysis

Once the diffracted intensities had been corrected for detector response and background then integrated, the following corrections were applied:

(1) Acceptance angle. The projection of the quartz slide along the normal to the neutron beam is dependent upon its relative angle to the beam. If the slide presents a very low angle (θ) to the incident beam, it only samples a small fraction of the total neutron beam width and, therefore, flux. This means that the diffraction peaks recorded for the lower orders will be correspondingly weaker than if the slide were able to sample the whole width of the neutron beam. As long as the neutron beam is wider than the maximum projected width of the sample slide and the neutron flux constant across the width of the beam, the angular correction factor, takes the form:

$$C_{\mathrm{Ang}(h)} = 1/\sin\,\theta_h$$

(2) Lorentz factor. For the geometry used in this study, the appropriate correction factor is:

$$C_{\mathrm{Lor}(h)} = \sin(2\theta_h)$$

(3) Absorption. When the angle of diffraction is low, the incident and diffracted beam have a significant path length within the sample and thus will be subject to a greater degree of absorption than when the angle is high and the corresponding path lengths low. Moreover, the degree of absorption will also be affected by the H_2O/D_2O composition of the sample. The appropriate correction for absorption by the lipid film, was applied:

$$C_{\mathrm{Abs}(h)} = 1/(\sin\,\theta/2ut)(1 - \exp[-2ut/\sin\,\theta])$$

where $u = (6.04–0.75d)$, d being the mole fraction of D_2O [10]. The mass of lipid on each slide, the area over which it was spread and the unit cell size, as determined by diffraction, were used to calculate a value of 30 μm for t, the thickness of the lipid film.

(4) Sampling by the detector. As a result of lattice disorder in the sample, the diffraction peaks may be so wide that the whole of each diffraction peak is not recorded by the detector, and a correction must be applied to the data to account for this. In this study the mosaic spread of each sample was small enough to ensure that each diffraction peak was regular in shape and contained wholly within the central part of the detector so no correction was applied in this case.

The final neutron structure factor amplitudes were therefore calculated as:

$$F_h^2 = I_h \cdot C_{\mathrm{Ang}(h)} \cdot C_{\mathrm{Lor}(h)} \cdot C_{\mathrm{Abs}(h)}$$

Phasing

Electron density or neutron scattering profiles may only be obtained upon solving the individual phases of the recorded amplitudes. In this study three different techniques were employed to phase the data sets: swelling series, D_2O/H_2O exchange and isomorphous replacement.

The X-ray structure factors were phased using a five point swelling series [11]. Our methodology comprised of selecting from the swelling series one working set of eight diffraction peaks and using this to compute a continuous transform [12] against which the fit of all the other observed sets were compared. The best fit minimised the difference between the calculated and the observed intensities for each of the possible 256 phase combinations. The selected working set alternated until all five had been used and sampled against. The resulting transform represented the best, integrated fit for all data over all possible phases. This process was carried out independently for the DOPC, DOPC/amantadine HCl and DOPC/amantadine FB swelling series.

Neutron data are routinely phased by carrying out experiments hydrated at various H_2O/D_2O ratios [9,10,13,14]. This method was used in the present study, with additional phasing information coming from a variation of the isomorphous derivative technique [15] in which use was made of the presence or absence of amantadine in the multilayers. Assigning phases to the neutron data proceeded by altering the sign of the individual structure factors until a result was achieved in which both the differences caused by replacing H_2O with D_2O and the DOPC/amantadine minus DOPC differences were consistent within each set of comparable data.

The two techniques, using X-rays and neutrons, emphasise different features within the bilayer structure, and further confirmation that the correct phases had been assigned was given by the fact that the two methods agreed and thereby showed the complementary nature of the techniques.

White and his co-workers [16] have produced an elegant method for scaling neutron data. This approach was used in the present study and basically involved using the size of the D_2O and the amantadine distributions to scale the different sets of data to each other. The results put the profiles on a 'relative absolute' scale in which they are scaled with respect to the unit cell contents, but not on an absolute per volume scale. The method is also readily applicable to X-ray data, although for this there is no equivalent of the D_2O peak therefore scaling is carried out on the size of the amantadine distribution alone.

Results

Fig. 2 is a representative X-ray diffraction pattern, in this instance obtained from DOPC with 5% (mol) amantadine FB at 90% rh. Fig. 3 shows the relationship between the relative humidity of the sample chamber and the bilayer repeat distance as observed by X-ray and neutron diffraction. Fig. 4 shows the swelling series data used to phase the X-ray diffraction patterns of pure DOPC (a), DOPC with 5% (mol) amantadine HCl (b) and DOPC with 5% (mol) amantadine FB (c). In each case the continuous transform calculated from 98% rh data is shown superimposed upon the observed diffraction amplitudes for 98, 90, 81, 74 and 57% rh. Table 1 gives the corrected, scaled neutron diffraction structure factors for all three samples at 0% and 100% D_2O. Fig. 5 shows reconstructed transbilayer profiles of DOPC alone (a, b) and difference profiles calculated by subtraction of structure factor data sets of corresponding *D*-repeat to define the distribution of amantadine HCl (c, d) and FB (e, f), respectively.

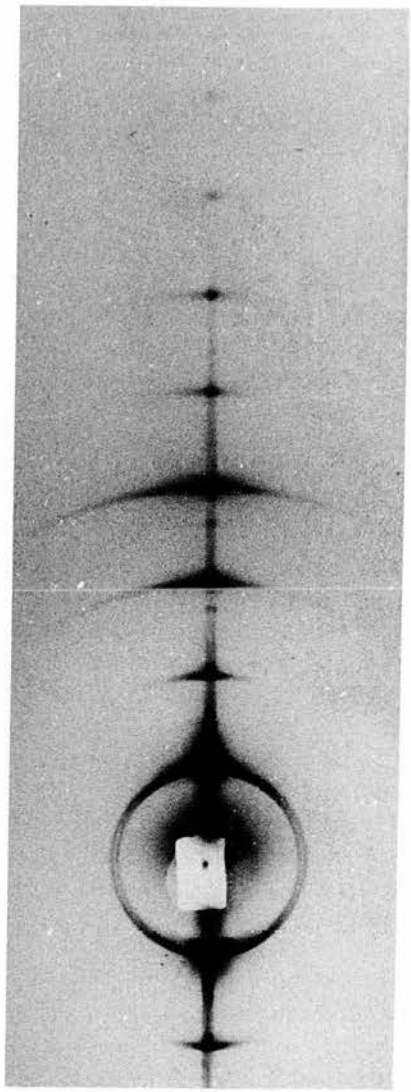

Fig. 2. X-ray diffraction pattern of lamellar arrays of DOPC with 5% (mol) amantadine FB at 90% relative humidity and 20°C.

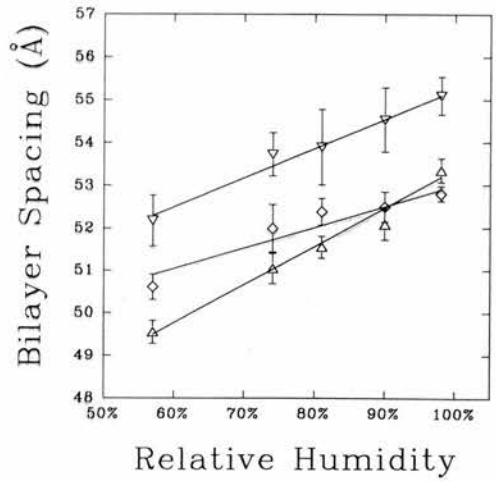

Fig. 3. The relationship between the relative humidity at 20°C of the sample and the observed bilayer spacing (in ångströms, Å). ▽, pure DOPC; △, amantadine hydrochloride; ◇, amantadine free base. The error bars represent the standard deviation for each point. Sample size varied from 3 to 9.

The mosaic spread of the DOPC bilayers ranged from 0.4° to 0.6°, these very low values being quite characteristic of unsaturated fatty acyl phospholipids. The mosaic spread was not significantly changed upon the addition of amantadine.

Discussion

DOPC

Fig. 5 displays both X-ray and neutron scattering density profiles across the phospholipid bilayer with the water component occupying the outer region of the graphs. With X-rays, the DOPC profile (a) agrees with previously published data [17,18] in that it displays the classic phospholipid leaflet form with a main peak representing the electron-dense region which encompases the phosphate groups and fatty acyl ester bonds. A secondary peak appears within the hydrophobic region which corresponds to the double-bond in the oleic

acid chains. It can be seen from (b) that less detail results from the neutron data. This is probably due to the lower contrast characteristic of neutron scattering (all diffraction experiments were sampled through eight orders so this phenomenon does not involve the X-ray data being collected to a higher resolution than the neutron).

The differences between the X-ray and neutron profiles are due to inherent atomic scattering differences across the unit cell. X-rays are more strongly scattered by the phosphate groups in the repeat motif whereas maximum neutron scattering corresponds to the fatty acyl ester bond positions [19]. Profile (b) clearly displays this scattering dichotomy with the neutron data peak appearing markedly closer to the hydrophobic interior of the bilayer than the X-ray result (a). The sharper X-ray profile displays a second highly defined peak in the fatty acyl chain region of the leaflet.

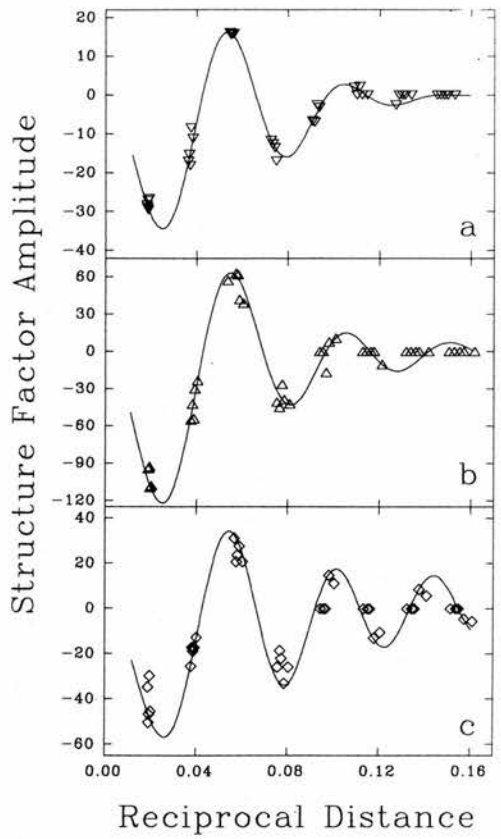

Fig. 4. Structure factors of lamellar arrays of bilayers of (a) pure DOPC, (b) DOPC with 5% (mol) amantadine HCl and (c) DOPC with 5% (mol) amantadine FB, plotted against corresponding reciprocals of Bragg spacings ($Å^{-1}$). The amplitudes of the structure factors are equal to the square roots of the Bragg intensities, their signs are those derived from the phasing procedure described in the text. The swelling series data sets were collected at 98, 90, 81, 74 and 57% relative humidity. The continuous transforms calculated from the 98% rh data is shown.

TABLE I

Relative absolute neutron structure factors of lamellar arrays of pure DOPC and DOPC with 5% (mol) amantadine HCl or FB at 98% rh and 20°C. The accuracy is estimated to be ± 0.15 units

Order	DOPC 20°C, 98%rh (D_2O)	DOPC+5 mol% amantadine HCl 20°C, 98%rh (D_2O)	DOPC+5 mol% D-amantadine FB 20°C, 98%rh (D_2O)
1	−89.31	−61.22	−96.41
2	25.56	10.02	18.80
3	−4.34	−1.68	−2.76
4	1.00	0.32	1.21
5	−2.84	−1.86	−2.97
6	0.77	0.06	0.57
7	−0.67	0.15	−0.16
8	0.00	−0.27	−0.15
Order	DOPC 20°C, 98%rh (H_2O)	DOPC+5 mol% amantadine HCl 20°C, 98%rh (H_2O)	DOPC+5 mol% D-amantadine FB 20°C, 98%rh (H_2O)
1	−6.47	−19.74	−13.55
2	−12.09	−8.66	−17.65
3	5.16	3.17	6.53
4	0.34	0.00	0.00
5	−1.44	−1.37	−1.98
6	0.33	−0.18	0.33
7	−0.30	0.26	0.00
8	0.00	−0.30	0.00

Amantadine HCl

Fig. 5. (c) to (f) are difference profiles which were calculated by subtracting the lipid component from the lipid + amantadine structure factors and therefore represent only the amantadine distribution across the bilayer. They are displayed in the same orientation as the pure DOPC but it can be seen that these profiles, both X-ray and neutron, are substantially different from the DOPC data. Amantadine, in both its hydrochloride and free base forms, appears to have been incorporated into the multilayer system.

The highest peak in the X-ray profile (c), representing the greatest distribution of amantadine HCl, lies between the phosphate and ester linkages. This surface location is also represented in the neutron (d) profile but its shape has changed with additional density encroaching into the water. It is proposed that the difference between the X-ray and neutron profiles is due to the relatively higher scattering length of nitrogen for neutrons compared to that for X-rays, which emphasises the amine group in the neutron profiles. These results therefore orientate amantadine HCl in the bilayer; the hydrophobic, cyclic region of the drug located between the phosphate and ester linkages of the phospholipids with the NH_3^+ group protruding into the water space.

This interpretation is supported by changes in the distribution of water between adjacent bilayers when amantadine HCl is added. Fig. 6 shows difference profiles representing the location of the deuterons of

heavy water, calculated by subtracting neutron scattering profiles of multi-bilayers containing H_2O from corresponding ones hydrated with D_2O. It can be seen that incorporation of amantadine HCl into the DOPC bilayers reduces the area under the water profiles, indicating that the drug is displacing some of the water from the system.

Both profiles (c) and (d) of Fig. 5 include additional features in the lipid tail region which may be caused by termination error. The resolution of the present study procludes unambiguous assignment of these features to the presence of amantadine deep within the bilayer, but it should be noted that evidence from the FB profiles (see below) indicates that full penetration of the bilayer by a proportion of the amantadine can occur. This is particularly noticeable in the neutron profiles and is either a product of the relatively high concentration of drug used saturating preferential surface sites, or it may represent amantadine which has reverted to the uncharged, FB form by deprotonation.

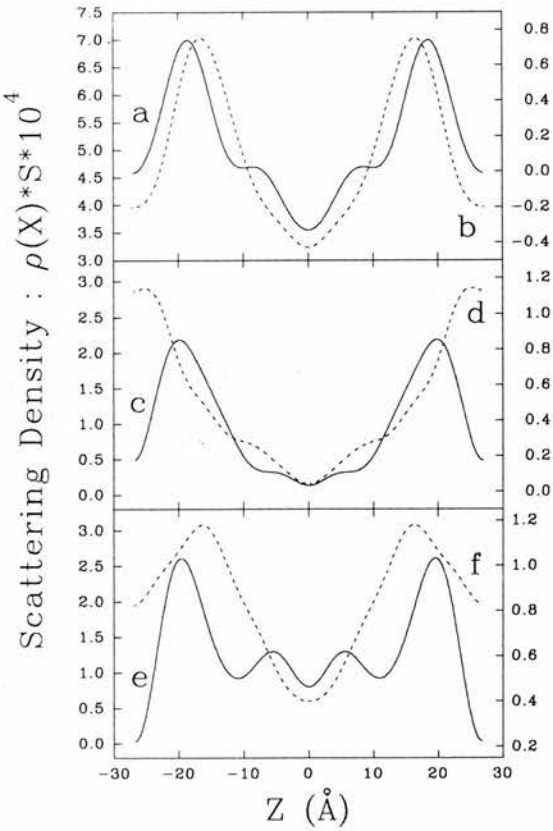

Fig. 5. Reconstructed trans-bilayer X-ray scattering profile of pure DOPC (a, left-hand scale) and neutron scattering profile of pure DOPC (b, right-hand scale) at 98% rh and 20°C. (d) and (f) are neutron scattering difference profiles of amantadine hydrochloride and amantadine free base, respectively. (c) and (e) are the corresponding X-ray scattering difference profiles. The difference profiles were calculated by subtracting structure factors of pure DOPC from those of DOPC with 5% (mol) amantadine, after correction for variations in bilayer repeat and placed on a relative absolute scale using the method of Weiner et al. [18]). The horizontal scale (Z) is distance, measured from the bilayer centre, in ångströms.

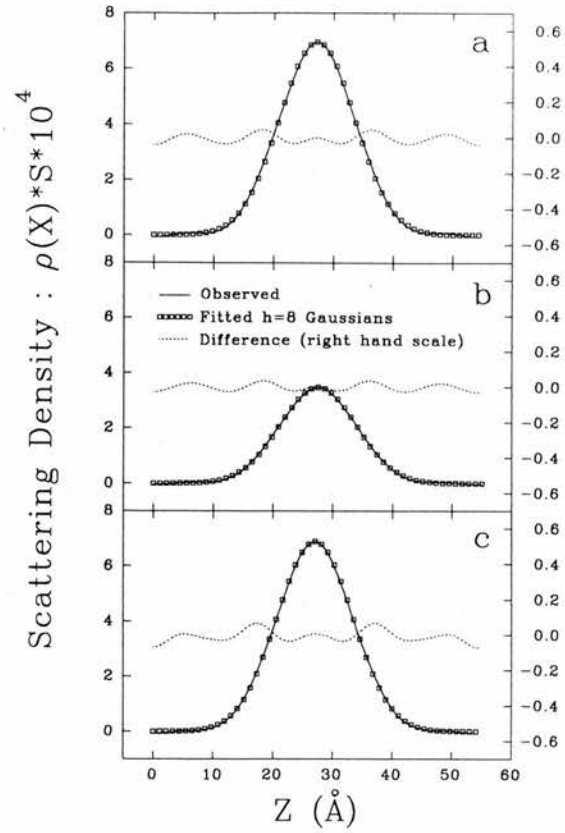

Fig. 6. Difference neutron density scattering profiles showing the distribution of water between bilayers of (a) pure DOPC, (b) DOPC with 5% (mol) amantadine HCl and (c) DOPC with 5% (mol) amantadine FB, all at 20°C. Also shown are Gaussian distributions fitted to the water profiles in reciprocal space over all eight observed orders of diffraction, using a development of the method of Wiener et al. [18]. Each curve consists of the sum of two Gaussians with the following parameters: (a) Z (distance from centre of bilayer) = $\pm 26.53 \pm 0.35$ Å, A_w (1/e halfwidth) = 8.82 ± 0.20 Å; (b) $Z = 26.04 \pm 0.55$ Å, $A_w = 8.75 \pm 0.25$ Å; (c) $Z = \pm 25.58 \pm 0.45$ Å, $A_w = 8.65 \pm 0.25$ Å. The difference between the observed and modelled water profiles may be taken as a crude approximation of error in the reconstructions. Each graph therefore also shows this difference, plotted on an enlarged scale, corresponding to that used in Fig. 5 (right-hand side).

Amantadine FB

At this resolution, both amantadine peaks are in the same position in the X-ray profile (e) as in the amantadine HCl result (c). Positionally, therefore, the data are identical. However, there is a difference in the proportional representation of amantadine across the bilayer with relatively more now appearing in the fatty acid tail region of the phospholipids. The neutron results (f) support these findings. Here the main scattering density at the surface location has moved slightly into the bilayer reflecting the fact that the amantadine FB is deuterated on the hydrophobic carbons only and that the NH_2 amine group is unlabelled and therefore scatters much less intensely compared to the labelled

mass; it can be observed as a shoulder on the water side of the main peak. This observation again orientates the amantadine with its NH_2 group at the lipid/water interface.

Profiles (e) and (f) clearly show that a proportion of amantadine has penetrated almost to the centre of the bilayer. Once again, the features in this region may represent some part of the amantadine structure, or may just be termination error. However, the height of the profiles above zero can only be explained in terms of a considerable mass of drug being present in this region. Consistent with this finding, the amount of water associated with the bilayers containing amantadine FB is much greater than that for bilayers containing amantadine HCl (Fig. 6) and almost equates with that present in the bilayers in the absence of either form of amantadine. Clearly a proportion of the drug has moved away from the water-penetrated surface of the bilayers to take up a deeper location in the bilayers. This evidence, taken together with the HCl results, leads us to propose that the interaction between amantadine and DOPC bilayers takes the form of an equilibrium between two possible regions. One of these is located at the water/bilayer interface, the other is less defined and broadly represents the fatty acid tail region. The balance of this equilibrium between the two sites appears to depend upon the starting protonation state of amantadine. However, this does not necessarily imply that the initial charge state of the amine is preserved throughout the experiment. This result compares with tetracaine where its interaction with phospholipids is also reported to be influenced by the charge state of the drug [20,21].

Amantadine–phospholipid interactions

If the optical parameters and the sample dimensions are kept constant throughout a series of diffraction experiments then the mosaic spread may be used as a measure of the macroscopic order of each sample; the smaller the mosaic spread, the less the degree of disorder of the bilayers [22,23]. The values obtained for stacked bilayers of pure DOPC in this study are in good agreement with previous observations [16,17]. The mosaic spread did not change upon the addition of 5 mol% amantadine, which indicates that the interaction between the drug and the bilayer did not disturb the macroscopic order of the system. There was no evidence of phase separation in the multilayers containing amantadine. Unfortunately, in the liquid phase, DOPC does not give discrete 4.5–4.8 Å reflections so we are unable to comment on the effect of amantadine on chain packing. We can, however, conclude that, under these experimental conditions, amantadine does not markedly perturb the bilayer system.

It has been reported that amantadine reduces the extent of dissociation of clathrin from coated vesicles [6] in a study which used relatively small amounts of the amine. The ability of amantadine and related compounds to stabilise or destabilise phospholipid bilayers has also been extensively investigated. Cheetam and Epand [8] concluded from NMR studies that amantadine perturbs the organisation and increases the fluidity of bilayers. Our present study, using a much lower drug/lipid molar ratio, does not indicate any such perturbation but it may be that this anomaly reflects the different drug concentrations used in such studies.

Another variable involves the lipid type used. The work reported here employed DOPC which has a large headgroup and two unsaturated chains giving the phospholipid a quasi-hourglass shape, creating an area of increased steric freedom in the neck region when the lipids are formed into a bilayer. The amantadine may be accomodated within such an area, fitting in between the phospholipid molecules. Our data, which indicate that the cyclic carbon component of amantadine orientates on the hydrophobic side of the phospholipid headgroup, support this model. This would suggest that the effects of amantadine upon bilayer structure and stability are likely to be complex and to be dependant upon intrinsic and environmental factors.

Fig. 2 shows that the bilayer repeat distance was reduced by up to 2.5 Å at low humidities. A similar effect is produced by the addition of 1,2-dioleoyl-*s*-glycero-3-phosphoethanolamine (DOPE) [17] to DOPC, where the smaller PE headgroup allows the choline moiety of DOPC to lie in a more perpendicular orientation and therefore closer to the plane of the bilayer surface (unpublished data). Amantadine may have a similar effect on DOPC. Unfortunately, the relatively low contrast between the PC headgroup and water makes it impossible to determine the headgroup conformation with the present data. However, this does mean that any drug-induced changes in headgroup conformation will not have an adverse effect on the profile subtractions. Future neutron work using specifically deuterated phospholipid headgroups may be able to resolve this question.

Our finding that uncharged, amantadine FB has the ability to penetrate more easily into the bilayer is supported by diffusion data performed on other similar compounds [24]. This phenomenon could be related to the zwitterionic nature of DOPC, the lipid chosen for our study. Further work will investigate the possible relationship between the lipid composition of the bilayer and the nature of its interaction with amantadine. For example, including a proportion of negatively-charged lipid may induce major changes [25] particularly with the charged amantadine HCl.

Acknowledgements

The deuterated amantadine was prepared by Dr. M.R. Alecio (Shell Research Centre, Sittingbourne,

UK) who also read and made helpful comments on the manuscript. Neutron data collection and initial reduction were performed on instrument DI6 at the Institut Max von Laue - Paul Langevin, Grenoble, France. The work was supported by both SERC and ILL grants.

References

1 Oxford, J.S. and Galbraith, A. (1980) Pharmacol. Therap. 11, 181–262.
2 Obeso, J.A. and Martinez-Lage, J.M. (1987) in: The Handbook of Parkinson's Disease (Koller, W.C., ed.), pp. 312–316, Marcel Dekker, New York.
3 Hay, A.J. (1989) in Concepts in Viral Pathogenesis, Vol. 3, pp. 561–567, Springer-Verlag, New York.
4 Sugrue, R.J., Bahadur, G., Zambon, M.C., Hall-Smith, M., Douglas, A.R. and Hay, A.J. (1990) EMBO. J. 9, 3469–3476.
5 Gilman, A.G., Rall, T.W., Nies, A.S. and Taylor, P. (1990) The Pharmaceutical Basis of Therapeutics, 8th Edn., pp. 472–473, Pergamon Press, New York.
6 Phonphok, Y. and Rosenthal, K.S. (1991) FEBS Lett. 281, 188–190.
7 Sugrue, R.J. and Hay, A.J. (1991) Virology 180, 617–624.
8 Cheetham, J.J. and Epand, R.M. (1987) Biosci. Rep. 7, 225–230.
9 Franks, N.P. and Lieb, W.R. (1979) J. Mol. Biol. 133, 469–500.
10 Worcester, D.L. and Franks, N.P. (1976) J. Mol. Biol. 100, 359–378.
11 Torbet, J. and Wilkins, M.H.F. (1976) J. Theor. Biol. 62, 447–458.
12 Lesslauer, W., Cain, J.J. and Blaisie, J.K. (1972) Proc. Natl. Acad. Sci. USA 69, 1499–1503.
13 Büldt, G., Gaily, H.U., Seelig, J. and Zaccai, G. (1979) J. Mol. Biol. 134, 673–691.
14 Jacobs, R.E. and White, S.H. (1989) Biochemistry 28, 3421–3437.
15 Büldt, G., Gaily, H.U., Seelig, A., Seelig, J. and Zaccai, G. (1978) Nature 271, 182–184.
16 Weiner, M.C., King, G.I. and White, S.H. (1991) Biophys. J. 60, 568–576.
17 Bradshaw, J.P., Edenborough, M., Sizer, P.J.H. and Watts, A. (1989) Biochim. Biophys.. Acta 987, 101–110.
18 Weiner, M.C. and White, S.H. (1991) Biochemistry 30, 6997–7008.
19 Franks, N.P. and Lieb, W.R. (1981) in Liposomes: From Physical Structure to Therapeutic Applications (Knight, ed.), pp. 243–272, Elsevier/North-Holland Press, Amsterdam.
20 Smith, I.C., Auger, M. and Jarrell, H.C. (1991) Ann. NY. Acad. Sci. 625, 668–684.
21 Shinooka, T., Shibata, A. and Terada, M. (1992) Biochim. Biophys. Acta. 1104, 261–268.
22 Schwartz, S., Cain, J.E., Dratz, E.A. and Blasie, J.K. (1975) Biophys. J. 15, 1201–1233.
23 Blaurock, A.E. and Nelander, J.C. (1976) J. Mol. Biol. 103, 421–431.
24 Miller, D.K. and Lenard, J. (1981) Proc. Natl. Acad. Sci. USA. 78, 3605–3609.
25 Kim, J., Mosior, M., Chung, L.A., Wu, H. and McLaughlin, S. (1991) Biophys. J. 60, 135–148.

Reprinted from

Biophysical Chemistry

Biophysical Chemistry, 49 (1994) 71–76
Elsevier Science B.V., Amsterdam

BIOCHE 1829

X-ray diffraction studies using a novel synthetic phospholipid

A.J. Cudmore [a], J.P. Bradshaw [a,b,*] and M.R. Alecio [c]

[a] *Department of Biochemistry, University of Edinburgh, Hugh Robson Building, George Square, Edinburgh EH8 9XD, Scotland (UK)*
[b] *Department of Preclinical Veterinary Sciences, University of Edinburgh, Summerhall, Edinburgh EH9 1QH, Scotland (UK)*
[c] *Shell Research Centre, Sittingbourne, Kent ME9 8AG (UK)*

(Received 25 July 1993; accepted in revised form 4 October 1993)

ELSEVIER

BIOPHYSICAL CHEMISTRY

An International Journal devoted to the Physics and Chemistry of Biological Phenomena

Aims and Scope of the Journal

The journal is devoted to the interpretation of biological phenomena in terms of the principles and methods of physics and chemistry. It is receptive to articles which deal with biological molecules and systems, and to papers which treat systems serving as models for these. Treatments, phenomenological as well as molecular, of the interactions, structure and biological functions of individual biological macromolecules and of supramolecular structures are also within the journal's domain.

Biophysical Chemistry is published monthly. For 1994, 4 volumes, volumes 48–51, are scheduled for publication. Subscription prices are available upon request from the publisher. Subscriptions are accepted on a prepaid basis only. The Journal will be sent by SAL (Surface Air Lifted) mail whenever this service is available. Airmail rates are available upon request. Subscription orders can be entered only by calender year and should be sent to: ELSEVIER SCIENCE B.V., P.O. Box 211, 1000 AE Amsterdam, The Netherlands. Tel.: 31-20-5803642, FAX: 31-20-5803598, or to your usual subscription agent. A specimen copy will be sent on request. Claims for issues not received should be made within six months of publication of the issues. If not, they cannot be honoured free of charge. Customers in the U.S.A. and Canada wishing information on this and other Elsevier Journals, please contact Elsevier Science Company Inc., Journal Information Center, 655 Avenue of the Americas, New York, NY 10010. Tel.: (212) 633-3750, FAX: (212) 633-3764. For advertising rates apply to the publishers

US mailing notice – Biophysical Chemistry (ISSN 0301-4622) is published monthly by Elsevier Science B.V., Molenwerf 1, P.O. Box 211, 1000 AE Amsterdam, The Netherlands. Annual subscription price in the U.S.A. is US$ 908.00, including air speed delivery, valid in North, Central and South America only. Application to mail at second class postage pending at Jamaica, NY 11431.

USA POSTMASTERS: Send address changes to Biophysical Chemistry, Publications Expediting, Inc., 200 Meacham Avenue, Elmont, NY 11003. Airfreight and mailing in the USA by Publication Expediting.

Biophysical Chemistry, 49 (1994) 71–76
Elsevier Science B.V., Amsterdam

BIOCHE 1829

X-ray diffraction studies using a novel synthetic phospholipid

A.J. Cudmore [a], J.P. Bradshaw [a,b,*] and M.R. Alecio [c]

[a] *Department of Biochemistry, University of Edinburgh, Hugh Robson Building, George Square, Edinburgh EH8 9XD, Scotland (UK)*
[b] *Department of Preclinical Veterinary Sciences, University of Edinburgh, Summerhall, Edinburgh EH9 1QH, Scotland (UK)*
[c] *Shell Research Centre, Sittingbourne, Kent ME9 8AG (UK)*

(Received 25 July 1993; accepted in revised form 4 October 1993)

Abstract

A novel brominated phospholipid has been designed and synthesised for future use in X-ray diffraction studies. It is an analogue of dipalmitoyl-phosphatidylcholine (DPPC), with the sn-2 chain terminal methyl group exchanged for a bromine atom. This bromine atom "label" has been incorporated into a phospholipid by substitution for a group of similar atomic radius, 1.85 versus 2.00 Å, thus creating a molecule which is sterically similar to its unlabelled analogue. The "bromolipid" has been studied using the swelling series method in conjunction with Patterson mapping in the gel phase at 20°C. It diffracts well to 12 orders in its pure form at 20°C and between 57% and 98% relative humidity. A combination of two phasing methods have allowed the diffraction patterns of bilayers incorporating the bromolipid to be phased unambiguously. We suggest that the bromolipid is excellently suited as a phasing agent for use in future isomorphous replacement and multiple anomalous diffraction (MAD) experiments.

Keywords: X-ray diffraction; Phospholipid; Bromolipid; Patterson mapping

1. Introduction

Brominated phospholipids have been utilised before in the study of lipid bilayers [1]. Synthetic bromolipids have been used in fluorescence, as well as X-ray diffraction, studies [2,3]. These studies have however focused on the production of a bromolipid, typically by the addition of two bromine atoms across a double bond, resulting in a phospholipid "isomorph" lacking a double bond, with two relatively large atoms sticking out from the lipid chain. Other methods of placing bromine in a bilayer include the approach of labelling a small molecule with bromine, which is then inserted into the bilayer [4].

The present study has set out to make and study a close structural isomorph of dipalmitoylphosphatidylcholine, which can be used as a phasing agent in isomorphous replacement studies. DPPC, a benchmark lipid, has been studied many times and is well characterised [5]. This bromolipid was designed so that it would have only one bromine per molecule, would not hinder chain packing by having been added across a double bond, and would have approximately the

* Corresponding author.

SSDI 0301-4622(93)E0083-H

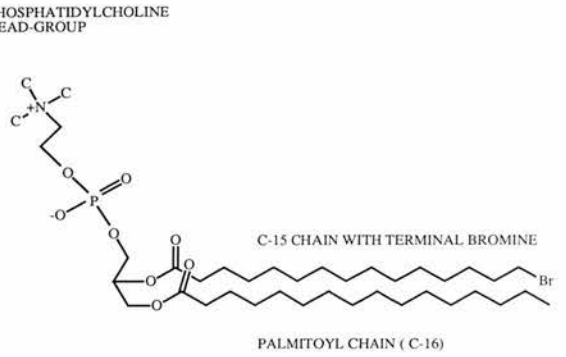

Fig. 1. The structure of the bromolipid used in this study. This shows the position of the bromine atom in the molecule, which replaces the sn-2 palmitoyl terminal methyl group of DPPC.

same molecular volume as DPPC. The optimum place to locate such a phasing agent "label" would be in the centre of the bilayer. This has been achieved by switching the terminal methyl of the sn-2 palmitoly chain of DPPC for a bromine atom, see fig. 1. The methyl group and bromine atom are of similar radius and so the substitution results in little difference in the overall volume of the two molecules and therefore similar packing in the membrane.

In this paper the fully hydrated structure of bromolipid has been studied, together with that for pure DPPC at 20°C. X-ray diffraction photographs of each have been collected to at least 12 orders, and swelling series have been created by repeating the experiments at varying sample humidity, using the method of Torbet and Wilkins, [6]. Diffraction spots have been phased using a combination of this swelling series method and by using one-dimensional Patterson maps to help phase ambiguous reflections. From these results electron density maps have been created showing the structure of bromolipid and DPPC to 4 Å.

2. Possible future uses of the bromolipid

2.1. Isomorphous replacement

This is a method, used extensively in protein crystalography for phasing, where a heavy atom is added into the sample as a "label". On introducing a known amount of heavy atoms into a system, one has a way of scaling the relative electron density scale into one of absolute density per unit cell. This is a great advantage over the swelling series which is always only on a relative scale. The use of heavy atom methods go back some time and have had limited success with biological membranes [7–9]. Phases have been determined for bilayer of fatty acids associated with a series of alkaline earth metals [10]. Franks et al. [11] have used halogenated cholesterol analogues in isomorphous experiments. They showed that the analogue could be isomorphously exchanged with cholesterol and this exchange be used to phase the signs of the lamellar reflections. This cholesterol labelled method works well, but obviously, only when one is studying a cholesterol containing system.

2.2. Multiple anomalous dispersion (MAD) experiments

Anomalous scattering as a method of phasing is still very new to protein crystalography [12,13], and has still yet to be used in membrane diffraction experiments. If possible this method would be the finest application for a phospholipid such as the bromolipid synthesised and studied as reported here.

MAD experiments have a major advantage over isomorphous replacement experiments. In a typical isomorphous replacement experiment one might study several samples, each with increasing amounts of heavy atom present, and hope for phase assignment to be successful, that there is no major structural change around the heavy atom. In the MAD experiment one need only study one sample with a percentage of label incorporated. The experiment is performed using X-rays, at energies either side of a heavy atom absorption edge, the difference being used as the phasing method, Hendrickson [14]. Therefore throughout the experiment there are no structural variations in the sample whatsoever, as it is the X-ray source and not the sample that is varied.

By using the swelling series as the phasing method to characterise this novel molecule, we

have shown that this molecule has great potential, in itself, as a phasing agent.

3. Materials and methods

1,2-dipalmitoyl-sn-glycero-3-phosphocholine (DPPC) was purchased from Sigma Chemical Company Ltd. (Fancy Road, Poole, U.K.). The synthesis of the novel bromolipid shall be covered elsewhere. Both phospholipids were confirmed to be a single species by thin layer chromatography prior to use.

3.1. X-ray diffraction

Oriented bilayer stacks of phospholipid were prepared by pipetting 2 mg of sample, dissolved in chloroform, onto a curved glass slide of area 1 cm^2. The chloroform was then evaporated off by a stream of nitrogen, before the slide was placed in a vacuum for 2 h. The sample was then rehydrated over water, and reannealled at 70°C for 1 h. Samples were then held in a temperature controlled cell at 20°C. The relative humidity of the cell was varied from 57% to 98%, using varying salt solutions in a bath under the sample, for the swelling series experiments. The data were corrected for absorption, as described in Franks and Leib [15], and with the Lorentz factor. For the geometry used, this latter factor takes the form of h^2, where h is the order of diffraction.

Previous methods which attempt the determination of phases using only a single data set have been attempted. Luzzati et al. [16] used a pattern recognition approach. In this procedure all possible phase combinations are considered and the correct solution chosen on the basis of known or postulated properties of the electron density profile, such as levels of electron density and partial specific thicknesses of particular components. For a good pattern however, with a large number of orders, there are a large number of possibilities. Using only one data set also can allow in errors in data collection, that would stand out in a data series. This paper however uses a similar approach to this method for distinguishing ambiguous phases, i.e. the case where most phases are determined from the swelling series but one or two orders could be either phase. The properties of the electron density profile, in this case, coming from the Patterson maps.

3.2. Differential scanning calorimetry

The lipids, DPPC and bromolipid, were prepared by dissolving the weighed out mixtures in chloroform, drying down in a rotary evaporator, washing twice with acetone and again drying down to a mixed solid in a rotary evaporator. The dry phospholipid was then placed in a platinum pan and the mass of lipid weighed using a four point balance. An exact amount of water, 40 μl of water to 7 mg of lipid for water in excess experiments, were then measured into a sample pan, of volume 50 μl, by syringe. A lid was placed on top of the pan and sealed by cold welding using a Perkin Elmer sealing press. A reference pan containing only water was prepared in the same way as the sample pans. Samples were loaded into a Perkin Elmer DSC 7 machine with a Perkin Elmer Tac 7/7 instrument controller. Samples were then typically cycled from 10°C to 70°C, so as to anneal and homogenise the sample. The sample was then allowed to sit at 10°C for 30 minutes before an experimental run from 10°C to 70°C was recorded. A scan rate of 3.0°C per minute was used.

4. Results and discussion

The DSC results, table 1, compare the phase behaviour of two lipids, DPPC and bromolipid, calorimetrically. The results show that the phase behaviour of bromolipid is similar to that of

Table 1

DSC results for DPPC and bromolipid samples

Lipid	Main transition temperature (°C)	Pretransition temperature (°C)	Main transition enthalpy (J/g)	Main peak width at half height $\Delta T_{1/2}$ (°C)
DPPC	42.3	37.1	54.5	1.45
bromolipid	33.4	30.5	52.4	1.55

DPPC. Although the main phase transition temperature, for the bromolipid, occurs at ≈ 9°C lower than that found for DPPC, it melts with a similar enthalpy. The width of the melting peak, which is an indicator of the cooperativity of the event [17], is also similar for the two species. The bromolipid also has a pretransition peak, indicating it too forms the pretransition ripple phase, found for DPPC.

Scheme 1 shows a typical X-ray diffraction photograph of pure bromolipid, showing twelve orders of diffraction. Films were scanned and data corrected before a Patterson map of each data set was constructed. The Patterson maps show the interatomic distances of the major electron dense regions of the molecule in the bilayer without using any phase information whatsoever. An electron density graph constructed using data that is putatively phased should therefore show the same approximate interatomic distances. Because the Patterson map has no phase information involved in its construction it is a useful alternative test of accurate phasing.

Fig. 2 shows the Patterson map for pure bromolipid and pure DPPC, see also table 1. The graph for pure bromolipid naturally has more features to it, it having extra regions of high electron density, compared with DPPC. The bromines are close together giving rise to a peak from the origin out to ≈ 7 Å. The phosphate headgroup to bromine atom distance gives the peak at 18.5 Å. This partially masks the headgroup separation peak at ≈ 14 Å. Swelling series have been constructed for pure bromolipid and pure DPPC, figs. 3 and 4, using the method of Torbet and Wilkins [6]. Although ideally for phasing using the swelling series method, water lost

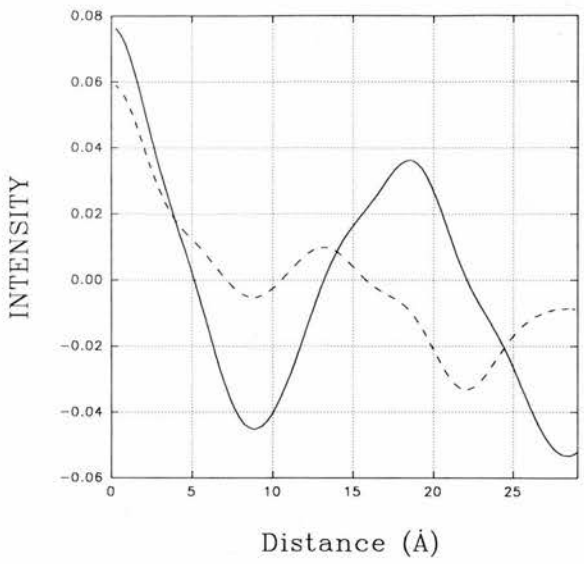

Fig. 2. One-dimensional Patterson maps of bromolipid (solid) and DPPC (dash), fully hydrated at 20°C. The bromolipid has increased intensity near the origin due to the closeness in space of the bromine atoms in the center of the bilayer. It also shows the bromine to phosphate distance as being about 18.5 Å.

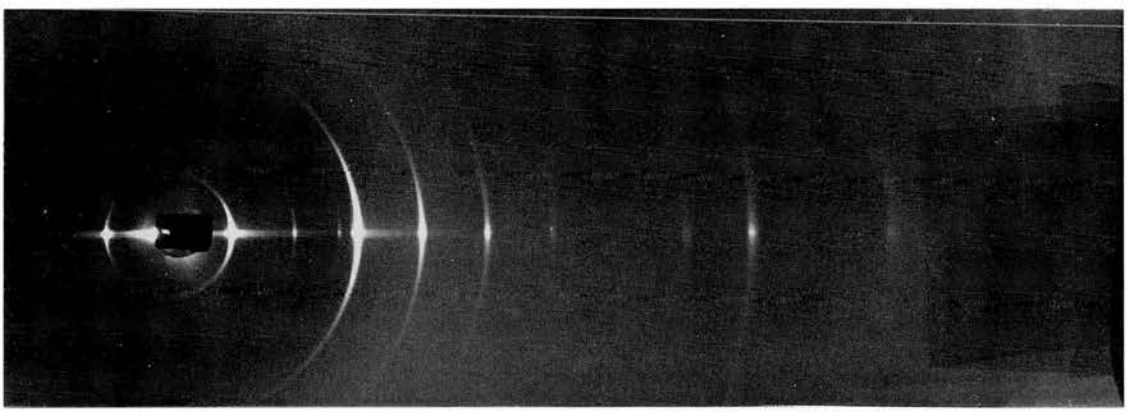

Scheme 1.

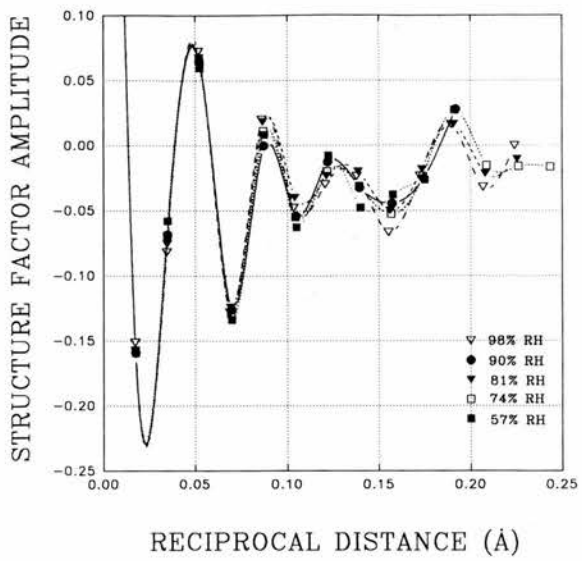

Fig. 3. Swelling series data for pure DPPC at 20°C. The humidity was varied from 57% to 98% using varying salt solutions. The corrected square roots of intensity are plotted against reciprocals of Bragg spacing.

from the water layer is the only structural change in the sample, varying humidity has other known effects on the structure and thickness of the

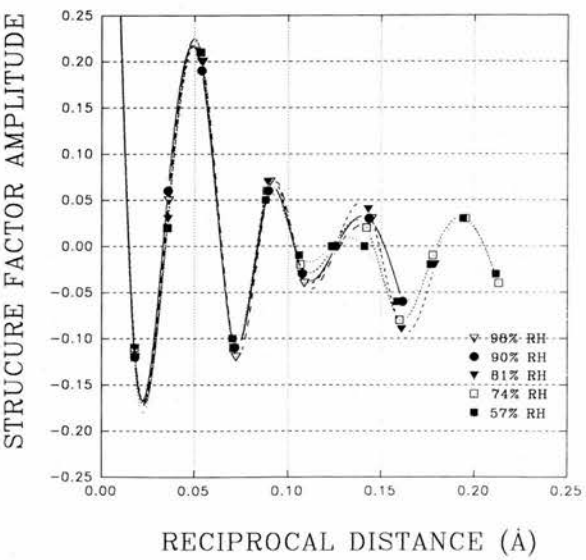

Fig. 4. Swelling series data for pure bromolipid at 20°C. The relative structure factors show a general displacement in the positive direction compared with those for pure DPPC.

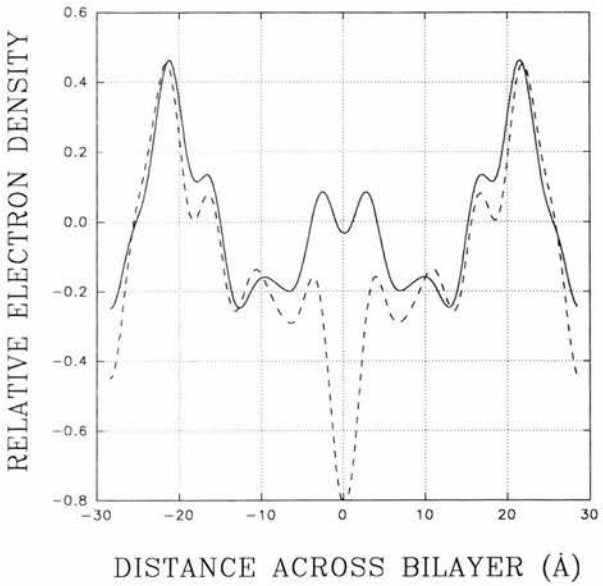

Fig. 5. Reconstructed electron density maps of bromolipid (solid) and DPPC (dash) using the phases from the swelling series, figs. 3 and 4. The maps clearly show the bromine atoms at the centre of the bilayer.

bilayer. As the humidity decreases so does the chain tilt angle, which acts to increase the bilayer thickness [18,19]. At the same time water is removed from around the head group, and the N^+ end of the phosphocholine group moves closer to the hydrocarbon layer, acting to reduce the bilayer thickness [20]. In spite of this the swelling series method is still usable. The phases shown have been constructed by fitting data to continuous Fourier transforms, and comparison of putatively phased electron density graphs to Patterson maps. These show data collected out to fourteen orders in one case for DPPC and twelve orders for bromolipid. One can note the general tendency of the continuous transform of bromolipid being positively shifted, compared with DPPC, as one would expect for a large atom placed in the centre of the DPPC bilayer [21].

Fig. 5 shows the electron density graph of both pure bromolipid and DPPC each to twelve orders using the phases shown. From the electron density graph can be measured the same interatomic distances that give rise to maxima in the Patterson function. Table 2 summarises these distances,

Table 2

Inter-atomic distances inferred from Patterson functions versus those from phased electron density graphs

Phospholipid	Phosphate headgroup to headgroup distance	Phosphate headgroup to bromine distance
bromolipid		
Patterson	≈ 14 Å	≈ 18.5 Å
electron density map	13.6 Å	18.7 Å
DPPC		
Patterson	≈ 13.2 Å	
electron density map	13.0 Å	

as obtained from the Patterson function or electron density map. The correlation of the two are very good suggesting the right phases have been used in obtaining the electron density maps.

5. Summary

A novel structural isomorph of the benchmark phospholipid DPPC has been successfully synthesised for use in X-ray diffraction experiments. This bromolipid analogue of DPPC has a terminal bromine on the sn-2 lipid chain in place of a methyl group. This new molecule forms membrane bilayers very similar to those of pure DPPC and diffracts well to twelve orders. The diffraction patterns here have been successfully phased using the swelling series method and one-dimensional Pattersons. The resultant electron density maps show the two bromines close together in the centre of the bilayer structure.

We hope that in this paper we have prepared the way for future X-ray experiments where the bromolipid hopefully can be used as a phasing agent in isomorphous replacement experiments or in anomalous dispersion experiments which should be able to utilise the absorption edge of the bromine atom.

References

1 M.C. Wiener and S.H. White, Biochemistry 30 (1991) 6997–7008.
2 P.W. Holloway, T.C. Markello and T.L. Leto, Biophys. J. 57 (1982) 63–44.
3 J. Everett, A. Zlotnick, J. Tennyson and P.W. Holloway, J. Biol. Chem. 261 (1986) 6725–6729.
4 J. Katsaras, R.H. Stinson, J.H. Davis and E.J. Kendall, Biophys. J. 59 (1991) 645–653.
5 M.C. Wiener, R.M. Suter and J.F. Nagle, Biophys. J. 55 (1989) 315–325.
6 J. Torbet and M.H.F. Wilkins, J. Theoret. Biol. 62 (1976) 447–458.
7 C.K. Akers and D.F. Parsons, Biophys. J. 10 (1970) 116–136.
8 A. Harker, Biophys. J. 12 (1972) 1285–1295.
9 A.E. Blaurock, Biophys. J. 13 (1973) 1261–1262.
10 T.J. McIntosh, R.C. Wallbillig and J.D. Robertson, Biochim. Biophys. Acta 448 (1976) 15–33.
11 N.P. Franks, T. Arunachalam and E. Caspi, Nature 276 (1978) 530–532.
12 W.A. Hendrickson, NATO ASI series A: Life sciences, Vol. 126, paper a, Crystallography in molecular biology, eds. D. Moras and J. Drenth (1985) pp. 81–87.
13 W.A. Hendrickson, Methods in enzymology, Vol. 115, paper b (1985) pp. 41–55.
14 W.A. Hendrickson, Science 254 (1991) 51–58.
15 N.P. Franks and W.R. Leib, J. Mol. Biol. 131 (1979) 469–500.
16 V. Luzzati, A. Tardieu and D. Taupin, J. Mol. Biol 64 (1972) 269–286.
17 R.N. McElhaney, Biochim. Biophys. Acta 864 (1986) 361–421.
18 J. Katsaras, D. Yang and R.M. Epand, Biophys. J. 63 (1992) 1170–1175.
19 J. Katsaras and R.H. Stintson, Biophys. J. 57 (1990) 649–655.
20 B. Bechinger and J. Seelig, Chem. Phys. Lipids 58 (1991) 1–5.
21 N.P. Franks and W.R. Leib, Liposomes: from physical structure to therapeutic applications, ed. C.G. Knight (Elsevier, Amsterdam, 1981).